

NATURAL MUMMIFICATION IN HUMAN  
CARCASSES AND ANALOGUES IN A  
TEMPERATE AUSTRALIAN ENVIRONMENT

Alisha Deo

Thesis written in the School of Mathematical and Physical Sciences at the  
University of Technology Sydney

in fulfilment of the requirements for the

Degree of Doctor of Philosophy

2023

## CERTIFICATE OF AUTHORSHIP AND ORIGINALITY

I, Alisha Deo, declare that this thesis, is submitted in fulfilment of the requirements for the award of Doctor of Philosophy, Science, in the School of Mathematical and Physical Sciences at the University of Technology Sydney. This thesis is wholly my own work unless otherwise referenced or acknowledged. In addition, I certify that all information sources and literature used are indicated in the thesis. This document has not been submitted for qualifications at any other academic institution.

This research is supported by the Australian Government Research Training Program.

Production Note:

Signature removed prior to publication.

Signature: \_\_\_\_\_

Date: 06.09.2023

## ACKNOWLEDGEMENTS

First, thank you to my supervisors, Maiken and Barb, for all your guidance through my candidature. Thank you for believing that I could complete such a busy task and for holding my hand through the hard parts and putting up with all my stupid questions. Thank you to the entire time at AFTER and everyone in the analytical forensics lab group who sacrificed many days and even weekends to help me out during my sampling days. Thank you for the catch-up sessions and concerts in those hour-long car rides. You all made for great company!

Thank you to all my wonderful friends who would always check in on me by asking “How’s the thesis going?” (Especially you Anju), to which I would respond “It’s going”. Thank you for listening to me whinge about all of my hurdles and hear me complain literally every time we met. I can stop complaining now (hopefully!).

Also, thank you to everyone at Uni, my incredible friends, and my fun little cubicle. To Vitor, Helen, Amber, Minh, John, Blake, Swasti (bae) and TTP- thank you for keeping me sane through the process with all your therapy, motivation, and insane support. Thank you for all the lunches, spontaneous desk drinks, weekend getaways, and for all endless laughter. Thank you for never judging me, watching me breakdown a million times, and for helping to put me back together with your sunshine. I honestly don’t think I could have done it without you all.

Finally, thank you to my wonderful parents, Arvind and Babita, and my beautiful sisters, Ashnay and Aksita. This is all for you. Thank you for all the incredible love and support you have given me, and not just through my PhD. I love you all so much.

## Table of Contents

CERTIFICATE OF AUTHORSHIP AND ORIGINALITY .....	II
ACKNOWLEDGEMENTS .....	III
LIST OF FIGURES .....	VIII
LIST OF TABLES .....	XII
ABBREVIATIONS.....	XIV
ABSTRACT .....	XVI
CHAPTER 1 INTRODUCTION .....	1
1.1 DECOMPOSITION .....	4
1.1.1 ENVIRONMENTAL EFFECTS ON DECOMPOSITION .....	5
1.1.2 LIPIDS .....	8
1.2 TISSUE AND SKIN MATRIX IN DECOMPOSITION .....	8
1.3 LIPID ANALYSIS .....	9
1.3.1 GC-MS/MS IN LIPID ANALYSIS .....	10
1.4 STUDY RATIONALE .....	11
1.5 PROJECT AIMS.....	12
CHAPTER 2 MATERIALS & METHODS .....	14
2.1 GENERAL APPROACH .....	15
2.2 RESEARCH FACILITY .....	15
2.3 ETHICS .....	17
2.4 SURFACE DECOMPOSITION AND BODY PLACEMENT .....	17
2.5 SAMPLE COLLECTION AND ANALYSIS .....	20
2.5.1 SELECTION OF ANALYTES FOR TARGETED GC-MS/MS ANALYSIS .....	21
2.5.2 REFERENCE STANDARDS.....	23
2.5.3 CHEMICAL REAGENTS .....	23
2.6 GC-MS/MS METHOD .....	24
2.6.1 SAMPLE PREPARATION .....	24
2.6.2 INSTRUMENT PARAMETERS .....	24
CHAPTER 3 GC-MS/MS METHOD OPTIMISATION .....	27
3.1 INTRODUCTION.....	28



3.2	MATERIALS AND METHODS .....	28
3.2.1	PREPARATION OF STANDARDS FOR IDENTIFICATION .....	28
3.2.2	PREPARATION OF STANDARDS FOR CALIBRATION .....	29
3.2.3	MRM MODE OPTIMISATION .....	29
3.2.4	SAMPLE EXTRACTION OPTIMISATION .....	29
3.2.5	EXTRACTION EFFICIENCIES AND MATRIX EFFECTS .....	30
3.3	RESULTS AND DISCUSSION .....	32
3.3.1	STANDARD IDENTIFICATION AND CALIBRATION .....	32
3.3.2	OPTIMISED MRM METHOD .....	33
3.3.3	SAMPLE EXTRACTION OPTIMISATION .....	36
3.3.4	MATRIX EFFECTS RESULTS .....	39
3.4	FINAL METHOD .....	42
CHAPTER 4	PIG VS HUMAN: WARMER SEASON STUDY .....	44
4.1	MATERIALS AND METHODS .....	45
4.2	RESULTS .....	46
4.2.1	VISUAL COMPARISON AND OBSERVATIONS .....	46
4.2.2	PIG VS HUMAN TISSUE .....	49
4.2.3	PCAS .....	49
4.2.4	ANOVA .....	51
4.2.5	SUMMARY .....	54
4.2.6	PIG VS HUMAN SKIN .....	54
4.2.7	PCAS .....	54
4.2.8	ANOVA .....	56
4.2.9	SUMMARY .....	58
4.3	WARMER CLIMATE STUDY CONCLUSIONS .....	58
CHAPTER 5	PIG VS HUMAN: COOLER SEASON STUDY .....	60
5.1	MATERIAL AND METHODS .....	61
5.2	RESULTS .....	62
5.2.1	VISUAL COMPARISON AND OBSERVATIONS .....	62
5.2.2	PIG VS HUMAN TISSUE .....	64
5.2.3	PCAS .....	65
5.2.4	ANOVA .....	66
5.2.5	SUMMARY .....	68
5.2.6	PIG VS HUMAN SKIN .....	69
5.2.7	PCAS .....	69
5.2.8	ANOVA .....	70

5.2.9	SUMMARY.....	76
5.3	COOLER CLIMATE STUDY CONCLUSIONS .....	76
CHAPTER 6	LONGITUDINAL STUDY OF HUMAN TISSUE AND SKIN.....	78
6.1	MATERIALS AND METHODS .....	79
6.2	VISUAL OBSERVATIONS AND WEATHER DATA.....	81
6.3	TISSUE RESULTS .....	84
6.3.1	PCAS .....	84
6.3.2	COMPOUND COMPARISONS .....	85
6.4	TISSUE CONCLUSIONS .....	93
6.5	HUMAN SKIN.....	93
6.5.1	PCAS .....	93
6.5.2	COMPOUND COMPARISONS .....	95
6.6	SKIN CONCLUSIONS .....	107
CHAPTER 7	CONCLUSIONS AND FUTURE WORK .....	108
CHAPTER 8	REFERENCES .....	114
APPENDIX A-	CALIBRATION CURVES.....	124
APPENDIX B-	WARMER SEASON STUDY: PIG VS HUMAN SKIN.....	133
APPENDIX C-	WARMER SEASON STUDY: PIG VS HUMAN TISSUE .....	143
APPENDIX D-	COOLER SEASON STUDY: PIG VS HUMAN SKIN.....	153
APPENDIX E-	COOLER SEASON STUDY: PIG VS HUMAN TISSUE.....	163
APPENDIX F-	WARMER SEASON STUDY: PCA AND LOADINGS PLOT OF COMPOUNDS FOR PCA IN PIG VS HUMAN .....	173
APPENDIX G-	COOLER SEASON STUDY: PCA AND LOADINGS PLOT OF COMPOUNDS FOR PCA IN PIG VS HUMAN .....	177
APPENDIX H-	LOADINGS PLOTS OF COMPOUNDS FOR PCA IN ALL HUMAN BODIES (HUMAN 2= H2, HUMAN 3= H3, HUMAN 4= H4, HUMAN 5= H5) .....	181

APPENDIX I- INDIVIDUAL COMPOUND TREND COMPARISON WITHIN THE SKIN OF ALL HUMAN BODIES .....	184
APPENDIX J- INDIVIDUAL COMPOUND TREND COMPARISON WITHIN THE TISSUE OF ALL HUMAN BODIES.....	198
APPENDIX K- PHOTOGRAPHS OF ALL STUDIED BODIES.....	211

## LIST OF FIGURES

Figure 2.1: Map of Australia highlighting the location of the Australian Facility for Taphonomic Experimental Research (AFTER). Source adapted from National Museum Australia [URL]: <a href="https://www.google.com/search?q=map+of+australia+with+states&amp;tbm=isch&amp;ved=2ahUKewiU3OTH8vGDaxUnQmwGHQfjAhttps://digital-classroom.nma.gov.au/images/map-australia-showing-states-and-territories">https://www.google.com/search?q=map+of+australia+with+states&amp;tbm=isch&amp;ved=2ahUKewiU3OTH8vGDaxUnQmwGHQfjAhttps://digital-classroom.nma.gov.au/images/map-australia-showing-states-and-territories</a> . .....	16
Figure 2.2: A HOBO® U30 weather station.....	37
Figure 2.3: Plots used for human body placement.....	38
Figure 2.4: Metal cages used to cover bodies. ....	38
Figure 3.1: Solvents tested for the optimal extraction of lipids from human tissue samples. Relative abundance reported in log base10. Error bars represent margin of error in data, relative to standard deviation of 4 replicate points).....	37
Figure 3.2: Solvents tested for the optimal extraction of lipids from human skin samples. Relative abundance reported in log base10. Error bars represent margin of error in data, relative to standard deviation of 4 replicate points).....	37
Figure 3.3: Comparison of skin extract volumes, 10 µL and 100 µL (relative abundance log base10). Error bars represent margin of error in data, relative to standard deviation of 4 replicate points. Y-axis represents relative abundance in log base10.....	38
Figure 3.4: Comparison of tissue extract volumes, 10 µL and 100 µL (relative abundance log base10). Error bars represent margin of error in data, relative to standard deviation of 4 replicate points). Y-axis represents relative abundance in log base10.....	38
Figure 4.1: Stages of decomposition (fresh, bloat, active and advanced decay) shown as a comparison between human 4 (H4), pig 1 (P1) and pig 2 (P2). First signs of observed natural mummification is denoted by the black line. ....	47
Figure 4.2: Final sampling day (Day 202) for human 5 (H5) depicting preserving effects of natural mummification within human body .....	48

Figure 4.3: Final sampling days for P1 (day 42) and P2 (day 70) depicting hard tissue (bones) due to lack of mummified skin present. (a). = P1 remains, (b). = P2 remains..... 48

Figure 4.4: Principal component analysis (PCA) of fatty acid variation within the tissue of H4 and pigs (P1 and P2 averaged). Purple circle highlighted D0-D6 sampling days for H4. Orange circle highlights D0-D7 sampling days for pigs..... 50

Figure 5.1: Stages of decomposition (fresh, bloat, active and advanced decay) shown as a comparison between Human 5 (H5), Pig 3 (P3) and Pig 4 (P4). First signs of observed mummified tissue is denoted by the black line. .... 63

Figure 5.2: Day 69 for H5, exhibiting effects of natural mummification..... 64

Figure 5.3: Day 69 for a). P1 and b). P2, exhibiting effects of natural mummification. .... 64

Figure 5.4: Principal component analysis (PCA) of fatty acid variation within the tissue of human 5 (H5) and pigs (P1 and P2 averaged). Early and middle stages samples for H5 is highlighted in orange oval. Middle and late stages of decomposition for both pigs and H5 is highlight in purple oval. .... 65

Figure 5.5: Principal component analysis (PCA) of sterol variation within the tissue of human 5 (H5) and pigs (P1 and P2 averaged). .... 66

Figure 5.6: Comparison of oleic acid relative abundance within the tissue, through decomposition period of H5 (human 5), P3 (pig 3) and P4 (pig 4). Error bars represent standard deviation variation of (4) replicates..... 68

Figure 5.7: Principal component analysis (PCA) of fatty acid variation within the skin of human 5 (H5) and pigs (P1 and P2 averaged). .... 70

Figure 6.1: Comparison of stages of decomposition for human 2 (H2), human 3 (H3), human 4 (H4) and human 5 (H5) reported in accumulated degree days (ADD). Highlighted range depicts first signs of observed mummified tissue. .... 82

Figure 6.2: Weather data comparison of H2 (human 2), H3 (human 3), H4 (human 4) and H5 (human 5).  
..... 83

Figure 6.3: PCA comparison of fatty acid profile within the tissue matrix of human 2 (H2), human 3 (H3), human 4 (H4) and human 5 (H5), grouped by stages of decomposition. Bloat and active stage samples for most humans highlighted by purple circle..... 84

Figure 6.4: PCA comparison of sterol profile within the tissue matrix of human 2 (H2), human 3 (H3), human 4 (H4) and human 5 (H5), grouped by stages of decomposition. Purple circle highlights most fresh and bloat stage samples for humans..... 85

Figure 6.5: Comparison of myristic acid during the decomposition periods of H2 (human 2), H3 (human 3), H4 (human 4) and H5 (human 5). Error bars represent standard deviation variation of (4) replicates. .... 87

Figure 6.6: Adipocere formation on the surface of human 5 (H5). .... 88

Figure 6.7: Comparison of oleic acid within tissue matrix during the decomposition periods of H2 (human 2), H3 (human 3), H4 (human 4) and H5 (human 5). Error bars represent standard deviation variation of (4) replicates. .... 90

Figure 6.8: Comparison of Palmitoleic acid during the decomposition periods of H2 (human 2), H3 (human 3), H4 (human 4) and H5 (human 5). Error bars represent standard deviation variation of (4) replicates..... 92

Figure 6.9: PCA comparison of fatty acid profile within the skin matrix of human 2 (H2), human 3 (H3), human 4 (H4) and human 5 (H5), grouped by stages of decomposition. Purple circle highlights fresh stage sampling days for most humans. Orange oval highlights bloat stage samples for most humans.94

Figure 6.10: PCA comparison of sterol profile within the skin matrix of human 2 (H2), human 3 (H3), human 4 (H4) and human 5 (H5), grouped by stages of decomposition..... 95

Figure 6.11: Comparison of lauric acid during the decomposition periods of H2 (human 2), H3 (human 3), H4 (human 4) and H5 (human 5). Error bars represent standard deviation variation of (4) replicates. .... 97

Figure 6.12: Comparison of myristic acid during the decomposition periods of H2 (human 2), H3 (human 3), H4 (human 4) and H5 (human 5). Error bars represent standard deviation variation of (4) replicates. .... 99

Figure 6.13: Comparison of palmitoleic acid during the decomposition periods of H2 (human 2), H3 (human 3), H4 (human 4) and H5 (human 5). Error bars represent standard deviation variation of (4) replicates. .... 101

Figure 6.14: Comparison of oleic acid during the decomposition periods of H2 (human 2), H3 (human 3), H4 (human 4) and H5 (human 5). Error bars represent standard deviation variation of (4) replicates. .... 103

Figure 6.15: Comparison of cholesterol during the decomposition periods of H2 (human 2), H3 (human 3), H4 (human 4) and H5 (human 5). Error bars represent standard deviation variation of (4) replicates. .... 104

Figure 6.16: Comparison of lithocholic acid during the decomposition periods of H2 (human 2), H3 (human 3), H4 (human 4) and H5 (human 5). Error bars represent standard deviation variation of (4) replicates. .... 106

## LIST OF TABLES

Table 2.1: Information of human bodies used in this study. Orange colour indicates bodies studied in warmer seasons (Australian summer and spring). Blue colour indicates bodies studied in cooler seasons (Australian autumn and winter). .....	19
Table 2.2: Information of pigs used in this study. Orange colour indicates pigs studied during warmer seasons (summer). Blue colour indicates pigs studied during cooler seasons (winter).....	20
Table 3.1: Organic solvents tested for optimal lipid extraction from decomposing human skin and tissue. ....	30
Table 3.2: Trials conducted for calculation of extraction efficiency and matrix effects. ....	31
Table 3.3: GC-MS/MS MRM method results for the targeted lipid analytes including the limit of detection (LOD) and limit of quantitation (LOQ) reported in parts per million (PPM). ....	32
Table 3.4: GC-MS/MS MRM ion transitions and optimised collision energies (CE) for the targeted lipids. ....	34
Table 3.5: Matrix effects results showing the matrix effects percentage (ME %) and recovery percentage (RE %) of tissue matrix for fresh samples (Day 0) and decomposed sample (Day 40), with both samples being spiked with deuterated compounds of 1 ppm and 10 ppm . ME % is calculated as the ratio of the mean peak area in set 2 (matrix spiked with mixture after extraction) and set 1 (deuterated compound mixture - no matrix), multiplied by 100 (Table 3.2). Ionisation enhancement is indicated by ME % values > 100 % and ion suppression is indicated by values < 100 %. RE % was calculated as the ratio of the mean peak area in set 3 (matrix spiked with mixture before extraction) to the mean peak area in set 2 (matrix spiked with mixture after extraction), multiplied by 100 [80].....	40
Table 3.6: Matrix effects results showing the matrix effects percentage (ME %) and recovery percentage (RE %) of skin matrix for fresh samples (Day 0) and decomposed sample (Day 40), with both samples being spiked with deuterated compounds of 1 ppm and 10 ppm. ME % is calculated as the ratio of the mean peak area in set 2 (matrix spiked with mixture after extraction) and set 1 (deuterated compound mixture - no matrix), multiplied by 100 (Table 3.2). Ionisation enhancement is indicated by ME % values > 100 % and ion suppression is indicated by values < 100 %. RE % was calculated as the ratio of the mean peak area in set 3 (matrix spiked with mixture before extraction) to the mean peak area in set 2 (matrix spiked with mixture after extraction), multiplied by 100 [80].....	41



Table 4.1: Warmer climate study information of pig 1 (P1), pig 2 (P2) and human 4 (H4)..... 45

Table 4.2: Depiction of compound significance in tissue comparison because of t-test, with Bonferroni correction, where H4 = human 4, P1= pig 1 and P2= pig 2 (i.e., H4 vs P1 = human 4 vs pig 1 compound comparison). Compounds showing statistical significance between two sample groups indicated through the denomination 'x'. ..... 51

Table 4.3: Depiction of compound significance in skin comparison because of t-test, with Bonferroni correction, where H4 = human 4, P1= pig 1 and P2= pig 2. (i.e., H4 vs P1 = human 4 vs pig 1 compound comparison) Compounds showing statistical significance between two sample groups indicated through the denomination..... 56

Table 5.1: Cooler climate study information of pig 3 (P3), pig 4 (P4) and human 5 (H5). ..... 61

Table 5.2: Depiction of compound significance within tissue samples because of t-test, with Bonferroni correction, where H5 = human 5, P3= pig 3 and P4= pig 4. (i.e., H5 vs P3 = human 5 vs pig 3 compound comparison) Compounds showing statistical significance between two sample groups indicated through the denomination 'x.' ..... 67

Table 5.3: Depiction of compound significance within skin samples because of t-test, with Bonferroni correction, where H5 = human 5, P3= pig 3 and P4= pig 4. (i.e., H5 vs P3 = human 5 vs pig 3 compound comparison) Compounds showing statistical significance between two sample groupings indicated through the denomination 'x'. ..... 71

Table 6.1: Information on bodies used for this study. Orange colour indicates bodies studied in warmer seasons (Australian Summer and Spring). Blue colour indicates bodies studied in cooler seasons (Australian Autumn and Winter) (H2= human 2, ca ..... 79

Table 6.2: Sampling information for human 2 (H2), human 3 (H3), human 4 (H4) and human 5 (H5).. 80

## ABBREVIATIONS

ADD	Accumulated Degree Day
AFTER	Australian Facility for Taphonomic Experimental Research
ANOVA	Analysis of Variance
BMI	Body Mass Index
BSTFA + TMCS	N,O-bis(trimethylsilyl) trifluoroacetamide + trimethylchlorosilane
CE	Collision Energy
CID	Collision Induced Dissociation
DCM	Dichloromethane
D-	Day -
GC	Gas Chromatography
GC-MS	Gas Chromatography-Mass Spectrometry
GC-MS/MS	Gas Chromatography-Tandem Mass Spectrometry
HPLC	High-Performance Liquid Chromatography
H1	Human 1
H2	Human 2
H3	Human 3
H4	Human 4
H5	Human 5
IS	Internal Standard
LOD	Limit of Detection
LOQ	Limit of Quantitation
ME %	Matrix Effects (%)
MRM	Multiple Reaction Monitoring
MS	Mass Spectrometry
PCA	Principal Component Analysis
PMI	Post-Mortem Interval
PTFE	Polytetrafluoroethylene
P1	Pig 1

P2	Pig 2
P3	Pig 3
P4	Pig 4
RE %	Recovery Extraction (%)
SIM	Selected Ion Monitoring
SRM	Selected Reaction Monitoring
TBS	Total Body Scoring
VOC	Volatile Organic Compound

## ABSTRACT

Natural mummification is a phenomenon that occurs during the decomposition of human bodies, where the external surface is preserved, while internal decomposition progresses. This event inhibits the traditional stages of decomposition (fresh, bloat, active decay, advanced decay and skeletonisation) and therefore makes staging of decomposing bodies difficult. Traditional progression of decomposition results in visual changes and biochemical degradation of internal lipids, proteins, and carbohydrates. Of these compounds proteins and carbohydrates are known to easily degrade with the environment, with lipids to surviving harsh environmental conditions due to difficult breakdown. With little knowledge surrounding the causes and biochemical analysis of natural mummification, it is crucial to investigate the visual and lipid characteristics of this event to strengthen our understanding of this phenomenon.

This thesis reports an investigation of the lipid profile within naturally mummifying skin and tissue of decomposing human and pig bodies through targeted analysis using gas chromatography tandem mass spectrometry (GC-MS/MS). A method was developed and optimised for the detection of volatile, low-molecular weight lipids within the skin and tissue of human bodies. This method was applied to investigate naturally mummifying tissue and skin within four (4) deceased humans across various seasons, and in seasonal trials comparing pig versus human skin and tissue in warmer (summer) and (cooler) winter. All studies were conducted outdoors at the Australian Facility for Taphonomic Experimental Research (AFTER).

All individuals (both human and pig) depicted signs of natural mummification during the decomposition process. Visual decomposition of the humans and pigs showed dissimilarities in staging of the bodies and with the onset of mummification. Skin preservation was observed within humans due to natural mummification, but this was not observed in pigs. Distinctions within the lipid profile of humans and pigs for both tissue and skin can be made to a statistically significant degree. This supports the idea that although both species undergo natural mummification, the extent and effect of this occurrence is not similar. This further indicates that pigs are not suitable analogues for human decomposition studies from a biochemical (lipid) stance or in the instances of natural mummification.

Human studies revealed that all humans underwent the process of natural mummification, regardless of the seasonal placement. The first signs of natural mummification were depicted at a range of 150-250 ADD. Natural mummification appeared to affect the skin matrix of humans more than the tissue matrix. This occurred due to the surface-level effect of this phenomenon, which does not

penetrate through the skin. The effect of natural mummification at a lipid level within the skin shows variability, according to seasonal placement. Myristic acid was the only compound showing a positive correlation (increase in relative abundance) with the presence of naturally mummified skin. The anti-virulent and anti-microbial properties of myristic acid indicate inhibition of fungal and bacterial activity, which consequently results in skin preservation (instead of degradation) and by extension, natural mummification.

It was proved that pigs are unsuitable as human analogues when investigating natural mummification visually and at a lipid level. This directs future studies to use caution when using pig data for human forensic cases. Findings from this project allows for prediction of natural mummification within a temperature environment and has the potential to be incorporated into visual interpretation and staging techniques. Furthermore, these findings have potential to strengthen the estimation of time-since-death for more accurate calculations. The application of this research into forensic investigations is holistic, as skin and tissue are typically present in all instances of non-archaeological forensic investigations. Naturally mummified skin being present in both archaeological and non-archaeological forensic investigations further validates the impact of this research, with the use of lipids such as myristic acid, as potential biomarkers in both instances.

# CHAPTER 1 INTRODUCTION

Forensic taphonomy is defined as the scientific study of the stages and processes that are involved in the decomposition and fossilisation of an organism [1]. The term 'taphonomy' was originally devised in 1940 by Efremov, translating from the Greek *taphos* meaning 'burial' and *nomos*, meaning 'law'-defining this sub discipline of forensics as the "science of burial"[2]. It is a complex, multidisciplinary field, comprising knowledge from an array of scientific disciplines including chemistry, microbiology, and anthropology [3-5]. The application of taphonomy into a forensic context did not occur until the 1970s, when it was applied to the study of prehistoric remains and furthermore the recovery of more recent human bodies [5, 6]. Forensic taphonomy delves into the intricate processes of human body decomposition from the moment of death, with the objective of understanding how the pace of decay is influenced by diverse variables. As the realm of forensic taphonomy continually advances, its applications hold significant advantages for forensic inquiries. A fundamental purpose of forensic taphonomy is to offer invaluable support to the legal and justice system. This encompasses tasks such as the identification of remains, estimation of the post-mortem interval (PMI), and comprehensive investigation into an individual's demise, encompassing the circumstances, causes, and manners of death [3, 5, 7-11]. Human remains serve as the most relevant and accurate model for forensic investigations, providing insights that are directly applicable to legal and justice contexts. Ethical and legal restrictions pose significant limitations on the use of human bodies in taphonomic studies, rendering research involving the comprehensive use of whole human bodies a complex endeavour.

To overcome these ethical challenges, researchers often resort to using animal analogues, particularly pigs (*Sus scrofa*), which share certain anatomical, physiological, and microbial characteristics with humans [12]. However, contemporary research has indicated that the complex nature of decay in conjunction with the high degree of physical and chemical variability within each instance of decomposition results in the unreliable translation of pig decomposition data to human medico-legal forensic death investigations [12, 13]. While these analogues provide valuable insights, they inherently lack the complexity and specificity of human systems. The challenge, therefore, lies in striking a balance between the need for accurate forensic knowledge and the ethical obligations surrounding the treatment of human remains. This has resulted in the global introduction of licensed research facilities of various biomes, that enable the study of human decomposition in an ethical and legal manner. Within Australia, this includes the Australian Facility for Taphonomic Experimental Research (AFTER) (see Figure 2.1 in section 2.2 for map of AFTER), a research facility located in the greater Sydney region. This environment features eucalyptus forests and other temperate vegetation, with a mix of both wet and dry sclerophyll forests. With the differing impacts of climate and environment on the method and rate of decomposition [14, 15], research from this facility ensures

accurate reflection of Australian medico-legal forensic death investigations in a temperature environment.

Natural mummification is a prime example of an environmentally induced post-mortem phenomenon that occurs when the body loses fluids to the environment via evaporation, causing retardation of decomposition due to drying of tissues below the threshold of bacterial activity [1, 16]. This can be facilitated by extremes of dry heat or cold causing the rapid dehydration of the external body whilst preserving the internal tissue and has been well attested both in forensic and archaeological literature [1, 13, 14, 16-18]. In this research, the initial characterisation of natural mummification relies on visual observations, specifically involving desiccation and the manifestation of orange colour changes within the skin. This is followed by skin appearing leathery, shrunken, and tightly drawn due to the loss of moisture, as well as preserving features. Alternative explanations of natural mummification found in scholarly literature encompass the thorough desiccation of the remains, including subcutaneous tissues and viscera [19-22], rather than focusing solely on the skin, as discussed in this thesis. Incorporating research on natural mummification in forensic taphonomy is pivotal in Australian investigations as this phenomenon occurs in almost all cases of outdoor human decomposition with presently insufficient knowledge surrounding it [10, 13, 14, 23, 24]. Among the approximately 38,000 reported missing persons in Australia, around 2,600 are classified as long-term missing individuals (exceeding 3 months) [25]. In such cases, especially when human remains have undergone extended decomposition in a temperate Australian environment, the presence of naturally mummified skin is likely due to the preservation-like effects of this phenomenon. The presence or absence of mummification on a decomposing body can have substantial influence on the estimation of PMI due to its ability to preserve the body in an unpredictable manner [16]. The lack of research and current knowledge in this area has resulted in inaccuracies in the reporting of this event, and discrepancies in accurate case numbers. This is imperative from a forensic investigative perspective as an educated construction of PMI can greatly assist in helping law enforcement, forensic scientists, and researchers reconstruct events, identify individuals, and contribute to the understanding of historical and contemporary human remains.

PMI refers to the estimation of time that has elapsed since an individual's death with the intention of reconstructing events surrounding the death, determining the circumstances, causes, and manners of death. These estimations are based on various aspects of research including volatile organic compound (VOC) profiling, lipid degradation, total body scoring (TBS) and categorisation into decomposition stages in association with acquired weather data. Estimating the PMI is crucial in forensic investigations, helping forensic experts understand the timeline of events surrounding a death



and assessing the condition of remains. Accurate PMI estimation is a cornerstone of forensic taphonomy, as it enables forensic experts to interpret the stage of decomposition and the effects of environmental variables on the remains. This information is invaluable for forensic investigators, allowing them to reconstruct events leading to death and aiding in the identification of remains.

## 1.1 DECOMPOSITION

Mammalian decomposition is a complex, multifaceted process involving the biological, chemical and physical reactions that result in the degradation of macromolecules into smaller compounds [26]. This process commences immediately when an individual dies.

The post-mortem processes of human bodies are often categorised into five stages, namely fresh, bloat, active decay, advanced decay and skeletonisation/dry remains [7, 9, 13]. This classification system was first developed by Payne in 1965 [27], and is still used as the preferred method of categorisation to date [28]. Each stage of decomposition is characterised by its own unique qualities and decomposition manner [13].

During the early stage of decomposition, autolysis is initiated by lysosomes organelles, specifically hydrolytic enzymes. The lack of internal oxygen combined with a decrease in cytoplasmic pH [11], results in the enzymatic self-digestion of cells [29]. The ensuing breakdown liberates intracellular constituents like lipids, proteins, carbohydrates, and nucleic acid [7, 30, 31]. Organs rich in lysosomes and enzymes, such as the pancreas, liver, and stomach, deteriorate rapidly due to the abundance of hydrolytic enzymes. Subsequently, cell catabolism initiates putrefaction, a process fuelled by microbial activity, predominantly anaerobic bacteria, which liquefies and disintegrates tissues [11]. This results in gas production, purple/green body discolouration (initially on the abdominal region) and body bloating, referred to as the bloat stage. This bloat-effect occurs due to fermentative gas accumulation within the body [11]. Owing to pressure build-up, fluids emerge from post-mortem skin ruptures and natural body orifices, triggering body deflation and ushering in the active decay stage. This stage witnesses the expulsion of most decomposition fluids and odours from the body, accompanied by heightened insect activity [32]. Advanced decay ensues, where significant soft tissue loss occurs due to liquefaction, leaving primarily skin and bones. The terminal stage, known as skeletonisation, sees the carcass reduced to bones, cartilage, and hard tissues. Should mummified tissue persist, this stage is often categorized as dry remains. Dry remains typically exhibit reduced tissue density accompanied by leather-like skin [16].

Traditional decomposition stages can be visually characterized by physical transformations and identified by entomological species present on the decomposing bodies. However, the initiation times of decomposition stages vary widely due to a plethora of factors, both extrinsic and intrinsic [28]. Extrinsic factors encompass insect activity, temperature, humidity, concealment through burial or water, location in sunlight versus shade, wind, and rainfall. Intrinsic factors influencing decomposition rates include enteric enzymatic and microbial activity, fat distribution, and biomass [28, 33, 34]. Contemporary literature also notes instances of simultaneous presence of multiple decomposition stages on a body, known as differential decomposition [13, 35]. Decomposition of this nature can be influenced by extrinsic factors [13]. This further creates a degree of uncertainty when categorising remains into the traditional 5-stages developed by Payne, indicating a shift for reform required to these traditional stages. This uncertainty is further heightened by the contribution and presence of mummification. The desiccated tissue is rarely subjected to putrefactive change due to the moisture threshold dropping until microbial activity is significantly inhibited, resulting in the internal tissue predominantly retaining its integrity [11, 34]. The unpredictable emergence of mummification, accompanied by the formation of a protective external layer that preserves internal tissues, complicates the categorisation of individuals into specific decomposition stages, as the visual indicators of physical changes become less discernible.

#### 1.1.1 ENVIRONMENTAL EFFECTS ON DECOMPOSITION

In any taphonomic analysis it has been well documented that temperature as an extrinsic factor plays a crucial role in relation to the decomposition rate of an organism [6, 8, 11, 15, 36]. Increased temperatures lead to an increase in biological activity as insects and bacteria become more active and will proliferate [6], consequently leading to an increase in soft tissue degradation and mass loss [33]. Comparatively, lower temperatures result in prolonged decomposition of bodies due to the decrease in insect and microbial activity. This decrease causes slower initiation of post-mortem biochemical reactions [28]. Furthermore, factors including humidity levels, composition and pH of soil, exposure to sunlight and burial conditions, including depth and soil characteristics, add another layer of complexity to the decomposition process, influencing the activity of insects and microorganisms. These environmental variables collectively shape the intricate ballet of decomposition, influencing the timeframe, preservation, and observable changes in human remains. Forensic investigators carefully analyse these factors to estimate PMI and unravel the circumstances surrounding a person's demise, underscoring the crucial intersection of environmental conditions and forensic taphonomy in medico-legal investigations. Placement of bodies in different environmental conditions have shown substantial influence on the method of decomposition. For instance, in a study conducted by Janaway et al. (2009)

[37] on pig remains, it was observed that placing the carcass in arid conditions (sand) led to the development of a hard layer on the exterior tissue, while the internal core retained moisture. This phenomenon is commonly referred to as natural mummification.

#### 1.1.1.1 NATURAL MUMMIFICATION

The term mummification can be interpreted to define carcasses with overall soft-tissue preservation, including but not limited to the skin, muscles, internal organs, and ligaments [11, 20]. Extreme arid environments can facilitate natural preservation such as natural mummification (arrested decay) of a human body rather than traditional decomposition [11, 17, 18, 38]. Natural mummification preserves the tissue, making features identifiable for many years. In contrast, putrefactive decomposition obscures external marks [11]. Unlike artificial mummification, which involves deliberate human actions like removing organs and using preservatives, natural mummification occurs spontaneously due to environmental conditions that inhibit microbial and enzymatic activities responsible for decomposition. Typically, it involves the drying out of tissues and the formation of a desiccated, leathery, or shrivelled appearance. Natural mummification can be influenced by factors such as temperature, humidity, sun, and air exposure [11, 38].

This widespread phenomenon has been observed to occur unpredictably in all seasons. As a result, forecasting the manifestation of this natural occurrence has become extremely challenging. Natural mummification has been documented in almost all instances of decomposition within Australia [10, 13, 14, 23, 24, 39]. Furthermore, this phenomenon not only occurs in outdoor environments, but has been documented in indoor settings [17, 36, 38] and burials [40]. The consequence of this inhibits the traditional progression of decomposition into the five stages of decay (fresh, bloat, active decay, advanced decay, and skeletonisation). As a result, natural mummification causes preservation of remains. This further complicates estimating time-since-death, as visual interpretation and staging of bodies are a key aspect of PMI estimation, with natural mummification and variable timing of preservation unaccounted for. This preservation occurs due to the premature discontinuation of decomposition, excluding and hindering activity of biotic agents such as bacteria, fungi, insects, and scavengers from the decomposition process, classically by loss of moisture and tissue desiccation [13, 20, 22, 41]. Absence or removal of water from a corpse will result in cessation of decomposition due to most enzymes operating within an aqueous environment [42]. Mummified tissue has been reported in many archaeological cases [43, 44], dating back to approximately 5000 years ago [45]. The long-term presence of this natural preservation technique indicates great potential to provide valuable information in both archaeological and forensic investigative contexts. This results in a promising matrix

that can be located and used as a contributing indicator of PMI estimations in environments of arid conditions where a carcass is prone to mummification.

Currently, methods of estimating time-since-death include total body scoring (TBS) through visual observations and the use of accumulated degree days (ADD). ADD is based on the principle that the rate of decomposition is influenced by temperature. The formula involves calculating the accumulated heat units or degree days over a specific period and is commonly used in research surrounding forensic taphonomy [30]. TBS involves scoring the overall state of decomposition based on visual and olfactory assessments of the body, where different aspects of the body, such as skin, eyes, fluids, and soft tissues, are individually scored [36]. Recordings of natural mummification are being noted using the TBS method [13, 40]; nonetheless, the impact of this phenomenon remains unaddressed within the confines of this method due to the variable timing and presentation of natural mummification [17].

As a result, inaccuracies are being observed with respect to calculations of TBS in instances of natural mummification. This was exhibited through study conducted by Pittner et al., who observed natural mummification at each part of the body in a burial setting, and as a result assigned inaccurate visual scoring to the remains, due to natural mummification [40]. Furthermore, Cecilason et al., quantified natural mummification for indoor settings with the use of a TBS system and highlighted the inaccuracies and potential errors in using current methods for staging for natural mummification, [17]. Akin to simpler qualitative stage-based descriptions of decomposition progression, the TBS scoring criteria lack accommodation for the diverse timing of natural mummification presentation. While the TBS system does incorporate natural mummification, its limitation in addressing the variable timing poses challenges when striving for precise post-mortem interval (PMI) estimation in cases involving natural mummification. The significant gap in literature and medico-legal investigations surrounding the incorporation of natural mummification creates room for inaccuracies in estimating time-since-death. This necessitates a precise modification of existing PMI estimation methods tailored to distinct environmental conditions, with a special focus on integrating natural mummification, given its frequent prevalence. Alternative methods to encompass natural mummification more accurately in PMI estimation is quantitative biochemical investigation through the lipid analysis. Lipid analysis emerges as a promising alternative method, offering a more accurate means of integrating natural mummification into PMI estimation. This approach is driven by the recognition that the biochemical changes associated with lipid composition can provide valuable insights into the preservation effects associated with natural mummification, enhancing the precision of time-since-death estimations.

### 1.1.2 LIPIDS

Lipid molecules break down into their foundational components (e.g., fatty acids and amino acids) during decomposition, resulting in the release of decomposition fluids, triggering a range of reactions. Lipid analysis is commonly carried out in a broad range of disciplines including, but not limited to, environmental, agricultural, biological, and forensic sciences [46-55]. This is primarily due to their ubiquitous presence and abundance in nature, as well as their hydrophobic properties, promoting their ability to withstand harsh environmental conditions [49]. Ninety to 99 percent of lipids found in adipose (fat) tissue are triacylglycerols, molecules that are composed of a triester-glycerol backbone linked with three fatty acids [11, 34]. The major fatty acids present in adipose tissue include palmitoleic, linoleic, palmitic acids and oleic acid [34]

The first step in the lipid degradation process is hydrolysis of neutral lipids. Here, intrinsic lipases free fatty acids from their glycerol backbone in a lipid, creating a mixture of glycerol, unsaturated and saturated free fatty acids [11, 34]. The second step involves the degradation of these free fatty acids, which can occur in two ways: aerobically or anaerobically. Aerobic conditions enable fatty acids to undergo oxidation, typically from atmospheric oxygen, bacteria, and fungi. The process is initiated by oxygen attacking the double bonds present in unsaturated fatty acids, producing peroxides (two oxygen) linkages, which then eventuates into the production of ketones and aldehydes [34]. Anaerobic degradation involves the domination of anaerobic microorganisms in tissues due to the lack of oxygen, and as a result, promotes anaerobic degradation through hydrogenation (the addition of hydrogen). During the hydrogenation process, hydrogen atoms are added to the double bonds of unsaturated fatty acids, converting them to their single bond, saturated counterparts [11]. For example, palmitoleic acids and oleic acid hydrogenation will result in the production of palmitic acids and stearic acid, respectively [34]. As decomposition progresses, neutral lipid concentrations decrease while fatty acid concentrations increase.

In a medio legal context, lipid analysis may provide valuable information due to its resilience in the environment as well as its presence in varying matrices, such as skin, tissue, soil and textiles [24]. Patterns including the type and quantities of lipid present in various matrices, can potentially provide insight as an indicator of PMI.

## 1.2 TISSUE AND SKIN MATRIX IN DECOMPOSITION

Lipids are abundantly present in the human body, can be harvested from a variety of tissues, and encompass approximately 60-85% of adipose tissue found within the body [34]. Skeletal muscle

has recently been the preferred tissue of sampling as it can be sampled with minimal disturbance to the body and is also one of the last soft tissues to decompose [8, 56]. These properties enable lipids to be monitored and studied over longer periods of times and have even indicated the predictive capacity for PMI estimation [56]. Previous studies including that by Wood and Shirley and Langley et al., [56, 57] have successfully indicated the reliable monitoring of complex lipid structures and lipid biomarkers within skeletal muscle tissue and its potential forensic application in regard to establishing a biochemical criterion for PMI [46,47].

During decomposition, the first observations made on the skin include fluid-filled blisters during autolysis resulting in insect activity attraction [34]. Putrefaction occurs resulting in greenish discolouration of the skin due to sulfhaemoglobin formation in blood, eventually leading to skin slippage whereby large sheets of the skin slough off during putrefaction, particularly on the limbs [58]. The internal buildup of gases including carbon dioxide, methane and ammonia results in distension of tissues and eventual rupturing of the skin [58]. The skin then continued to deteriorate with the aid of beetle activity. However, during mummification, the exterior tissue hardens and forms a shell over the interior tissue, preserving it while remaining moist. As a result, external tissue refrains from sloughing off and instead acts as a protective barrier for the internal tissue from insect activity. The hardening of the skin does not prevent all insect activity from occurring as many beetle and larvae activity is still observed [16]. During mummification, generally, the skin on the face, hands and feet are the first to harden and darken into a leather-like appearance, followed by the chest and torso, arms and legs.

While the phenomenon of natural mummification in human remains unveils intriguing insights into the preservation of tissues through external means, the application of advanced scientific techniques becomes paramount in unraveling the biochemical intricacies associated with this process. Lipid analysis emerges as a crucial tool in comprehending the molecular changes occurring during natural mummification. By delving into the lipid composition of mummified tissues, researchers gain valuable information on the substances involved in preservation and their potential role in hindering microbial and enzymatic activities. This analytical approach not only deepens our understanding of the mechanisms behind natural mummification but also opens avenues for forensic applications and archaeological investigations.

### 1.3 LIPID ANALYSIS

The analysis of trace compounds in complex matrices requires effective separation and detection through analytical instrumentation. A highly advantageous technique for analysis of trace

lipids includes the use of chromatographic separation coupled with mass spectrometry (MS). The quantitative use of gas chromatography (GC) has been the preferred method of separation in chemical investigations associated with complex fatty acids since early 1950s. Kamer et al., first discovered the effective trace separation of volatile short-chain fatty acids in the gas phase [59]. The low viscosity of the mobile phase enabled longer columns to be used within the GC gas-liquid system, resulting in increased efficiency compared to previously used liquid-liquid columns [59]. GC coupled with mass spectrometry (GC-MS) detection has since become a commonly used technique in lipidomics for fatty acid analysis in complex biological mixtures [59]. Recent studies have illustrated the use of GC-MS in forensic investigations for the detection and quantification of human and non-human decomposition products [10, 60, 61]. However, due to the single fragmentation of compounds, the output from GC-MS analysis is resultant in less specificity and sensitivity compared with analytical methods involving multiple fragmentations. Gas chromatography-tandem mass spectrometry (GC-MS/MS) is an alternative method to conventional GC-MS that enables increased specificity and selectivity in trace compound analysis.

### 1.3.1 GC-MS/MS IN LIPID ANALYSIS

GC-MS/MS is a powerful analytical technique used for analysis due to its high sensitivity and ability to analyse samples that are complex or have low molecular weight, with its uses in lipid analysis being well documented [24, 47, 53, 54, 62, 63]. This technique enables target compounds to be detected at trace levels [53, 54], making it an ideal analytical technique in the identification of lipids for decomposition due to the degrading nature of these compounds [53, 64]. The process of analysis using GC-MS/MS begins with separation of analytes in the gas chromatography (GC) column via a carrier gas (such as helium), to the detector (MS/MS). The MS/MS then operates by selecting the target ion(s)/parent ion based on a known mass-to-charge ratio in the first detection mode resulting in separation of ions from the chemical matrix. The selected parent ions are then further dissociated by collision energy in the collision cell, resulting in unique product ions that confirm the presence of the target analyte [62]. The MS/MS portion of this technique is a highly selective mass spectrometric technique, where specific analytes are detected regardless of coeluting interferences or sample matrix and is recommended for complex matrix analysis [53, 54, 62]. Additionally, GC-MS/MS has an increased signal-to-noise ratio, due to the reduction of noise from interference ions, lowering the detection limit of the multiple reaction monitoring (MRM) mode relative to selected ion monitoring (SIM) [63], proving it to be a superior technique to conventional GC-MS. An array of forensic-archaeological investigations has successfully demonstrated the efficiency of the GC-MS/MS analytical technique in the detection and quantification of low molecular weight lipids [24, 53, 54, 64-68].

#### 1.3.1.1 MULTIPLE REACTION MONITORING

Multiple reaction monitoring (MRM) is a method of analyte quantitation in GC-MS/MS which enables optimisation of collision energies and retention times of analytes of interest [53]. This is possible through the determination of the mass and retention times of the analytes of interest, through which the MRM will determine the most intense product ions that occur, because of collision [53, 54]. This is known as the precursor study. This is followed by the product study, where product ions are scanned to get an energy range for the best product ions. The product study is then followed by the selected reaction monitoring (SRM) optimisation study, wherein the SRM acquires these transitions at multiple collision energies. This method therefore enables optimisation of collision energies and retention times, thus reducing errors in collision energy and improving the confidence in retention times to allow shortened windows [53]. This method has been used in many studies including those by Luong et al. [53, 54, 64] who used it for the quantitation of analytes in complex mixtures, including archaeological samples. By facilitating analyte quantitation in complex sample mixtures GC-MS/MS paired with MRM analysis results in a highly specific and sensitive mass spectrometry technique.

#### 1.4 STUDY RATIONALE

Out of the roughly 190,000 annual deaths in Australia [69], 10-20% undergo medico-legal investigations [70]. The extent to which instances of natural mummification occur within these coronial cases remains challenging to assess due to underreporting. Nevertheless, forensic research conducted in the Australian environment has consistently identified occurrences of natural mummification in all cases of pig and human bodies studied [10, 13, 14, 24, 33, 39]. This information underscores the importance of delving into natural mummification and integrating it into medico-legal casework. It enhances the accuracy of estimating the post-mortem interval, determining cause-of-death, and facilitating victim identification.

The Australian environment creates an optimal setting to assess the occurrence of natural mummification. The interplay of extreme temperature fluctuations, combined with minimal air moisture, gives rise favourable conditions for mummification in Australia [13, 14, 23, 24]. This spontaneous occurrence during the decay process at unpredictable time periods [13, 71], makes monitoring challenging [72]. Methods including the Megeysi et al. method of TBS (total body scoring) are currently used for PMI estimation, incorporating ADD to evaluate different body sections based on decomposition criteria [36]. Regrettably, these methods typically exclude consideration of mummification, potentially leading to inaccurate timeline assessments. These features prevent the TBS method from being universally applicable in forensic contexts of environmental variability.



Furthermore, the limited extent of research encompassing mummification in general, and more specifically, human decomposition within the Australian context, suggests PMI estimations are unreliable in instances of natural mummification. Understanding the intricacies of natural mummification is crucial for forensic taphonomy, as it can directly influence the accuracy of PMI estimates. Factors such as temperature, humidity, and the availability of microbial activity play pivotal roles in both decomposition and mummification processes. The lack of research in this area hinders the development of precise and reliable methods for PMI estimation in cases involving natural mummification

Addressing this research gap requires a comprehensive investigation into the mechanisms of natural mummification, its impact on the decomposition timeline, and the specific changes it induces in tissue composition, particularly at a biochemical level. Bridging this gap would not only advance the field of forensic taphonomy but also contribute to refining PMI estimation methods, ensuring their applicability in diverse forensic scenarios, including those involving natural mummification. The research further seeks to address a notable gap in the existing methodologies for evaluating the progression of decomposition. The motivation stems from the recognition that stage-based and TBS-based systems, commonly employed in decomposition assessment, lack true quantitative effects. The post-mortem biochemical approach emerges as a promising alternative, offering the advantage of capturing genuine changes in the tissue's constituents. This departure from qualitative appraisal, inherent in systems like TBS, becomes crucial as qualitative descriptions are not only subjective but also constrained by predefined system definitions. While attempts have been made, such as the separate scoring of three body regions in the TBS method, the inherent sequential consideration within those regions still poses challenges. Therefore, there is a compelling need to transition towards truly quantitative methods for a more accurate measurement of the progression of decomposition.

### 1.5 PROJECT AIMS

The primary objective is to explore and monitor lipid degradation trends and patterns in the skin and tissue during the mummification process in human bodies for the accurate, quantitative, measurement of decomposition. To achieve this, a novel method for lipid analysis on a GC-MS/MS system was developed and optimised, formulating aim 1.

The second and third aims involve conducting a lipid-level comparison of pig and human skin and tissue in varied climates, including both warm (aim 2) and cool conditions (aim 3). This is accomplished through lipid analysis of remains from humans and pigs studied concurrently in different climates. Aim

4 is to compare instances of natural mummification in humans across diverse climates (both warm and cool) and to establish a timeline estimating the initial visible signs of natural mummification. These aims entail a combination of visual observations and analysis of weather data. By isolating temperature as the primary variable of interest, the research aimed to establish a focused understanding of its impact on natural mummification. This approach allows for a more in-depth analysis of temperature-related effects without introducing the complexities associated with multiple variables. An objective within this aim is to identify the specific lipids involved in the mummification process within the skin and tissue matrix of humans, employing statistical analysis of the lipid profile within human remains.

Analysis of this nature would allow detailed insight into the processes of mummification from a lipid standpoint. Moreover, acquiring this knowledge would enable comprehension of the roles played by both the skin and tissue matrix in instances involving natural mummification. With the common use of pig as human analogues in research surrounding forensic taphonomy [12, 13, 23, 27, 50, 61, 73] lipid analysis in pig skin and tissue is conducted to compare with mummified or non-mummified human skin and tissue.

The persevering nature of mummified skin and tissue of decomposing carcasses enable the provision of a stable matrix and biochemical compound that is present years after an individual has died. This is extremely beneficial from a forensic perspective as it enables the investigation of long-term missing persons in an Australian environment. Furthermore, with current PMI estimation techniques not incorporating natural mummification due to lack of research – the outcome of this study will assist in providing valuable information and further optimise PMI estimations. An added benefit to this research includes insights into the physical/visual changes with consideration of mummification and hence potential adaptation to the traditional decomposition stages categorisation method. Each project aim (aims 1-4) is organised into thesis chapters, each with self-contained discussions.

# CHAPTER 2 MATERIALS & METHODS

## 2.1 GENERAL APPROACH

The enigmatic nature of natural mummification has created a void in research, causing uncertainty in forensic taphonomy when dealing with human bodies affected by this occurrence. The scarcity of research in this area makes predicting and integrating this natural process exceptionally intricate. The objective of this study was to rectify this knowledge gap by examining the lipid composition within the skin and tissue of mummified human bodies. The identification and quantification of these lipids will be juxtaposed against concurrent studies involving pigs. This allows for a biochemical comparison of human and pig skin and tissue, aiding in evaluating the suitability of pigs as analogues in taphonomic investigations.

Moreover, a comparison will be drawn between the skin and tissue of mummified human bodies and non-mummified bodies to augment our comprehension of the patterns in lipid composition during this phenomenon across both types of samples. Visual documentation and observations were systematically recorded on each experimental day to provide visual references illustrating the state of the decomposing bodies. The stages of decomposition for each donated body and pig were evaluated following the classifications devised by Payne [27].

## 2.2 RESEARCH FACILITY

Australia is characterized by various biomes, each with its unique ecological features. These biomes include a variety of temperate, grassland (sclerophyll), tropical, aquatic and desert biomes. As 75 % of Australia's total forest area is dominated by Eucalypt Forest type [74], there is an increasing regional demand for forensic taphonomy studies in these environments. The project was undertaken at the Australia Facility for Taphonomic Experimental Research (AFTER) – a UTS owned research facility located in the Greater Sydney Region, classified as a Cumberland Dry Sclerophyll (Eucalypt) Forest. Figure 2.1 highlights the location of AFTER relative to Australia. This facility was designed for studying human decomposition, with ethics approval for experimental research at AFTER granted under program approval (HREC#ETH18-2999). Through the UTS Body Donation Program, humans are able contribute by donating their bodies to the enhancement for forensic science. This process incorporates body donation, screening of bodies to ensure they are safe for research and placement out at the facility. The facility has secured fencing with restricted access. This facility has been used in prior research to determine baseline data for decomposition [13, 14, 33].

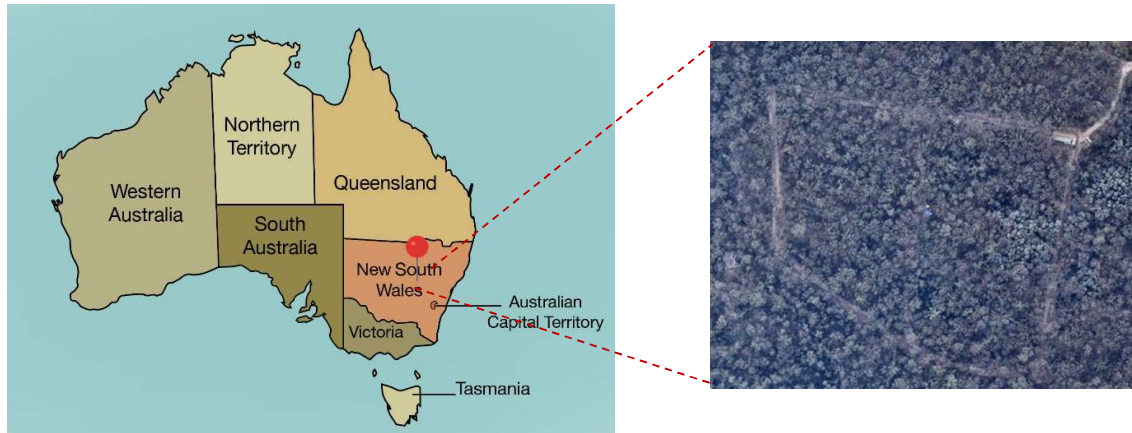


Figure 2.1: Map of Australia highlighting the location of the Australian Facility for Taphonomic Experimental Research (AFTER). Source adapted from National Museum Australia [URL]: <https://www.google.com/search?q=map+of+australia+with+states&tbm=isch&ved=2ahUKEwiU3OTH8vGDAXUnQmwGHQfjA> <https://digital-classroom.nma.gov.au/images/map-australia-showing-states-and-territories>.

The premises are described as open eucalypt Australian woodland, built for the purposes of studying whole human bodies in a secure and ethical manner for research and medio-legal casework applicability. Situated in an open eucalypt forest within the Greater Sydney Region, this facility experiences variable average temperatures and rainfall throughout the warmer and cooler seasons. Summer (warmer) temperatures fluctuate between averages of 18°C to 26°C, with an average rainfall of approximately 99 mm. In contrast, winter (cooler) temperatures range from averages of 17°C to 9°C, accompanied by an average rainfall of approximately 103 mm [75]. A HOBO® U30 weather station (Figure 2.2) erected within the facility allowed weather data to accurately be recorded on an hourly basis. Data recorded included temperature (°C), rainfall (mm), wind direction (°), wind speed and gusts (m/s), and solar radiation (W/m<sup>2</sup>). All bodies researched at this facility are donated through the UTS Body Donation Program.



Figure 2.2: A HOBO® U30 weather station.

### 2.3 ETHICS

It is understood there are many ethical issues surrounding research using human bodies for research. To protect the welfare, dignity, rights, and safety of donated bodies and the obtained data from this research in accordance with the National Statement on Ethical Conduct in Human Research (2007), ethical approval was granted under program approval (HREC#ETH18-2999). This ensures the protection of privacy and confidentiality of body donor information, and ensures the appropriate management of security, storage and disposal of confidential data and biological samples throughout the duration of the project.

### 2.4 SURFACE DECOMPOSITION AND BODY PLACEMENT

Plots measuring 5m<sup>2</sup>, (Figure 2.3), were cleared of environmental debris and used for human body placement. Human bodies were placed in the centre of the plot, in a supine position, on the soil surface.



Efforts were made to avoid placement on uneven ground due to potential pooling from rainfall. Placement of bodies were standardised to allow for equal exposure to the microenvironment, including sun exposure and surface contact.



*Figure 2.3: Plots used for human body placement.*

Metal cages (Figure 2.4) were assembled from aluminium frames with 25 mm wire mesh on the top and side panels measuring 960 mm (H) x 2090 mm (L) x 1260 mm (W). These anti-scavenging cages were placed over each body when not sampling, allowing for invertebrate activity to occur, whilst preventing large vertebrate activity. Recognising the enhanced forensic relevance and real-world applicability of research involving scavengers in outdoor decomposition cases, it is acknowledged that intentionally excluding scavengers may limit the study's practical utility. Nevertheless, ethical constraints associated with uncaged human body research and the additional objective of mitigating scavenging activity as a potential confounding factor led to the decision to employ metal cages.

Five (n=5) human bodies were used. Two of these bodies were placed out during warmer seasons (Australian summer and spring) and three of the bodies were placed out during cooler seasons (Australian autumn and winter) (Table 2.1). The bodies varied in sex and weight. Human body numbers

3, 4 and 5 (Table 2.1) were clothed in a cotton t-shirt due to concurrent decomposition studies conducted.



Figure 2.4: Metal cages used to cover bodies.

Table 2.1: Information of human bodies used in this study. Orange colour indicates bodies studied in warmer seasons (Australian summer and spring). Blue colour indicates bodies studied in cooler seasons (Australian autumn and winter).

Human body No.	Sex	Height (cm)	Weight (kg)	Body Mass Index (BMI)	Cause-of-death
1	M	174	96	31.7	Aspiration Pneumonia, Congestive Cardiac Failure, Pulmonary Embolism, Acute Kidney Injury
2	F	156	89	36.6	Liver Failure, Metastatic Cancer - Duodenal Adenocarcinoma
3	F	154	53	22.2	Pneumonia
4	M	174	63	20.8	Alzheimer's Disease
5	M	175	94	30.7	Metastatic Bladder Cancer, Prostate Cancer, Peripheral Vascular Disease, Atrial Fibrillation



Four (n=4) pigs (*Sus scrofa domesticus*) were also used for comparative data to human bodies. Pigs 1 and 2 were placed during Australian summer and pigs 3 and 4 were placed out during Australian Winter. All pigs were approximately 70 kg in weight and were clothed in a cotton t-shirt due to concurrent decomposition studies. Clothing was adjusted to fit over pig's body shape to ensure similar conditions to human bodies were maintained.

Table 2.2: Information of pigs used in this study. Orange colour indicates pigs studied during warmer seasons (summer). Blue colour indicates pigs studied during cooler seasons (winter).

Pig No.	Breed	Sex	Weight (kg)
Pig 1	<i>Sus scrofa domesticus</i>	M	70
Pig 2	<i>Sus scrofa domesticus</i>	M	70
Pig 3	<i>Sus scrofa domesticus</i>	F	70
Pig 4	<i>Sus scrofa domesticus</i>	M	70

All pigs were obtained fresh and killed by captive-head bolt according to the Australian abattoir procedure standard guidelines. They were then transported to the AFTER facility in polyethylene tarpaulins. The animals do not require animal ethics (adults that are not bred for research purposes) as they are readily available for human consumption [13, 76].

## 2.5 SAMPLE COLLECTION AND ANALYSIS

A single 1 × 1 cm<sup>2</sup> skin sample was collected on each sampling day using CYNAMED surgical grade scalpel blades (Lorton, Virginia). Samples were taken from the deltoid, biceps brachii and triceps brachii. This was done by making incisions on the skin with the blade and collecting the skin sample in an eppendorf tube. This opening from this incision was then used to collect tissue samples using a BARD® MAGNUM® Reusable Core Biopsy System gun with a BARD® MAGNUM® 14G x 16cm needle (New Jersey, USA). Upon collection, samples were freeze dried using a Martin Christ Alpha 2-4 LD Plus freeze drier (Osterode am Harz, Germany) and stored in the freezer at -17°C until required for extractions. Project sampling dates and sampling periods can be observed in Table 2.3.

Table 2.3: Sample frequency and length of each individual studied across project period.

Individual No.	Date of Placement	Sampling Day	Final Sampling Date
Human 2 (H2)	25/03/2020	0, 1, 2, 3, 4, 5, 6, 7, 10, 12, 14, 16, 18, 20, 22, 24, 26, 28, 30, 35, 40, 45, 50, 55, 60, 65, 70, 75	13 <sup>th</sup> May 2021
Human 3 (H3)	12/08/2020	0, 1, 2, 3, 4, 5, 6, 9, 12, 16, 19, 23, 26, 30, 33, 37, 40, 47, 55, 68, 82, 114, 153, 274	8 <sup>th</sup> June 2020
Human 4 (H4)	29/01/2021	0, 1, 2, 3, 4, 5, 6, 7, 8, 10, 14, 17, 20, 28, 35, 42, 70, 105, 185, 202	19 <sup>th</sup> August 2021
Human 5 (H5)	11/06/2021	0, 1, 2, 3, 4, 5, 6, 10, 17, 19, 26, 31, 35, 42, 49, 56, 63, 69, 84, 105, 132	21 <sup>st</sup> December 2021
Pig 1 (P1)	01/02/2021	0, 1, 2, 3, 4, 5, 6, 7, 8, 10, 14, 17, 20, 28, 35, 42	15 <sup>th</sup> March 2021
Pig 2 (P2)	01/02/2021	0, 1, 2, 3, 4, 5, 6, 7, 8, 10, 14, 17, 20, 28, 35, 42, 70	12 <sup>th</sup> April 2021
Pig 3 (P3)	11/06/2021	0, 1, 2, 3, 4, 5, 6, 10, 17, 19, 26, 31, 35, 42, 49, 56, 63, 69, 84, 105, 132	21 <sup>st</sup> December 2021
Pig 4 (P4)	11/06/2021	0, 1, 2, 3, 4, 5, 6, 10, 17, 19, 26, 31, 35, 42, 49, 56, 63, 69, 84, 105, 132	21 <sup>st</sup> December 2021

### 2.5.1 SELECTION OF ANALYTES FOR TARGETED GC-MS/MS ANALYSIS

The target analytes were carefully selected based on their diagnostic value in the context of human decomposition chemistry, as lipids are ubiquitous in nature being found in both animal and plant sources in varying quantities [49, 73]. Lipids are insoluble in water and are a major component of adipose tissue, with the dominant type being triacylglycerols [77].

As decomposition progresses, unsaturated fatty acids are hydrogenated into their saturated fatty acid form. This process led to the selection of both types of fatty acids for analysis [24, 50]. This study targeted fatty acids containing a carbon count between C10 (decanoic acid) and C28 (octacosanoic acid), to ensure the degradation of larger carbons chains into smaller carbon chains were monitored (Table 2.4). Oleic, palmitoleic and linoleic fatty acids have been reported as the most prevalent unsaturated fatty acid detected in adipose tissue of humans and were also selected in this study [34, 78]. Zoosterols, particularly cholesterol and coprostanol, were selected as the biomarkers to assess sterol degradation patterns within the human body during the decomposition process, commonly used in previous archaeological studies [53, 79]. Additionally, a suite of phytosterols (B-sitosterol, stigmasterol and ergosterol) were included as markers to capture a more holistic insight to the decomposition ecology.

Table 2.4: Analytes targeted in this study in their lipid subgroup.

<i>Saturated Fatty Acids</i>	Arachidic Acid (C <sub>20</sub> H <sub>40</sub> O <sub>2</sub> )
	Behenic Acid (C <sub>22</sub> H <sub>44</sub> O <sub>2</sub> )
	Decanoic Acid (C <sub>10</sub> H <sub>20</sub> O <sub>2</sub> )
	Dodecanoic Acid (C <sub>12</sub> H <sub>24</sub> O <sub>2</sub> )
	Hexacosanoic Acid (CH <sub>3</sub> (CH <sub>2</sub> ) <sub>24</sub> COOH)
	Lignoceric Acid (C <sub>24</sub> H <sub>48</sub> O <sub>2</sub> )
	Myristic Acid (C <sub>14</sub> H <sub>28</sub> O <sub>2</sub> )
	Nonadecanoic Acid (C <sub>19</sub> H <sub>38</sub> O <sub>2</sub> )
	Pentadecanoic Acid (C <sub>15</sub> H <sub>30</sub> O <sub>2</sub> )
	Tricosanoic Acid (C <sub>23</sub> H <sub>46</sub> O <sub>2</sub> )
	Tridecanoic Acid (CH <sub>3</sub> (CH <sub>2</sub> ) <sub>11</sub> COOH)
<i>Unsaturated Fatty Acids</i>	Linoleic Acid (C <sub>18</sub> H <sub>32</sub> O <sub>2</sub> )
	Oleic Acid (C <sub>18</sub> H <sub>34</sub> O <sub>2</sub> )
	Palmitoleic Acid (C <sub>16</sub> H <sub>30</sub> O <sub>2</sub> )

<i>Dicarboxylic Acids</i>	Azelaic Acid (C <sub>9</sub> H <sub>16</sub> O <sub>4</sub> )
	Sebacic Acid (C <sub>10</sub> H <sub>18</sub> O <sub>4</sub> )
<i>Bile Acids</i>	Lithocholic Acid (C <sub>24</sub> H <sub>40</sub> O <sub>3</sub> )
<i>Sterols</i>	5 $\alpha$ -cholestanone (C <sub>27</sub> H <sub>40</sub> O <sub>3</sub> )
	Cholesterol (C <sub>27</sub> H <sub>46</sub> O)
	Ergosterol (C <sub>28</sub> H <sub>44</sub> O)
	Stigmasterol (C <sub>29</sub> H <sub>48</sub> O)
	$\beta$ -sitosterol (C <sub>29</sub> H <sub>50</sub> O)
	Coprostanol (C <sub>27</sub> H <sub>48</sub> O)

### 2.5.2 REFERENCE STANDARDS

High-performance liquid chromatography (HPLC) grade reference standards were sourced from a variety of manufacturers and ranged in purity from  $\leq 85\%$  to  $\geq 99.5\%$ . Saturated fatty acids including: pentadecanoic acid, tricosanoic acid, tridecanoic acid, arachidic acid, behenic acid, decanoic acid, hexacosanoic acid, myristic acid, and stearic D<sub>3</sub> ( $\geq 95 - \geq 99\%$ ) were sourced from Sigma-Aldrich (Missouri, United States). Nonadecanoic acid ( $\geq 99.5\%$ ) was obtained from Honeywell (Sydney, Australia), while lauric acid ( $\geq 98\%$ ) was sourced from European Pharmacopeia (Strasbourg, France). All unsaturated fatty acids including linoleic acid, oleic acid, palmitoleic acid ( $\geq 98.5 - \geq 99\%$ ) were sourced from Sigma-Aldrich (Missouri, United States). Dicarboxylic acids including: azelaic acid ( $\geq 98.5\%$ ) and sebacic acid ( $99\%$ ) were sourced from Honeywell and Sigma-Aldrich, respectively. Bile acid, lithocholic acid ( $\geq 95\%$ ), was sourced from Sigma-Aldrich (Missouri, United States). Sterols including: 5 $\alpha$ -cholestanone, cholesterol, ergosterol, stigmasterol,  $\beta$ -sitosterol and coprostanol ( $\leq 85 - \geq 99\%$ ), were sourced from Sigma-Aldrich (Missouri, United States), while cholesterol D<sub>7</sub> ( $\geq 99\%$ ), was sourced from Avanti Polar Lipids, Inc (Alabama, United States). Tridecanoic D<sub>25</sub>, palmitoleic D<sub>13</sub>, palmitic D<sub>2</sub> and arachidic D<sub>2</sub> ( $\geq 99\%$ ) were purchased from Sapphire Bioscience (Sydney, Australia).

### 2.5.3 CHEMICAL REAGENTS

Acetonitrile, hexane and dichloromethane (DCM) (all HPLC grade) were obtained from RCI Labscan Ltd. (Gillman, South Australia). N,O-bis (trimethylsilyl) trifluoroacetamide (BSTFA) with w/1 %

trimethyl-chlorosilane (TMCS) silylation reagent was purchased from United Chemical Reagents (Bristol, Pennsylvania, USA). Chloroform (HPLC grade) was purchased from Chem-Supply Pty Ltd (Port Adelaide, Australia) and acetone (HPLC grade) was purchased from Sigma-Aldrich Pty Ltd (New South Wales, Australia).

## 2.6 GC-MS/MS METHOD

### 2.6.1 SAMPLE PREPARATION

Sample preparation was adapted from Ueland et al. (2021) [24]. Samples were prepared by weighing 3 mg of freeze-dried tissue/skin. These were then homogenised in 2 mL of hexane (for tissue) and chloroform:acetone (for skin) before being sonicated using an FXP12 (Unisonics, Australia) for 20 min. The extract was then filtered through a 0.2 µm hydrophobic polytetrafluoroethylene (PTFE) syringe filter (MicroAnalytix, Sydney, Australia), and 100 µL was transferred to a glass GC vial. Fifty microlitres of 10 ppm of cholesterol D<sub>7</sub> and 20 µL of 10 ppm stearic acid D<sub>3</sub> were added as internal standards (IS) to the sample extract, which was then dried down under a gentle stream of nitrogen for approximately 5 min at 40 °C. Samples were then reconstituted in 40 µL BSTFA + TMCS and 10 µL, prior to being heated at 70 °C for 30 min using a heating block and then transferred into 250 µL polymer inserts (Agilent Technologies, Australia) for analysis on the GC-MS/MS.

### 2.6.2 INSTRUMENT PARAMETERS

Gas chromatography (GC) conditions for this project was adapted from Luong et al. (2017), where low molecular weight lipids were targeted using gas-chromatography-tandem mass spectrometry (GC-MS/MS) [53]. The GC-MS/MS used for method development and sample analysis was a GCMS-TQ8040 fitted with an AOC-20i auto injector (Shimadzu, Kyoto, Japan). Three modes of splits were investigated at 50:1, 20:1 and 10:1 ratio, to identify the most effective split ratio for efficient compound analysis with limited saturation, with 50:1 ratio indicating the most optimal results. Samples were injected using a 50:1 split at 270 °C and injected onto an Agilent HP-5MS (30 m x 0.250 mm) column with a film thickness of 0.25 µm. The column temperature upon injection was at 80 °C and was held here for 3 min before being increased at a rate of 20 °C per min, until reaching 315 °C, where it was held for 4 min. Sample flow through the column was at a rate of 1.40 mL/min with total run time of 18.75 min, including an 8-min solvent delay. This was selected to ensure that the detector was not being oversaturated from solvent and bleed. Further, no analytes of interest within this project were found before 8 min, with the earliest time of relevant lipid elution at 8.03 min. An 18.75 min run time

was selected to enable efficient separation and detection of lighter analytes (fatty acids and dicarboxylic acids) and heavier analytes (bile acids and sterols). Helium was used as carrier gas. Samples were analysed using GCMS RealTime Analysis (LabSolutions, Shimadzu Corporation) and data was processed using GCMS Postrun Analysis (LabSolutions, Shimadzu Corporation). The two most abundant product ion fragments identified and reported in transition 2 and 3, produce a unique 'signature' when combined with transition 1, the parent compound, enabling specific detection of compounds. The optimal collision energy for molecule dissociation per transition is also reported for each analyte, at 15 eV for all compounds

#### 2.6.2.1 CALIBRATION AND MATRIX EFFECTS METHODS

Calibration curves spectrum were exported, plotted, and integrated on OriginPro 2019 (64-bit) version 9.6.0.172, with limit of detection (LOD) and limit of quantitation (LOQ) calculated in Microsoft Excel® (Table 3.3). The LOD and LOQ were calculated using a signal-to-noise ratio criterion of  $\geq 3$  and  $\geq 10$ , respectively. This was done to provide reference concerning sensitivity of detection and overall performance of the analytical method being used. The following equations were used to determine LOD and LOQ:

- a.  $LOD = 3.3 \times (SD^* \text{ of } S^{**} / 100) / S^{**}$
- b.  $LOQ = 10 \times (SD^* \text{ of } S^{**} / 100) / S^{**}$

\*SD = standard deviation

\*\*S = slope of calibration curve

Matrix effects were analysed in accordance with Matuszewski et al. [80], where the matrix effect (ME %) and recovery of the extraction procedure (RE %) was determined by comparing the peak areas attained from sets 1-3 (Tables 3.5 and 3.6). ME % results can vary to indicate ion enhancement (increase in response) or suppression (loss in response) of compounds occurring due to the co-eluting compounds within matrix. The ME % and RE % was calculated as follows:

- c.  $ME \% = \text{Set } 2 / \text{Set } 1 \times 100$
- d.  $RE \% = \text{Set } 3 / \text{Set } 2 \times 100$

### 2.6.2.2 DATA AND STATISTICAL ANALYSIS

Samples were collected in duplicate and injected in duplicate, resulting in four datapoints per sampling day. The relative abundance data was then averaged [14] and exported to Microsoft Excel<sup>®</sup> for pre-processing, where the compounds were manually normalised to the internal standard per sampling day– stearic D<sub>3</sub> for acids and cholesterol D<sub>7</sub> for sterols. Analytes were then normalised to most abundant compound per each sampling day. Normalised abundance data was used to graph the trend of each lipid throughout the decomposition period for each individual (Appendix B, C, D, E, I and J).

The Unscrambler<sup>®</sup> X (version 10.5: CAMO software, Oslo, Norway) was used to visually investigate groupings and separation within a dataset through Principal Component Analysis (PCA). PCAs were used for data exploration as it enables projection of data onto principal components which can be indicative of variability within a dataset. Data pre-processing steps such as mean centring, variance scaling and unit vector normalisation was performed on the dataset [13, 14]. This process was repeated for the different sample groups within a dataset depending on focus. Comparisons included: warmer (summer) pig tissue vs human tissue (tissue of human 4, pig 1, pig 2), warmer (summer) pig skin vs human skin (skin of human 4, pig 1, pig 2), cooler (winter) pig tissue vs human tissue (tissue of human 5, pig 3, pig 4), cooler (winter) pig skin vs human skin (skin of human 5, pig 3, pig 4), human skin comparison (skin of humans 2-5), human tissue comparison (tissue of humans 2-5).

A one-way ANOVA was conducted on compounds of interest to determine which compounds were of significance within a dataset ( $p < 0.05 = \alpha$ ). Once the compounds were identified, a post-hoc t-test, namely student t-tests with Bonferroni correction, was conducted comparing the compound of interest within a dataset among the individuals. For example, if myristic acid was identified as a compound of interest, this compound would be compared within human 1 > pig 1, human 1 > pig 2, pig 1 > pig 2 datasets to identify between which dataset(s) the compound is indicating significance. The Bonferroni adjusts significance level to become stricter, helping to mitigate the increased chance of obtaining false positives when conducting multiple tests. This process was repeated for both skin and tissue sample type.

# CHAPTER 3 GC-MS/MS

## METHOD OPTIMISATION



### 3.1 INTRODUCTION

The complex nature of this project required a comprehensive analytical method for lipid detection, which has been optimised for the purposes of human decomposition. This process involved development of two methods: firstly, sample preparation and sample analysis and then optimisation using gas chromatography-tandem mass spectrometry (GC-MS/MS). To identify lipids most effectively, standards were used to build an analytical method of detection using the multiple reaction monitoring (MRM) mode of GC-MS/MS. This involved optimising transitions and collision energies for each compound of interest to ensure the instrument is detecting each compound accurately. Sample preparation optimisation involved the determination of optimal solvents for lipid extraction and the volume of extract manipulated prior to drying down.

### 3.2 MATERIALS AND METHODS

#### 3.2.1 PREPARATION OF STANDARDS FOR IDENTIFICATION

Twenty-four standards (Table 3.3) were prepared at 10 ppm concentration for full scan identification by GC-MS/MS. HPLC grade Hexane obtained from RCI Labscan Ltd. (Gillman, South Australia), was used as the preferred solvent, where standards were dissolved. Standards including cholic acid, azelaic acid and lithocholic acid were prepared in HPLC grade dichloromethane (DCM) obtained from RCI Labscan Ltd. (Gillman, South Australia), due to their inability to dissolve in hexane because of their non-polar chemical composition. Once prepared at 10 ppm, compounds were derivatised and reconstituted using a silylation method [50]. This was done due to the presence of 'active' hydroxyl (-OH) groups within the analytes of interest, thus requiring addition of N,O-bis(trimethylsilyl) trifluoroacetamide (BSTFA) with w/1 % trimethyl-chlorosilane (TMCS), which facilitates the conversion of the polar -OH groups to non-polar trimethylsilyl (TMS) groups in the presence of heat, effectively making compounds thermally stable and increasing volatility [81]. The silylation method selected was based on that reported by Ueland et al. [24], involving standards being dried down under a gentle stream of nitrogen for approximately 5 min at 40 °C [45]. Samples were then reconstituted in 40 µL BSTFA + TMCS (from United Chemical Reagents (Bristol, Pennsylvania, USA) and 10 µL acetonitrile (RCI Labscan Ltd. (Gillman, South Australia) prior to being heated at 70 °C for 30 min using a heating block and then transferred into 250 µL polymer inserts (Agilent Technologies, Australia).

### 3.2.2 PREPARATION OF STANDARDS FOR CALIBRATION

After identification, all standards were serially diluted from 0.5 to 8 ppm to make a 5-point calibration curve (Table 3.3). Samples were diluted in HPLC grade hexane, except for azelaic acid and lithocholic acid, which were prepared in dichloromethane (DCM). Once standards were diluted to the desired concentration, they were dried down under a gentle stream of nitrogen for approximately 5 min, at 40 °C. Samples were then reconstituted with 40 µL BSTFA + w/1 % TMCS and 10 µL acetonitrile before being heated at 70 °C for 30 min and transferred into 250 µL polymer inserts.

### 3.2.3 MRM MODE OPTIMISATION

Full scan mode was used to identify and obtain the spectrum of each reference standard. MS optimisation was then conducted to allow for MRM analysis, involving selection of the highest abundance m/z ions as precursor ions (Table 3.4). These precursor ions were selected for collision induced dissociation (CID), resulting in a precursor-to-product ion reaction. The product ion of highest abundance was allocated as the quantitative transition. The two qualitative transitions were allocated to the second and third highest abundance product ions.

### 3.2.4 SAMPLE EXTRACTION OPTIMISATION

Samples were prepared according to Ueland et al. [24], whereby 6 mg of freeze-dried tissue/skin samples were weighed out. Samples were then homogenised in 2 mL of organic solvent and sonicated for 20 min prior to being filtered through a 0.2 µm hydrophobic PTFE syringe filter (MicroAnalytix, Sydney, Australia).

Tissue and skin extraction optimisation tests were conducted using samples from human body 1 (refer to Chapter 2 (Table 2.1) for donor details), sampling day 44, to represent a mid-decomposition sample timepoint. Two skin samples and two tissue samples were collected. This ensures that the sample is analytically complex in nature and representative of what many of the sample types will be. Optimisation firstly involved testing several organic solvents at different ratios (Table 3.1) to determine the optimal solvent to extract most abundant number of lipids across all fatty acid groups for both skin and tissue matrix. Once the most suitable organic solvent was identified, the amount of sample ratio with the organic solvent was tested to ensure the optimal and most efficient extraction of lipids from skin and tissue without experiencing any analyte carryover. These included testing: 3 mg of skin/tissue in 2 mL of solvent, 6 mg of skin/tissue in 2 mL of solvent, 3 mg of skin/tissue in 1 mL of solvent and 6

mg of skin/tissue in 1 mL of solvent. Optimal extract volume (prior to the drying down step) was also tested at 10  $\mu$ L and 100  $\mu$ L. All sample extraction tests were carried out in duplicates with two injections per sample, resulting in a total of four replicates per sampling area per sampling day.

Table 3.1: *Organic solvents tested for optimal lipid extraction from decomposing human skin and tissue.*

Method	Solvent(s) used
1	Hexane
2	Chloroform
3	Acetone
4	Chloroform:Acetone (1:1)
5	Chloroform:Methanol (1:1)

Solvents (Table 3.1) were selected based on a review of the literature, which revealed diverse extraction methods and matrices in lipidomics. Method 5 (chloroform:methanol (1:1)) was derived from Folch et al., who had developed a method using the aforementioned solvents at a 2:1 ratio (chloroform:methanol) for total lipid profile extraction in animal tissue [55]. This was one of the first methods used in extracting lipids from animal tissue. More recent studies, such as that by Ueland et al. [49], and Luong et al. [64], have demonstrated the use of single solvents for lipid extraction. Ueland et al. used chloroform to extract lipids from textiles exposed to decomposition fluid [49], whereas Luong et al. used hexane to extract cholesterol from soil surrounding human decomposition fluids [64]. These methods were also included due to the single solvent usage as well as both methods extracting lipids from matrices surrounding decomposition.

### 3.2.5 EXTRACTION EFFICIENCIES AND MATRIX EFFECTS

Tests for matrix effects and extraction efficiencies were conducted on sampling day 0 and day 40 of human body 3 (refer to Chapter 2 (Table 2.1) for donor details). These two sampling days were selected in an attempt to represent a fresh tissue/skin sample in comparison with tissue/skin sample that has undergone a substantial amount of decomposition, to reflect an analytically challenging sample type with a complex matrix.

Due to the endogenous nature of the compounds of interest, it was not possible to obtain a matrix similar or identical to skin and tissue without these compounds present. Therefore, deuterated compounds, stearic D<sub>3</sub>, cholesterol D<sub>7</sub>, tridecanoic D<sub>25</sub>, palmitoleic D<sub>13</sub>, palmitic D<sub>2</sub> and arachidic D<sub>2</sub> were

used to spike the matrices at different intervals (pre- and post-extraction) to calculate the percentage of compound lost during the extraction process as well as the interaction of the matrix with the extraction process. A combined mixture of deuterated compounds was prepared at 0.5 ppm and 5 ppm to compare extraction efficiency at both concentrations on both day 0 and day 40. Matrix effects and extraction efficiency trials were split into 4 sets (Table 3.2). To prepare each of these samples, 3 mg of either tissue or skin samples were prepared in 2 mL of hexane (tissue) or chloroform:acetone (skin) and prepared according to Section 2.4.4.1.

Table 3.2: *Trials conducted for calculation of extraction efficiency and matrix effects.*

Set 1	Deuterated compound mixture (no matrix)
Set 2	Matrix (skin and tissue) spiked with deuterated compound mixture after extraction
Set 3	Matrix (skin and tissue) spiked with deuterated compound mixture before extraction
Set 4	Baseline matrix (skin and tissue) (no spike)

Set 2 was prepared by weighing 3 mg of sample and adding 2 mL of solvent (hexane for tissue and chloroform:acetone for skin) before being homogenised and sonicated for 20 min. The extract was then filtered through a 0.2 µm hydrophobic PTFE syringe filter (MicroAnalytix, Sydney, Australia) and 100 µL of the deuterated spike mixture was then added. 100 µL of sample extract was then dried down under a gentle stream of nitrogen for approximately 5 min at 40° C. Samples were then reconstituted in 40 µL BSTFA + TMCS and 10 µL, prior to being heated at 70 °C for 30 min using a heating block and then transferred into 250 µL polymer inserts (Agilent Technologies, Australia).

For set 3, 3 mg of sample was weighed out and 100 µL of the deuterated mixture was spiked directly onto the matrix. 2 mL of solvent (hexane for tissue and chloroform:acetone for skin) was then added to the matrix and the mixture was homogenised and then sonicated for 20 min. The extract was then filtered through a 0.2 µm hydrophobic PTFE syringe filter. 100 µL of sample extract was then dried down under a gentle stream of nitrogen for approximately 5 min at 40 °C. Samples were then reconstituted in 40 µL BSTFA + TMCS and 10 µL, prior to being heated at 70 °C for 30 min using a heating block and then transferred into 250 µL polymer inserts.

Due to the compounds of the deuterated mixtures being dried down under nitrogen and further reconstituted, this results in re-concentration and dilution of deuterated compounds from 0.5 and 5 ppm to 1 and 10 ppm, respectively. Set 2 and 3 were compared to provide percentage recovery

of spike mixture before and after the extraction process. This was the indicator for extraction efficiency. Set 1 and 3 comparisons were indicative of how the matrix interacts within the sample extraction process and indicate whether the matrix itself affects the extraction process. All set tests were carried out in duplicates with two injections per sample, resulting in a total of four replicates per set, per sampling day.

### 3.3 RESULTS AND DISCUSSION

#### 3.3.1 STANDARD IDENTIFICATION AND CALIBRATION

Calibration curves were produced for each biomarker with standards being prepared at serial dilutions of 0.5 – 8 ppm as per Section 3.2.2. The limit of detection (LOD) and limit of quantitation (LOQ) was calculated for each analyte that was investigated within the scope of this project using a signal-to-noise ratio criterion of  $\geq 3$  and  $\geq 10$ , respectively. All values were reported in parts-per-million. LOD and LOQ of saturated fatty acids ranged from 0.020 – 0.076 ppm and 0.061 – 0.152 ppm, respectively (Table 3.3). Unsaturated fatty acids indicated a range in LOD and LOQ of 0.029 – 0.067 ppm and 0.087 – 0.203 ppm, respectively. Sebacic acid illustrated the highest LOQ of any analyte at 0.376 ppm. Sterol LODs and LOQs ranged from 0.018 – 0.075 ppm and 0.054 – 0.228 ppm.

*Table 3.3: GC-MS/MS MRM method results for the targeted lipid analytes including the limit of detection (LOD) and limit of quantitation (LOQ) reported in parts per million (PPM).*

Analyte	LOD (ppm)	LOQ (ppm)
<i>Saturated Fatty Acids</i>		
Arachidic Acid	0.049	0.147
Behenic Acid	0.020	0.061
Decanoic Acid	0.042	0.129
Dodecanoic Acid	0.021	0.065
Hexacosanoic Acid	0.047	0.142
Myristic Acid	0.048	0.146
Nonadecanoic Acid	0.035	0.105
Pentadecanoic Acid	0.076	0.230
Tricosanoic Acid	0.029	0.089

Tridecanoic Acid	0.037	0.111
Stearic Acid d <sub>3</sub>	0.073	0.224
<i>Unsaturated Fatty Acids</i>		
Linoleic Acid	0.062	0.188
Oleic Acid	0.067	0.203
Palmitoleic Acid	0.029	0.087
<i>Dicarboxylic Acids</i>		
Azelaic Acid	0.061	0.186
Sebacic Acid	0.124	0.376
<i>Bile Acids</i>		
Lithocholic Acid	0.018	0.054
<i>Sterols</i>		
5 $\alpha$ -cholestanone	0.028	0.085
Cholesterol	0.075	0.228
Cholesterol d <sub>7</sub>	0.063	0.192
Ergosterol	0.025	0.077
Stigmasterol	0.044	0.132
$\beta$ -sitosterol	0.018	0.054
Coprostanol	0.044	0.133

### 3.3.2 OPTIMISED MRM METHOD

The first transition (transition 1) for each compound detected within the MS is referred to as the parent compound (Table 3.4). The following two transitions (transition 2 and 3) are qualitative assessments, where the fragmentation of the parent compounds (product compounds) is reported. Table 3.4 summarises the criterion for the detection of each compound including the retention time of identification, mass of each reference standard, along with the two qualifier ion transitions for each analyte.

Table 3.4: GC-MS/MS MRM ion transitions and optimised collision energies (CE) for the targeted lipids.

Analyte	Retention time (RT)	Transition 1 (quant.)	Transition 1 collision energy (eV)	Transition 2 (qual. 1)	Transition 2 collision energy (eV)	Transition 2 (qual. 2)	Transition 3 collision energy (eV)
<i>Saturated Fatty Acids</i>							
Arachidic Acid	13.27	369.00>75.00	15	369.00>131.00	15	369.00>95.00	15
Behenic Acid	13.94	397.00>75.00	15	397.00>131.00	15	397.00>95.00	15
Decanoic Acid	8.03	229.00>75.00	15	229.00>131.00	15	229.00>81.00	15
Hexacosanoic Acid	15.61	453.00>75.00	15	453.00>131.00	15	453.00>95.00	15
Lauric Acid	9.28	257.00>75.00	15	257.00>131.00	15	257.00>95.00	15
Myristic Acid	10.39	285.00>75.00	15	285.00>131.00	15	285.00>95.00	15
Nonadecanoic Acid	12.71	355.00>75.00	15	355.00>131.00	15	355.00>95.00	15
Palmitic Acid	11.47	313.00>141.00	15	313.00>113.00	15	313.00>75.00	15
Pentadecanoic Acid	10.90	299.00>75.00	15	299.00>131.00	15	299.00>95.00	15
Stearic Acid-D3	12.26	344.00>75.00	15	375.00>213.00	15	344.00>95.00	15
Tricosanoic Acid	14.34	411.00>75.00	15	411.00>131.00	15	411.00>81.00	15
Tridecanoic Acid	9.90	271.00>75.00	15	271.00>131.00	15	271.00>95.00	15
<i>Unsaturated Fatty Acids</i>							
Linoleic Acid	12.15	337.00>75.00	15	220.00>79.00	15	337.00>93.00	15

Oleic Acid	12.27	339.00>75.00	15	339.00>131.00	15	222.00>67.00	15
Palmitoleic Acid	11.28	311.00>75.00	15	236.00>67.00	15	311.00>131.00	15
<i>Dicarboxylic Acids</i>							
Azelaic Acid	10.17	201.00>83.00	15	317.00>149.00	15	317.00>123.00	15
Sebacic Acid	10.63	331.00>149.00	15	215.00>55.00	15	331.00>95.00	15
<i>Bile Acids</i>							
Lithocholic Acid	16.70	257.00>161.00	15	215.00>105.00	15	430.00>325.00	15
<i>Sterols</i>							
5 $\alpha$ -cholestanone	16.30	429.00>167.00	15	458.00>429.00	15	401.00>195.00	15
Cholesterol	16.15	329.00>95.00	15	368.00>353.00	15	368.00>339.00	15
Cholesterol d7	16.23	336.00>95.00	15	375.00>213.00	15	375.00>255.00	15
Ergosterol	16.90	379.00>69.00	15	379.00>255.00	15	379.00>83.00	15
Stigmasterol	16.90	255.00>105.00	15	394.00>83.00	15	394.00>211.00	15
$\beta$ -sitosterol	17.27	357.00>95.00	15	396.00>381.00	15	396.00>367.00	15
Coprostanol	15.98	403.00>73.00	15	370.00>215.00	15	370.00>355.00	15



### 3.3.3 SAMPLE EXTRACTION OPTIMISATION

The optimal method for skin extraction was determined to be chloroform:acetone (1:1) (Figure 3.2). Although this method did not result in the highest relative abundances across all compounds, it was selected due to the consistent results generated across both fatty acids and sterols. In addition, it was the only organic solvent mixture to produce results across all sterols. Hexane was determined to be the most efficient solvent in extraction lipids from tissue samples. This is confirmed with hexane not only producing the highest relative abundance for most compounds (Figure 3.1), but also through the fact that it was consistently generating results for sterols, where possible. Chloroform:acetone (1:1) also generated similar results, however due to the simplicity and added cost benefit of using a single solvent rather than two solvents, hexane was determined to be the most efficient solvent. Hexane was similarly used as the preferred extraction solvent in recent research conducted by Ueland et al. [24] on tissue of decomposing humans.

When comparing the sample volume of the lipid extract (prior to dry down), skin in chloroform:acetone (1:1) and tissue in hexane samples revealed 100  $\mu\text{L}$  as the optimal volume of starting sample extract for effective compound identification. Compounds which had complete dropout in both 10  $\mu\text{L}$  and 100  $\mu\text{L}$  were deemed as not present within the sample and removed from Figures 3.3 and 3.4. Within the skin extract test (Figure 3.3), complete compound drop-out is observed when 10  $\mu\text{L}$  extract is analysed for the compounds: linoleic acid, hexacosanoic acid, and b-sitosterol, resulting in 100  $\mu\text{L}$  being the preferred extract volume prior to dry-down for skin extract.

Similarly, within the tissue extract tests (Figure 3.4), 10  $\mu\text{L}$  volume indicated no detection of the compounds ergosterol and b-sitosterol, making 100  $\mu\text{L}$  the preferred sample dry down volume for tissue extract. There were some instances, such as decanoic acid, nonadecanoic acid, stigmasterol and 25-hydroxycholesterol for skin extract (Figure 3.3) and nonadecanoic acid, cholesterol, and cholesterol  $d_7$  for the tissue extract (Figure 3.4), where 10  $\mu\text{L}$  dry down volume abundance was higher than 100  $\mu\text{L}$  dry down volume abundance. Although this results in high retention for these compounds, due to most compound abundances being higher in 100  $\mu\text{L}$  than 10  $\mu\text{L}$ , 100  $\mu\text{L}$  was the preferred sample dry down volume in both type of extracts (tissue and skin).

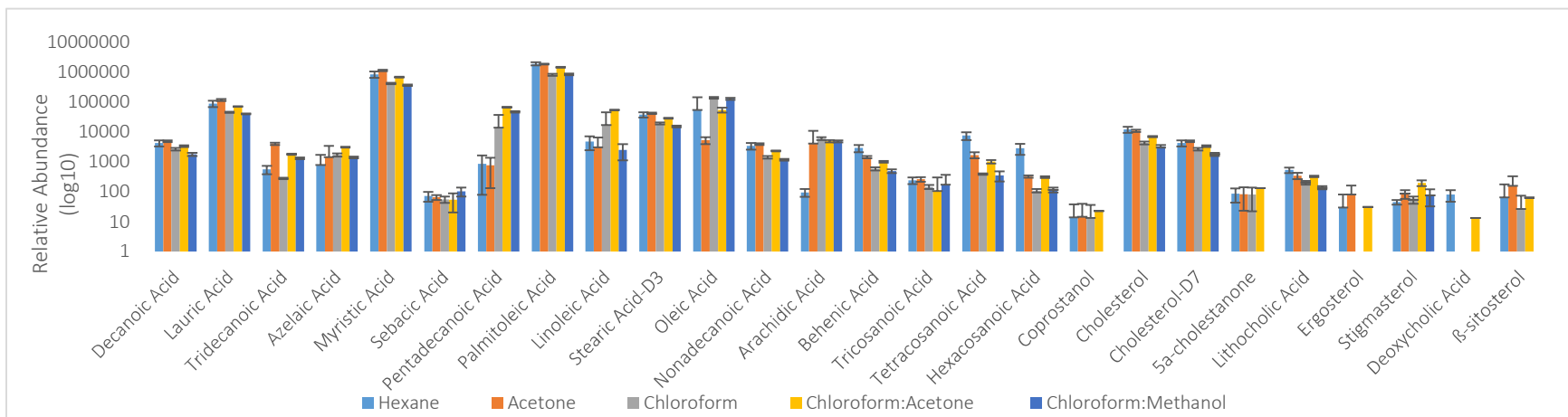


Figure 3.1: Solvents tested for the optimal extraction of lipids from human tissue samples. Relative abundance reported in log base10. Error bars represent margin of error in data, relative to standard deviation of 4 replicate points).

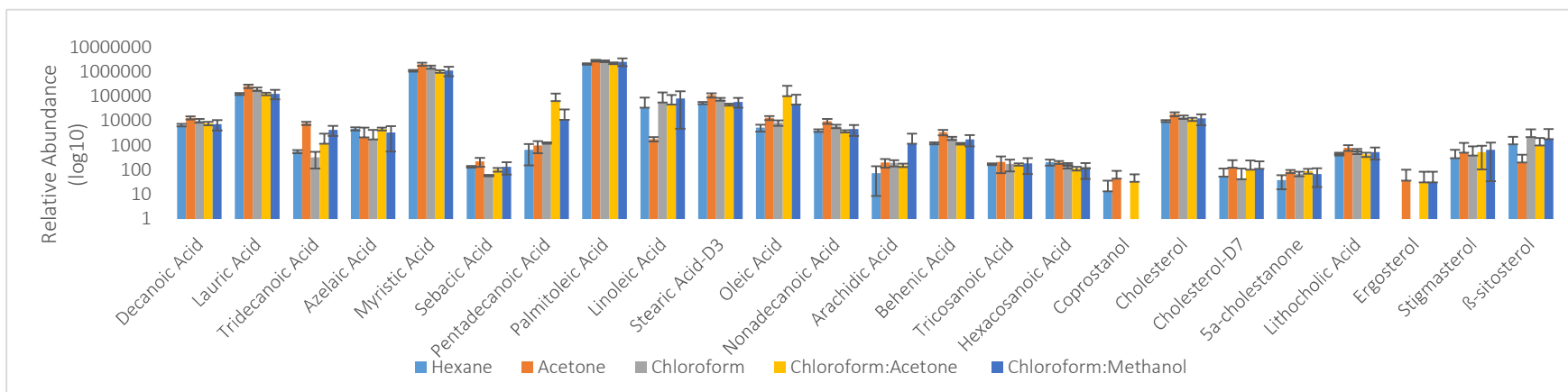


Figure 3.2: Solvents tested for the optimal extraction of lipids from human skin samples. Relative abundance reported in log base10. Error bars represent margin of error in data, relative to standard deviation of 4 replicate points).

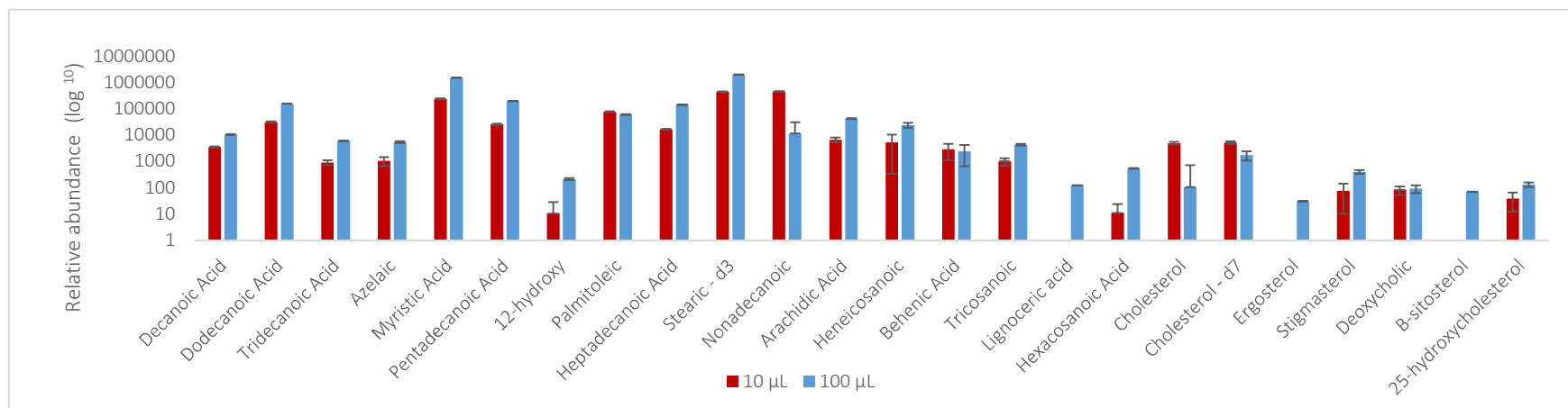


Figure 3.3: Comparison of skin extract volumes, 10 µL and 100 µL (relative abundance log base10). Error bars represent margin of error in data, relative to standard deviation of 4 replicate points. Y-axis represents relative abundance in log base10.

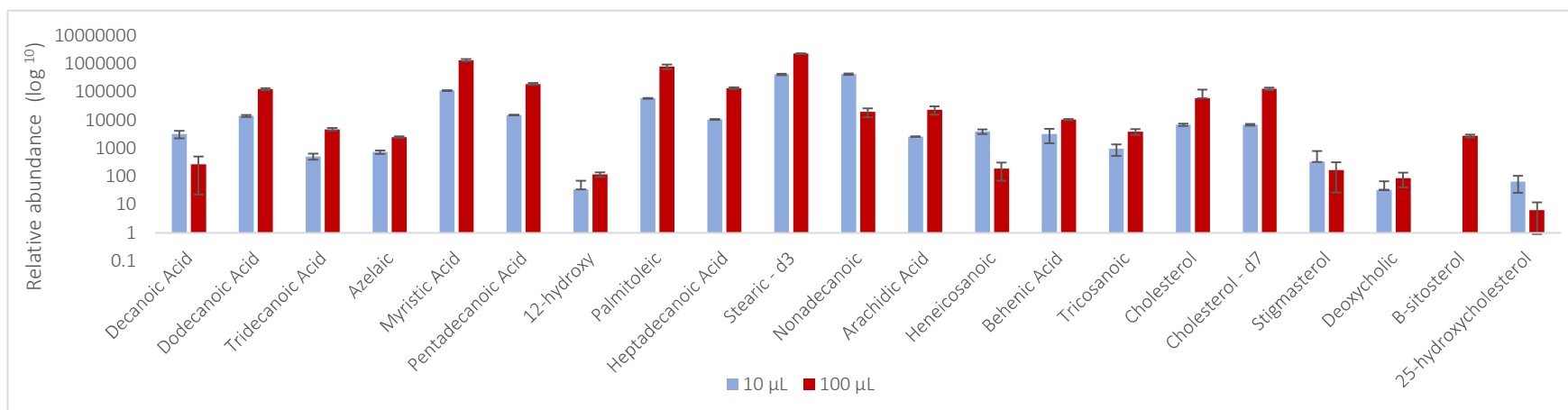


Figure 3.4: Comparison of tissue extract volumes, 10 µL and 100 µL (relative abundance log base10). Error bars represent margin of error in data, relative to standard deviation of 4 replicate points. Y-axis represents relative abundance in log base10.

### 3.3.4 MATRIX EFFECTS RESULTS

Overall, ME % results varied substantially within tissue samples (Table 3.5), with d-tridecanoic acid and d-stearic acid indicating large amounts of ion suppression for both 1 ppm and 10 ppm spikes on day 0 and day 40 sample days. This was also observed with d-arachidic acid for day 0 samples at 10 ppm. ME % for day 40 tissue samples (Table 3.5) indicated a large amount of ion enhancement for d-palmitoleic acid and d-palmitic acid for both 1 ppm and 10 ppm spiked samples and 1 ppm sample for d-cholesterol. RE % refers to the percentage of analytes that have successfully been extracted from the matrix, with values ranging from 65.3 – 151.9 % for day 0 samples at 1 ppm, 78.5 – 114.3 % for day 0 samples at 10 ppm, 89.1 – 264.0 % for day 40 samples at 1 ppm and 93.2 – 4243.1 % for day 40 samples at 10 ppm. These values indicate relatively good extraction of compounds from the matrix with 100 % being optimal. Day 40 sample at 10 ppm for d-cholesterol indicated an unusually large amount of recovery at 4243.1 %. A possible explanation of this could be contamination that may have occurred during the preparation of the day 40 tissue sample, particularly during the drying down phase when a potentially contaminated nozzle which disperses nitrogen was inserted into the vials.

Ionisation enhancement can be illustrated by ME values > 100 %, which indicate an increase in the intensity of the ions present due to other coeluting molecules present which have reacting capabilities with the primary ions [80, 82]. Ion suppression is illustrated by ME values < 100 %, where there is a loss in analyte response, wherein primary ions are indicating interference of analyte detection due to competing compounds in the matrix [80, 82]. RE % values illustrate the amount of compound that has been extracted successfully from matrix. While variation in matrix effects and ion enhancement is acknowledged and accounted for, standard addition, internal standards, replicate analyses and careful data analyses have collectively contributed to the accuracy of these results, allowing for data to be confidently interpreted.

Table 3.5: Matrix effects results showing the matrix effects percentage (ME %) and recovery percentage (RE %) of tissue matrix for fresh samples (Day 0) and decomposed sample (Day 40), with both samples being spiked with deuterated compounds of 1 ppm and 10 ppm. ME % is calculated as the ratio of the mean peak area in set 2 (matrix spiked with mixture after extraction) and set 1 (deuterated compound mixture - no matrix), multiplied by 100 (Table 3.2). Ionisation enhancement is indicated by ME % values > 100 % and ion suppression is indicated by values < 100 %. RE % was calculated as the ratio of the mean peak area in set 3 (matrix spiked with mixture before extraction) to the mean peak area in set 2 (matrix spiked with mixture after extraction), multiplied by 100 [80].

Compound	Day 0				Day 40			
	1 ppm		10 ppm		1 ppm		10 ppm	
	ME %	RE %	ME %	RE %	ME %	RE%	ME %	RE%
d-Tridecanoic acid	17.6	73.0	38.7	114.3	16.7	264.0	44.2	174.9
d-Palmitoleic acid	1453.1	151.9	303.6	100.8	191899.0	112.5	16978.5	116.0
d-Palmitic acid	400.2	104.3	137.5	105.5	35116.0	144.1	6388.1	139.4
d-Stearic acid	0.7	65.3	0.4	83.8	14.7	89.1	15.6	93.2
d-Arachidic acid	89.4	82.3	37.2	87.1	661.6	129.8	129.2	139.7
d-Cholesterol	312412.6	96.5	313.5	78.5	176622.3	172.1	122.7	4243.1

Table 3.6: Matrix effects results showing the matrix effects percentage (ME %) and recovery percentage (RE %) of skin matrix for fresh samples (Day 0) and decomposed sample (Day 40), with both samples being spiked with deuterated compounds of 1 ppm and 10 ppm. ME % is calculated as the ratio of the mean peak area in set 2 (matrix spiked with mixture after extraction) and set 1 (deuterated compound mixture - no matrix), multiplied by 100 (Table 3.2). Ionisation enhancement is indicated by ME % values > 100 % and ion suppression is indicated by values < 100 %. RE % was calculated as the ratio of the mean peak area in set 3 (matrix spiked with mixture before extraction) to the mean peak area in set 2 (matrix spiked with mixture after extraction), multiplied by 100 [80].

Compound	Day 0				Day 40			
	1 ppm		10 ppm		1 ppm		10 ppm	
	ME %	RE %	ME %	RE %	ME %	RE%	ME %	RE%
d-Tridecanoic acid	3.3	86.8	0.2	114.3	4.9	148.9	0.3	459.5
d-Palmitoleic acid	171370.9	617.3	2855.7	100.8	201438.0	943.8	3499.5	1236.8
d-Palmitic acid	1.1	3670.4	0.5	105.5	1.7	6658.5	0.2	11126.9
d-Stearic acid	0.7	958.0	0.2	83.8	0.8	2277.5	2.9	620.5
d-Arachidic acid	75.3	110.1	2.5	87.1	189.7	22.9	1.7	171.1
d-Cholesterol	16432.1	29.4	429.7	78.5	31919.9	5.7	117.2	931.4

Fresh and decomposed skin samples both showed considerable variation in ME %, illustrating both enhancement and suppression of compounds analysed (*Table 3.6*). Substantially low amounts of ME % were reported for d-tridecanoic acid, d-palmitoleic acid and d-stearic acid at both concentrations on both sampling days. D-arachidic acid depicted less matrix effects within samples that were spiked at 1 ppm compared to the 10 ppm spike, which indicated relatively high amounts of matrix effects. D-palmitoleic and d-cholesterol both depicted considerably large amounts of ion enhancement for both sampling days at both concentrations. Large variation was also observed for the recovery data within skin samples. It is speculated due to the consistently large results for d-palmitoleic acid across both skin and tissue samples, that there may have been interaction of this compound within the deuterated compound mix or on the matrix itself, which may have affected the chemical composition of this compound and therefore skewed the results.

RE % values ranged from 29.4 – 3670 % for day 0 samples at 1 ppm, 78.5 – 114.3 % for day 0 samples at 10 ppm, 5.7 – 6658.5 % for day 0 samples at 1 ppm and 171.1-11126.9 % for day 40 samples at 10 ppm. The substantially variable RE % from this method of skin extraction illustrates that samples that are more decomposed have a larger effect on the recovery of compounds. This is speculated to occur due to the degrading nature of the samples in question, which may result in increased concentrations and potential contamination of similar compounds to be saturating the detection of the deuterated compounds. Day 0 recovery demonstrates that d-palmitic, d-stearic and d-palmitoleic acid have a substantially large volume of recovery compared to d-cholesterol, which illustrates low recovery.

The overall skin matrix and recovery effect results illustrate that the method of extraction being used is not as effective on tissue samples as it is on skin samples. While there is potential for consistency in sample results, as observed in instances such as day 0 with 10 ppm RE %, this uniformity is not consistently reflected in the results obtained from tissue samples.

To improve this method, a range of deuterated compounds (ideally the deuterated form of each compound of interest) should be tested on both matrices in different solvents to ensure that solvent choice is not affecting the composition of deuterated compounds prior to analysis or spike. Matrix effects and recovery should be considered across multiple time points of decomposition, to verify the effects (if any) that the extent of degradation has on deuterated compounds.

### 3.4 FINAL METHOD

The final method developed had many similarities to that of Ueland et al. [24], including the use of hexane as the extraction solvent for tissue samples, and the processing steps post-solvent

addition. Ueland et al. [24] used 6 mg of sample within 2 mL of solvent, whereas this method uses 3 mg of sample in 2 mL of solvent resulting in more sample preservation without compromising results. 100  $\mu\text{L}$  of extract was used in this study in comparison to the 500  $\mu\text{L}$  used in the Ueland et al. [24] study. This was selected due to column saturation from higher volumes of extract being tested. Comparatively, Luong et al. analysed 1000  $\mu\text{L}$  of extract volume, possibly due to the presence of lipids being analysed in trace amounts on stone artefacts [53].

To conclude, a method was developed and optimised for the detection and analysis of lipids within decomposing human skin and tissue. Further work needs to be conducted to identify which compounds of interest would be most ideal for detection within this method and which compounds could benefit through alterations to this method. This method could be further refined by analysing samples at various stages of decomposition to assess how the detection of compounds is impacted and to determine the most suitable method, if any, for such analyses

This developed method was applied to the remainder of this thesis to detect and analyse lipids within samples of decomposing human bodies to improve the understanding of the lipid profile within these samples, focusing on natural mummification and its effects.



# CHAPTER 4 PIG VS HUMAN: WARMER SEASON STUDY

This chapter provides a comparative study of skin and tissue of human and pigs post-mortem, established during the Australian summer season. The differences in the lipid profile of fatty acid and sterol compositions of human versus pig tissue, and human versus pig skin have been investigated. The visual trends and stages of decomposition are also compared between the two species. This is crucial for an understanding of the effect that warmer climates have on the lipid degradation in the tissue and skin of both species. A warmer season in this instance is defined as a period of the year characterised by higher temperatures compared to the other seasons. These are associated with increased sunlight, longer days, and a general rise in temperature. Furthermore, the extent of these effects and how this is impacted by natural mummification is also explored. Visual observations of the initial signs of natural mummification are defined through desiccation, and orange colour changes within the skin. Knowledge from this study will assist in understanding the reliable use of pigs as human analogues from a biochemical perspective.

#### 4.1 MATERIALS AND METHODS

One human and two pigs were used for the warmer climate study, all three being clothed in a cotton t-shirt due to concurrent decomposition studies. The trial commenced on the 29<sup>th</sup> of January 2021, during Australian summer, with the final sampling day carried out on the 11<sup>th</sup> of August 2021 (Table 4.1). The individuals used in this study were human 4 (H4) and pigs 1 (P1) and 2 (P2). P1 and P2 were placed two days after H4 was placed (*Table 4.1*) to ensure a consistency in environmental conditions affecting the two species. Samples for all three specimens were collected on the same sampling day post-mortem to ensure the same amount of decomposition time had passed before sample collection. Sampling was conducted until samples could no longer be retrieved. Images of P1, P2 and H4 were taken on all sampling days to capture visual decomposition at the time of samplings (refer to tables K3, K5 and K6 from Appendix K).

*Table 4.1: Warmer climate study information of pig 1 (P1), pig 2 (P2) and human 4 (H4).*

Individual	Date of placement	Days sampled post-mortem	Final sampling date
Human 4 (H4)	29 <sup>th</sup> January 2021	0, 1, 2, 3, 4, 5, 6, 7, 8, 10, 14, 17, 20, 28, 35, 42, 70, 105, 185, 202	19 <sup>th</sup> August 2021

Pig 1 (P1)	1 <sup>st</sup> February 2021	0, 1, 2, 3, 4, 5, 6, 7, 8, 10, 14, 17, 20, 28, 35, 42	15 <sup>th</sup> March 2021
Pig 2 (P2)	1 <sup>st</sup> February 2021	0, 1, 2, 3, 4, 5, 6, 7, 8, 10, 14, 17, 20, 28, 35, 42, 70	12 <sup>th</sup> April 2021

Skin and tissue samples were collected from human and pig bodies in accordance with the method described in section 2.4. Once collected, samples were homogenised, and the lipids of interest were extracted from the matrix. Targeted analysis was then conducted on the samples using gas chromatography tandem mass spectrometry (GC-MS/MS). Resultant data was exported to Microsoft Excel<sup>®</sup> for pre-processing. Normalised abundance data was then imported onto the Unscrambler<sup>®</sup> X (version 10.5: CAMO software, Oslo, Norway) to produce Principal Compound Analysis (PCA) plots.

## 4.2 RESULTS

### 4.2.1 VISUAL COMPARISON AND OBSERVATIONS

P1 and P2 both had mummified skin present on day 1 post-placement with both pigs entering the bloat stage on day 2 (see Table K-5 and K-6 from Appendix K). Signs of mummified tissue were observed on day 6 post-placement for H4 (Table K-4 from Appendix K). Bloating was only observed on day 8, by which time the face of the human was well into the active stage of decay. Active decay was entered for pig 1 on day 7, while pig 2 entered active decay on day 8. Day 14 for both P1 and P2 showed excessive mass loss, indicating advanced stages of decomposition. H4 appeared to have mummified tissue during the bloat stage, retarding the onset of active decay and resulting in a direct transition into advanced decay by day 28. This meant there was mass loss without excessive eruption and loss of external tissue. By day 17 post-placement for both pigs, the unclothed areas of skin samples that were exposed had disintegrated, with both skin and tissue samples only being retrieved under the clothed areas of the pigs. Although the skin for H4 was also exposed, the effect of mummification appeared to preserve the skin of the human body throughout the period of decomposition. Comparatively, although the porcine indicated signs of mummified tissue during the earlier stages of decomposition, this did not result in preservation of the pig soft tissues. This dissimilarity could be attributed to differences in internal organ distribution between humans and pigs, indicating that pig decomposition may not accurately represent human decomposition. Samples were no longer retrievable by day 42 and day 70 for P1 and P2, respectively. Samples were collected until day 202 for H4.

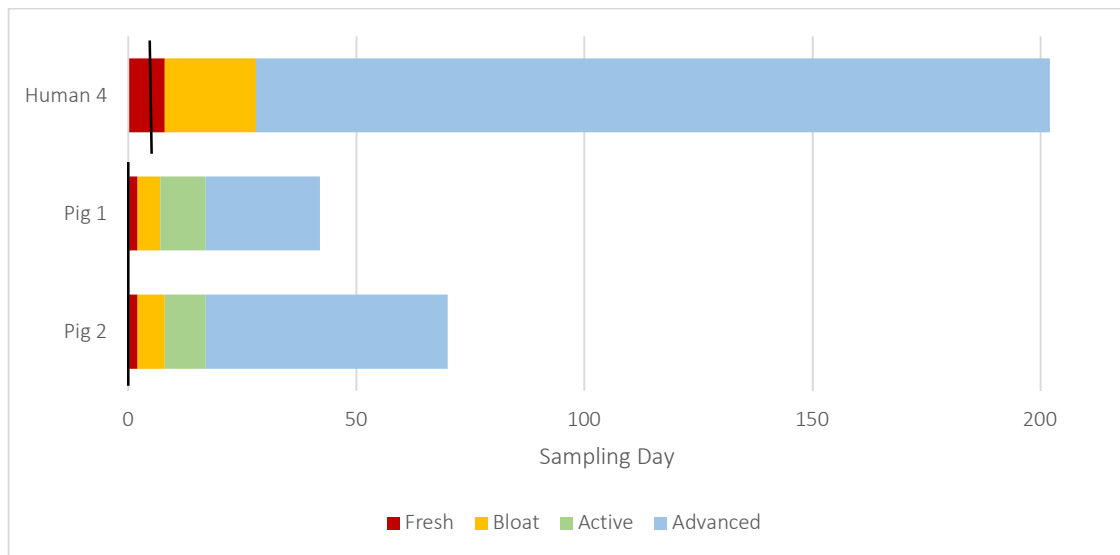


Figure 4.1: Stages of decomposition (fresh, bloat, active and advanced decay) shown as a comparison between human 4 (H4), pig 1 (P1) and pig 2 (P2). First signs of observed natural mummification is denoted by the black line.

When the stages of decomposition are compared for H4, P1 and P2 (Figure 4.1), both pigs followed a similar timeline from the fresh stage, into bloat, active decay, and advanced decay. However, the human did not show visual signs of active decay, resulting in a prolonged bloat stage, which directs into the advanced stage of decay (due to natural mummification). The first signs of observed natural mummification (orange colour change in the skin) are highlighted in Figure 4.1 through the black line across each body.

The long-term visual effects of natural mummification can be exhibited through Figure 4.2, which shows the final sampling day for H4. At this point, a substantial amount of skin remained on the body, and minimal disruptions to the skeletal structure were observed. This encapsulates the preservation effect that natural mummification has for decomposing humans.



Figure 4.2: Final sampling day (Day 202) for human 5 (H5) depicting preserving effects of natural mummification within human body

In contrast to the effects of natural mummification in humans, both pigs showed early signs of mummified tissue, but the outcomes differed significantly. Within the pigs, natural mummification appeared through orange colour changes on the skin, in a spotting manner. The human depicted orange colour changes of the skin more evenly, with a lot more of the skin affected. Natural mummification has not prohibited the progression of decomposition within the pigs and as a result, both pigs continued to decompose into the active and advanced stages of decomposition. Figure 4.3 exhibits the lack of naturally mummified skin or tissue remaining on pig 1 and pig 2.



Figure 4.3: Final sampling days for P1 (day 42) and P2 (day 70) depicting hard tissue (bones) due to lack of mummified skin present. (a). = P1 remains, (b). = P2 remains.

#### 4.2.2 PIG VS HUMAN TISSUE

Human and pig tissue were chosen as the target matrix for lipid analysis due to the abundant presence of lipids within the tissue matrix of both species. Tissue matrix was deemed an appropriate means to compare the lipid profile within the two species, with particular emphasis on any trends that can be allocated to stages of decomposition or natural mummification. Refer to methods section 2.5 and 2.6 for full method details.

#### 4.2.3 PCAS

PCA plots were created as a visual statistical tool to identify the underlying patterns and relationships in the data by pinpointing the variables that explain the most variation in the dataset. These plots were created in a split of fatty acids and sterols due to the differences in function between fatty acids and lipids. Pig data (P1 and P2) were averaged and treated as replicates. Upon investigation, PC1 vs PC2 appeared to consist of the most valuable data and was used in all instances of PCA analysis.

##### 4.2.3.1 FATTY ACIDS

Fatty acid variation within the tissue was plotted in a PCA to visualise any groupings within the tissue matrix of H4 and both pigs (P1 and P2 averaged) (Figure 4.4). The general PCA trends illustrate a cluster of human samples during the early period of decomposition (D0-D6), highlighted in the purple circle. This clustering suggests that the fatty acid profile during the early period of decomposition within the human has limited variability. Mummification was first visually identified on the human body on sampling day 6 (Figure 4.1), which also depicts a shift in relation to the lipids influencing the fatty acid profile post-day 6. These changes can be attributed to an increase in myristic acid, lauric acid and pentadecanoic acid (see Figures C-2, C-5, and C-10 from Appendix C). Mummification was first observed on sampling day 1 for pigs 1 and 2, but this observation did not result in a fatty acid profile shift (such as that observed within the human samples). This could be due to the inconsistent visual changes (orange spotting of the skin) that the effect that natural mummification had within the pigs. This indicates that the influence of mummification between the two species has a differing effect. Early-day samples of the pigs show similarities in the lipid profile being exhibited (highlighted in orange oval). A progression in decomposition from sampling day 10 onwards depicts a shift in the fatty acid profile within pigs. A similar shift was observed with decomposition progression within the human samples. This suggests that the earlier period of decomposition for the human and porcine show limited variability within the lipid profile and as both species progress into decomposition, a shift in fatty acid profile is depicted. The shift in fatty acid profile within the human tissue samples are attributed to an increased expression of myristic acid (See Figure F-1 in Appendix F).

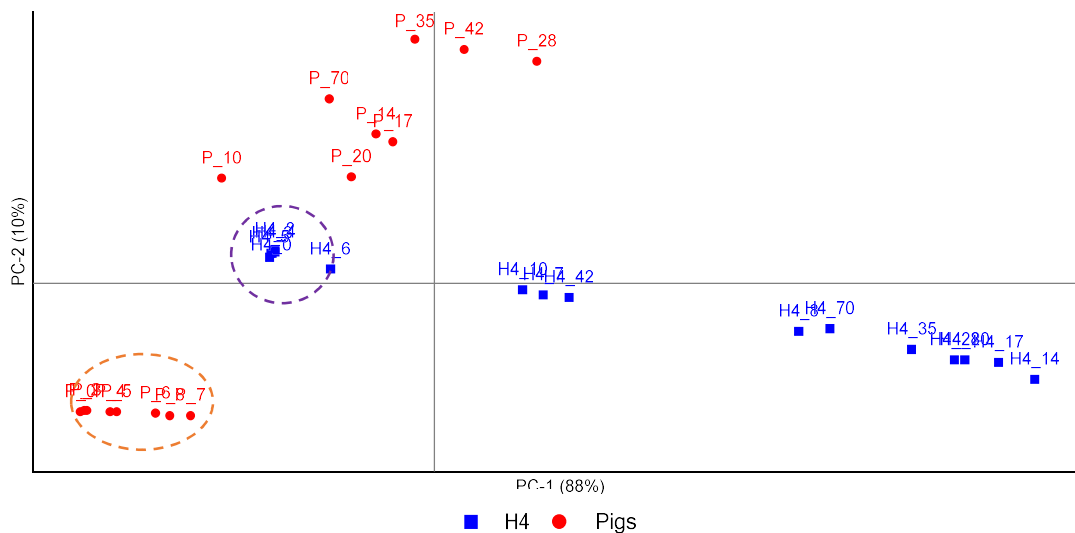


Figure 4.4: Principal component analysis (PCA) of fatty acid variation within the tissue of H4 and pigs (P1 and P2 averaged). Purple circle highlighted D0-D6 sampling days for H4. Orange circle highlights D0-D7 sampling days for pigs.

Of all the compounds investigated, palmitoleic acid showed statistically significant differences between P2 and P1, and P2 and H4 (Table 4.2). Palmitoleic acid is traditionally most abundant in serum in tissue, especially within the adipose tissue and liver [83]. Although, P2 had a similar mass compared to P1, the fat distribution within the pig as well as the internal biome and consequently, the internal method of decomposition, may have caused these differences in palmitoleic acid.

These trends suggest that although mummification was observed in both humans and pigs, the effect of this mummification is not the same between the species. It also indicates that during the earlier stages of decomposition, the lipid profile of pig is more comparable to humans and as decomposition progresses there is a greater biochemical shift within the sample type, at least in the instance where mummified tissue is present.

#### 4.2.3.2 STEROLS

Sterol variation within the tissue was plotted in a PCA to visualise any groupings within the tissue matrix of H4 and both pigs (P1 and P2) (Figure F-2 from Appendix F). Sterol distribution within the appears to indicate substantial differences between the two species, although there is little variation throughout decomposition. No trends were discernible concerning decomposition stages or natural mummification.



#### 4.2.4 ANOVA

A one-way analysis of variance (ANOVA) was conducted on the relative abundance data of all compounds between H4, P1 and P2 to identify compounds which had statistical significance between the three sample groupings. Once a compound was deemed significant, a student t-test ( $p \leq 0.5$ ) with the Bonferroni correction t-test were applied to identify where the significance lies within the sample grouping. This correction was used to help maintain a reasonable balance between identifying genuine significant findings and reducing the likelihood of mistakenly identifying significance due to random chance when dealing with multiple comparisons. This method of adjustment has been used in previous forensic science literature for accurate 'family-wise' error rates [84, 85].

Table 4.2: Depiction of compound significance in tissue comparison because of t-test, with Bonferroni correction, where H4 = human 4, P1= pig 1 and P2= pig 2 (i.e., H4 vs P1 = human 4 vs pig 1 compound comparison). Compounds showing statistical significance between two sample groups indicated through the denomination 'X'.

Fatty acids	H4 vs P1	H4 vs P2	P1 vs P2	Sterols	H4 vs P1	H4 vs P2	P1 vs P2
Decanoic Acid	x			Coprostanol			
Lauric Acid	x		x	Cholesterol			
Tridecanoic Acid			x	5 $\alpha$ -cholestanone			
Azelaic Acid				Lithocholic			
Myristic Acid	x	x		Ergosterol			
Sebacic Acid				Stigmasterol			
Pentadecanoic Acid				Deoxycholic acid			
Palmitoleic Acid		x	x	$\beta$ -sitosterol			
Linoleic Acid				25- hydroxycholesterol			
Oleic Acid							
Nonadecanoic Acid							
Arachidic Acid							
Behenic Acid	x						
Tricosanoic Acid							
Hexacosanoic Acid							



Myristic acid was the only compound showing statistically significant differences between the two species types (i.e., human and both pigs) (Table 4.2). This can be attributed to the spike in myristic acid from the onset of mummification (day 6) onwards throughout the decomposition of the human (Figure 4.5). Although signs of mummified tissue were first observed in both pigs on day 1 (orange colour change of skin), an increase in myristic acid was not reflected during the onset of this event.

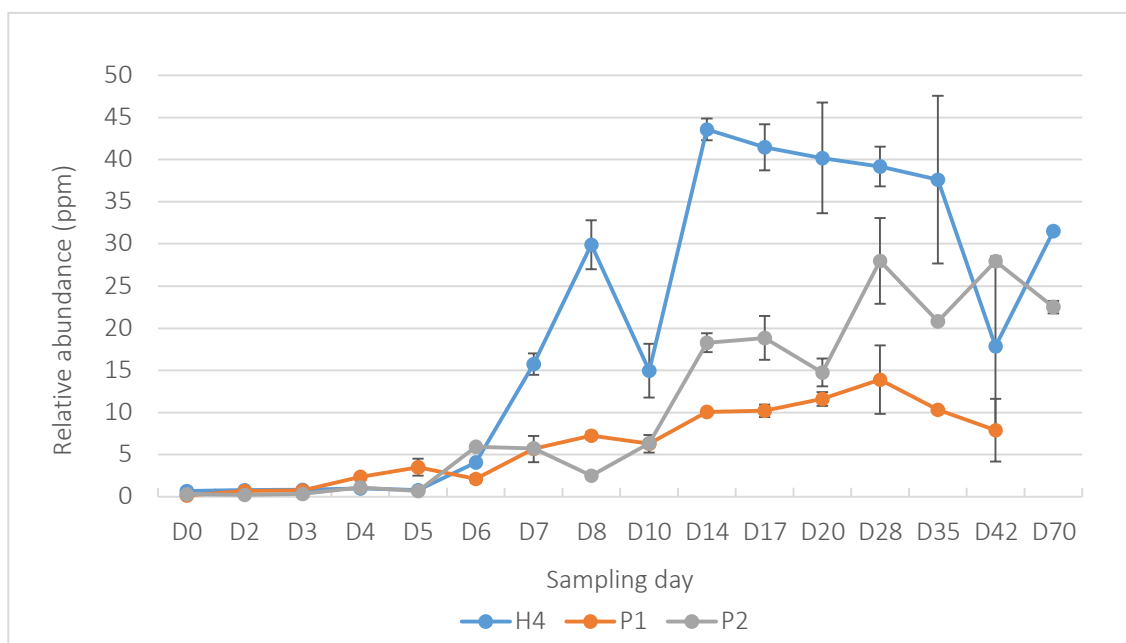


Figure 4.5: Comparison of myristic acid relative abundance trends within the tissue, through decomposition period of H4 (human 4), P1 (pig 1) and P2 (pig 2). Error bars represent standard deviation variation of (4) replicates.

Myristic acid is produced in the mammary gland and can also be ingested through diet. It is directly involved with hormonal and protein changes, and is also responsible for metabolic process control [86]. A 2011 study by Prasath et al. [87] also found that myristic acid has anti-fungal and anti-virulent properties, enabling it to mitigate systemic candidiasis of fungal species including *C. albicans* and *C. tropicalis*. This was observed through the reduction in spread of yeast cells within the host via increase of myristic acid. Although, this study was conducted on a Zebrafish host, this concept could provide potential insight into the natural mummification that is depicted in the human (H4) comparative to the pigs (P1 and P2). Furthermore, these antimicrobial properties within myristic acid have been discovered in a series of studies including those on mice, by Juárez-Rodríguez et al. [88] and is also discussed at length in review paper by Kumar et al. [89]. Visual observations illustrated signs of mummified tissue in both species. This phenomenon however, appeared to stunt decomposition within the human, whereas

the pigs only depicted little mummified tissue, early in decomposition and as a result, continued to decompose. The increased abundance of myristic acid and its anti-fungal properties may provide an explanation as to why decomposition failed to progress in the same manner as that observed within the pigs. Day 10 displays a decrease in relative abundance of myristic acid within the human, which is approximately during the period where the human had entered the bloat stage (day 8) (Figure 4.1). The biochemical changes and degradation of tissue resulting in gas building (during the bloat stage) may have impacted the abundance of myristic acid within the body. This is as enzymatic activity and the action of lipases responsible for chemical degradation during the bloat stage led to lipid breakdown, causing decrease in myristic acid levels [11, 16, 32].

A significant difference was observed in the amount of palmitoleic acid between P2 and P1 and between P2 and H4. This indicates that P2 had significantly higher levels of palmitoleic acid present within the tissues (Figure 4.6. Palmitoleic acid is abundantly found within the tissues and serum of liver and adipose tissue in humans and also in ruminant fat and dairy products [83].

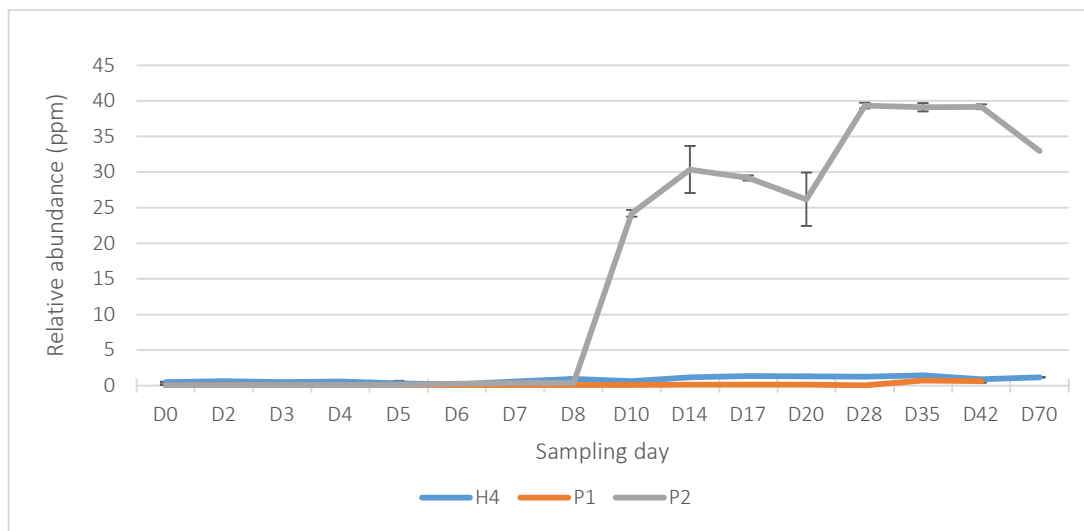


Figure 4.6: Comparison of palmitoleic acid relative abundance trends within the tissue, through decomposition period of H4 (human 4), P1 (pig 1) and P2 (pig 2). Error bars represent standard deviation variation of (4) replicates.

A large spike in palmitoleic acid was observed in P2 on day 10 (Figure 4.6) by which time the pig was in full bloat stage, whereas P1 was well into active decay. It is unclear what may have caused this spike in P2 and not in P1. Although both pigs weighed approximately 70 kg (Table 2.2) and were of similar age, these can differ due to differences in genetics, metabolism, physical activity, health, and age [90]. These factors can collectively contribute to the distinctions in fatty acid levels.

#### 4.2.5 SUMMARY

The fresh stages of decomposition showed little similarities in the fatty acid profile for the human (H4) and both pigs (P1 and P2). Myristic acid appeared to be the only compound present during mummification, within the tissue matrix of H4, but this was not observed in P1 and P2. Palmitoleic acid showed statistically significant differences between P2 and both other individuals (P1 and H4). Myristic acid was the only compound to show a statistically significant difference between the human and *both* pigs. This was driven by the large increase in myristic acid from the onset of mummification. Sterols within the tissues showed large variation between the species. Mummification had little effect on the sterol profile of the human and both pigs.

Among all the investigated compounds, myristic acid was the only one within the tissue that exhibited statistically significant differences between the human and both pigs. Although present in different abundances, the general lipid trends across both the human and pigs remain consistent as the stages of decomposition progressed.

#### 4.2.6 PIG VS HUMAN SKIN

Human and pig skin was the target matrix for lipid analysis in this study due to abundance of lipids within the skin matrix of both species. Skin matrix was thus examined in this study to investigate trends and patterns which could be allocated to stages of decomposition and furthermore, natural mummification. Visual observation accuracy is also highlighted, particularly within the skin, to examine the accuracy of visual changes in relation to fatty acid changes. Refer to section 2.5 and 2.6 for full method details.

#### 4.2.7 PCAS

##### 4.2.7.1 FATTY ACIDS

The fresh stage of decomposition for the human indicates some variability in the fatty acid profile until the time at which the first signs of mummified tissue appear (D0-D5) (Figure 4.7). This profile shares similarities with the final sampling days of the human (sampling days 105-202) indicating that the fresh and final sampling days within the human skin show parallels. A similar effect is in VOC studies where fresh and advanced/skeletonisation stages of decomposition show similar profiles to one another, while variation is observed during the middle period of decay [14, 33].

A shift in fatty acid profile is depicted during the middle period of decomposition (highlighted in the purple circle). This clustering suggests that once the first signs of mummified tissue are depicted,

there is fatty acid deviation from the early-day samples, followed by secondary deviation once later sampling periods are achieved. Limited variation is depicted within the middle period of decomposition, leading to the cluster of sampling days (highlighted in purple circle). This cluster is due to the dominance in myristic acid observed within the loadings plot (See F-6 in Appendix F). The early day samples for the pigs appear to cluster near a few of the early-day and late-day human samples (highlighted in the orange circle). This suggests that the fatty acids within the skin of pigs during early decomposition have limited variability. These sampling days also share similarities to the fatty acid profile during the early and later periods of decay within human skin. The compound responsible for this clustering is oleic acid (See Figure F-4 from Appendix F). Progression into decomposition for pigs depicts a shift in the fatty acid profile (D5 onwards), dissimilar to the shift observed within the human samples. This shift is attributed to palmitoleic acid (Figure F-4 from Appendix F). Natural mummification did not appear to impact the fatty acid profile of the pigs.

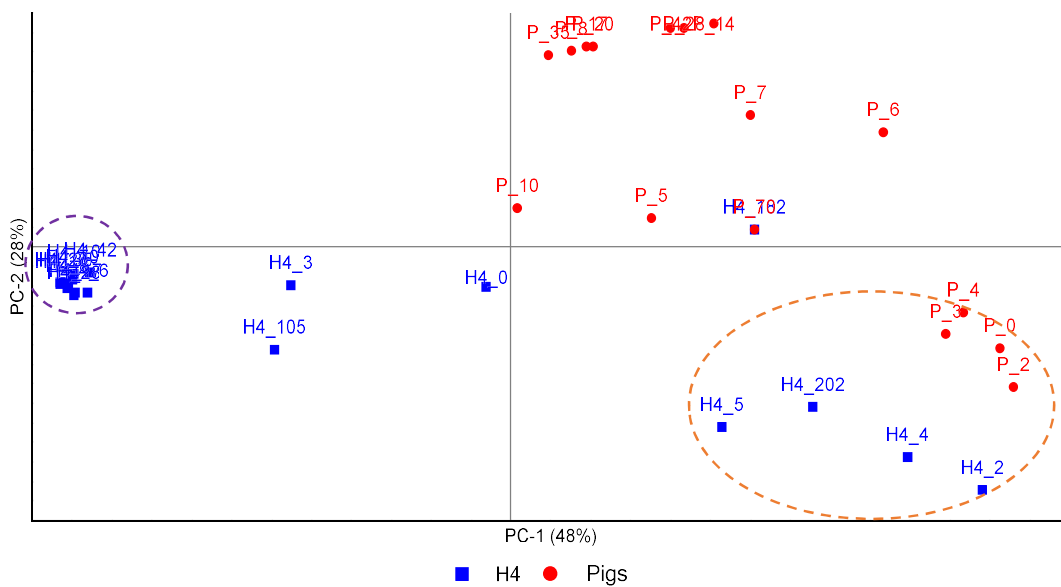


Figure 4.7: Principal component analysis (PCA) of fatty acid variation within the skin of human 4 (H4) and pigs (pig 1 and pig 2 averaged). Orange circle highlights D0-D4 for pigs and a few early (D2, D4, and D5) and late (D202) samples for human. Purple circle highlights middle period of decomposition for H4.

#### 4.2.7.2 STEROLS

Sterols generally showed variation between the human and pigs, with an overlap in sterol composition during the fresh stage of decay (Figure F-5 from Appendix F). Differences were observed in the sterol composition of the two species with the progression of decomposition, showing clear

distinctions between both species. Sterols did not appear to show large variation within each species. This trend is commonly observed in sterol behavior, with limited variation detected [91-93]. Mummification did not appear to have any effect on the sterol profile within the human or pigs.

#### 4.2.8 ANOVA

A one-way analysis of variance (ANOVA) was conducted on the relative abundance data of all compounds between H4, P1 and P2 to identify compounds that had statistical significance between the three sample groupings. This was conducted separately for fatty acids and sterols. Once a compound was deemed significant, a student t-test ( $p \leq 0.5$ ) with the Bonferroni correction t-test were applied to identify where the significance lies within the sample grouping.

Table 4.3: Depiction of compound significance in skin comparison because of t-test, with Bonferroni correction, where H4 = human 4, P1= pig 1 and P2= pig 2. (i.e., H4 vs P1 = human 4 vs pig 1 compound comparison) Compounds showing statistical significance between two sample groups indicated through the denomination.

Fatty acids	H4 vs P1	H4 vs P2	P1 vs P2	Sterols	H4 vs P1	H4 vs P2	P1 vs P2
Decanoic Acid	x			Coprostanol			
Lauric Acid				Cholesterol			
Tridecanoic Acid	x	x		5 $\alpha$ -cholestanone			
Azelaic Acid		x		Lithocholic			
Myristic Acid	x	x		Ergosterol			
Sebacic Acid		x		Stigmasterol			
Pentadecanoic Acid				Deoxycholic acid		x	x
Palmitoleic Acid	x	x	x	$\beta$ -sitosterol		x	
Linoleic Acid		x	x	25-hydroxycholesterol			
Oleic Acid							
Nonadecanoic Acid							
Arachidic Acid							
Behenic Acid							
Tricosanoic Acid	x						
Hexacosanoic Acid							

Tridecanoic acid, myristic acid and coprostanol all showed statistically significant differences between H4 and both pigs (P1, P2) (Table 4.3). Of these compounds, myristic acid was of most interest, due to tridecanoic acid and coprostanol being present in levels (Figure B-3 and B-17 from Appendix B) lower than the LOQ (Table 3.3). During the earlier stages of decomposition, similarities are observed within the myristic acid profile of H4, P1 and P2 (Figure 4.8). The onset of mummification in H4 (D6 onwards) appeared to have direct influence on the levels of myristic acid within the lipid profile creating a large variation of this acid compared with both pigs. As investigated in section 4.2.4, myristic acid has been known to carry anti-fungal and anti-virulent properties [87-89]. These properties may have inhibited the persistence of microbial and fungal activity within the skin of the human, and therefore stunted matrix decomposition. As a result, the large abundances of myristic acid during decomposition has resulted in natural mummification of the skin.

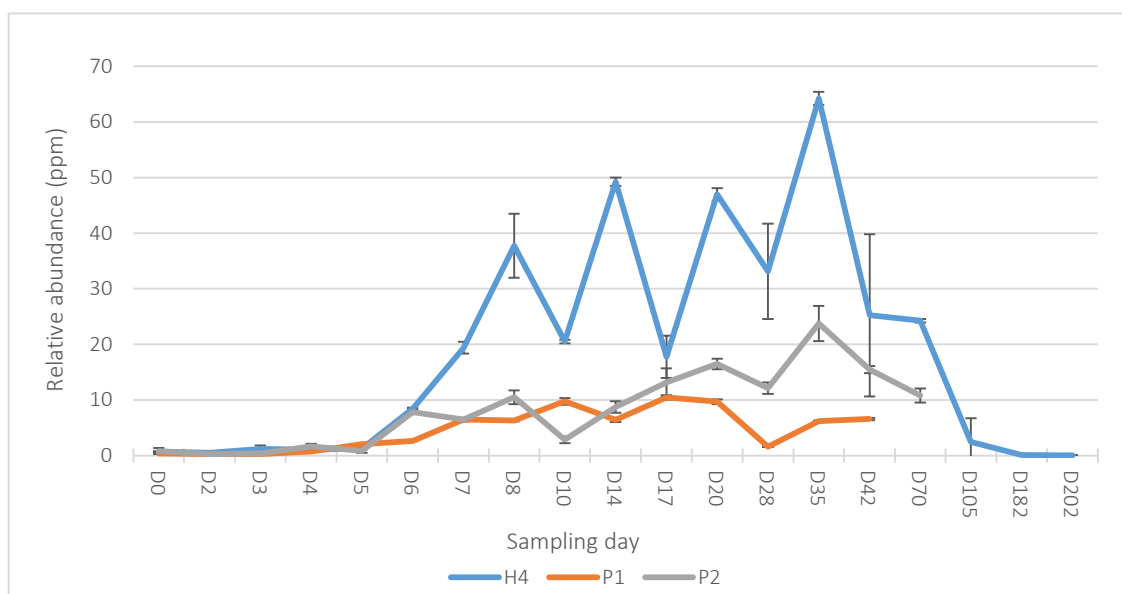


Figure 4.8: Comparison of myristic acid relative abundance within the skin, through decomposition period of H4 (human 4), P1 (pig 1) and P2 (pig 2). Error bars represent standard deviation variation of (4) replicates.

Deoxycholic acid was found to show statistically significant differences between H4 vs P2 and P1 vs P2 (Table 4.3). Upon investigation, P2 appeared to show much lower values of deoxycholic acid compared to H4 and P1 (Figure B-23 from Appendix B). Deoxycholic is a bile acid which is naturally found within the bile of the body and acts to solubilise and absorb fats within the intestine [94]. It is suspected that the gut microbiome composition of P2 has affected the synthesis of bile acids, leading to variation in deoxycholic acid compared to P1. This will need to be further investigated.

Palmitoleic acid was observed at very large abundance within P2 skin samples throughout decomposition, when compared with H4 and P1 (Figure B-8 from Appendix B). As evident in section 4.2.3.1, palmitoleic acid is commonly found within in ruminant fat and dairy products [83]. The consistently increased amounts of palmitoleic acid found within the skin of P2 suggest that the composition of the skin layer was quite fatty in nature compared to P1 and H4. This trend was also observed within the tissue matrix, where P2 had higher relative abundances of palmitoleic acid compared to P1 and H4. This further supports the concept of variability within age, lifestyle and health contributing as a large factor to the differences of this acid.

#### 4.2.9 SUMMARY

General lipid trends across the human and pigs were consistent between both species, although present in different abundances. Fatty acid composition within the skin of the decomposing human during the fresh stage did not show consistent patterns. The bloat stage results in shift of fatty acid influence, caused by myristic acid, which is consistent through most of the remaining period of decomposition for the human.

In the fresh stage of decay, sterols exhibited similarities between humans and pigs. Once the bloat stage was observed for the human, the sterol profile depicts differences from the pig, however, does not show large variation for the remainder of decomposition. A similar trend was depicted for the pigs, illustrating sterol composition having differences in pigs and humans, once the fresh period of decay has passed.

Tridecanoic acid, myristic acid, hexacosanoic acid and coprostanol all showed statistically significant difference between the human and both pigs, although myristic acid was the only compound to display this difference at quantifiable concentrations.

### 4.3 WARMER CLIMATE STUDY CONCLUSIONS

The skin and tissue matrix within human and pigs appeared to show similarities in relation to the method of lipid behavior and progression of the two species within both matrices. However, dissimilarities were observed in terms of the relative abundance of these compounds within each species. A similar trend was observed within the skin matrix samples, whereby the fatty acid and sterol

content within the skin was generally slightly higher in abundance compared with the pig skin. These fatty acids and sterols will need further investigation, potentially on a large-scale study.

Myristic acid in both the skin and tissue of the human matrix appeared to show much larger variation in relative abundance compared with the pigs. An increase in abundance of myristic acid was observed once the onset of mummification occurs, which affects both the skin and tissue matrix. The anti-fungal and anti-viral properties of this compound present in large amounts on both matrices are speculated to have inhibited microbial and fungal activity, which consequently may have depleted the onset of traditional decomposition (fresh, bloat, active, advanced decay).

The study noted larger abundances of various compounds in human samples compared to pigs. This may be attributed to the diverse range of compounds that humans are exposed to, potentially influenced by factors such as diet and lifestyle. These differences in compound abundances further highlight the distinct metabolic and biochemical characteristics between the two species.

Pigs and humans exhibit distinct responses to natural mummification. While pigs showed signs of mummification early in decomposition (day 1) without hindering the subsequent stages, humans demonstrated a preservation-like effect with a prolonged bloat stage and a direct transition into the advanced stage. This difference suggests that the impact of natural mummification varies significantly between the two species. Notably, natural mummification in humans resulted in the preservation of the skeletal structure and substantial levels of skin remaining on the body. This preservation effect contrasts sharply with the decomposition observed in pigs, where mummification did not prevent the progression through the bloat, active, and advanced stages

The variation in decomposition experiences between humans and pigs due to natural mummification implies that the mechanisms and effects of this phenomenon differ significantly. Pigs, despite undergoing mummification, continued decomposition, indicating that their response to this process does not mirror the preservation observed in humans.

It can be concluded that during the warmer seasonal trial, pigs and humans indicate variation in decomposition both visually and at a lipid level (both skin and tissue matrix), in the instances of natural mummification. Pigs are therefore not suitable analogues when investigating human decay in instances of natural mummification as evidenced by differences in progression through decomposition stages, preservation of skeletal structure, and variations in compound abundances.



# CHAPTER 5 PIG VS HUMAN: COOLER SEASON STUDY

This section involves a comparative analysis of the skin and tissue found in human and pig bodies after death, specifically during the Australian winter period. The focus is on examining variations in the lipid makeup, encompassing fatty acid and sterol compositions, between human and pig tissue, as well as human and pig skin. The objective is to pinpoint disparities in the lipid profiles of these two species and gauge the degree of such distinctions. Additionally, a comparison is drawn regarding the observable patterns and stages of decomposition in both human and pigs. This analysis holds particular significance in unveiling how colder climates influence lipid degradation within the tissue and skin of these species. A cooler season in this instance refers to a period of the year characterised by lower temperatures compared to the warmer seasons. This is associated with autumn and winter, which are known for shorter days, longer nights, and a decline in temperatures. Moreover, the study delves into the extent of these influences and how they interplay with the process of natural mummification. The identification of natural mummification is initially established by visual assessments that involve desiccation and the manifestation of orange colour changes in the skin. The insights garnered from this research will be instrumental in enhancing our comprehension of the dependable utilisation of pigs as biochemical counterparts for humans.

5.1 MATERIAL AND METHODS

One human and two pigs were used for the cooler climate study, all three being clothed in a cotton t-shirt due to concurrent decomposition studies. The trial commenced on the 11<sup>th</sup> of August 2021 (Australian Winter), with the final sampling day carried out on the 21<sup>st</sup> of December 2021. The individuals used in this study were human 5 (H5) and pigs 3 (P3) and 4 (P4). H5, P3 and P4 were out on the same day (Table 5.1) to ensure as consistency in environmental conditions that affect the two specimens. Samples for all three individuals were taken on the same sampling day post-mortem to ensure the same amount of decomposition time had passed before sample collection. Images of P3, P4 and H5 were taken on all sampling days to capture visual decomposition at the time of sampling. Refer to section 2.5 and 2.6 for full method details on sampling collection and preparation.

Table 5.1: Cooler climate study information of pig 3 (P3), pig 4 (P4) and human 5 (H5).

Individuals	Date of placement	Days sampled post-mortem	Final sampling date
-------------	-------------------	--------------------------	---------------------

Human 5 (H5)	11 <sup>th</sup> June 2021	0, 1, 2, 3, 4, 5, 6, 10, 17, 19, 26, 31, 35, 42, 49, 56, 63, 69, 84, 105, 132	21 <sup>st</sup> December 2021
Pig 3 (P3)	11 <sup>th</sup> June 2021	0, 1, 2, 3, 4, 5, 6, 10, 17, 19, 26, 31, 35, 42, 49, 56, 63, 69, 84, 105, 132	21 <sup>st</sup> December 2021
Pig 4 (P4)	11 <sup>th</sup> June 2021	0, 1, 2, 3, 4, 5, 6, 10, 17, 19, 26, 31, 35, 42, 49, 56, 63, 69, 84, 105, 132	21 <sup>st</sup> December 2021

## 5.2 RESULTS

### 5.2.1 VISUAL COMPARISON AND OBSERVATIONS

Human 5 (H5) exhibited first signs of change on sampling day 13, with the face transitioning from fresh to active decay (see Table K-4 from Appendix K). The torso of H5 began bloating on day 17 post-placement, where the first signs of mummified tissue were observed on the arms and face. Pig 3 and pig 4 entered bloat on day 10 and 17 respectively (see Table K-5 and K-6 from Appendix K). By this stage the head and neck for both pigs were in active decay. Day 23 for both pigs showed signs of mummified tissue, predominantly on and around the limbs. Human 5 had completely mummified by day 42, where the face had reached a more advanced stage of decomposition, being declared in advanced decay stage with no active decay depicted (Figure 5.1). Large mass loss was depicted for both pigs by day 35, where they were both staged as being in active decay. Advanced decay for pig 3 was illustrated on day 63 and on day 69 for pig 4.

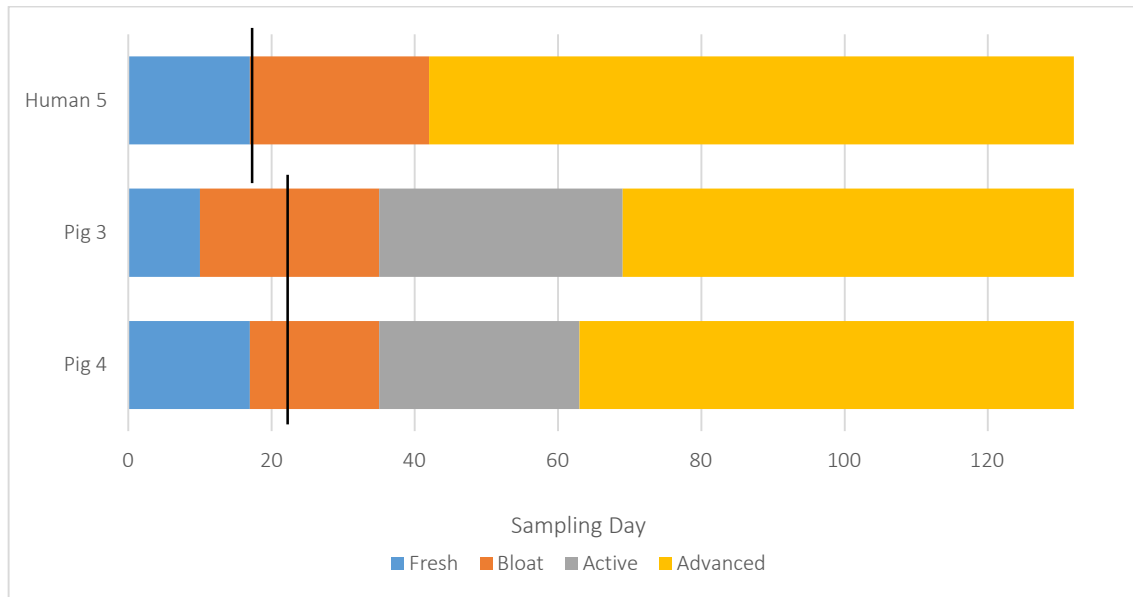


Figure 5.1: Stages of decomposition (fresh, bloat, active and advanced decay) shown as a comparison between Human 5 (H5), Pig 3 (P3) and Pig 4 (P4). First signs of observed mummified tissue is denoted by the black line.

When the stages of decomposition are compared for H5 and pigs 3 and 4 (Figure 5.1), H5 and P4 followed a similar fresh and bloat stage timeline. H5 did not undergo active decay and therefore transitioned from the bloat stage into advanced decay. Pig 3 and P4 both finished their bloat stage at the same time, resulting in similarities for the remainder of their decomposition period. The first signs of mummified tissue observed is highlighted in Figure 5.1, denoted by the black line (day 17 for human and day 23 for both pigs).

Signs of mummified tissue were observed on both the human and porcine investigated, but only appeared to have preservation-like effects for the human. Within the pigs, natural mummification presented itself through spotted orange colour changing of the skin. Within the human, the effects of natural mummification appeared more consistently (See Appendix K-4). Figure 5.2 displays the long-term effects of natural mummification, where the human is observed in an advanced mummified stage (day 69). It can be depicted that the effects of natural mummification have resulted in conservation of the skeletal structure with minimal disruption to the body. This has occurred due to the absence of the active decay stage, resulting in decreased insect activity. In contrast, the same sampling day (day 69) for the pigs can be exhibit through Figure 5.3, both also being categorised at an advanced stage. However, it is apparent that the effect of natural mummification in the pigs has not resulted in a similar preservation to the human, as they have both progressed through all stages of decomposition and are now nearing a skeletal state.



Figure 5.2: Day 69 for H5, exhibiting effects of natural mummification.



Figure 5.3: Day 69 for a). P1 and b). P2, exhibiting effects of natural mummification.

### 5.2.2 PIG VS HUMAN TISSUE

Lipid analysis centered on human and pig tissue, chosen as the focal matrix due to its widespread presence across both species. This selection made the matrix a fitting basis for contrasting the lipid composition between the two, with specific attention directed towards identifying trends linked to decomposition stages and natural mummification. Refer to section 2.5 and 2.6 for full method details.

### 5.2.3 PCAS

#### 5.2.3.1 FATTY ACIDS

Fatty acid variation is depicted throughout decomposition for both the human and pigs (Figure 5.4). The samples from the early and middle stages for the human show general clustering in the bottom-right quadrant of the PCA (highlighted in the orange oval), illustrating that during these periods of decay, the fatty acid profile within the skin matrix is similar. This cluster is attributed to large abundance of oleic acid, which is further investigated below (section 5.2.4). A shift was observed in the fatty acid profile with the progression of decomposition in the human, where the samples appear to cluster on the left-side of the PCA (highlighted by purple oval). The fatty acid profile of the early sampling days for the pigs (D0-D10) more closely resembles that of the early-middle human samples (highlighted in the orange oval), when compared to the middle-late stages of the pigs. The progression of decomposition within the pigs showed a similar pattern to the human, whereby the fatty acid profile changes. This shift is highlighted by the purple circle, caused by the large influence of myristic acid (see Figure G-1 from Appendix G). These changes depict that for both the human and pigs, the fatty acid profile during the earlier stages of decay is different to the middle and late stages of decay. Natural mummification could not be correlated to any changes within the fatty acid profile.

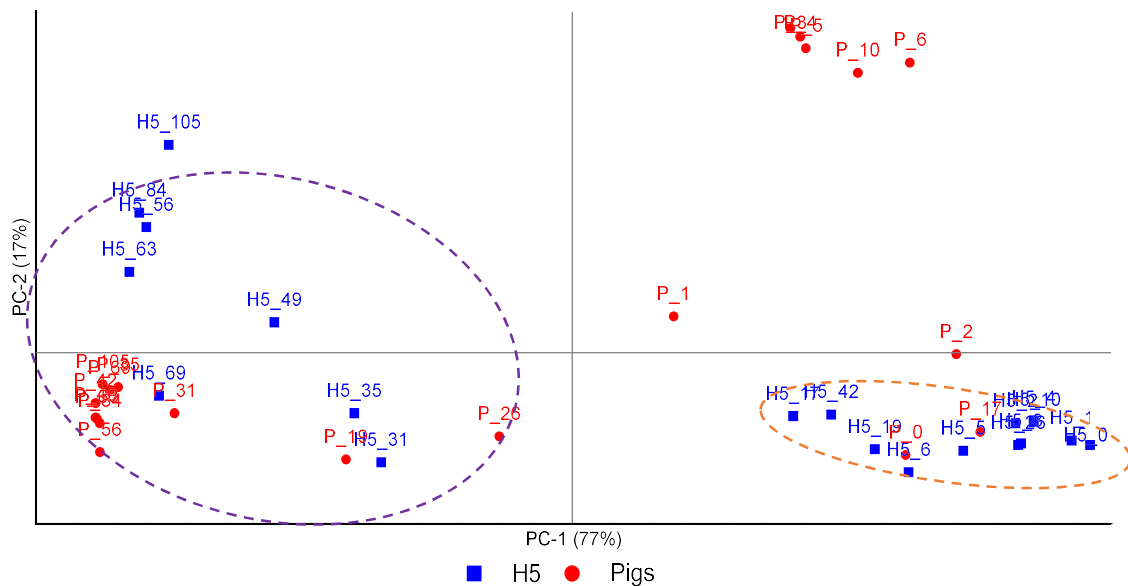


Figure 5.4: Principal component analysis (PCA) of fatty acid variation within the tissue of human 5 (H5) and pigs (P1 and P2 averaged). Early and middle stages samples for H5 is highlighted in orange oval. Middle and late stages of decomposition for both pigs and H5 is highlight in purple oval.

### 5.2.3.2 STEROLS

Sterol behaviour within the tissues showed similar patterns between the human and pig samples. This can be illustrated by the large cluster which consists of all the human and pig samples, except for sampling day 105 for the human and day 42 for the pigs (Figure 5.5). This cluster is largely attributed to cholesterol influence. No real trends were observed within the sterol profile, which indicated that decomposition has little impact on the sterol profile of both the human and pigs. Variation in the levels of b-sitosterol and lithocholic acid appear to impact the outlier days (day 105 for human and day 42 for pigs) (Figure G-2 from Appendix G). Natural mummification and stages of decay did not appear to impact the sterol profile within the tissue of the human or the pigs. This is in-line with literature investigating the use of sterols as biomarkers, due to its ability to persist in decomposing environments [91-93]. This indicates that sterols may not be suitable when investigating natural mummification as sterols remained unaffected by this phenomenon.

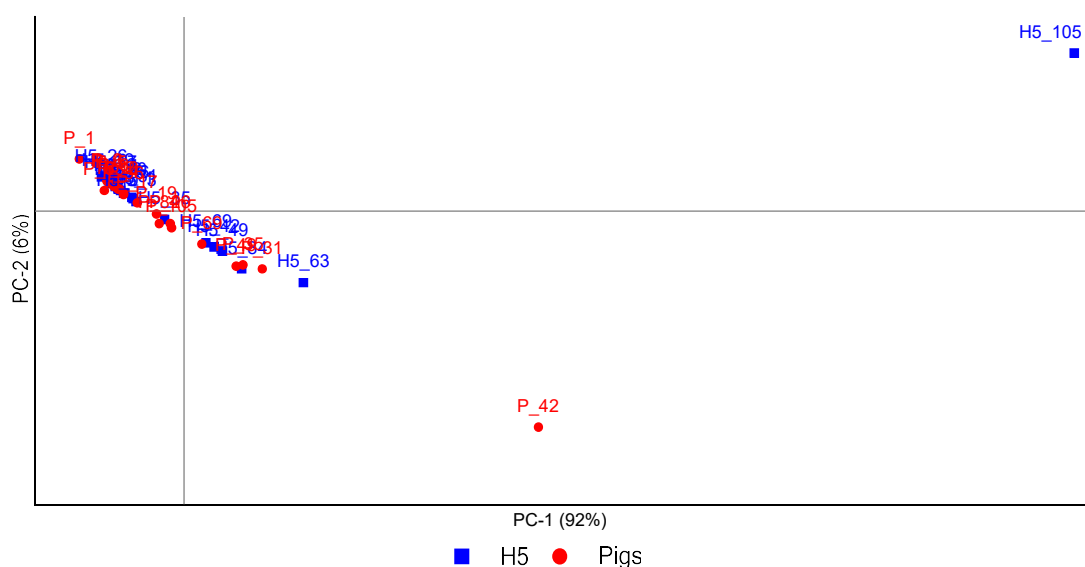


Figure 5.5: Principal component analysis (PCA) of sterol variation within the tissue of human 5 (H5) and pigs (P1 and P2 averaged).

### 5.2.4 ANOVA

A one-way analysis of variance (ANOVA) was conducted on the relative abundance data of all compounds between H5, P3 and P4 to identify compounds which had statistical significance between the three sample groupings. Once a compound was deemed significant, a student t-test ( $p \leq 0.5$ ) with the Bonferroni correction t-test were applied to identify where the significance lies within the sample grouping.

Table 5.2: Depiction of compound significance within tissue samples because of t-test, with Bonferroni correction, where H5 = human 5, P3= pig 3 and P4= pig 4. (i.e., H5 vs P3 = human 5 vs pig 3 compound comparison) Compounds showing statistical significance between two sample groups indicated through the denomination 'x.'

Fatty acids	H5 vs	H5 vs	P3 vs	Sterols	H5 vs	H5 vs	P3 vs
	P3	P4	P4		P3	P4	P4
Decanoic Acid				Coprostanol			
Lauric Acid				Cholesterol			
Tridecanoic Acid	x		x	5 $\alpha$ -cholestanone			
Azelaic Acid				Lithocholic	x	x	
Myristic Acid				Ergosterol			
Sebacic Acid				Stigmasterol	x	x	x
Pentadecanoic Acid	X	X		Deoxycholic acid			
Palmitoleic Acid				$\beta$ -sitosterol			
Linoleic Acid				25-hydroxycholesterol			
Oleic Acid	X	X					
Nonadecanoic Acid							
Arachidic Acid							
Behenic Acid							
Tricosanoic Acid		x					
Hexacosanoic Acid	x						

The lipid profile within the tissues showed statistically significant differences between human and both pigs for compounds including: pentadecanoic acid, oleic acid, lithocholic acid and stigmasterol (Table 5.2). Of these compounds' oleic acid (Figure E-10 from Appendix E) was the only compound presenting relative abundance at levels greater than the calculated LOQ for compounds (Table 3.3). Oleic acid is the most abundant chemical compound found within the fatty tissues of meat-bearing animals [95]. The behaviours of oleic acid (Figure 5.6) depict fluctuation between H5, P3 and P4, post day 35. This time-point of decomposition reflects the transition of the bloat to the advanced stage of decay for the human and could be responsible for this shift.



When addressing the substantial error bars observed in the tissue matrix of humans concerning oleic acid levels (Figure 5.6), several factors warrant consideration in explaining this variation. Differences in decomposition dynamics, degradation of samples, and post-mortem redistribution of lipids within the body can cause fluctuations in the amount of lipid detected. Hence, the importance of conducting replicates is underscored as a means of addressing and capturing this variability comprehensively.

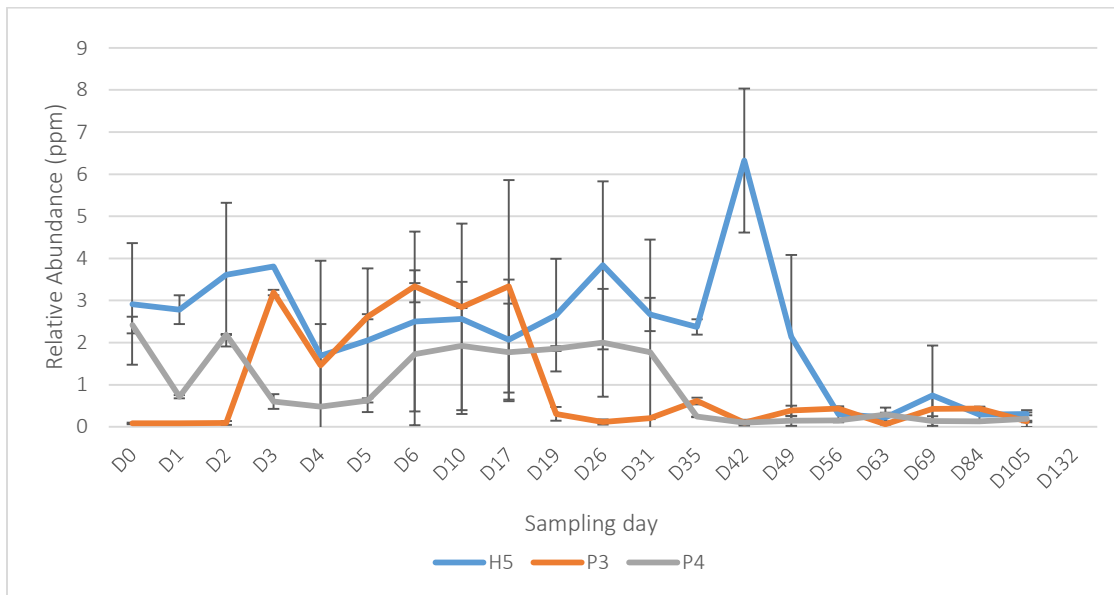


Figure 5.6: Comparison of oleic acid relative abundance within the tissue, through decomposition period of H5 (human 5), P3 (pig 3) and P4 (pig 4). Error bars represent standard deviation variation of (4) replicates.

### 5.2.5 SUMMARY

Small distinctions can be made in the fatty acid profile the human that can be loosely broken down into the early-middle (fresh and bloat) and middle-late (bloat, mummification, and advanced decay) stages of decay. The pigs showed a similar trend as that observed within the human, with early and middle (fresh and bloat) stages showing similarities in fatty acid profiles and the progression of decomposition (into the middle-late stages) indicating differences in the fatty acid profile. Oleic acid was the only compound showing statistically significant differences between both species, at relative abundances greater than the limit of quantification. Sterols within the tissue of the human and pigs showed little variation throughout decomposition, with cholesterol contributing highly to the lipid profile. Natural mummification did not appear to impact the fatty acid or sterol profile within the tissue matrix for the human or pigs.

The tissue matrix did not appear to show large differences regarding the fatty acid and sterol composition between the human and both pigs, with most compounds of large abundances following a similar pattern throughout decomposition. The prolonged onset of stages of decomposition in both humans and pigs, compared to warmer weather, may have resulted in reduced variations in lipid composition. Furthermore, it is concluded that natural mummification does not affect the composition of lipids within the tissue matrix, leaving it as a surface level (skin) effect.

#### 5.2.6 PIG VS HUMAN SKIN

Human and pig skin was the target matrix for lipid analysis due to its ubiquitous nature in both species. This matrix was therefore deemed an appropriate means to compare the lipid profile within the two species, with particular emphasis on any trends which can be allocated to stages of decomposition or natural mummification. The accuracy of visual observations is also tested to see how changes in visual decomposition, particularly in the skin, is reflected in the lipid profile. Refer to section 2.5 and 2.6 for full method details.

#### 5.2.7 PCAS

##### 5.2.7.1 FATTY ACIDS

A clear distinction was observed in the fatty acid profile of the human and pigs (Figure 5.7), with all pig samples generally clustering on the right side of the PCA, while most of the human samples are clustered on the left side of the PCA. This separation is a clear indication of the varying fatty acid profiles that are being exhibited by the human and pigs. This variation is attributed to the high levels of palmitoleic acid (see Figure G-4 from Appendix G), which was detected within the samples, which was statistically significant between the human and both pigs (Table 5.3), discussed further in section 5.2.8.

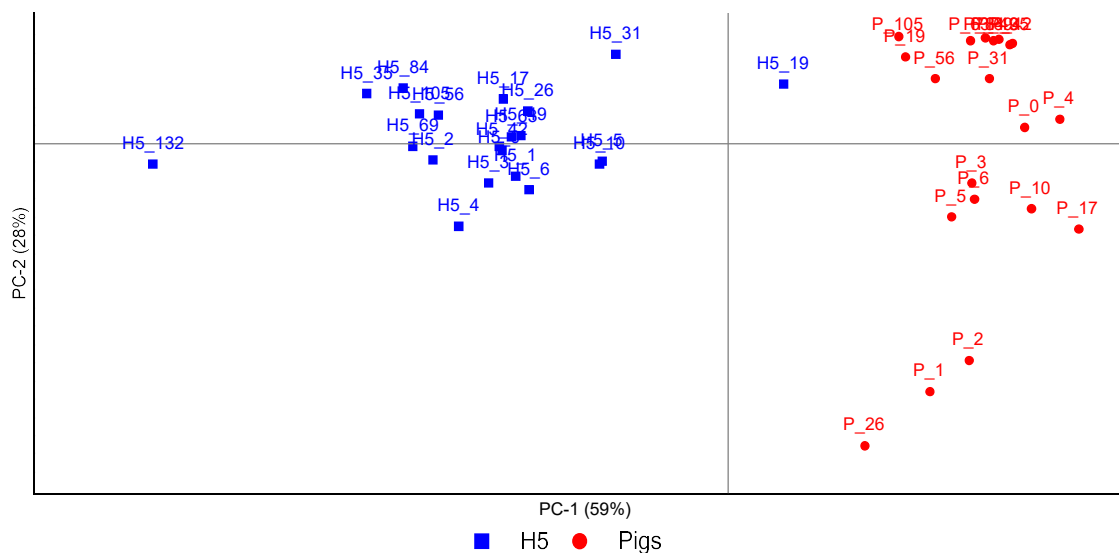


Figure 5.7: Principal component analysis (PCA) of fatty acid variation within the skin of human 5 (H5) and pigs (P1 and P2 averaged).

No trends could be depicted from the fatty acid profile of the human as far as stages of decay are concerned.

#### 5.2.7.2 STEROLS

No differences were observed in the sterol profile of the human and pigs.

#### 5.2.8 ANOVA

A one-way analysis of variance (ANOVA) was conducted on the relative abundance data of all compounds between H5, P3 and P4 to identify compounds which had statistical significance between the three sample groupings. Once a compound was deemed significant, a student t-test ( $p \leq 0.5$ ) with the Bonferroni correction t-test were applied to identify where the significance lies within the sample grouping.

Table 5.3: Depiction of compound significance within skin samples because of t-test, with Bonferroni correction, where H5 = human 5, P3= pig 3 and P4= pig 4. (i.e., H5 vs P3 = human 5 vs pig 3 compound comparison) Compounds showing statistical significance between two sample groupings indicated through the denomination 'x'.

Fatty acids	H5 vs P3	H5 vs P4	P3 vs P4	Sterols	H5 vs P3	H5 vs P4	P3 vs P4
Decanoic Acid	x	x		Coprostanol	x	x	
Lauric Acid	x			Cholesterol			
Tridecanoic Acid				5 $\alpha$ -cholestanone	x	x	
Azelaic Acid				Lithocholic			
Myristic Acid				Ergosterol	x	x	
Sebacic Acid				Stigmasterol	x	x	
Pentadecanoic Acid	x		x	Deoxycholic acid			
Palmitoleic Acid	x	x		$\beta$ -sitosterol	x		
Linoleic Acid				25-hydroxycholesterol	x	x	
Oleic Acid	x		x				
Nonadecanoic Acid	x	x	x				
Arachidic Acid	x	x					
Behenic Acid	x	x					
Tricosanoic Acid							
Hexacosanoic Acid							

Most of the sterol compounds showed statistically significant differences between the humans and both pigs (Table 5.3). Decanoic acid, palmitoleic acid, arachidic acid, behenic acid, 5 $\alpha$ -cholestanone, coprostanol, ergosterol, stigmasterol and 25-hydroxycholesterol all showed statistically significant differences between the two species type ((human (H5) and pigs (P3 and P4)). Of these compounds palmitoleic acid, lithocholic acid, coprostanol, 5 $\alpha$ -cholestanone, stigmasterol and 25-hydroxycholesterol were the only compounds that were detected at levels greater than LOQ and could therefore be further investigated. Palmitoleic showed large fluctuations in relative abundance within H5, compared to P3 and P4 whose abundance for the acid remained consistent (Figure D-8 from Appendix D). It is known that palmitoleic acid is commonly found in serum and adipose, in areas consisting of high fat levels [83]. It is therefore expected for H5 to have increased levels of palmitoleic

acid due to the large distribution of fatty tissue within and under the skin. Furthermore, palmitoleic acid is a known breakdown product of oleic acid [39], explaining the increase of this compound with the progression of decomposition within the human.

Lithocholic acid is a bile acid which is produced by intestinal flora and acts as a detergent in solubilising fat for absorption in the intestine [96]. Although the presence of lithocholic acid in high levels is not surprising due to increased possible production from the body to solubilise fat while the human was still living, it is unclear as to why such fluctuation were depicted through decomposition (Figure 5.8). It is possible that the progression of decomposition and breakdown of cells within the body resulted in increases and decreases of lithocholic acid release around the body (particularly on day 2). This is still a speculation and will need to be further investigated for confirmation.

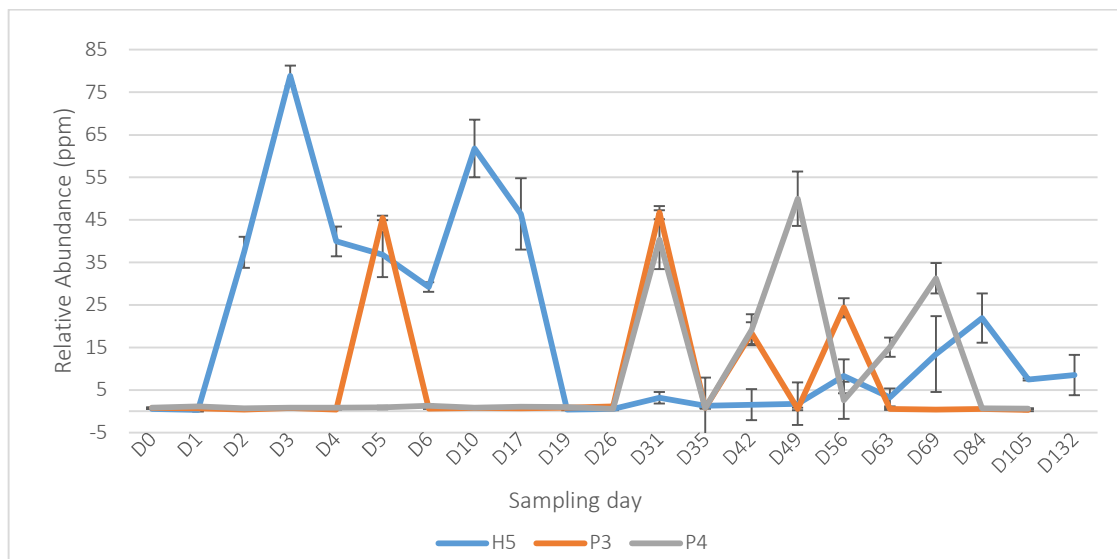


Figure 5.8: Comparison of lithocholic acid relative abundance within the skin, through decomposition period of H5 (human 5), P3 (pig 3) and P4 (pig 4). Error bars represent standard deviation variation of (4) replicates.

Stigmasterol appeared in low relative abundances for both pigs until approximately day 31 of sampling had commenced (Figure 5.9). This period coincides with the approximate onset of the active decay stage for both pigs. Stigmasterol is a phytosterol which has previously been detected in forensic lipid investigations, suggesting the presence of plant and fungal residue [53, 97]. The presence of this compound during the onset of active decay stages is suspected to occur with the increase in fungal activity occurring during the putrefaction stage. The fluctuating presence of this compound was also observed on the skin matrix of the human from day 3 onwards. Although this could not be correlated

to the onset of the active decay stage, the presence of this compound could be considered a ‘natural sterol background’ due to soil contamination [91, 93]. It is possible that rainfall experienced during the earlier periods of decomposition for the human (Figure 6.2) has resulted in soil and subsequently phytosterol transfer onto the skin matrix. It is speculated that rainfall did not have the same effect on the pigs, due to the excess amounts of hair found on the pig skin which may have shielded phytosterol transfer from soil. When addressing the presence of large error bars in the stigmasterol acid levels observed within the skin matrix, the contributing factors of this event were deduced to include the effects of decomposition dynamics and degradation of samples within replicates, the potential interaction of this compound with other compounds, and the post-mortem redistribution of lipids within the skin.

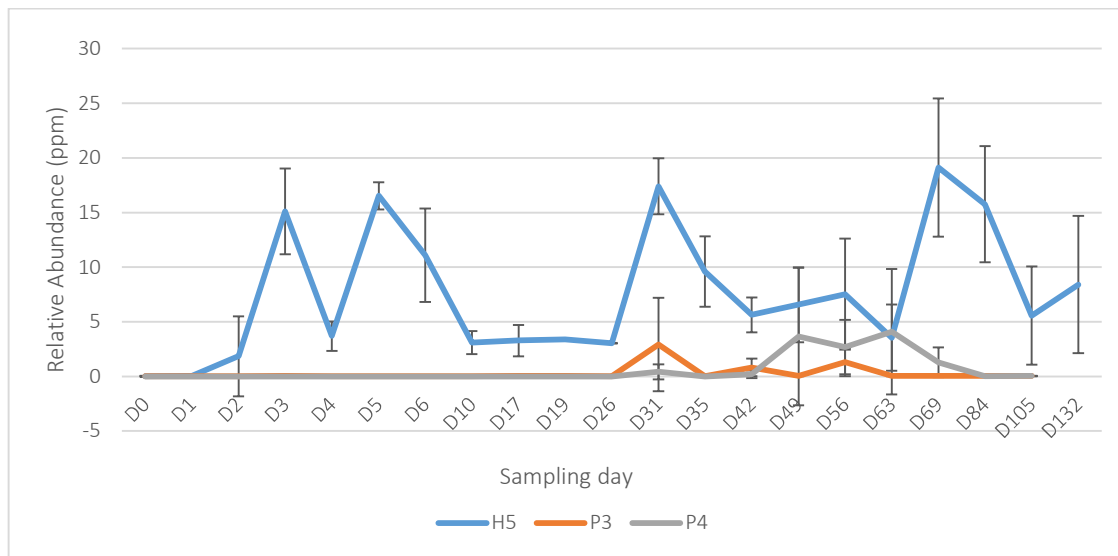


Figure 5.9: Comparison of stigmasterol relative abundance within the skin, through decomposition period of H5 (human 5), P3 (pig 3) and P4 (pig 4). Error bars represent standard deviation variation of (4) replicates.

Coprostanol is a known faecal steroid, which is produced in the gut of higher animals, commonly used as a faecal biomarker [91, 98, 99]. This occurs with the microbial degradation of cholesterol and constitutes approximately 60 % of the total sterol content in faeces [98]. Coprostanol was found in increasing concentrations in the human until day 5 after which a decline was observed (Figure 5.10). A secondary increase was detected on day 31 within the human, after which a general decrease occurred. The first increase of this compound (day 2-5) is suspected to occur due to the release of bodily and faecal fluids from the body and onto the skin matrix. A decline was then observed, which could be correlated to rainfall resulting in decreasing concentrations of this compound remaining

on the skin. A subsequent spike was then observed on day 31, which could be due to the excess amounts of fluid surrounding the sampling site due to the face of the human being in an active decay state, as well as continued faecal fluid release. Within the pigs, coprostanol was found as much lower concentrations throughout decomposition compared to the human (Figure 5.10). Lower abundances of coprostanol have been documented in ruminant and other animals (apart from humans), who instead contain a higher relative proportion of other sterols, including sitosterol and campersterol from their high herbivorous diet [98]. Factors such as variances in potential sample degradation, analytical variability (sample preparation and extraction), and the redistribution of lipids post-mortem within the body can all contribute to the observed fluctuations in detected lipid quantities.

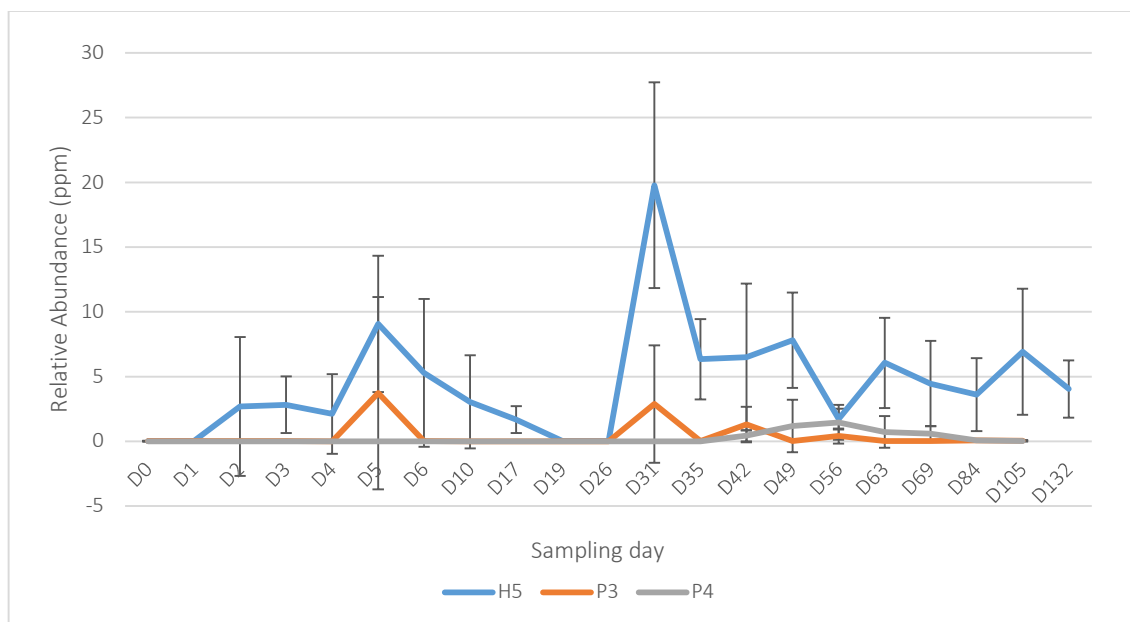


Figure 5.10: Comparison of coprostanol relative abundance within the skin, through decomposition period of H5 (human 5), P3 (pig 3) and P4 (pig 4). Error bars represent standard deviation variation of (4) replicates.

5 $\alpha$ -cholestanone is a sterol ubiquitously found within soils [93] and were present within both the human and pigs (Figure 5.11). The relative abundance of this compound was found at similar concentrations and at similar trends (increasing and decreasing) to stigmasterol (Figure 5.9). As discussed, the suspected rainfall (Figure 6.2) and soil movement aspect of decomposition within the human resulted in increase and decrease of relative abundances for stigmasterol. 5 $\alpha$ -cholestanone is therefore also expected to progress through the same trends as stigmasterol, due to both sterols being of plant and soil origin [93, 99]. The trends for both compounds were observed similar in both the human and pigs.

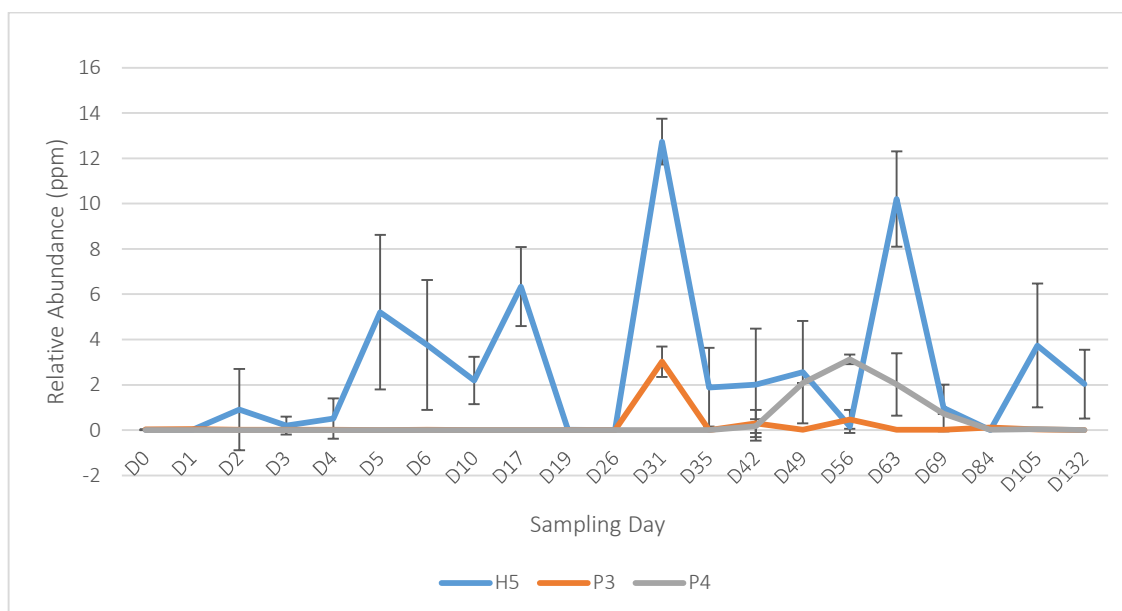


Figure 5.11: Comparison of 5 $\alpha$ -cholestanone relative abundance within the skin, through decomposition period of H5 (human 5), P3 (pig 3) and P4 (pig 4). Error bars represent standard deviation variation of (4) replicates.

25-hydroxycholesterol is an oxysterol typically found in arid conditions (absence of humidity) [100, 101]. A large increase of this compound was observed on day 17 for the human (when natural mummification was first observed) (Figure D-23 from Appendix D). This is then followed by a decrease and a subsequent increase on day 31 (mid-bloat). The variable levels of this compound during human decomposition make it unclear whether it correlates with naturally mummified skin. Review by Diczfalusy [102] states that although the role of 25-hydroxycholesterol within the body is still unclear, its presence within human tissue are at very low levels. These low levels were detected for the earlier sampling days for the human (day 0-5), after which an increase in observed. It is suspected the behaviour of this compound (both increasing and decreasing) could be related to a combination of arid conditions and progression of decomposition.

Nonadecanoic acid showed statistically significant differences in relative abundance between all three individuals. This compound was present in relative abundances (Figure D-11 from Appendix D) below the threshold of detection and quantitation (Table 3.3).



### 5.2.9 SUMMARY

PCAs revealed significant variations in the fatty acid profiles during the decomposition period for humans compared to pigs. The fatty nature of the skin led to increased abundances of palmitoleic and linoleic acids, demonstrating statistical significance between humans and both pigs. Interestingly, mummification exhibited a decrease in fatty acid abundances within H5, potentially attributed to the challenging extraction of fatty acids from the tough matrix of mummified skin.

In terms of sterols, the skin generally showed a similar chemical composition between humans and pigs, primarily influenced by the abundance of cholesterol. However, humans exhibited more significant sterol variation, particularly following the onset of mummification.

### 5.3 COOLER CLIMATE STUDY CONCLUSIONS

The tissue matrix between humans and pigs displayed minimal variation in terms of fatty acid and sterol composition. In contrast, the skin matrix demonstrated fluctuations in relative abundances, both within and among individuals. While mummification had little impact on the fatty acid profile of tissues, sterols appeared to increase in relative abundances. A similar trend was observed in the skin matrix, with sterols showing positive impacts from natural mummification, except for cholesterol, which exhibited a general decrease. Many compounds of fatty acids and sterols, in both skin and tissue, were present in low relative abundance, necessitating further investigation, potentially through large-scale studies or with greater amounts of matrix to accurately assess each compound's effects.

The high fat content within the human (H5) skin and tissue appeared to directly influence the abundance of fatty acids associated with adipose storage and breakdown. This was evident in both the skin and tissue matrices, with significantly larger abundances of oleic acid in the tissue and palmitoleic and linoleic acids in the skin of humans compared to pigs.

Human samples consistently showed larger abundances across various compounds, potentially attributed to the diverse compounds humans are exposed to, influencing lipid and sterol levels due to factors like diet and lifestyle. Another contributing factor may be the method itself, optimised for human matrix rather than pig matrix, resulting in more reliable results for humans.

Natural mummification, while observed in both humans and pigs, manifested differently between the two species. In humans, natural mummification preserved the skin and hindered the progression of decomposition into the active stage. In contrast, natural mummification in pigs did not result in preservation-like effects, as they continued to progress through the decomposition stages.

Given the visual and lipid-level differences between humans and pigs, it is concluded that pig models should not be used as human analogues when investigating natural mummification in humans.

CHAPTER 6 LONGITUDINAL  
STUDY OF HUMAN TISSUE  
AND SKIN

This section conducts a comparative analysis of post-mortem tissues and skin from human subjects over a two-year period. The investigation focuses on discerning differences in lipid profiles, specifically examining fatty acid and sterol compositions. Special attention is given to instances of natural mummification and its effects on lipid profiles. The primary goal is to identify specific trends related to natural mummification and gain insights into the underlying biochemical changes that lead to this phenomenon. The knowledge derived from this study is expected to contribute to a better understanding and, potentially, the prediction of natural mummification. Observing the natural mummification process involves identifying key visual cues, namely desiccation and alterations in the skin's colour to an orange hue.

## 6.1 MATERIALS AND METHODS

Four (4) human bodies (H2= human 2, H3= human 3, H4= human 4, H5= human 5), were used during the period of this project, details of which can be found in Table 6.1. Tissue samples were collected to identify different fatty acid and sterol trends during the period of decomposition for humans, with emphasis on the effects of natural mummification.

*Table 6.1: Information on bodies used for this study. Orange colour indicates bodies studied in warmer seasons (Australian Summer and Spring). Blue colour indicates bodies studied in cooler seasons (Australian Autumn and Winter) (H2= human 2, ca*

Human	Date of Placement	Cause of death	Sex	Height (cm)	Weight (kg)	Body Mass Index (BMI)	Mummified (yes or no)
H2	25 <sup>th</sup> March 2020	Liver Failure, Metastatic Cancer - Duodenal Adenocarcinoma	F	156	89	36.6	Yes
H3	12 <sup>th</sup> August 2020	Pneumonia	F	154	53	22.2	Yes
H4	29 <sup>th</sup> January 2021	Alzheimer's Disease	M	174	63	20.8	Yes
H5	11 <sup>th</sup> June 2021	Metastatic Bladder Cancer, Prostate Cancer, Peripheral	M	175	94	30.7	Yes

		Vascular Disease, Atrial Fibrillation					
--	--	--	--	--	--	--	--

Sampling of each human occurred daily from date of placement until sampling day 7. Sample collection decreased as decomposition progressed i.e., daily from date of placement to every second day for two weeks, to two times a week for two weeks, to once a week, and so on. Table 6.2 summarises the sampling schedule for H2-H5. Photographs of H2, H3, H4 and H5 were taken on all sampling days to capture the extent of visual decomposition at the time of sampling (see Appendix K).

Table 6.2: Sampling information for human 2 (H2), human 3 (H3), human 4 (H4) and human 5 (H5).

Human	Date of placement	Days sampled post-mortem	Final sampling date
H2	25 <sup>th</sup> March 2020	0, 1, 2, 3, 4, 5, 6, 7, 10, 12, 14, 16, 18, 20, 22, 24, 26, 28, 30, 35, 40, 45, 50, 55, 60, 65, 70, 75	8 <sup>th</sup> June 2020
H3	12 <sup>th</sup> August 2020	0, 1, 2, 3, 4, 5, 6, 9, 12, 16, 19, 23, 26, 30, 33, 37, 40, 47, 55, 68, 82, 114, 153, 274	13 <sup>th</sup> May 2021
H4	29 <sup>th</sup> January 2021	0, 1, 2, 3, 4, 5, 6, 7, 8, 10, 14, 17, 20, 28, 35, 42, 70, 105, 185, 202	19 <sup>th</sup> August 2021
H5	11 <sup>th</sup> June 2021	0, 1, 2, 3, 4, 5, 6, 10, 17, 19, 26, 31, 35, 42, 49, 56, 63, 69, 84, 105, 132	21 <sup>st</sup> December 2021

Refer to section 2.5 and 2.6 for full method details on sample collection and processing.

ADD was employed as a method to estimate the accumulation of heat energy influencing various biological and environmental processes. This method enables the comparison of humans placed outdoors at different time points, calculated through the cumulative sum of average daily temperatures from the date of placement, replacing traditional sampling days.

## 6.2 VISUAL OBSERVATIONS AND WEATHER DATA

Human 2 remained in the fresh stage of decomposition until day 10, where they had begun showing first signs of bloat (Table K-1 from Appendix K). By this stage, the face had mummified and become leathery in texture. The torso of H2 exhibited first signs of mummified tissue during the bloat stage, on day 18. Rupture of the torso was observed on day 35, on which D2 was declared as being in the active day stage. Mass loss was illustrated over the next few days, with advanced decay being entered on 50. Human 3 exhibited signs of mummified tissue on the upper limbs on day 13, while the torso was still in the fresh stage. Signs of bloating were first observed on day 19 with full bloat achieved by day 26 (Table K-2 from Appendix K). Mass loss (active decay) was first depicted on day 30, with the advanced stage of decay reached on day 40. From the bloat stage onwards, the skin on the torso of H3 was mummified in appearance. On day 114, the skin on the sampling site (arm) had completely turned black and hardened. By this time, no soft tissue was left and only skin and bones remain. The fresh stage for H4 persisted from day 0 to day 8, where the human was classed as being in the bloat stage (Table K-3 from Appendix K). During this period, the sampling site (upper arm) began exhibiting signs of mummified tissue. Human 4 mummified while in the bloat stage, resulting in a transition from the bloat stage directly to the advanced stage of decay. The human was classed as being in advanced decay on day 28. H5 only exhibited a shift from the fresh to bloat stage of decay in the torso on day 17. During this time, the first signs of mummified tissue was observed on the face and the arm (Table K-4 from Appendix K). Active decay was not detected in this body, with the transition from the bloat stage to advanced decay stage on day 42. By this time the human body had completely mummified.

Comparison of visual observations in Figure 6.1 are reported in ADD where the accumulated sum of weather data is used instead of sampling days. This method accounts for temperature and removes seasonal barrier impacts [13, 14]. The duration of fresh stages for H3 and H5 appeared similar in timeline compared to H2 and H4 lasted 10 and 8 days, respectfully. This is speculated to occur due to the closeness in terms of average temperature at which these human bodies were placed out (Figure 6.2). However, when reported in ADD (Figure 6.1), it was observed that all 4 bodies remained in the fresh stage of decomposition for similar periods. This event depicts the usage of ADD for accurate comparison of staging humans, instead of sampling days. First signs of mummified tissue were observed on each body as highlight through the shaded portion of Figure 6.1 (ADD 150-250).

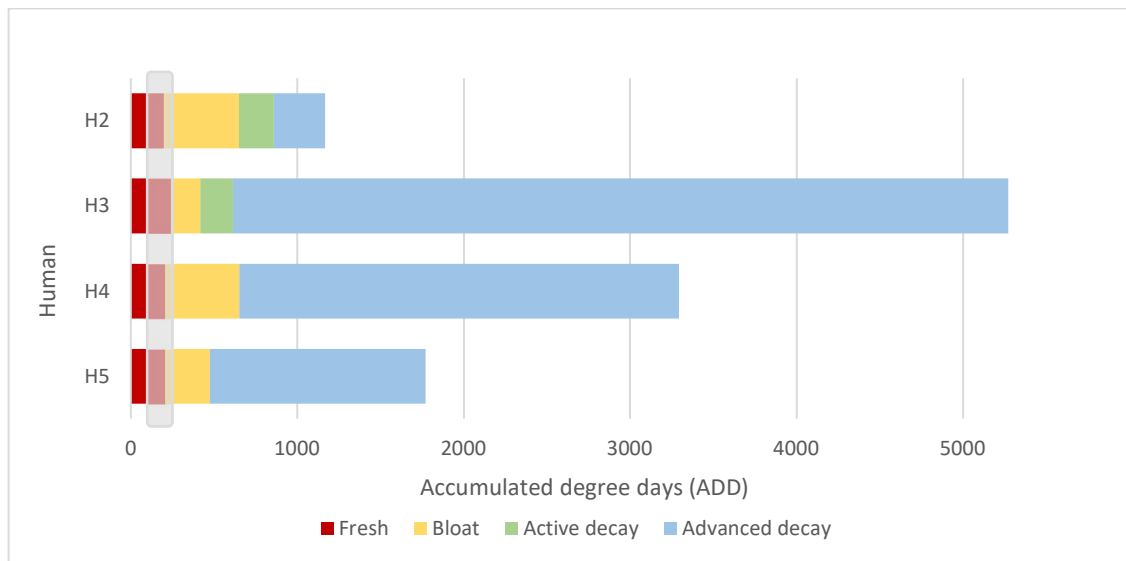


Figure 6.1: Comparison of stages of decomposition for human 2 (H2), human 3 (H3), human 4 (H4) and human 5 (H5) reported in accumulated degree days (ADD). Highlighted range depicts first signs of observed mummified tissue.

H2 and H4 were placed during Australian winter and averaged similar daily temperatures from when they were placed out. Similarly, H3 and H5 were placed during Australian summer and autumn, however weather data from Figure 6.2 depicts those average daily temperatures between the two humans were similar. Upon comparison, H2 and H3 were the only two humans to follow the traditional stages of decomposition as per Payne [27]. H4 and H5 did not appear to enter the active stages of decomposition and remained in prolonged bloat. This could potentially be linked to the increased amounts of rainfall depicted during the onset of H4 and H5 study, which may have caused retardation of crucial insect and microbiological active from progressing the body into an active state. The correlation between rainfall and progression in terms of stages of decomposition will need further trials for investigation. All four humans experienced natural mummification at some point during decomposition (highlight through shaded portion of Figure 6.1). The first signs of mummified tissue for all human bodies consistently appeared to take place on the face and upper limbs (arms). The first signs of mummified tissue for each human are as follows: H2 = 231 ADD (day 18), H3= 166 ADD (day 13), H4 = 201 ADD (day 8) and H5 = 200 ADD (day 17). These sampling days correlate to an approximate ADD range of 150-250 (Figure 6.1). This finding is extremely important as it allows for the approximately prediction of this occurrence within humans in an Australian temperate environment, regardless of seasonal placement. By determining such a temperature timeframe, this enables opportunity for the addition of this finding within staging and categorisation techniques.

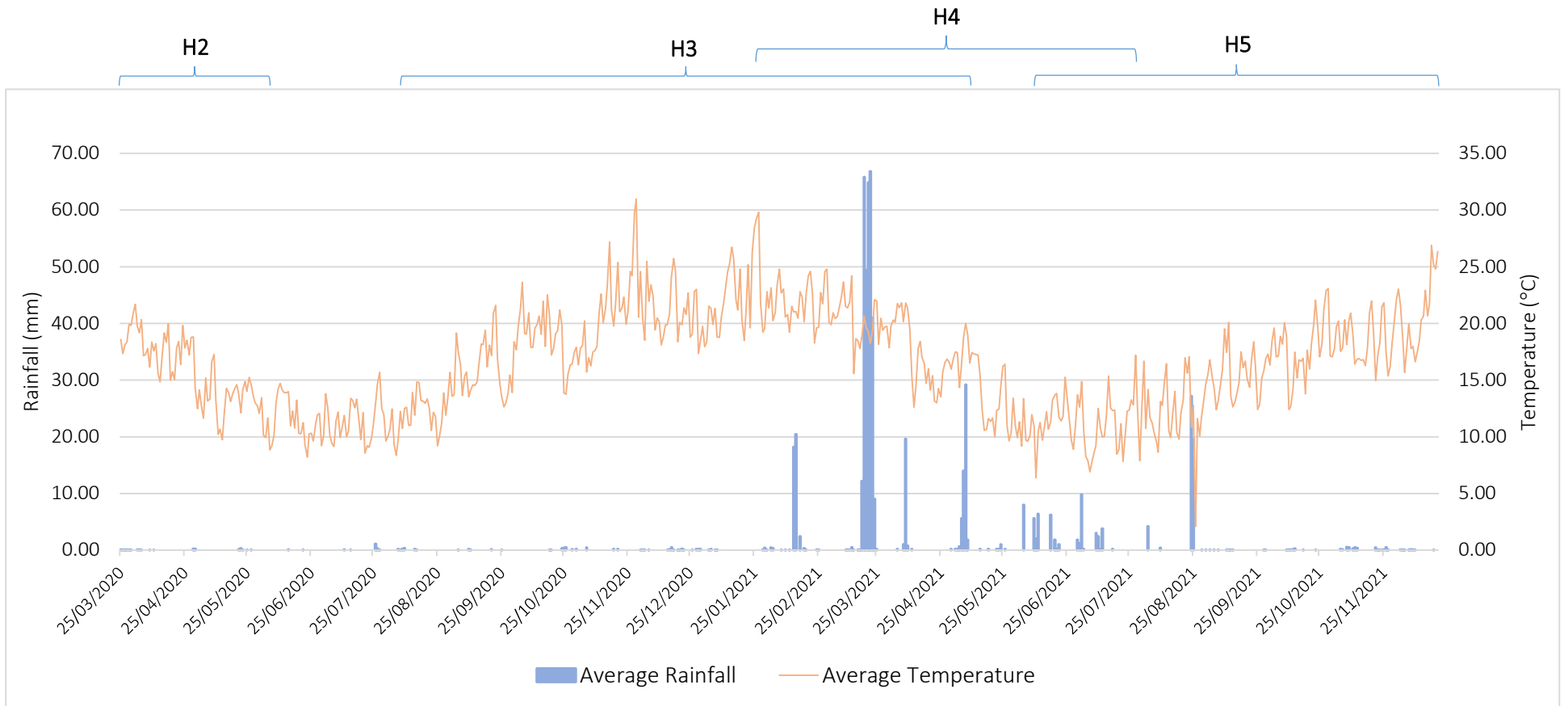


Figure 6.2: Weather data comparison of H2 (human 2), H3 (human 3), H4 (human 4) and H5 (human 5).



## 6.3 TISSUE RESULTS

### 6.3.1 PCAS

#### 6.3.1.1 FATTY ACIDS

Fatty acid variation within the tissue was plotted in a PCA to visualise any groupings within the tissue matrix of H2, H3, H4 and H5 which could be correlated to stages of decomposition (Figure 6.3). Most fresh stage samples showed general clustering on the PCA for all humans, attributed to the influence of oleic acid (see Figure H-3 from Appendix H). H5 showed some overlap in fatty acid influence between the fresh and bloat stages of decay. A cluster (highlighted in purple) is shown consisting of most of the bloat and active stage samples, which can be attributed to the large influence of palmitoleic acid (see Figure H-3 from Appendix H). These trends illustrate the break of compounds into breakdown products, with the progression of decomposition. The large influence of oleic acid was observed to transition into a large influence of palmitoleic acid (breakdown product of oleic acid), with the progression of decomposition. This is further discussed in 6.3.2.

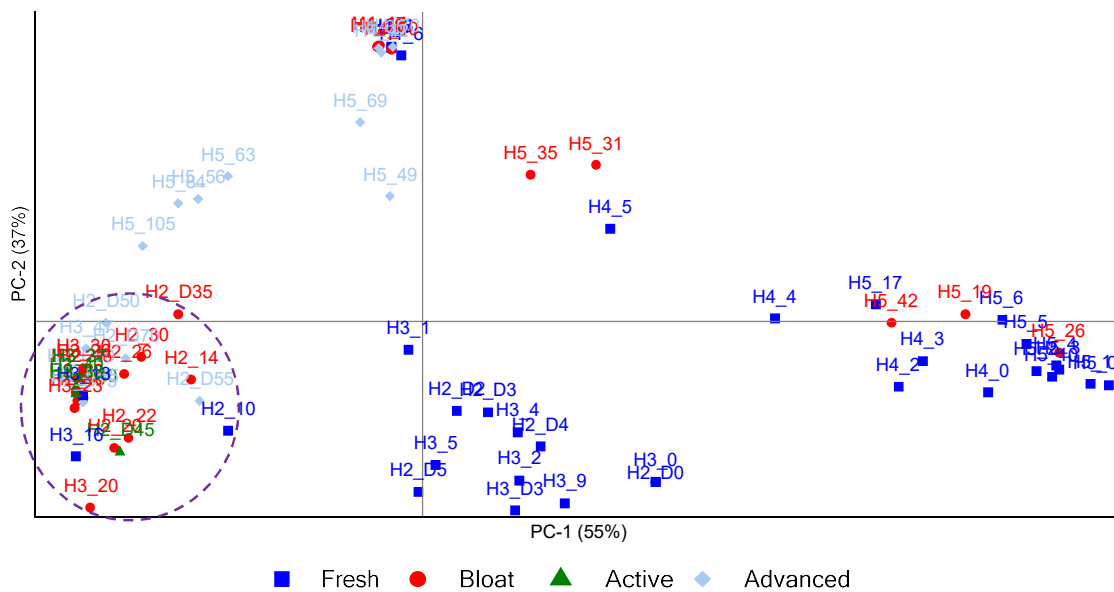


Figure 6.3: PCA comparison of fatty acid profile within the tissue matrix of human 2 (H2), human 3 (H3), human 4 (H4) and human 5 (H5), grouped by stages of decomposition. Bloat and active stage samples for most humans highlighted by purple circle.

All humans show a transition of fatty acid profile from the bloat and active stage into the advanced stage, which can be correlated to influence of myristic acid (Figure H-3 from Appendix H). The transition into stages of decay appear to show differences in fatty acids contributing to the profile

of the humans with oleic acid predominantly observed during the fresh and bloat stage, palmitoleic acid during the bloat and active stages, and myristic acid observed during the advanced stage.

### 6.3.1.2 STEROLS

The stages of decomposition do not affect the sterol composition (Figure 6.4), as no distinct patterns were observed. H2 and H3 fresh and bloat stages showed similarities in lithocholic acid influence (see Figure H-4 from Appendix H), compared to H4 and H5 (highlighted in purple). Samples highlighted in purple show a large influence attributed to cholesterol (H-3 from Appendix H).

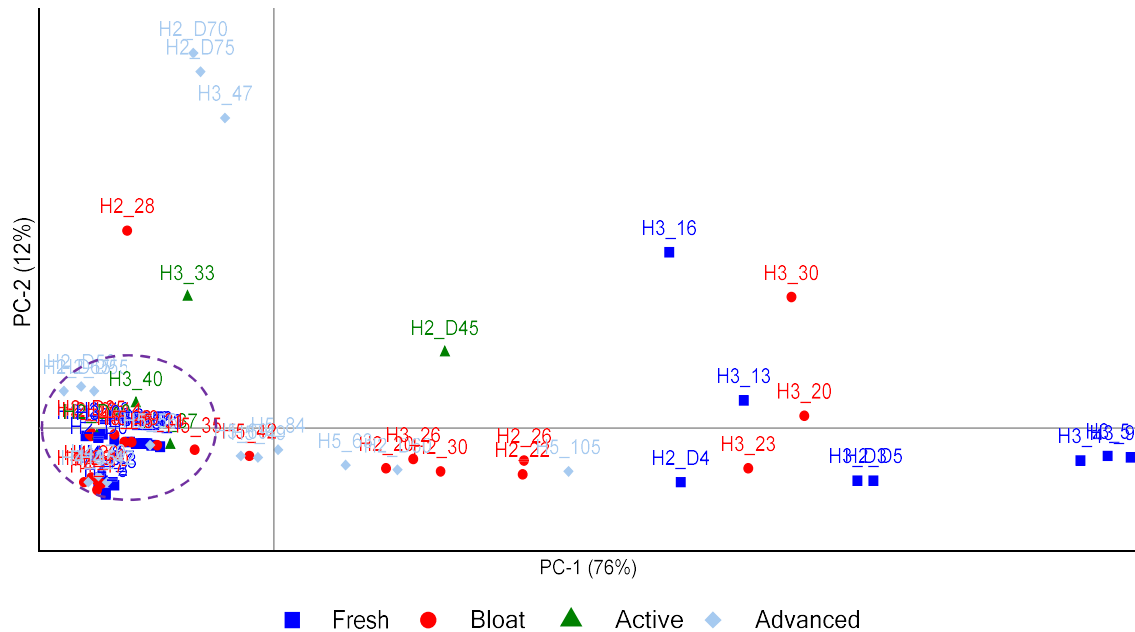


Figure 6.4: PCA comparison of sterol profile within the tissue matrix of human 2 (H2), human 3 (H3), human 4 (H4) and human 5 (H5), grouped by stages of decomposition. Purple circle highlights most fresh and bloat stage samples for humans.

Sterols showed little trends related to stages of decomposition and therefore may not be suitable for tracking transition of stages in human decomposition, compared to fatty acids.

### 6.3.2 COMPOUND COMPARISONS

After death, triacylglycerides within adipose tissue are hydrolysed to form free fatty acids once the body begins to breakdown [60, 103]. These fatty acids constitute of either single or double bonds,

making them either saturated or unsaturated acids. Post-mortem oxidation and hydrogenation processes, influenced by bacterial enzymes, lead to the breakdown of unsaturated acids into their corresponding saturated forms [34, 39, 104]. It is therefore predicated for a decrease in unsaturated acids and an increase in saturated acids to occur over the period of decomposition [73, 105]. Similarly, sterols also undergo various transformations which include oxidation and reduction, which can result in the formation of different compounds [34]. These formations are heavily dependent on factors such as the environment, body fat, and microbial activity.

Each compound of interest was compared across the period of decomposition for all humans (see Appendix J). Myristic acid, oleic acid, palmitoleic acid, were the only compounds with detectable relative abundances within the humans at levels above the reported LOQ (Table 3.3). In some instances, compounds were found at higher (quantifiable) relative abundances in some humans and not in others, as discussed below. Compounds investigated within the tissue matrix generally followed breakdown of fatty acids as literature outlines, in anaerobic decomposition [24, 34, 39]. This means that larger molecules were observed to undergo hydrogenation into their shorter 'building block' forms as decomposition progressed, resulting in a decrease in relative abundance over time. Simultaneously, the 'building block' compounds increased in relative abundance with the progression of decomposition. This is further discussed below.

Myristic acid was detected in similar relative abundance during the first 30 days of decomposition within all four human bodies. Myristic acid, a component of human sweat and adipocere, is produced in the mammary gland and can also be ingested through the diet. It plays a role in various biological processes, including hormone production, membrane stabilisation, and metabolic process control [86]. The gradual increase in myristic acid for H5 (Figure 6.5) could be attributed to hydrogenation of fatty acids including palmitic acid (C:16), which is known to break down into C:14 (myristic acid) [106].

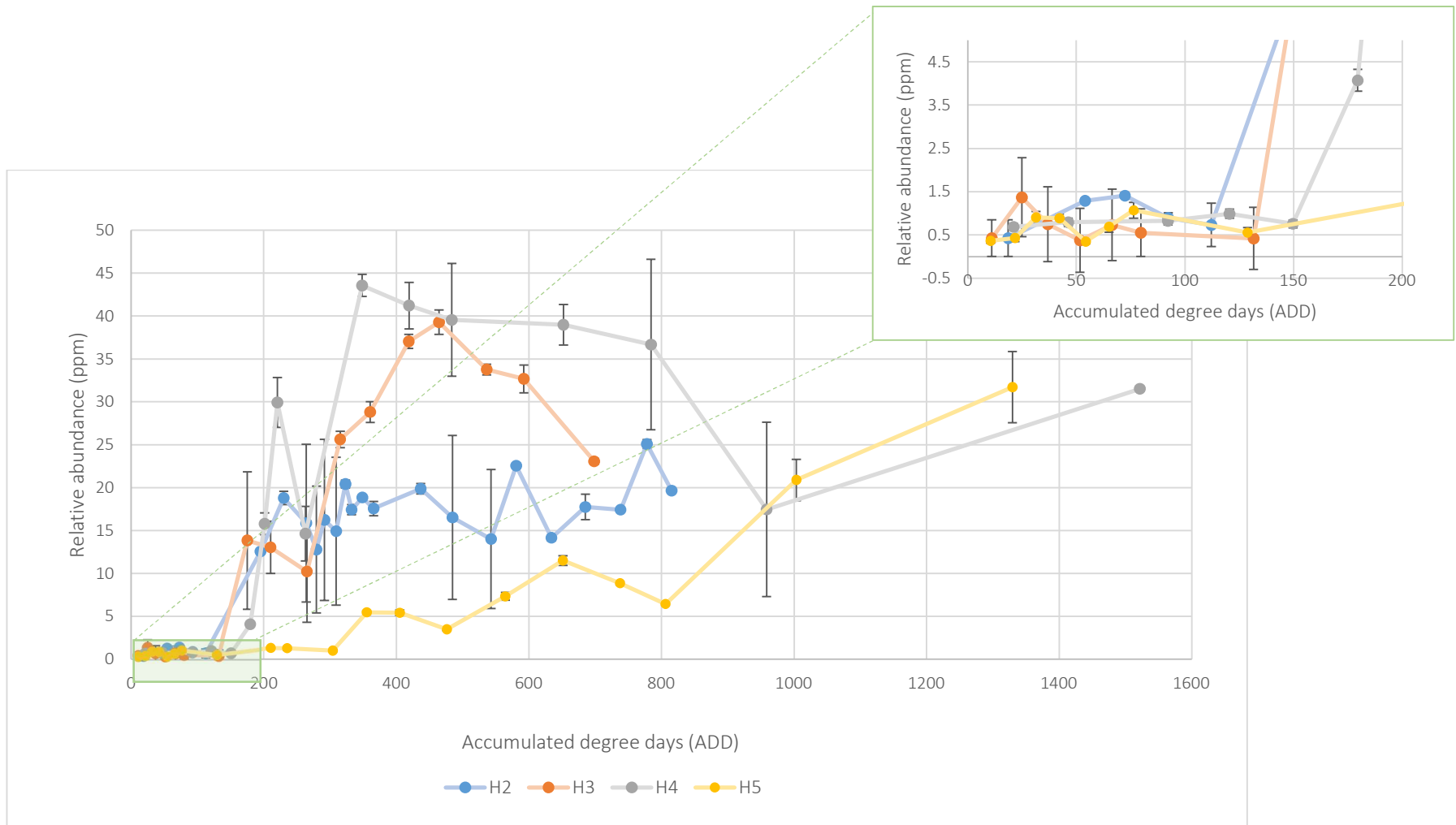


Figure 6.5: Comparison of myristic acid during the decomposition periods of H2 (human 2), H3 (human 3), H4 (human 4) and H5 (human 5). Error bars represent standard deviation variation of (4) replicates.

Adipocere formation was first observed on sampling day 13 in H5 (Figure 6.6), suspected to occur due to the presence of fatty tissue within the body, coupled with the cool climate. Adipocere is formed through saponification, a process wherein body fats are converted into soap, resulting in the formation of a wax-like substance on the surface [73, 104]. While palmitic, stearic, and myristic acids are the most abundant fatty acids present in adipocere [73], it's important to note that adipocere formation occurs on the skin surface rather than internally. Therefore, the observed increase in myristic acid is unlikely to be directly caused by adipocere formation. Instead, it is speculated that this increase is primarily attributed to the hydrogenation of palmitic acid [39].



*Figure 6.6: Adipocere formation on the surface of human 5 (H5).*

Oleic acid, a constituent of human sweat and adipocere, is commonly found in various animal and vegetable sources [73, 104]. Its presence within the human tissue matrix is expected. General trends of oleic acid reveal an initial increase in relative abundance, succeeded by a decline as decomposition progresses (Figure 6.7). This initial rise is suspected to be a result of the hydrogenation of linoleic acid, leading to the breakdown of this compound into oleic acid in its building block form. Subsequently, oleic acid levels tend to diminish with the advancement of decomposition. This trend is likely associated with the degradation of oleic acid over time, potentially resulting in an increase in its degradation product, palmitoleic acid [39, 83]. As illustrated in Figure H-3 from Appendix H and Figure

6.7, oleic acid prominently influences the fresh and bloat stages of decomposition. This suggests the potential utility of this compound in the early-stage detection of human bodies. However, the substantial variation observed in the early decomposition stages of H2 and H3 highlights challenges in discerning clear trends. This variability may arise from the intricate interplay between oleic acid and other compounds within the tissue matrix, the heterogeneous distribution of oleic acid within the tissues, and potential sample matrix degradation.

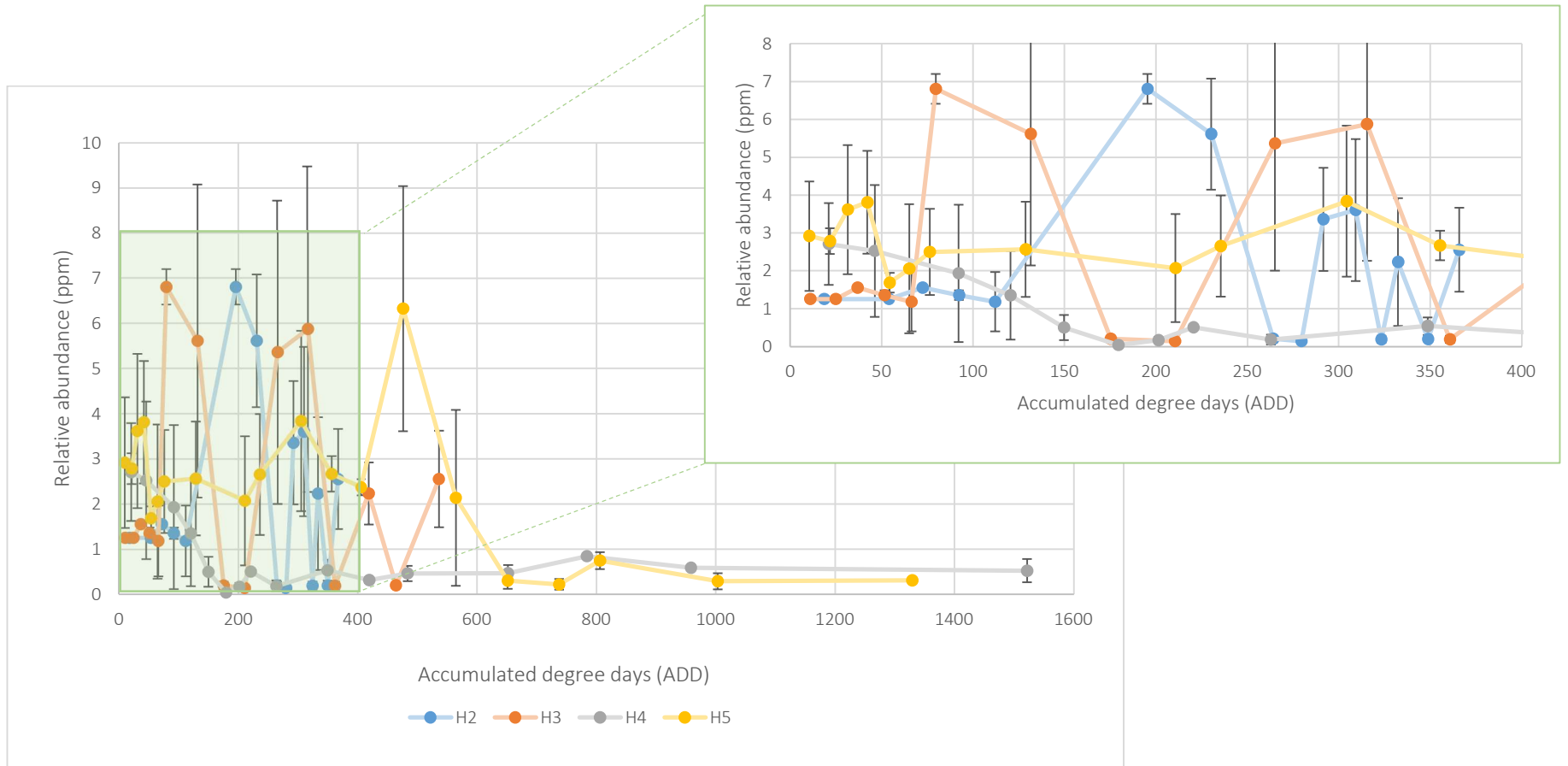


Figure 6.7: Comparison of oleic acid within tissue matrix during the decomposition periods of H2 (human 2), H3 (human 3), H4 (human 4) and H5 (human 5). Error bars represent standard deviation variation of (4) replicates.

Palmitoleic acid was generally found at quantifiable levels in all four humans (Figure 6.8). This acid is typically found within human serum and tissues [39, 83]. Consequently, low levels of palmitoleic acid are expected within the tissue matrix of all humans. The increase in palmitoleic acid (Figure 6.8) alongside a decrease in oleic acid (Figure 6.7) is anticipated to occur with the progression of decomposition, owing to the breakdown of oleic acid into palmitoleic acid [39]. However, a significant spike in relative abundance was observed for H2 from sampling day 10 (ADD 195) onwards, resulting in much higher levels of this compound compared to H3-H5. This increase occurred approximately during the period when natural mummification was first detected (ADD 231/sampling day 12). It remains unclear whether this increase in relative abundance is correlated with the onset of natural mummification, as this trend was not observed in the other humans. Therefore, it is suspected that this increase may be attributed to the breakdown of surrounding tissues, including fat, within H2, resulting in the excessive release of palmitoleic acid within the body.



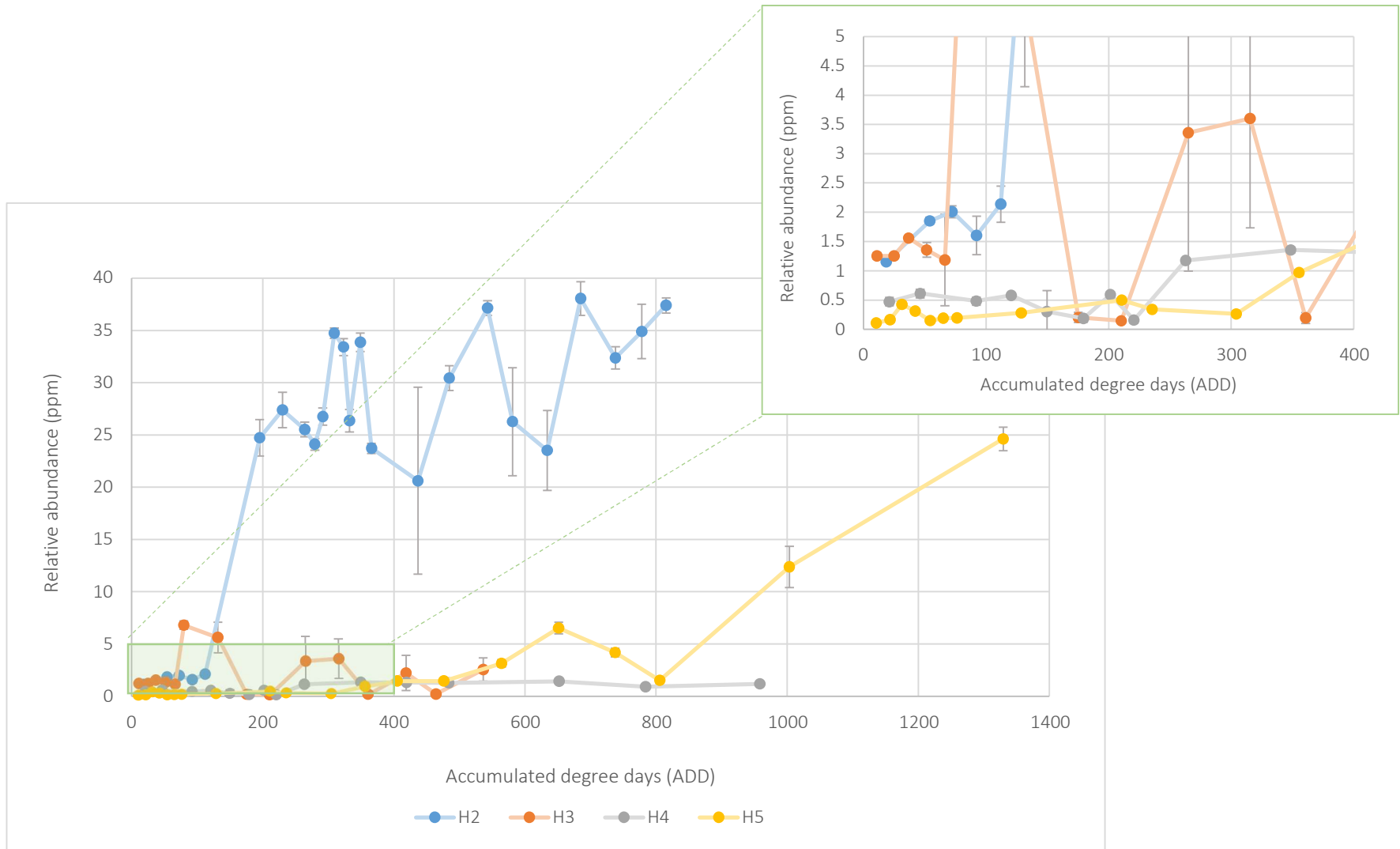


Figure 6.8: Comparison of Palmitoleic acid during the decomposition periods of H2 (human 2), H3 (human 3), H4 (human 4) and H5 (human 5). Error bars represent standard deviation variation of (4) replicates.

The general trend of compounds decreasing in relative abundance with the progression of decomposition and breakdown products increasing in relative abundance was observed in all compounds investigated (Appendix J). The onset or presence of natural mummification did not seem to influence the lipids found within the tissue matrix, as no trends could be correlated between the two variables. This lack of correlation is expected because natural mummification primarily occurs on the external surface (skin) of the bodies. It can be concluded that natural mummification does not affect the internal degradation process of decomposition, although visual changes external to the body are evident. The bloat and active stages of decomposition were identified as the stages at which palmitoleic acid increase is depicted (Figure H-3 from Appendix H and Figure 6.8), potentially making this an ideal compound for middle-stage decomposition identification.

#### 6.4 TISSUE CONCLUSIONS

PCAs illustrated that fatty acids, notably oleic acid, palmitoleic acid, and myristic acid, could be traced throughout the progression of decomposition. Oleic acid exhibited the most influence and large relative abundances during the fresh and early-bloat stages of decay for all humans. The transition between the bloat and active stages was characterized by an increase in palmitoleic acid, followed by myristic acid, impacting the fatty acid profile in the advanced stages of decay. However, sterol influence could not be correlated with the progression into any stages of decay.

Both fatty acids and sterols within the body showed a general trend of decrease over time with the progression of decomposition. The increase in degradation products, such as palmitoleic acid, was expectedly observed with the decrease of its larger chain form (oleic acid). Interestingly, natural mummification did not appear to have any measurable impact on the fatty acid and sterol composition within the tissue matrix.

In conclusion, it can be inferred that the effects of natural mummification result in visual changes external to the body, which cannot be linked to any fatty acid or sterol trends within the tissue matrix. This suggests that the effects of mummification are purely external and do not penetrate through the skin matrix, subsequently having no impact on the internal process of decomposition

#### 6.5 HUMAN SKIN

##### 6.5.1 PCAS

### 6.5.1.1 FATTY ACIDS

Fatty acid variation was visualized through a PCA to identify potential groupings within the skin matrix of H2, H3, H4, and H5 (Figure 7.1). While distinct clusters were challenging to interpret, general transitions were loosely identified. The purple circle in the figure highlights the early sampling days corresponding to the fresh stage for humans, with a transition into the bloat stage marked by the orange circle. The overlapping samples from the early and bloat stages suggest a general transition from the purple cluster to the orange cluster. This shift was attributed to the influence of oleic acid during the fresh-early bloat stage, transitioning to the influence of palmitoleic acid during the bloat stage (refer to Figure H-1 in Appendix H for details)

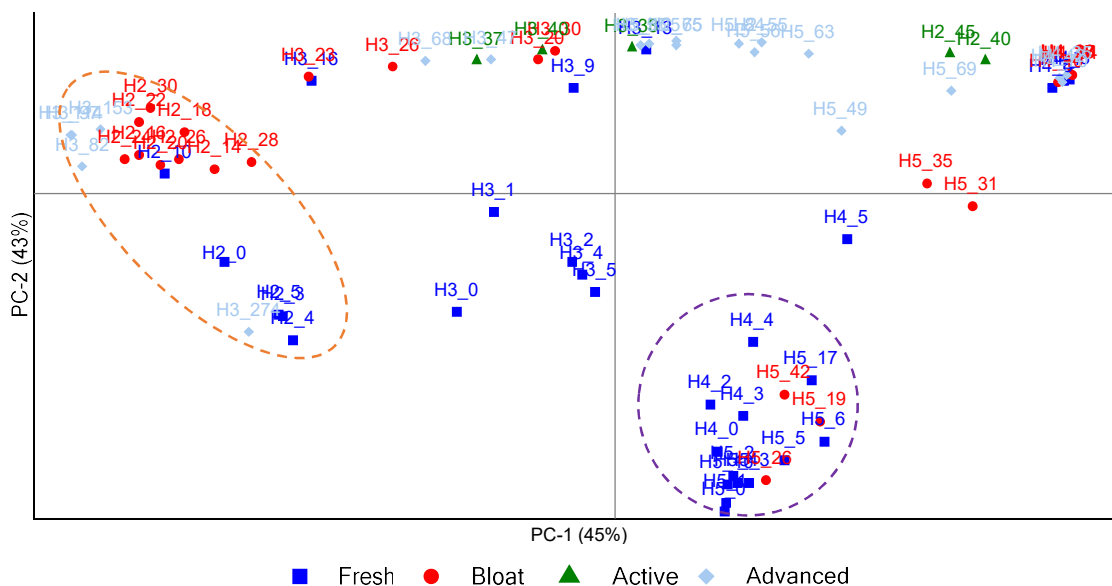


Figure 6.9: PCA comparison of fatty acid profile within the skin matrix of human 2 (H2), human 3 (H3), human 4 (H4) and human 5 (H5), grouped by stages of decomposition. Purple circle highlights fresh stage sampling days for most humans. Orange oval highlights bloat stage samples for most humans.

The active and advanced stages of decay could not be confidently correlated to any trends of fatty acid influence.

### 6.5.1.2 STEROLS

Sterol composition depicted little variation through the progression of decomposition for all humans (Figure 7.2). The purple circle highlights majority of the samples for all humans clustered, with

no trends able to be correlated with the transition of stage of decay. Scattering was observed on some sampling days, particularly within H3, due to the influence of lithocholic acid (Figure H-2 from Appendix H).

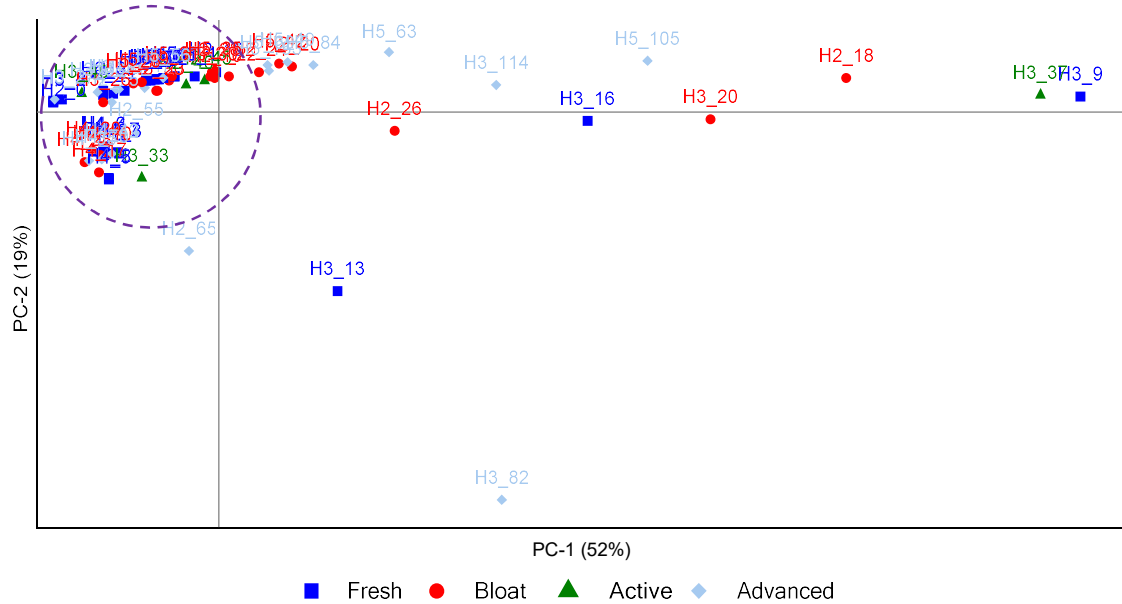


Figure 6.10: PCA comparison of sterol profile within the skin matrix of human 2 (H2), human 3 (H3), human 4 (H4) and human 5 (H5), grouped by stages of decomposition.

Similar to the sterol patterns within the tissue matrix, this PCA illustrates how sterols may not be useful in staging decomposing bodies.

### 6.5.2 COMPOUND COMPARISONS

Each compound of interest was compared across the decomposition period for all humans (refer to Appendix I). Among the investigated compounds, including lauric acid, myristic acid, palmitoleic acid, oleic acid, cholesterol, lithocholic acid, stigmasterol, deoxycholic acid,  $\beta$ -sitosterol, and 25-hydroxycholesterol, presented relative abundances exceeding the LOQ (Table 3.3) for most humans. Generally, a decrease in relative abundance was observed within compounds with the progression of decomposition. Breakdown/degradation products showed an increase followed by a decrease, aligning with expected trends during anaerobic decomposition [34].

Lauric acid was detected on the skin of all humans at low concentrations during the fresh stage of decomposition (Figure 7.3). An increase was observed in this compound, persisting for the

approximate duration of the bloat period for each human. As the decomposition progressed into the active and/or advanced stages, a subsequent decrease was observed in the levels of lauric acid. Lauric acid, known for its antimicrobial properties, is commonly found within sebum [107] and human sweat at the human skin surface [108]. Therefore, the detection of this compound on the skin of decaying humans was expected. The increase observed during the bloat stage is suspected to be a result of changes in the physical properties of the skin, including blistering and slippage [109]. These changes may have led to increased exposure of sebum and fluids within and on the skin, resulting in an elevation of relative abundances. The subsequent decrease in lauric acid abundance can be attributed to the breakdown of this compound.

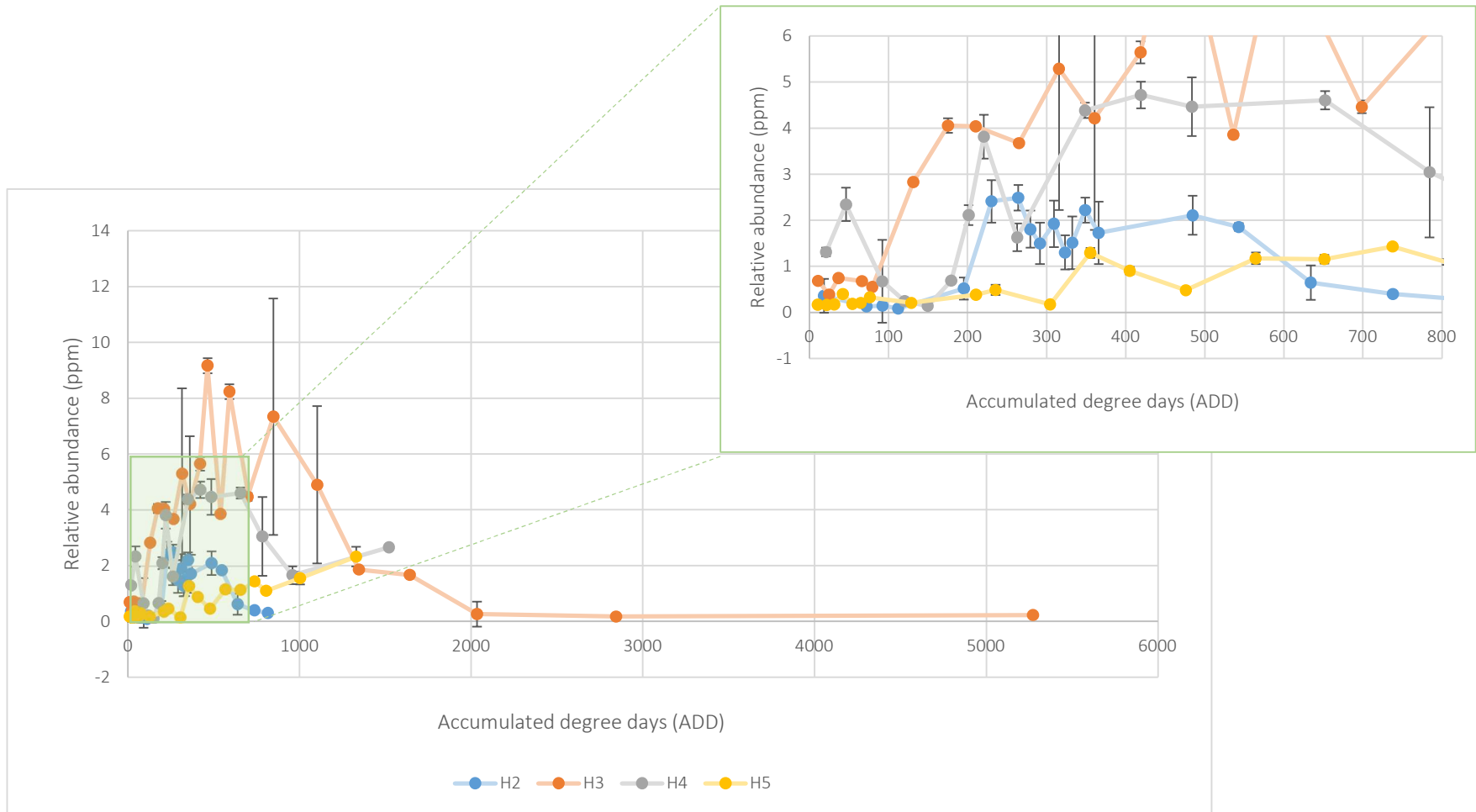


Figure 6.11: Comparison of lauric acid during the decomposition periods of H2 (human 2), H3 (human 3), H4 (human 4) and H5 (human 5). Error bars represent standard deviation variation of (4) replicates.

Myristic acid was found in substantially large amounts for all the humans (Figure 7.4). A spike in myristic acid was observed on day 14 for H2, day 9 for H3, day 6 for H4 and day 19 for H5. Each of these sampling days were approximately around the period where the first signs of mummified tissue were observed, between an ADD range of 150-250 or on sampling day 18 for H2, day 13 for H3, day 8 for H4 and day 17 for H5. The consistent increase of this compound in all humans enable for speculations that relative abundance levels of myristic acid within the skin matrix has correlation to natural mummification.

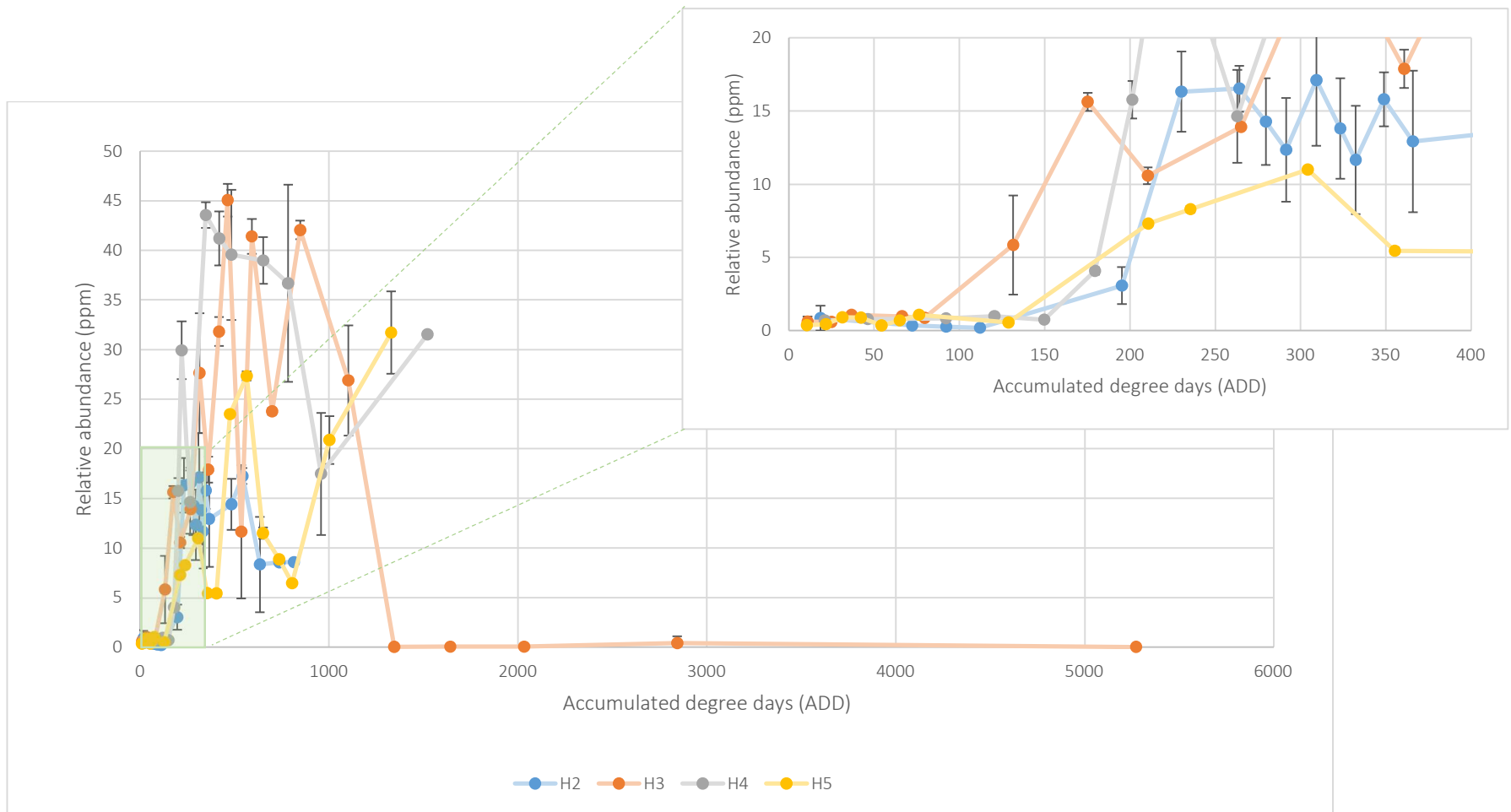


Figure 6.12: Comparison of myristic acid during the decomposition periods of H2 (human 2), H3 (human 3), H4 (human 4) and H5 (human 5). Error bars represent standard deviation variation of (4) replicates.



Myristic acid is identified as a component of adipocere, and it is also present in human sweat in both living organisms and human tissue [39, 106]. This fatty acid plays a direct role in influencing hormonal and protein shifts and is responsible for regulating metabolic processes [86]. Notably, myristic acid has been observed to possess antimicrobial and antifungal attributes [87, 88, 110, 111]. A 2011 study by Prasath et al. demonstrated the mitigation of systemic fungal infections, including *Candida albicans* and *Candida tropicalis*, attributing the decrease in yeast cell proliferation to increased myristic acid levels [87]. These qualities are also highlighted in research by Kim et al. and Khan et al., where a significant suppression of biofilms (consisting of bacterial, fungal, and yeast colonies) was attributed to the antibiofilm properties of myristic acid [110, 111]. It is therefore proposed that the increased amounts of the myristic acid present within the skin of all humans with its anti-fungal, anti-virulent properties have allowed resistance of skin degradation due to lack of biofilm activity. This consequently results in preservation of the skin on the humans in the form of natural mummification, rather than decomposition, which was consequently observed as a result in all humans studied. This substantial finding provides a link as to why natural mummification within humans result in preservation of the body, comparative to analogues (including pigs), where preservation is not observed (see sections 4.2.9 and 5.2.9 for details).

Palmitoleic acid was found at high levels, particularly in H2 and H3 samples (Figure 7.5), with an increase detected during the bloat stages of decomposition. This increase was observed from day 12 (230 ADD) within H2 and day 20 (265 ADD) within H3. Palmitoleic acid, commonly found in areas with high fat levels, is prevalent in serum and adipose tissues [83]. The extensive fat distribution within the skin matrix of H2 could account for why this was observed at very high levels (Table 6.1). H3 also depicts palmitoleic acids at high levels, although not as high as H2 (Figure 7.5). Being a known breakdown product of oleic acid [39], the increase in palmitoleic acid observed during the bloat stage for H3 may be linked to the breakdown of the skin matrix and the release of both palmitoleic and oleic acids. The heightened presence of this compound in the fatty content of the skin, coupled with the breakdown of oleic acid, might explain why H2 exhibited higher levels than H3. A similar trend was observed for H4 and H5 but on a smaller scale.

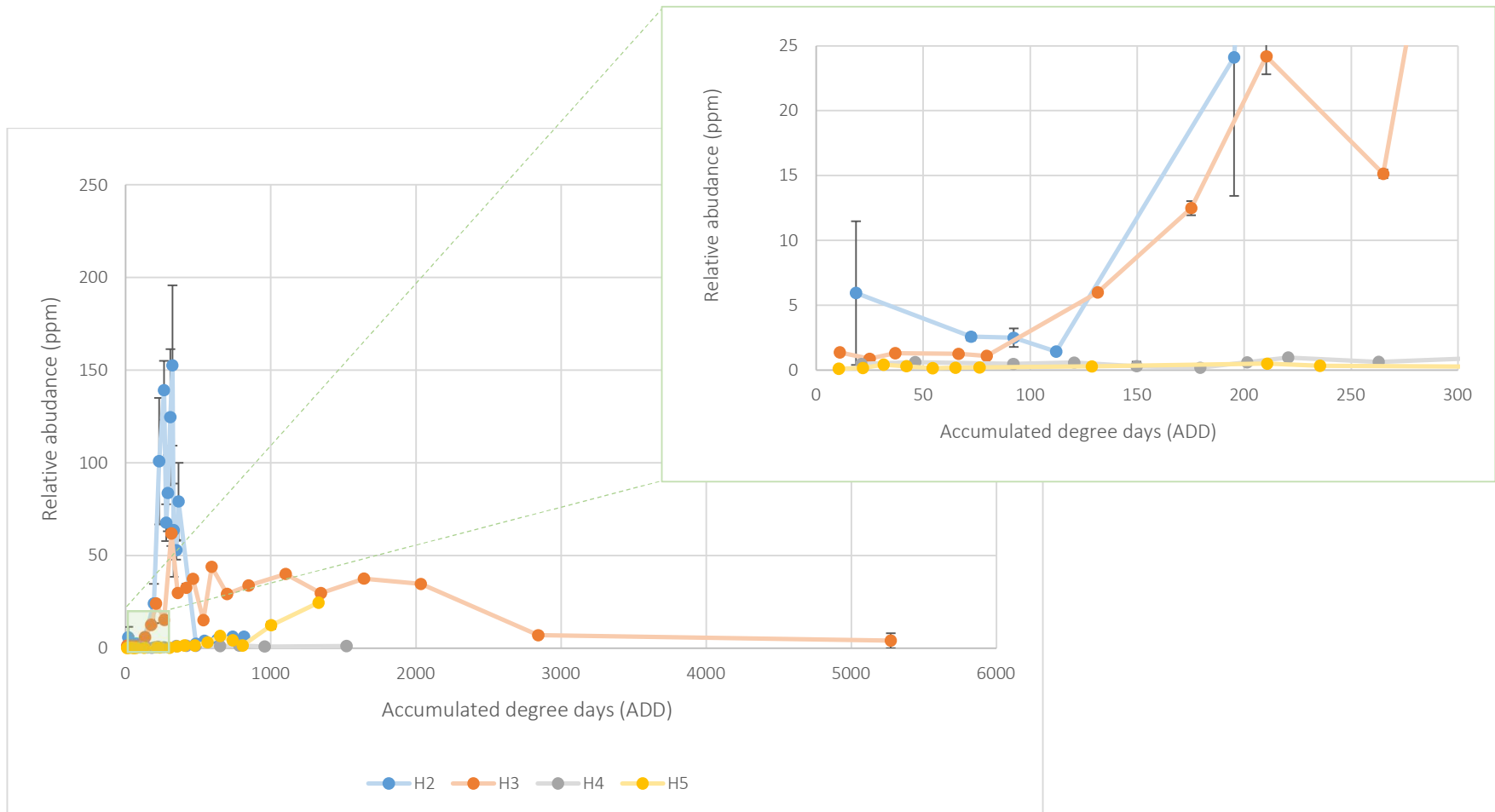


Figure 6.13: Comparison of palmitoleic acid during the decomposition periods of H2 (human 2), H3 (human 3), H4 (human 4) and H5 (human 5). Error bars represent standard deviation variation of (4) replicates.

Oleic acid is a constituent found in human sweat and adipose tissue, present across both human and animal sources [39, 73]. Additionally, it emerges as the breakdown product of linoleic acid [106, 112]. During the early stages of decomposition, oleic acid was found in moderate relative amounts in H2 and H5. Its levels elevate notably as decomposition advances into the bloat stage, only to gradually decrease in later stages (Figure 7.6). This pattern can be attributed to the initial occurrence of the compound within the skin matrix, followed by its degradation as the matrix undergoes decomposition. The notable increase in oleic acid concentration during the bloat stage could be linked to the liberation of oleic acid from the fatty skin matrix.

Examining the BMI and weight distribution (as presented in Table 6.1), both H2 (BMI = 36.6) and H5 (BMI = 30.7) were identified as the primary human donors with substantial amounts of adipose tissue. This observation could explain the higher concentrations of oleic acid in H2 and H5 compared to H3 and H4. Moreover, the breakdown of linoleic acid within the skin matrix might have contributed to the elevated levels of oleic acid [106, 112].

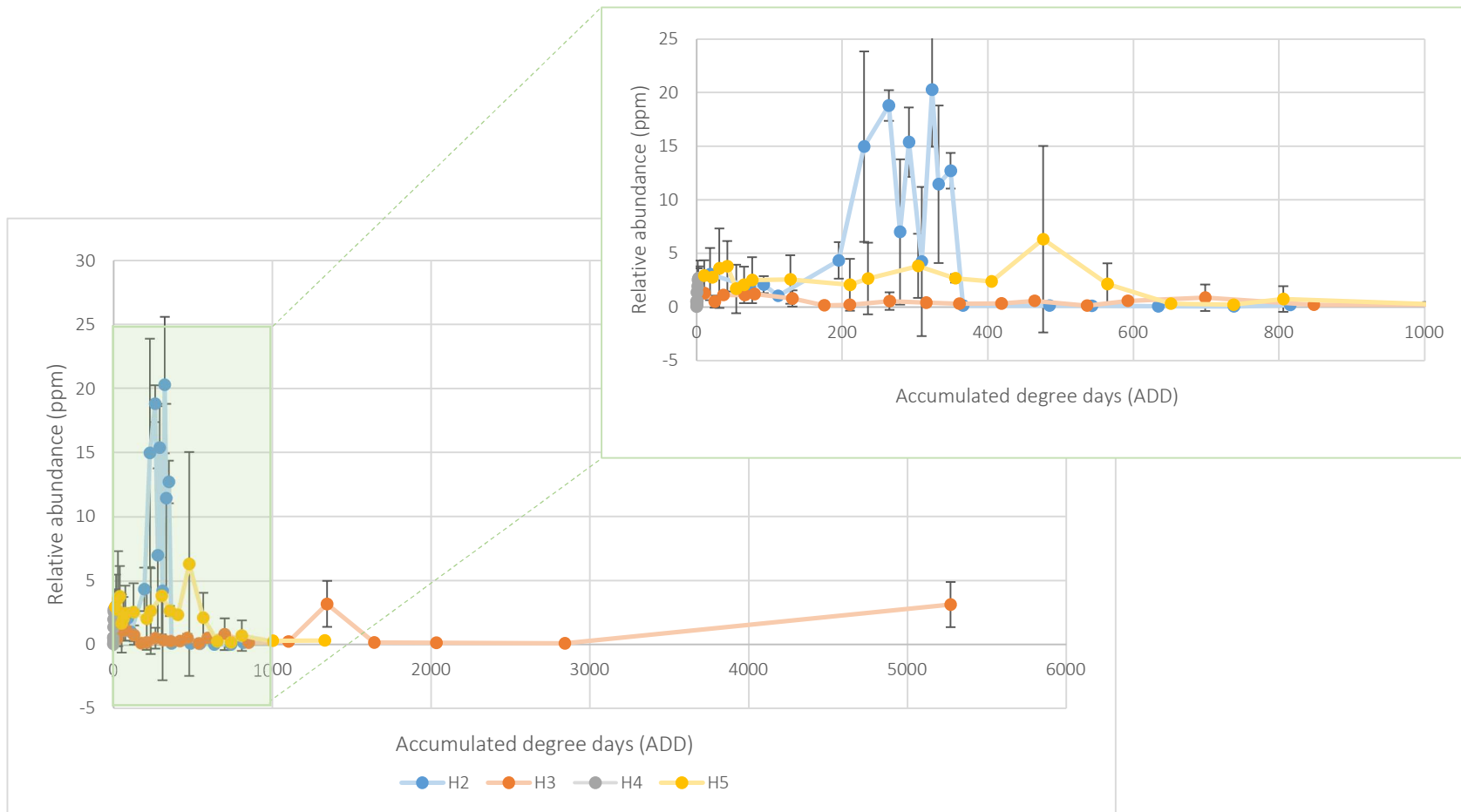


Figure 6.14: Comparison of oleic acid during the decomposition periods of H2 (human 2), H3 (human 3), H4 (human 4) and H5 (human 5). Error bars represent standard deviation variation of (4) replicates.

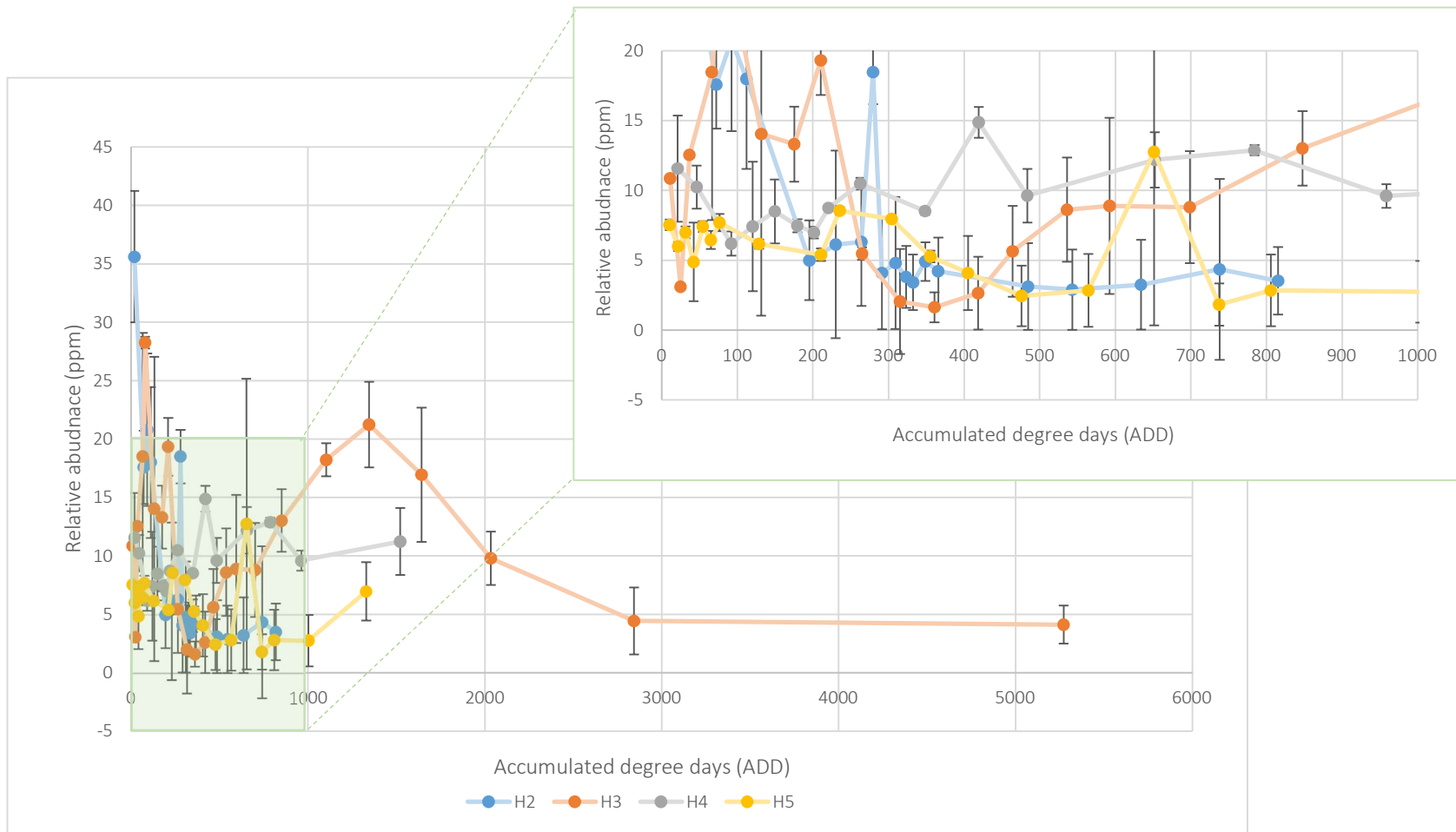


Figure 6.15: Comparison of cholesterol during the decomposition periods of H2 (human 2), H3 (human 3), H4 (human 4) and H5 (human 5). Error bars represent standard deviation variation of (4) replicates.

Cholesterol serves as a sterol commonly utilised as a biomarker in decomposition studies due to its stability over extended time periods [64, 91]. This compound is present within all eukaryotic cells, particularly in significant amounts within the tissues of higher animals, rendering it a valuable biomarker for detecting decomposition products [64, 105]. Throughout the fresh stage, cholesterol was moderately abundant in all humans, in alignment with expectations. Intriguingly, this phase was followed by a subsequent decline across all individuals. This decline was evident at ADD 195 for H2 and at ADD 265 for H3, roughly coinciding with the emergence of initial signs of mummified tissue. Although the changes in cholesterol levels for H4 and H5 are depicted in Figure 7.7, they manifest more gradually and therefore cannot be precisely tied to a specific ADD.

Upon scrutinizing weather data, it was discovered that H4 and H5 experienced substantial rainfall during the fresh and bloat stages of decomposition (as illustrated in Figure 6.1 and Figure 6.2). This significant rainfall might have led to a lack of microbial or insect activity, and subsequently resulted in a diminished rate of skin decomposition.

Consequently, the reduction in cholesterol levels for H4 and H5 was comparatively slower, contrasting with the drastic declines observed in H2 and H3. Uncertainties remain about whether the cholesterol decrease is directly linked to the onset of natural mummification. This relationship couldn't be confidently established across all four individuals and hence necessitates further investigation. This uncertainty calls into question the use of cholesterol as a reliable biomarker in decomposition cases involving natural mummification and demands further exploration.

Lithocholic acid is secondary bile acid which is produced within the intestines [110] through the action of intestinal bacteria [96] and can also be released from the body's bile ducts and gallbladder during decomposition. This compound was detected mostly in high abundances within the skin of H3 (Figure 7.8). Lithocholic acid is a bile acid produced by intestinal flora and acts as a detergent in solubilising fat for absorption in the intestine [96]. While the presence of lithocholic acid in high levels is not surprising due to its possible release from the body to solubilize fat while the human was still living, it is unclear why such fluctuations were depicted through decomposition. Lithocholic acid is suspected to be present due to the breakdown and disintegration of the epithelial tissue within the gastrointestinal tract. This may have resulted in the release of faecal particles from the intestinal tract to the approximately area of sampling and therefore resulted in the presence of this compound at the levels observed. This compound is not detected at levels greater than 10 ppm for H2, H4, and H5, further suggesting that lithocholic acid was present in H3 at such high levels due to contamination from bodily fluid release.

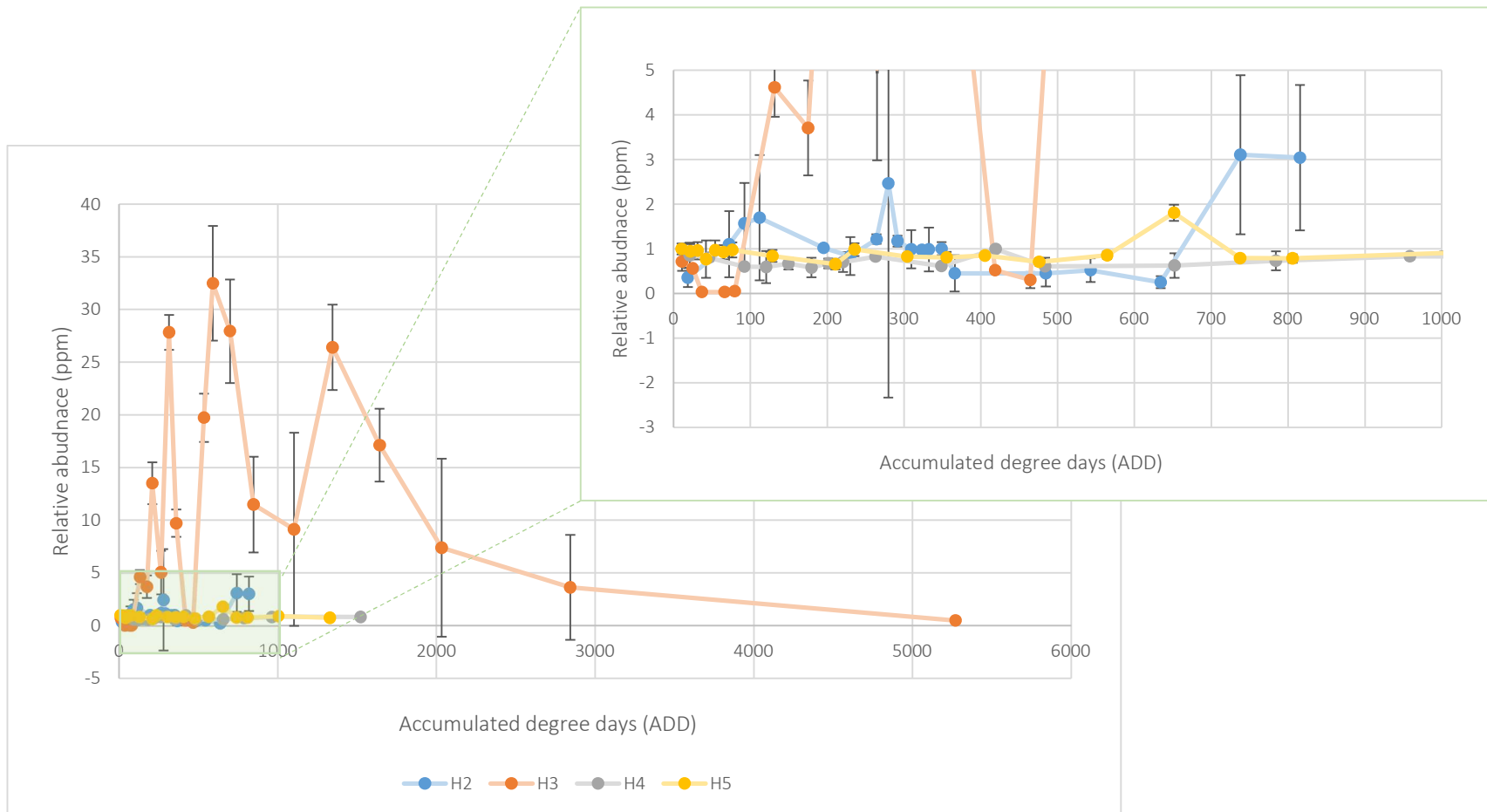


Figure 6.16: Comparison of lithocholic acid during the decomposition periods of H2 (human 2), H3 (human 3), H4 (human 4) and H5 (human 5). Error bars represent standard deviation variation of (4) replicates.

## 6.6 SKIN CONCLUSIONS

The detection of a variety of lipids at high relative abundances across the decomposition period for all four humans (H2-H5) indicates a dynamic lipid profile. Generally, the compounds degraded as decomposition progressed, while breakdown products initially increased and subsequently decreased—a pattern consistent with anaerobic compound breakdown.

Establishing trends in compounds concerning stages of decay posed challenges for both fatty acids and sterols. The transition of oleic acid into palmitoleic acid emerged as the sole observable trend in the fatty acids of the skin, specifically during the transition from the fresh to the bloat stage. Myristic acid, among all investigated compounds, consistently correlated with natural mummification. The presence of naturally mummified skin demonstrated higher myristic acid levels in all humans, attributed to the anti-fungal, anti-virulent, and anti-bacterial properties associated with myristic acid [87, 111, 112]. This inhibition of microbial and insect activity sheds light on the preservation achieved through natural mummification consistently observed across all individuals. This relationship

The challenge in categorising decomposing remains based on the fatty acid composition of the skin may be attributed to the influx of myristic acid during the initiation of mummification, presenting a distinct pattern within the skin matrix compared to the tissue matrix where myristic acid increase is evident during later phases of decomposition. The rise in myristic acid levels coinciding with the onset of natural mummification may contribute to the complexities in staging remains based on their lipid profiles.

Cholesterol exhibited some correlation with the onset of natural mummification, as indicated by a decrease in this compound in H2 and H3. However, these trends were not confidently observed in H4 and H5, potentially due to substantial rainfall. The impact of rainfall on concealing trends could be attributed to interference and interaction with the surrounding environment, resulting in potential contamination and disrupting microbial activity on the body's surface. Further investigation is necessary to establish a relationship and determine the influence of environmental factors on cholesterol breakdown during decomposition.



# CHAPTER 7 CONCLUSIONS AND FUTURE WORK

The aim of this research was to investigate the effect of natural mummification within the skin and tissue of decomposing human and pig bodies. A method for the detection of volatile, low molecular weight lipids were developed and optimised for the assessment of lipids within decomposing skin and tissue of humans. This method is proven useful as per the research conducted to accurately determine lipid abundances in human bodies and was applied to investigate both humans and pigs.

The findings of this research clearly establish distinct differences in the decomposition processes of human and pig decomposition, evident both visually and at a biochemical level. This disparity holds true for studies conducted on both human and pigs during both Australian summer and winter conditions, revealing numerous lipids that exhibit statistically significant variations between the two species. Furthermore, the study demonstrates that the occurrence of natural mummification is a consistent phenomenon observed across all decomposing bodies, irrespective of whether they are human or pig. While, natural mummification is a consistent feature, it is accompanied by variations in terms of its onset, impact, and lipid composition. The research design involved placing one (1) human and two (2) pig bodies in close temporal proximity during both Australian summer (warmer climate) and winter (cooler climate) trials to ensure comparable environmental conditions. Notably, the visual staging of humans and pigs differed, with natural mummification manifesting at distinct time points for the two species. In humans, this process led to the preservation of skin integrity and skeletal structure, both during seasonal trials, consequently preventing the active decay stage. In contrast, the porcine displayed non-preservation effects in both seasonal trials, progressing through all stages of decomposition. Lipid behavior exhibited some similarities as decomposition advanced; however, the levels of relative abundance unveiled significant statistical differences between humans and pigs. These differences were evident across both skin and tissue matrices, regardless of the season. Considering these findings, it is evident that while natural mummification is a shared characteristic in humans and pigs, its outcomes cannot be generalised across the two species. To validate these trends further, comprehensive studies encompassing all seasons should be conducted to ascertain the consistencies and disparities in lipid relative abundances for both species. While natural mummification is shared, its outcomes cannot be generalized across species, emphasising the unsuitability of pigs as human analogues. Consequently, the comprehension of natural mummification is deepened when viewed through the lens of lipid analysis in human decomposition and in the comparative context of decomposing humans and pigs. Prospective endeavors should encompass broader explorations into similar compounds discovered within naturally mummified human and pigs. This broader investigation could unveil insights into whether specific lipid observations could potentially endorse the utilisation of pigs as human analogues.

Four (4) humans were also investigated from a lipid profile and natural mummification perspective. It was documented that all humans, regardless of temperature and rainfall subjected, experienced natural mummification. It was observed, through using accumulated degree days (ADD) for visual monitoring of natural mummification, that initial indications of this process emerged within the range of 150-250 ADD for all humans. This pivotal discovery holds significant implications, as establishing such an ADD range enables the anticipation of what was once considered a 'random occurrence' of natural mummification within temperate settings. Moreover, this range can serve as a valuable framework for visually staging and categorising decomposing human bodies subject to natural mummification in such environments. In the realm of medico-legal casework, these discoveries carry substantial value, especially concerning the estimation of the post-mortem interval (PMI). Integrating the phenomenon of natural mummification in this context enables the establishment of precise timelines, achieved through a fusion of visual observations and analysis of weather data.

The manifestation of natural mummification primarily exerted its impact on the skin of decomposing bodies, yielding a higher degree of lipid variability when compared to the tissue. Despite comprehensive efforts, no discernible compound associations could be established regarding the onset of natural mummification within the tissue matrix. It is postulated that while natural mummification inhibits external decomposition, internal decomposition remains relatively unaffected or experiences a milder influence. The influence of natural mummification predominantly targets the surface layers of decomposing bodies.

In the domain of human skin matrix studies, myristic acid emerged with a direct and positive correlation to the presence of natural mummification. This consistent relationship raises speculation about myristic acid's role in the preservation effects, attributed to its antiviral and antibacterial properties, reducing microbial and insect activities. Myristic acid emerges as a promising biomarker for investigating natural mummification, with potential applications in estimating PMI and archaeological forensic investigations. Its utilisation holds potential significance in cases involving missing persons in a temperate Australian environment, where naturally mummified skin is likely present.

This biochemical approach offers the advantage of accurately representing actual changes in the composition of tissue, as opposed to systems relying on qualitative assessments such as the TBS method. In systems based on qualitative appraisal, including TBS, the description of decomposition progression is restricted by the predefined definitions of the system. This limitation arises not only from the subjectivity inherent in qualitative descriptions but also because the sequence of visual phenomena

is often perceived as sequential, contrary to the non-linear nature of decomposition processes, as seen in mosaic/differential decomposition and the rehydration of desiccated tissues post-rainfall.

To verify the potential antibiotic effects of myristic acid contributing to the observed natural mummification in the human remains from my research, additional investigations and experiments would be required. This could involve conducting controlled studies to assess the impact of myristic acid on microbial activity and decay processes in simulated conditions resembling the decomposition environment. By systematically varying the presence and concentration of myristic acid in these experiments, researchers can observe any inhibitory effects on bacterial and fungal growth, providing insights into its antibiotic properties. This could be explored by examining the post-mortem microbial succession on the skin, with a specific focus on organisms like *Enterobacteriaceae* and *Proteus mirabilis*. These microbes have been documented to play a crucial role in attracting insects to cadavers, thereby aiding in the process of decomposition [113]. Additionally, comparative analyses with and without myristic acid in similar decomposition settings could help confirm its role in natural mummification.

Further studies focusing on the utilisation of myristic acid as a biomarker to refine the understanding of the relationship between time-since-death and the accumulation of the compound could shed light on the nuances of this component. Such investigations could expand the application of this study within forensic inquiries. Given that the drying out of soft tissue is a crucial element in natural mummification, measuring and incorporating this process into upcoming studies could be valuable for potentially crafting PMI estimation methods using biomarker patterns over time. Comparable quantitative research, such as that by Lennartz et al., indicates the promise of creating a PMI estimation approach founded on the moisture content of desiccating tissue [114].

The application of this research within forensic contexts is all-encompassing, as skin and tissue are universally present in non-archaeological forensic cases, unlike matrices such as soil and clothing that might not always be available. The potential utilisation of naturally mummified skin in both archaeological and non-archaeological forensic investigations further highlights the significance of this research. While the research offers valuable insights into the occurrence and presentation of natural mummification, the specific influence of different clothing levels on this process remains an aspect that requires further investigation. The diverse nature of clothing materials, thickness, and coverage may contribute to variations in the rate and extent of natural mummification. The study acknowledges the potential impact of clothing on decomposition dynamics but does not extensively delve into the nuanced effects that varying clothing conditions might exert on the observed phenomenon. Therefore, future research endeavors focusing on the intricate interplay between clothing variables and natural

mummification could provide a more comprehensive understanding of the factors influencing this intriguing process.

The observed reduction in entomofauna, particularly influenced by weather factors like rainfall, prompts further investigation into the depth of this connection. This examination could encompass quantitative entomofauna analysis involving consistent monitoring, trapping, and identification of insect species to gauge their influence on decomposition. Additionally, delving into microbial community dynamics can shed light on the shifts in microbial communities associated with decomposition under varying weather conditions and entomofauna exclusion. The integration of weather data becomes crucial in correlating factors such as temperature, humidity, and precipitation with the identified preservation effects. This multifaceted approach ensures a comprehensive exploration of the intricate relationship between weather impacts, entomofauna activity, and the preservation of biological remains.

The discoveries related to natural mummification within humans within the temperate environment of Australia provides framework and holds promise for broader global applications, enhancing the significance of this research. Expanding on this, future investigations could involve examining natural mummification occurrences in diverse biomes worldwide, aiming to analyse the distinct influences that different environments have on the process. Such comprehensive studies would contribute to a more nuanced understanding of natural mummification and facilitate the differentiation of its instances across various global environments.

Acknowledging the limited sample size in this project underscores the need for additional replication and comprehensive evaluation with larger sample sizes under appropriately replicated conditions. Such efforts would enhance the robustness of the findings obtained in this research. Future endeavors will strive to achieve sufficient statistical power, aiming for approximately 80%, as suggested by Benbow et al. This will be accomplished through an expanded number of replicates to ensure precise measurements, considering the inherent variability among samples [115].

In conclusion, this research introduces a novel method for detecting volatile, low molecular weight lipids in decomposing human and pig bodies, offering accurate insights into lipid abundances. Distinct differences in the decomposition processes of humans and pigs are highlighted, both visually and biochemically, across Australian summer and winter conditions. Myristic acid emerges as a promising biomarker, exhibiting a direct correlation with natural mummification in human skin matrices, suggesting its potential role in preservation. The biochemical approach employed in this research,

compared to qualitative systems like the TBS method, accurately represents tissue composition changes and offers advantages in studying non-linear decomposition processes.

# CHAPTER 8 REFERENCES

1. Pless, J.E., M.B. Worrell, and M.A. Clark, *Chapter 9 - Postmortem changes in soft tissues [in] Forensic taphonomy: the postmortem fate of human remains*, in *Forensic Taphonomy: the postmortem fate of human remains*, W.D. Haglund and M.H. Sorg, ed. 1997, CRC Press: Boca Raton, London. p. 151-164.
2. Efremov, J., *Taphonomy: a new branch of paleontology: Pan-American Geologist*, v. 74. American Geologist, 1940.
3. Haglund, D.W. and H.M. Sorg, *Advances in Forensic Taphonomy: Method, Theory, and Archaeological Perspectives*. 2002, U.S: CRC Press.
4. Rowe, W., *Review of: Advances in Forensic Taphonomy: Method, Theory, and Archaeological Perspectives*. Journal of Forensic Sciences, 2002.
5. Haglund, D.W. and H.M. Sorg, *Forensic Taphonomy: The Postmortem Fate of Human Remains*. 1997, US: CRC Press.
6. Nawrocki, S., *Handbook of Forensic Anthropology and Archaeology*. Second ed, ed. S. Blau and D. Ubelakar. 2016, New York: Routledge.
7. Dekeirsschieter, J., et al., *Enhanced Characterization of the Smell of Death by Comprehensive Two-Dimensional Gas Chromatography-Time-of-Flight Mass Spectrometry (GCxGC-TOFMS)*. PLOS ONE, 2012. **7**(6): p. e39005.
8. Gill-King, H., *Chemical and Ultrastructural Aspects of Decomposition*. Forensic Taphonomy: The Postmortem Fate of Human Remains, ed. H.M. Sorg and D.W. Haglund. 1997, USA: CRC Press.
9. Iqbal, M.A., et al., *Forensic Decomposition Odour Profiling: A review of experimental designs and analytical techniques*. TrAC Trends in Analytical Chemistry, 2017. **91**: p. 112-124.
10. Perrault, K., B. Stuart, and S. Forbes, *A Longitudinal Study of Decomposition Odour in Soil Using Sorbent Tubes and Solid Phase Microextraction*. Chromatography, 2014. **1**(3): p. 120.
11. Schotsmans, E., N. Márquez-Grant, and S. Forbes, *Taphonomy of Human Remains : Forensic analysis of the dead and the depositional environment*. 2017, Chichester, West Sussex John Wiley & Sons Ltd.
12. Connor, M., C. Baigent, and E.S. Hansen, *Testing the Use of Pigs as Human Proxies in Decomposition Studies*. Journal of Forensic Science, 2018. **63**(5): p. 1350-1355.
13. Knobel, Z., et al., *A Comparison of Human and Pig Decomposition Rates and Odour Profiles in an Australian Environment*. Australian Journal of Forensic Sciences, 2018: p. 1-16.



14. Deo, A., et al., *Profiling the Seasonal Variability of Decomposition Odour from Human Remains in a Temperate Australian Environment*. Australian Journal of Forensic Sciences, 2020. **52**(6): p. 654-664.
15. W. Mann, R., W. M. Bass, and L. Meadows, *Time Since Death and Decomposition of the Human Body: Variables and Observations in Case and Experimental Field Studies*. Vol. 35. 1990. 103-11.
16. Janaway, R.C., S.L. Percival, and A.S. Wilson, *Decomposition of Human Remains*. 2009, Humana Press. p. 313-334.
17. Ceciliason, A.S., et al., *Quantifying Human Decomposition in an Indoor Setting and Implications for Postmortem Interval Estimation*. Forensic Science International, 2018. **283**: p. 180-189.
18. Brooks, J.W., *Postmortem Changes in Animal Carcasses and Estimation of the Postmortem Interval*. Vet Pathology, 2016. **53**(5): p. 929-40.
19. Pinheiro, J., *Decay Process of a Cadaver*, in *Forensic Anthropology and Medicine: Complementary Sciences From Recovery to Cause of Death*, A. Schmitt, E. Cunha, and J. Pinheiro, ed. 2006, Humana Press: Totowa, NJ. p. 85-116.
20. Lynnerup, N., *Mummies*. American Journal of Physical Anthropology, 2007. **134**(S45): p. 162-190.
21. Campobasso, C.P., et al., *The Mummified Corpse in a Domestic Setting*. The American Journal of Forensic Medicine and Pathology, 2009. **30**(3): p. 307-10.
22. Finaughty, D.A. and A.G. Morris, *Precocious Natural Mummification in a Temperate Climate (Western Cape, South Africa)*. Forensic Science International, 2019. **303**: p. 109948.
23. Nolan, A.-N.D., et al., *The Impact of Environmental Factors on the Production of Peptides in Mammalian Decomposition Fluid in Relation to the Estimation of Post-mortem Interval: A summer/winter comparison in Western Australia*. Forensic Science International, 2019. **303**: p. 109957-109957.
24. Ueland, M., et al., *Fresh vs. Frozen Human Decomposition – A preliminary investigation of lipid degradation products as biomarkers of post-mortem interval*. Forensic Chemistry, 2021. **24**: p. 100335.
25. Police, A.F. *Missing Persons*. 2022 [cited 2023 09.01.2024]; Available from: <https://www.missingpersons.gov.au/view-all-profiles>.
26. Perrault, K.A., K.D. Nizio, and S.L. Forbes, *A Comparison of One-Dimensional and Comprehensive Two-Dimensional Gas Chromatography for Decomposition Odour Profiling Using Inter-Year Replicate Field Trials*. Chromatographia, 2015. **78**(15): p. 1057-1070.

27. Payne, J.A., *A Summer Carrion Study of the Baby Pig Sus Scrofa Linnaeus*. Ecology, 1965. **46**(5): p. 592-602.
28. Perrault, K.A., et al., *Seasonal Comparison of Carrion Volatiles in Decomposition Soil using Comprehensive Two-dimensional Gas Chromatography - Time of flight Mass Spectrometry*. Analytical Methods, 2015. **7**(2): p. 690-698.
29. Ioan, B., et al., *The Chemistry Decomposition in Human Corpses*. Revista de Chimie, 2017. **68**: p. 1450-1454.
30. Marhoff, S.J., et al., *Estimating Post-mortem Interval using Accumulated Degree-days and a Degree of Decomposition Index in Australia: a validation study*. Australian Journal of Forensic Sciences, 2016. **48**(1): p. 24-36.
31. Statheropoulos, M., C. Spiliopoulou, and A. Agapiou, *A Study of Volatile Organic Compounds Evolved from the Decaying Human Body*. Forensic Science International, 2005. **153**(2): p. 147-155.
32. Stefanuto, P., Parrault, K., Stadler, S., Pesesse, R., Broki, M., Forbes, S., Focant, J, *Reading Cadaveric Decomposition Chemistry with a New Pair of Glasses*. ChemPlusChem, 2014. **79**(6): p. 786-789.
33. Forbes, S.L., et al., *Comparison of the Decomposition VOC Profile during Winter and Summer in a Moist, Mid-Latitude (Cfb) Climate*. PLOS ONE, 2014. **9**(11): p. e113681.
34. Stuart, B., *Decomposition Chemistry: Overview, Analysis, and Interpretation*, in *Encyclopedia of Forensic Sciences* P.J.S.a.M.M.H. Jay A. Siegel, ed. 2013, Academic Press. p. 11-15.
35. Troutman, L., C. Moffatt, and T. Simmons, *A Preliminary Examination of Differential Decomposition Patterns in Mass Graves*. Journal of Forensic Sciences, 2014. **59**(3): p. 621-626.
36. Megyesi, M.S., S.P. Nawrocki, and N.H. Haskell, *Using Accumulated Degree-days to Estimate the Postmortem Interval from Decomposed Human Remains*. Journal of Forensic Science, 2005. **50**(3): p. 618-26.
37. Janaway, R.C., et al., *Taphonomic Changes to the Buried Body in Arid Environments: An Experimental Case Study in Peru*, in *Criminal and Environmental Soil Forensics*, K. Ritz, L. Dawson, and D. Miller, ed. 2009, Springer Netherlands: Dordrecht. p. 341-356.
38. Galloway, A., et al., *Decay Rates of Human Remains in an Arid Environment*. Journal of Forensic Sciences, 1989. **34**(3): p. 607-616.
39. Collins, S., B. Stuart, and M. Ueland, *The use of Lipids from Textiles as Soft-tissue Biomarkers of Human Decomposition*. Forensic Science International, 2023. **343**: p. 111547.

40. Pittner, S., et al., *The Applicability of Forensic Time Since Death Estimation Methods for Buried Bodies in Advanced Decomposition Stages*. PLOS ONE, 2020. **15**(12): p. e0243395.
41. Finaughty, D. and A. Morris, *The Mummies of the Cape: precocious natural mummification in the Western Cape*. 2018.
42. Aufderheide, A.C., *Soft Tissue Taphonomy: A paleopathology perspective*. International Journal of Paleopathology, 2011. **1**(2): p. 75-80.
43. Petrella, E., et al., *CT Scan of Thirteen Natural Mummies Dating Back to the XVI-XVIII Centuries: An Emerging Tool to Investigate Living Conditions and Diseases in History*. PLoS One, 2016. **11**(6): p. e0154349.
44. Nerlich, A.G., A. Fleckinger, and O. Peschel, *Life and Diseases of the Neolithic Glacier Mummy "Ötzi"*, in *The Handbook of Mummy Studies: New Frontiers in Scientific and Cultural Perspectives*, D.H. Shin and R. Bianucci, ed. 2020, Springer Singapore: Singapore. p. 1-22.
45. Makristathis, A., et al., *Fatty Acid Composition and Preservation of the Tyrolean Iceman and other Mummies*. Journal of Lipid Research, 2002. **43**(12): p. 2056-2061.
46. Bligh, E.G. and W.J. Dyer, *A Rapid Method of Total Lipid Extraction and Purification*. Canadian journal of biochemistry physiology, 1959. **37**(8): p. 911-917.
47. Copley, M.S., et al., *Detection of Palm Fruit Lipids in Archaeological Pottery from Qasr Ibrim, Egyptian Nubia*. Biological Sciences, 2001. **268**(1467): p. 593-597.
48. Dudd, S.N., M. Regert, and R.P. Evershed, *Assessing Microbial Lipid Contributions during Laboratory Degradations of Fats and Oils and Pure Triacylglycerols Absorbed in Ceramic Potsherds*. Organic Geochemistry, 1998. **29**(5-7): p. 1345-1354.
49. Ueland, M., et al., *The Interactive Effect of the Degradation of Cotton Clothing and Decomposition Fluid Production Associated with Decaying Remains*. Forensic Science International, 2015. **255**: p. 56-63.
50. Ueland, M., S.L. Forbes, and B.H. Stuart, *Seasonal Variation of Fatty Acid Profiles from Textiles Associated with Decomposing Pig Remains in a Temperate Australian Environment*. Forensic Chemistry, 2018. **11**: p. 120-127.
51. Serafim, V., et al., *Development and Validation of a LC-MS/MS-Based Assay for Quantification of Free and Total Omega 3 and 6 Fatty Acids from Human Plasma*. Molecules, 2019. **24**(2): p. 360.
52. Reis, A., et al., *A Comparison of Five Lipid Extraction Solvent Systems for Lipidomic Studies of Human LDL*. Journal of Lipid Research, 2013. **54**(7): p. 1812-1824.

53. Luong, S., et al., *Development and Application of a Comprehensive Analytical Workflow for the Quantification of Non-volatile Low Molecular Weight Lipids on Archaeological Stone Tools*. Analytical Methods, 2017. **9**(30): p. 4349-4362.
54. Luong, S., et al., *Incorporating Terpenes, Monoterpenoids and Alkanes into Multiresidue Organic Biomarker Analysis of Archaeological Stone Artefacts from Liang Bua (Flores, Indonesia)*. Journal of Archaeological Science: Reports, 2018. **19**: p. 189-199.
55. Folch, J., M. Lees, and G.H. Sloane Stanley, *A Simple Method for the Isolation and Purification of Total Lipides from Animal Tissues*. Journal of Biological Chemistry, 1957. **226**(1): p. 497-509.
56. Langley, N.R., et al., *Forensic Postmortem Interval Estimation from Skeletal Muscle Tissue: A Lipidomics Approach*. Forensic Anthropology, 2019. **2**(3): p. 152-157.
57. Wood, P. and S. NR, *Lipidomics Analysis of Postmortem Interval: Preliminary evaluation of human skeletal muscle*. Metabolomics, 2013. **3**: p. 127.
58. A. Vass, A., *Beyond the Grave—Understanding human decomposition*. Vol. 28. 2001. 190-193.
59. Van de Kamer, J., K. Gerritsma, and E. Wansink, *Gas-liquid Partition Chromatography: the separation and micro-estimation of volatile fatty acids from formic acid to dodecanoic acid*. Biochemical Journal, 1955. **61**(1): p. 174-176.
60. Forbes, S.L., B.H. Stuart, and B.B. Dent, *The Identification of Adipocere in Grave Soils*. Forensic Science International, 2002. **127**(3): p. 225-230.
61. Cablk, M.E., E.E. Szlagowski, and J.C. Sagebiel, *Characterization of the Volatile Organic Compounds present in the Headspace of Decomposing Animal Remains, and Compared with Human Remains*. Forensic Science International, 2012. **220**(1-3): p. 118-25.
62. Actlabs. *GC/MS & GC/MS/MS Methods*. 2019 [cited 2019].
63. Homer, N., et al., *Gas Chromatography Tandem Mass Spectrometry offers Advantages for Urinary Steroids Analysis*. Analytical biochemistry, 2017. **538**: p. 34-37.
64. Luong, S., et al., *Monitoring the Extent of Vertical and Lateral Movement of Human Decomposition Products through Sediment using Cholesterol as a Biomarker*. Forensic Science International, 2018. **285**: p. 93-104.
65. Colombini, M.P., et al., *Characterisation of Organic Residues in Pottery Vessels of the Roman Age from Antinoe (Egypt)*. Microchemical Journal, 2005. **79**(1-2): p. 83-90.
66. Eerkens, J.W., *GC-MS Analysis and fatty acid ratios of archaeological potsherds from the wester great basin of North America* Archaeometry, 2005. **47**(1): p. 83-102.

67. Kimpe, K., et al., *Assessing the Relationship Between Form and use of Different Kinds of Pottery from the Archaeological Site Sagalassos (southwest Turkey) with Lipid Analysis*. *Journal of Archaeological Science*, 2004. **31**(11): p. 1503-1510.
68. Isaksson, S. and F. Hallgren, *Lipid Residue Analyses of Early Neolithic Funnel-beaker Pottery from Skogsmossen, Eastern Central Sweden, and the Earliest Evidence of Dairying in Sweden*. *Journal of Archaeological Science*, 2012. **39**(12): p. 3600-3609.
69. Statistics, A.B.o., *Deaths, Australia*. 2022, ABS Website: Australia.
70. Medicine, V.I.o.F. *For Medical Practitioners*. 2023 [cited 2024 09.01.24]; Available from: <https://www.vifm.org/home/medical-practitioners/>.
71. Aufderheide, A.C., *The Scientific Study of Mummies*. 2003: Cambridge University Press.
72. Henssge, C. and B. Madea, *Estimation of the Time Since Death in the Early Post-mortem Period*. *Forensic Science International*, 2004. **144**(2-3): p. 167-175.
73. Notter, S.J., et al., *The Initial Changes of Fat Deposits During the Decomposition of Human and Pig Remains*. *Journal of Forensic Sciences*, 2009. **54**(1): p. 195-201.
74. Department of Agriculture, F.a.F. *Australia's forests – overview*. 2018 [cited 2024 09.01.2024]; Available from: <https://www.agriculture.gov.au/abares/forestsaustralia/australias-forests/profiles/australias-forests-2019>.
75. Meterology, B.o., *Climate Statistics for Australian Locations*. 2020, Australian Government.
76. Stokes, K.L., S.L. Forbes, and M. Tibbett, *Human Versus Animal: Contrasting Decomposition Dynamics of Mammalian Analogues in Experimental Taphonomy*. *Journal of Forensic Sciences*, 2013. **58**(3): p. 583-591.
77. Collins, S., B. Stuart, and M. Ueland, *Monitoring Human Decomposition Products Collected in Clothing: An infrared spectroscopy study*. *Australian Journal of Forensic Sciences*, 2020. **52**(4): p. 428-438.
78. Pfeiffer, S., S. Milne, and R.M. Stevenson, *The Natural Decomposition of Adipocere*. *Journal of Forensic Sciences*, 1998. **43**(2): p. 368-370.
79. Bethell, P.H., et al., *The Study of Molecular Markers of Human Activity: The Use of Coprostanol in the Soil as an Indicator of Human Faecal Material*. *Journal of Archaeological Science*, 1994. **21**(5): p. 619-632.
80. Matuszewski, B.K., M.L. Constanzer, and C.M. Chavez-Eng, *Strategies for the Assessment of Matrix Effect in Quantitative Bioanalytical Methods Based on HPLC-MS/MS*. *Analytical Chemistry*, 2003. **75**(13): p. 3019-3030.
81. Moldoveanu, S. and V. David, *Derivatization Methods in GC and GC/MS*. 2018.

82. Zhou, W., S. Yang, and P.G. Wang, *Matrix Effects and Application of Matrix Effect Factor*. *Bioanalysis*, 2017. **9**(23): p. 1839-1844.
83. Frigolet, M.E. and R. Gutiérrez-Aguilar, *The Role of the Novel Lipokine Palmitoleic Acid in Health and Disease*. *Advances in Nutrition*, 2017. **8**(1): p. 173S-181S.
84. Dadour, I.R., et al., *Forensic Entomology: application, education and research in Western Australia*. *Forensic Science International*, 2001. **120**(1): p. 48-52.
85. Megreya, A.M., *Emotional Intelligence and Criminal Behavior*. *Journal of Forensic Sciences*, 2015. **60**(1): p. 84-88.
86. Ruiz-Núñez, B., D.A.J. Dijk-Brouwer, and F.A.J. Muskiet, *The Relation of Saturated Fatty Acids with Low-grade Inflammation and Cardiovascular Disease*. *The Journal of Nutritional Biochemistry*, 2016. **36**: p. 1-20.
87. Prasath, K.G., et al., *Anti-inflammatory Potential of Myristic Acid and Palmitic Acid Synergism against Systemic Candidiasis in Danio Rerio (Zebrafish)*. *Biomedicine & Pharmacotherapy*, 2021. **133**: p. 111043.
88. Juárez-Rodríguez, M.M., et al., *Tetradecanoic Acids With Anti-Virulence Properties Increase the Pathogenicity of Pseudomonas aeruginosa in a Murine Cutaneous Infection Model*. *Frontiers in Cellular and Infection Microbiology*, 2021. **10**.
89. Kumar, P., et al., *Fatty Acids as Antibiofilm and Antivirulence Agents*. *Trends in Microbiology*, 2020. **28**(9): p. 753-768.
90. Sarmiento-García, A. and C. Vieira-Aller, *Improving Fatty Acid Profile in Native Breed Pigs Using Dietary Strategies: A Review*. *Animals (Basel)*, 2023. **13**(10).
91. von der Lühe, B., et al., *Steroid Fingerprints: Efficient biomarkers of human decomposition fluids in soil*. *Organic Geochemistry*, 2018. **124**: p. 228-237.
92. von der Lühe, B., et al., *Investigation of Sterols as Potential Biomarkers for the Detection of Pig (S. s. domesticus) Decomposition Fluid in Soils*. *Forensic Science International*, 2013. **230**(1): p. 68-73.
93. von der Lühe, B., et al., *Steroids Aid in Human Decomposition Fluid Identification in Soils of Temporary Mass Graves from World War II*. *Journal of Archaeological Science: Reports*, 2020. **32**: p. 102431.
94. PubChem, *Compound Summary for CID 222528, Deoxycholic Acid*. 2017, National Center for Biotechnology Information (2023).
95. Smith, S.B. and D.R. Smith, *Fats: Production and Uses of Animal Fats*, in *Encyclopedia of Food and Health*, B. Caballero, P.M. Finglas, and F. Toldrá, ed. 2016, Academic Press: Oxford. p. 604-608.

96. Sheng, W., G. Ji, and L. Zhang, *The Effect of Lithocholic Acid on the Gut-Liver Axis*. *Frontiers in Pharmacology*, 2022. **13**: p. 910493.
97. Gabay, O., et al., *Stigmasterol: a phytosterol with potential anti-osteoarthritic properties*. *Osteoarthritis Cartilage*, 2010. **18**(1): p. 106-16.
98. Bull, I.D., et al., *The Origin of Faeces by means of Biomarker Detection*. *Environment International*, 2002. **27**(8): p. 647-654.
99. Prost, K., et al., *Steroid Biomarkers Revisited – Improved Source Identification of Faecal Remains in Archaeological Soil Material*. *PLOS ONE*, 2017. **12**(1): p. e0164882.
100. Luong, S., et al., *Combined organic biomarker and use-wear analyses of stone artefacts from Liang Bua, Flores, Indonesia*. *Scientific Reports*, 2019. **9**(1): p. 17553.
101. Copley, M.S., et al., *Gas Chromatographic, Mass Spectrometric and Stable Carbon Isotopic Investigations of Organic Residues of Plant Oils and Animal Fats Employed as Illuminants in Archaeological Lamps from Egypt*. *Analyst*, 2005. **130**(6): p. 860-71.
102. Diczfalusy, U., *On the Formation and possible Biological Role of 25-hydroxycholesterol*. *Biochimie*, 2013. **95**(3): p. 455-460.
103. Forbes, S.L., B.H. Stuart, and B.B. Dent, *The Effect of the Burial Environment on Adipocere Formation*. *Forensic Science International*, 2005. **154**(1): p. 24-34.
104. Notter, S.J., et al., *Solid-phase Extraction in Combination with GC/MS for the Quantification of Free Fatty Acids in Adipocere*. *European Journal of Lipid Science and Technology*, 2008. **110**(1): p. 73-80.
105. Forbes, S.L., B.B. Dent, and B.H. Stuart, *The Effect of Soil Type on Adipocere Formation*. *Forensic Science International*, 2005. **154**(1): p. 35-43.
106. Saraswathi, V., et al., *Myristic Acid Supplementation Aggravates High Fat Diet-Induced Adipose Inflammation and Systemic Insulin Resistance in Mice*. *Biomolecules*, 2022. **12**(6): p. 739.
107. Fischer, C.L., et al., *The Roles of Cutaneous Lipids in Host Defense*. *Biochim Biophys Acta*, 2014. **1841**(3): p. 319-22.
108. TAKEMURA, T., P.W. WERTZ, and K. SATO, *Free Fatty Acids and Sterols in Human Eccrine Sweat*. *British Journal of Dermatology*, 1989. **120**(1): p. 43-47.
109. Almulhim, A.M. and R.G. Menezes, *Evaluation of Postmortem Changes*, in *StatPearls*. 2023, StatPearls Publishing LLC: Treasure Island (FL) ineligible companies. Disclosure: Ritesh Menezes declares no relevant financial relationships with ineligible companies.
110. Gérard, P., *Metabolism of Cholesterol and Bile Acids by the Gut Microbiota*. *Pathogens*, 2014. **3**(1): p. 14-24.

111. Khan, N., et al., *Sponge-derived Fatty Acids Inhibit Biofilm Formation of MRSA and MSSA by Down-regulating Biofilm-related Genes Specific to each Pathogen*. Journal of Applied Microbiology, 2023. **134**.
112. Kim, Y.-G., et al., *Inhibition of Polymicrobial Biofilm Formation by Saw Palmetto Oil, Lauric Acid and Myristic Acid*. Microbial Biotechnology, 2022. **15**(2): p. 590-602.
113. Metcalf, J.L., D.O. Carter, and R. Knight, *Microbiology of Death*. Current Biology, 2016. **26**(13): p. R561-r563.
114. Lennartz, A., M.D. Hamilton, and R. Weaver, *Moisture Content in Decomposing, Desiccated, and Mummified Human Tissue*. Forensic Anthropology, 2020. **3**(1): p. 1-16.
115. Benbow, M.E., J.K. Tomberlin, and A.M. Tarone, *Carrion Ecology, Evolution, and their Applications*. 2015: CRC press.



## APPENDIX A- CALIBRATION CURVES

Calibration curve of compounds used for method optimisation. X-axis is concentration of compound in parts per million (ppm), Y-axis is relative abundance

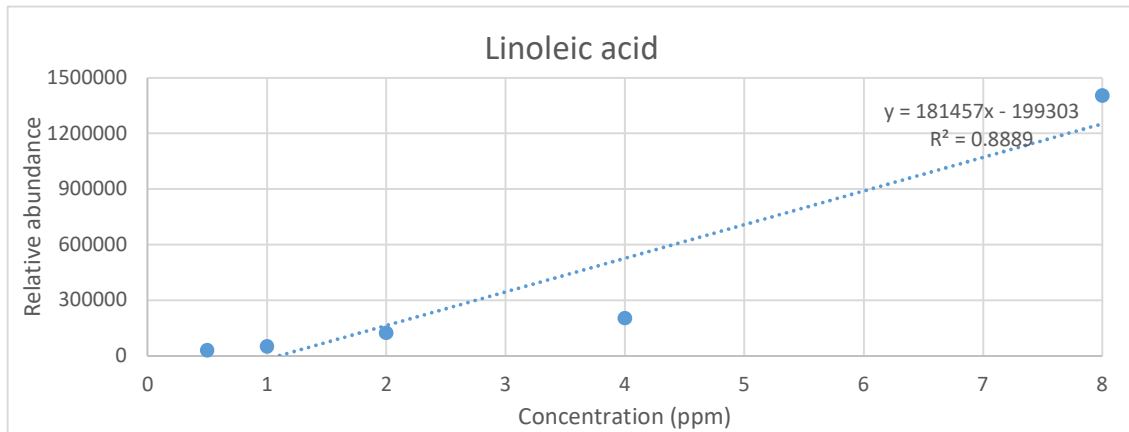


**Figure A-1:** Calibration curve of linoleic acid. X-axis represents concentration in ppm and y-axis is relative abundance.

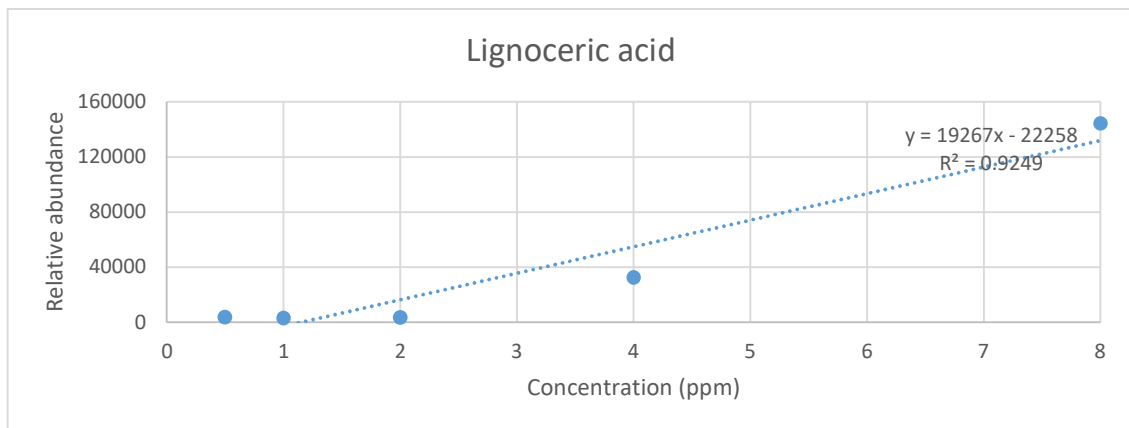


**Figure A-2:** Calibration curve of lignoceric acid. X-axis represents concentration in ppm and y-axis is relative abundance.

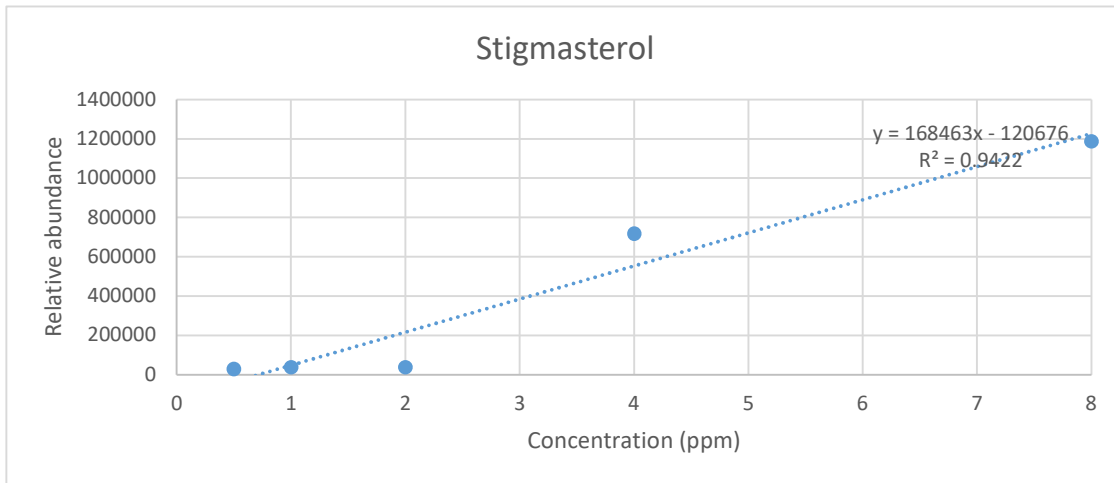


**Figure A-3:** Calibration curve of stigmasterol. X-axis represents concentration in ppm and y-axis is relative abundance.

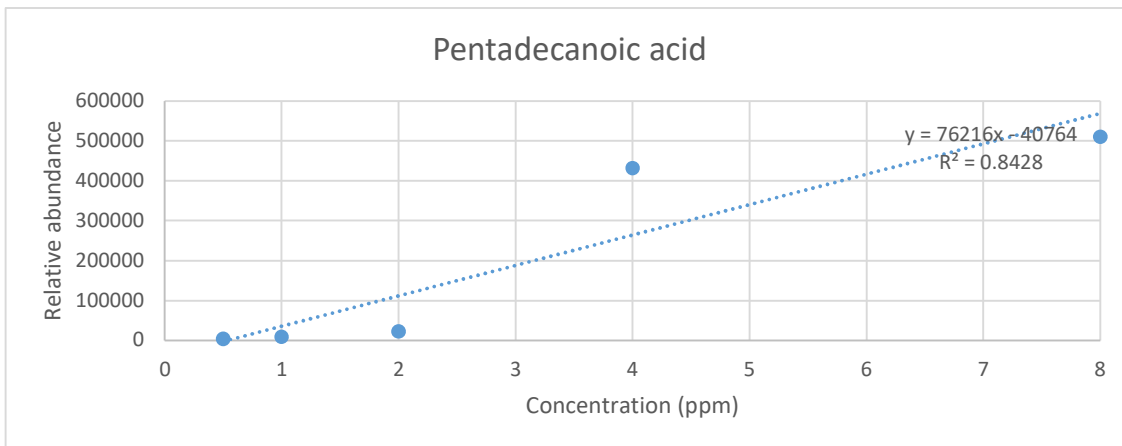


**Figure A-4:** Calibration curve of pentadecanoic acid. X-axis represents concentration in ppm and y-axis is relative abundance.

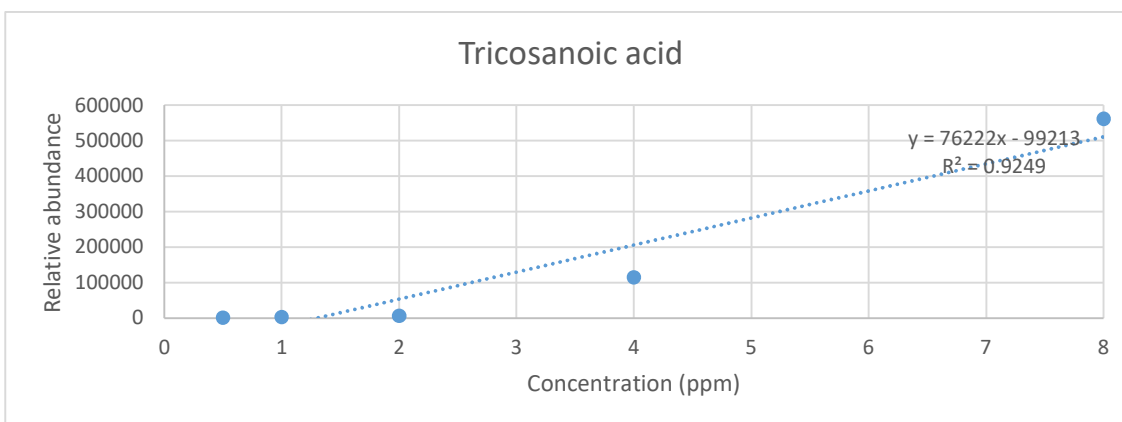


**Figure A-5:** Calibration curve of tricosanoic acid. X-axis represents concentration in ppm and y-axis is relative abundance.

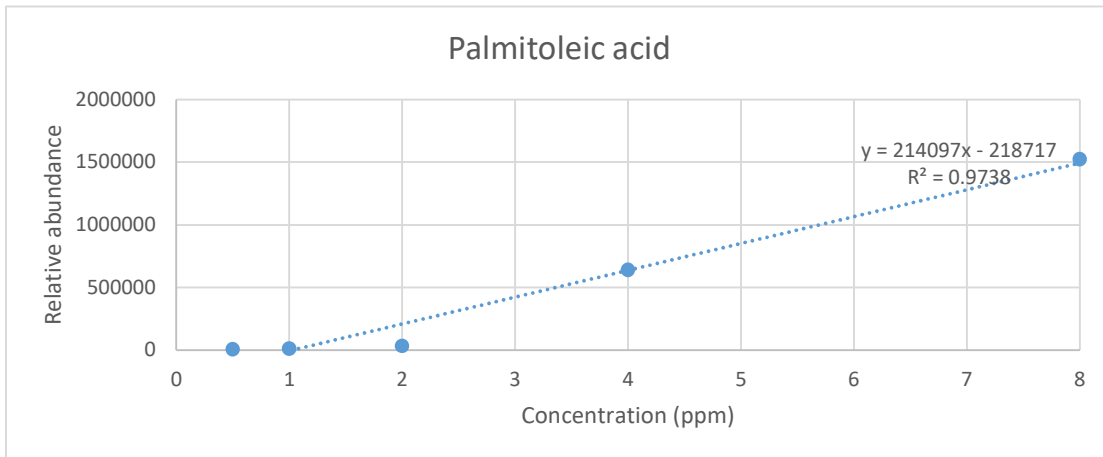


**Figure A-6:** Calibration curve of palmitoleic acid. X-axis represents concentration in ppm and y-axis is relative abundance.

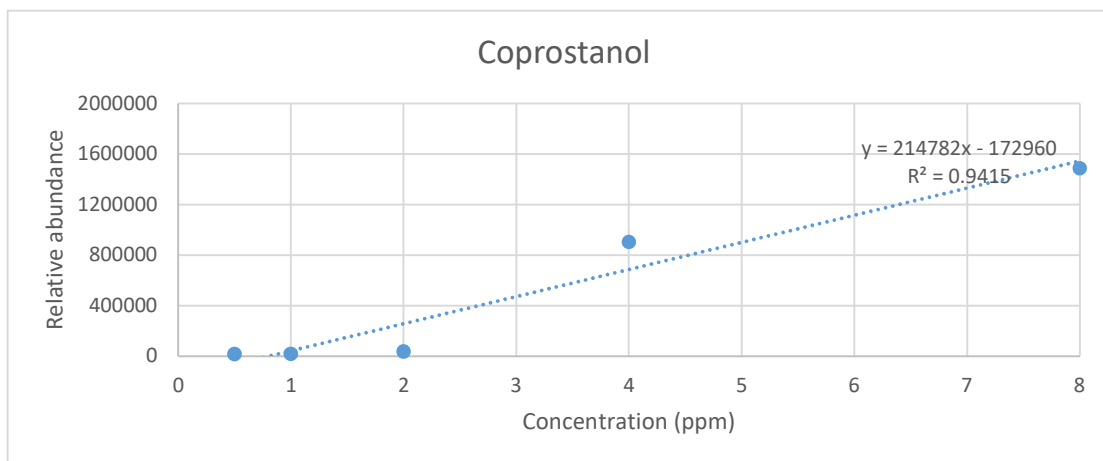


**Figure A-7:** Calibration curve of coprostanol. X-axis represents concentration in ppm and y-axis is relative abundance.

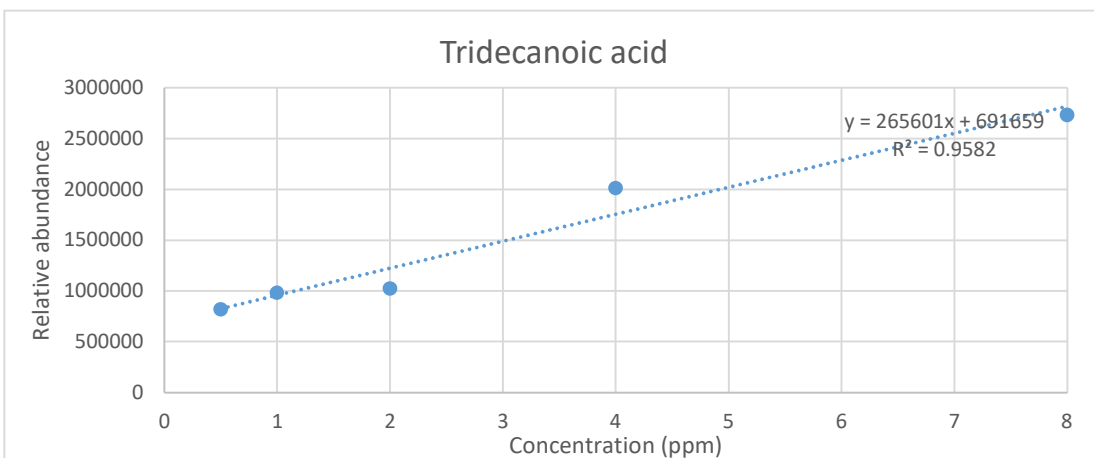


**Figure A-8:** Calibration curve of tridecanoic acid. X-axis represents concentration in ppm and y-axis is relative abundance

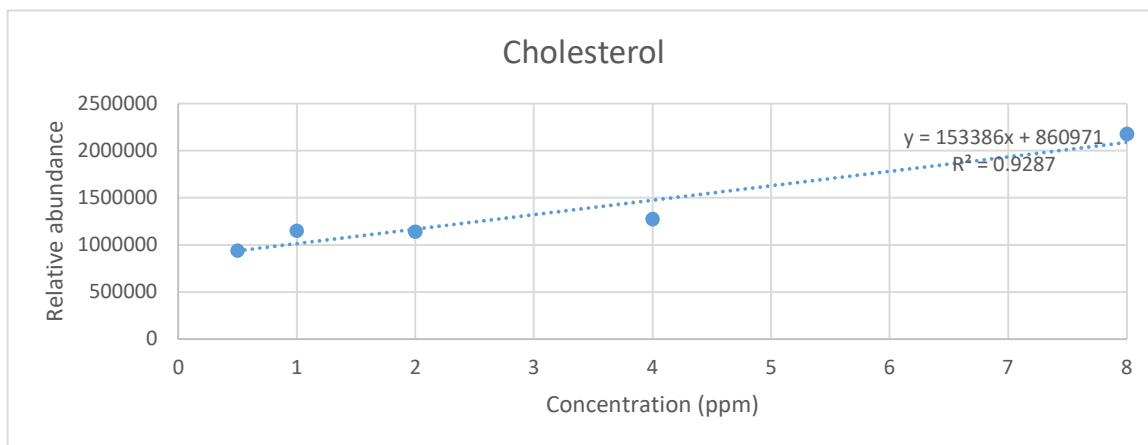


**Figure A-9:** Calibration curve of cholesterol. X-axis represents concentration in ppm and y-axis is relative abundance.

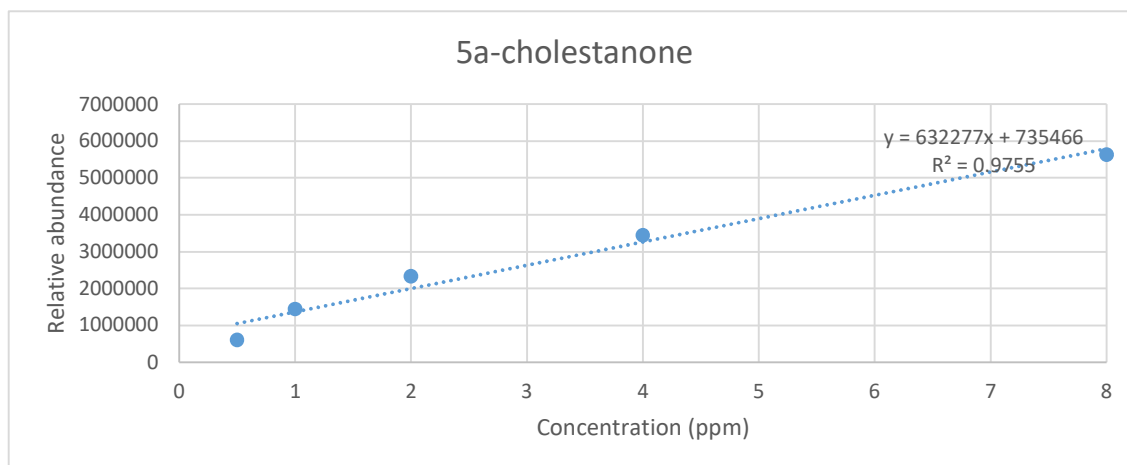


**Figure A-10:** Calibration curve of 5a-cholestanone. X-axis represents concentration in ppm and y-axis is relative abundance.

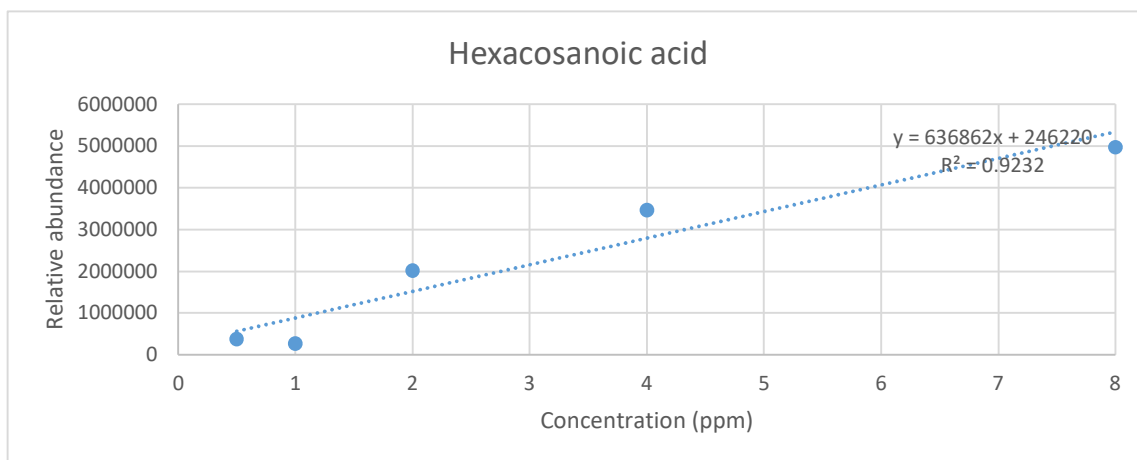


**Figure A-11:** Calibration curve of hexacosanoic acid. X-axis represents concentration in ppm and y-axis is relative abundance.

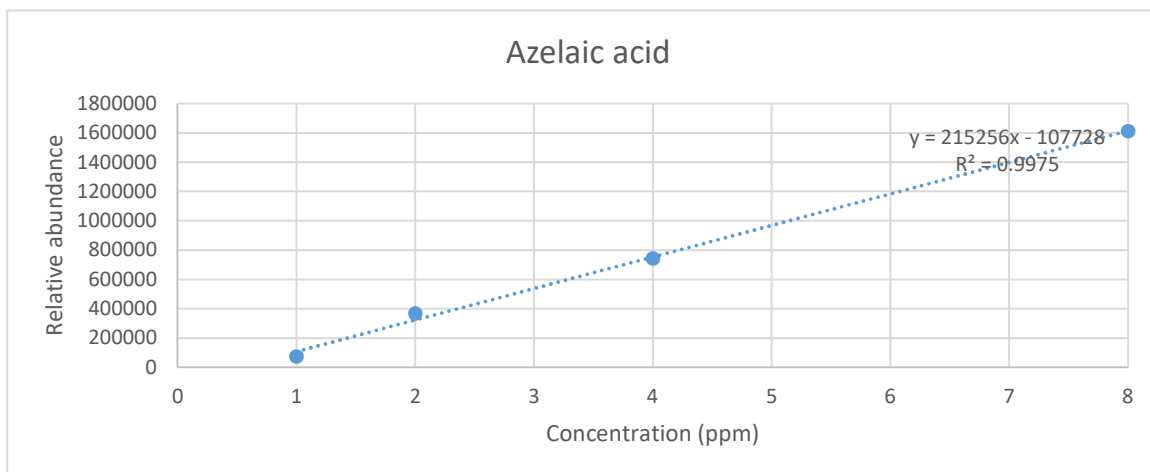


**Figure A-12:** Calibration curve of azelaic acid. X-axis represents concentration in ppm and y-axis is relative abundance.

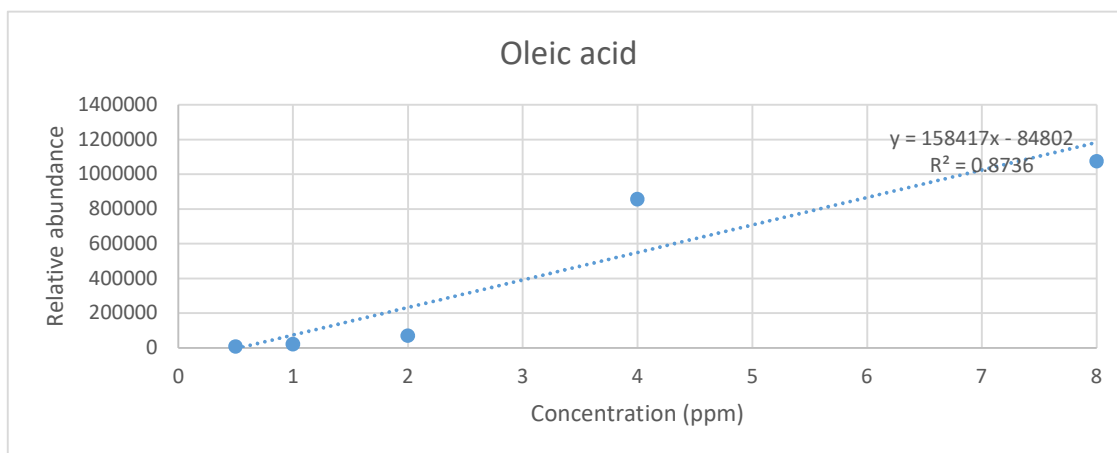


**Figure A-13:** Calibration curve of oleic acid. X-axis represents concentration in ppm and y-axis is relative abundance.

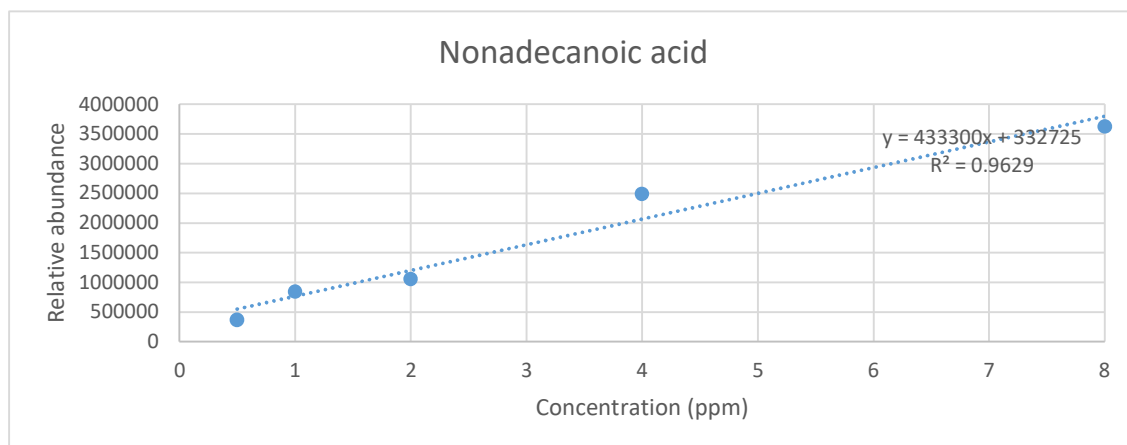


**Figure A-14:** Calibration curve of nonadecanoic acid. X-axis represents concentration in ppm and y-axis is relative abundance.

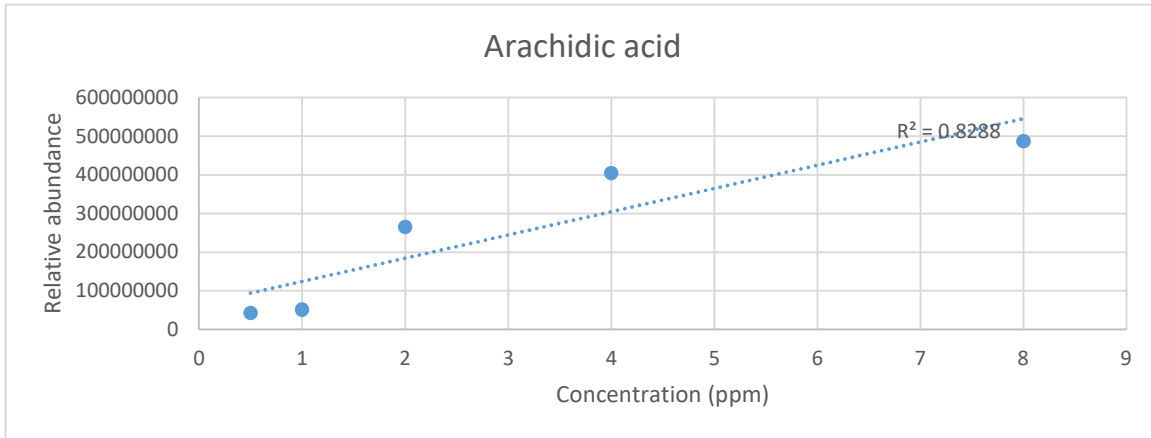


**Figure A-15:** Calibration curve of arachidic acid. X-axis represents concentration in ppm and y-axis is relative abundance.

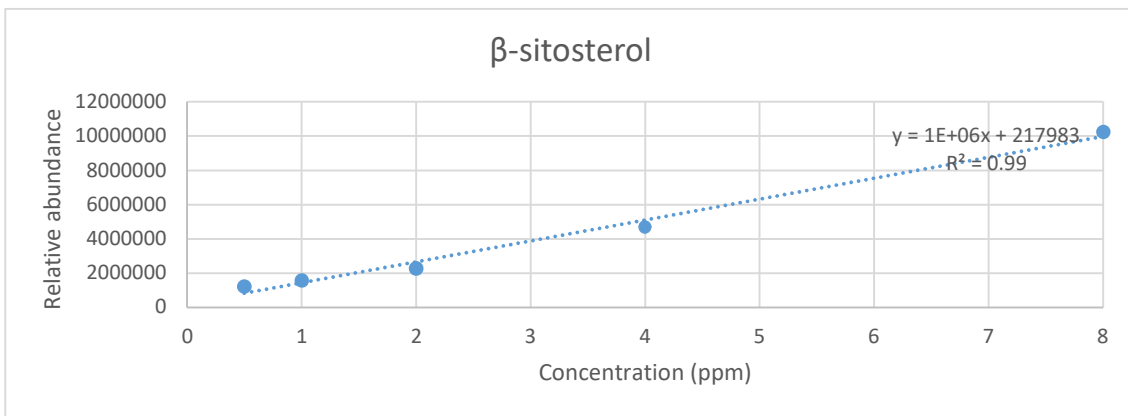


**Figure A-16:** Calibration curve of  $\beta$ -sitosterol. X-axis represents concentration in ppm and y-axis is relative abundance.

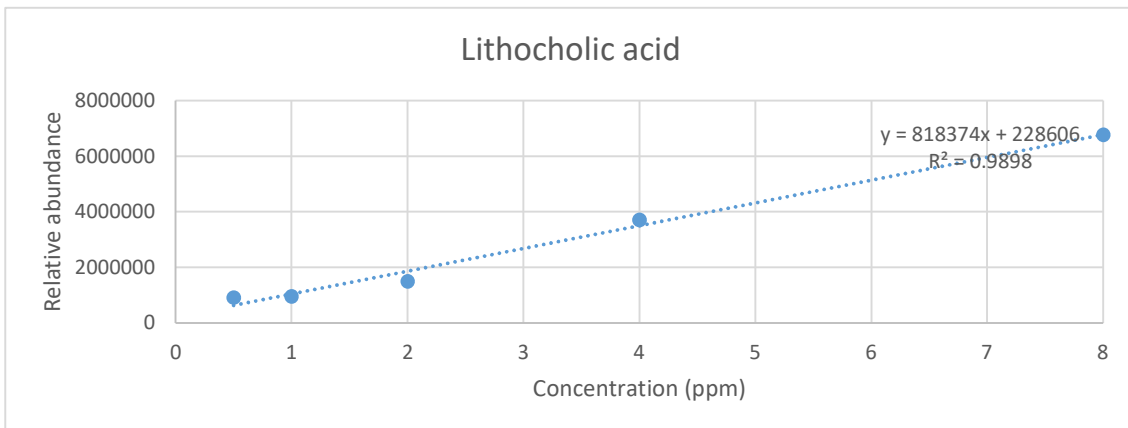


**Figure A-17:** Calibration curve of lithocholic acid. X-axis represents concentration in ppm and y-axis is relative abundance.

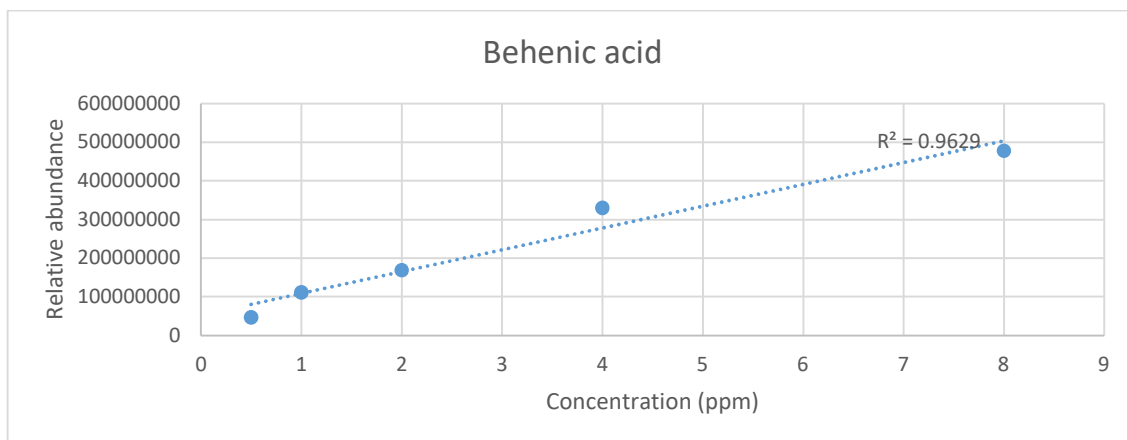


**Figure A-18:** Calibration curve of behenic acid. X-axis represents concentration in ppm and y-axis is relative abundance.

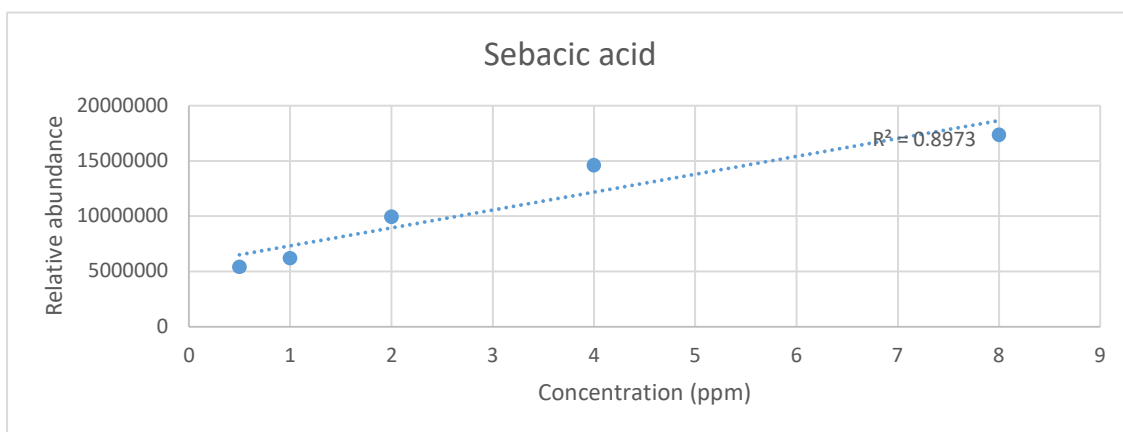


**Figure A-19:** Calibration curve of sebacic acid. X-axis represents concentration in ppm and y-axis is relative abundance.

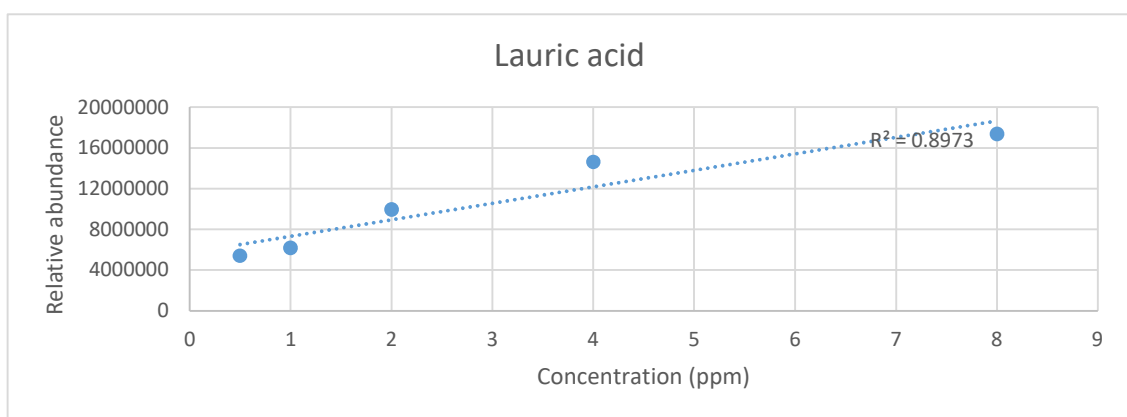


**Figure A-20:** Calibration curve of lauric acid. X-axis represents concentration in ppm and y-axis is relative abundance.



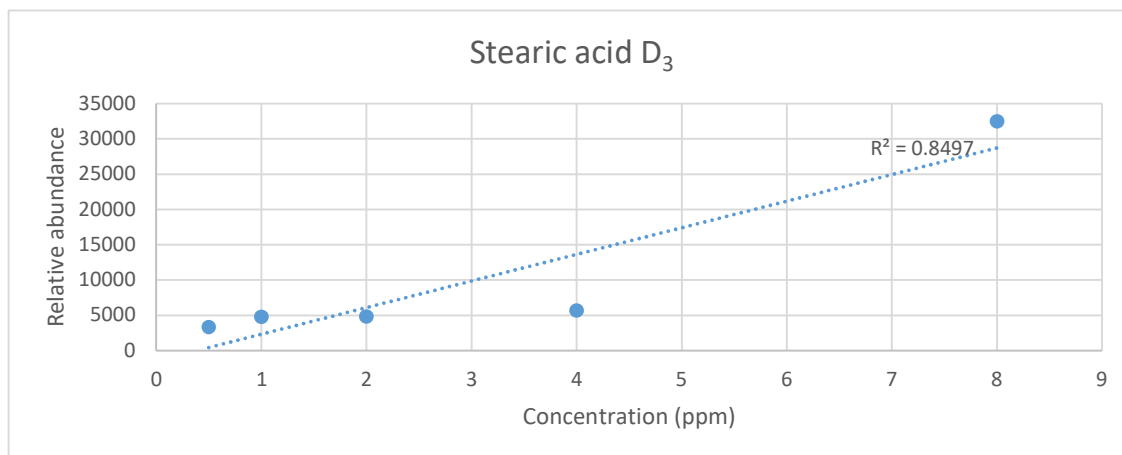


**Figure A-21:** Calibration curve of linoleic acid. X-axis represents concentration in ppm and y-axis is relative abundance.

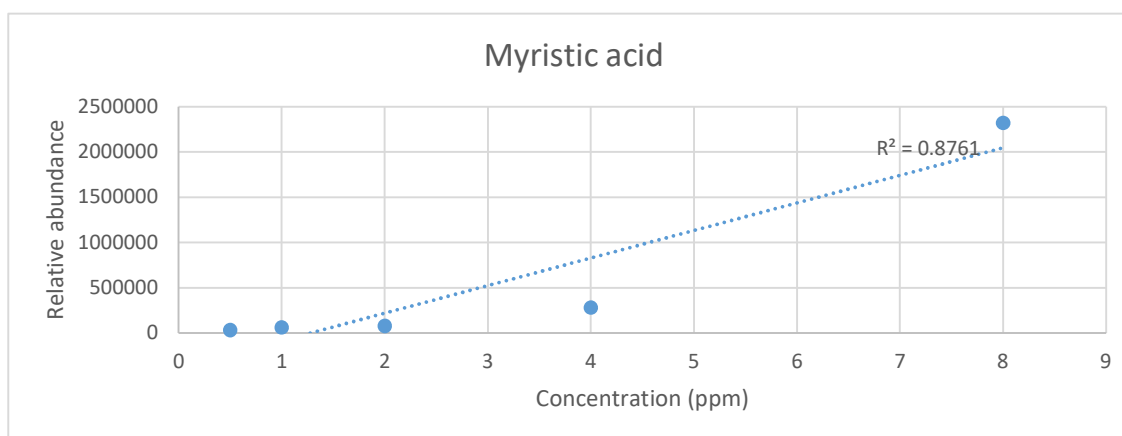


**Figure A-22:** Calibration curve of linoleic acid. X-axis represents concentration in ppm and y-axis is relative abundance.

## APPENDIX B- WARMER SEASON STUDY: PIG VS HUMAN SKIN

Comparison of H4, P1 and P2 individual lipid trends within the skin of pigs and humans. The x-axis for all graphs represents relative abundance in parts per million (ppm), y-axis represents sampling day

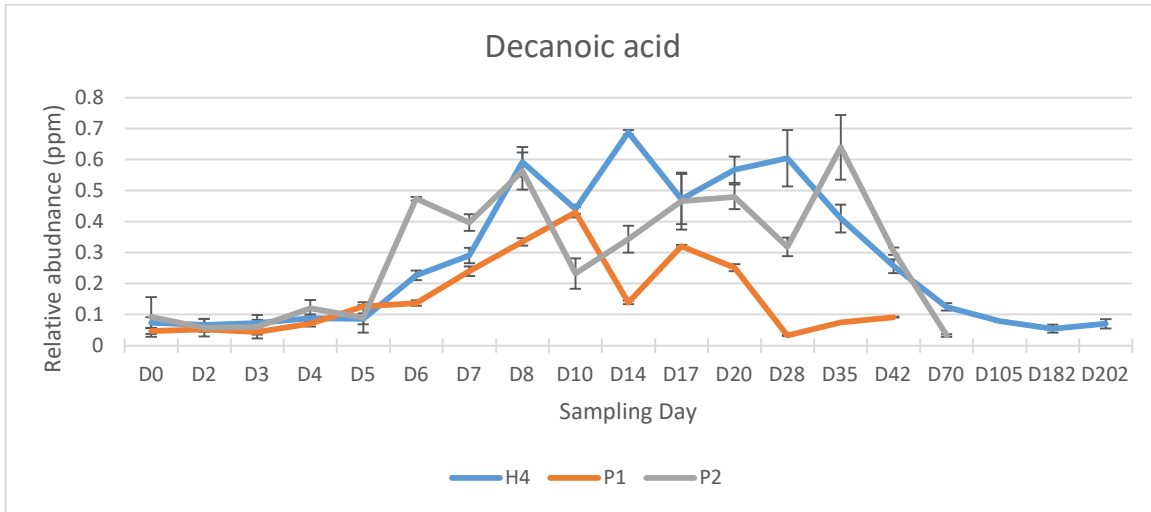


**Figure B-1:** Relative abundance graph of decanoic acid through decomposition period of H4, P1 and P2. X-axis represents sampling day and y-axis is relative abundance (ppm).

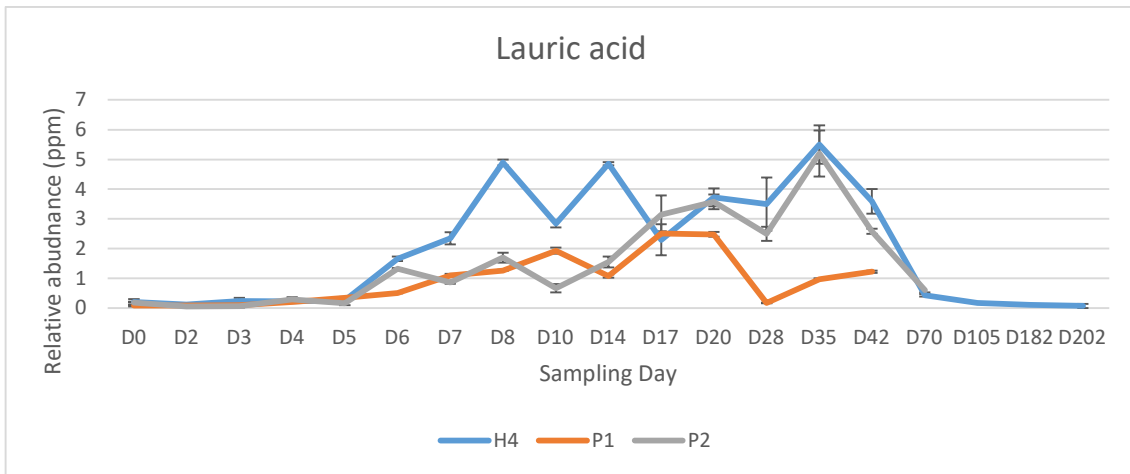


**Figure B-2:** Relative abundance graph of lauric acid through decomposition period of H4, P1 and P2. X-axis represents sampling day and y-axis is relative abundance (ppm).

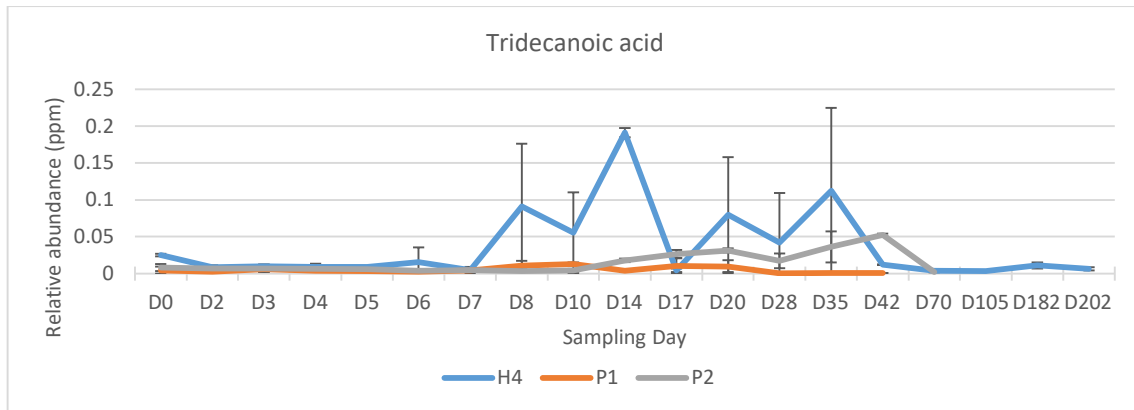


**Figure B-3:** Relative abundance graph of tridecanoic acid through decomposition period of H4, P1 and P2. X-axis represents sampling day and y-axis is relative abundance (ppm).

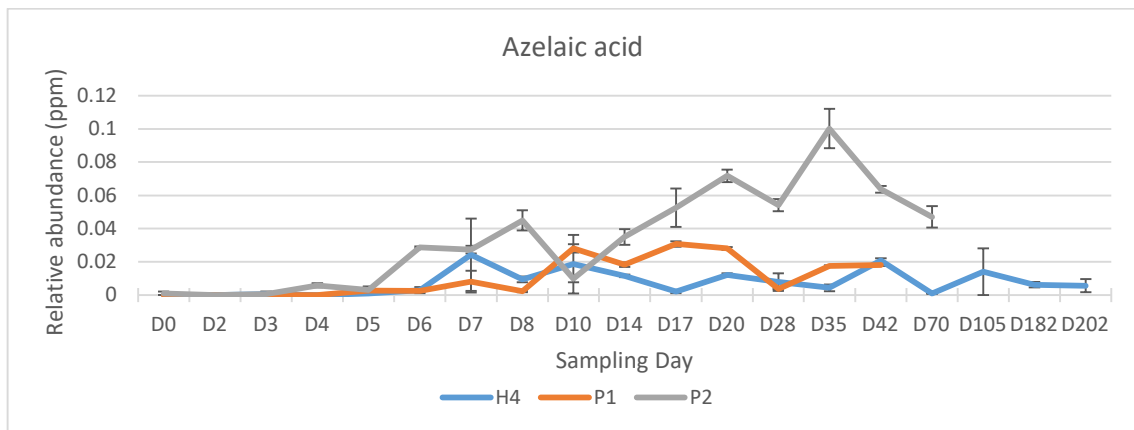


**Figure B-4:** Relative abundance graph of azelaic acid through decomposition period of H4, P1 and P2. X-axis represents sampling day and y-axis is relative abundance (ppm).

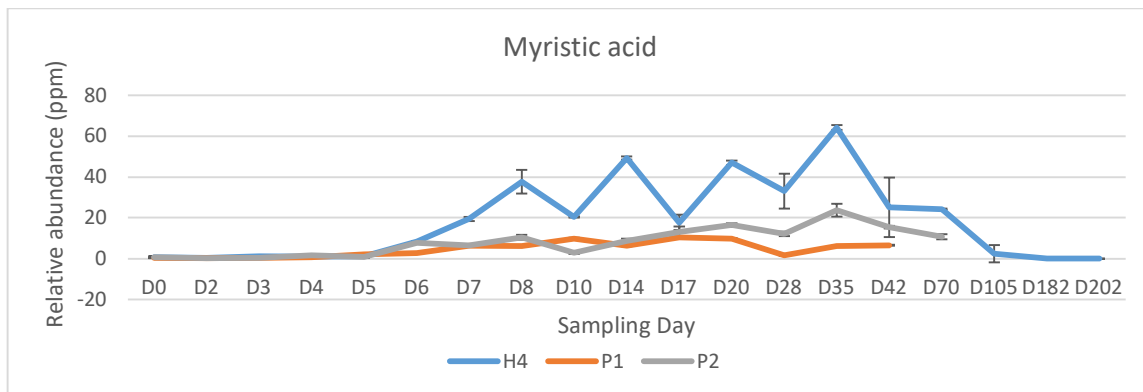


**Figure B-5:** Relative abundance graph of myristic acid through decomposition period of H4, P1 and P2. X-axis represents sampling day and y-axis is relative abundance (ppm).

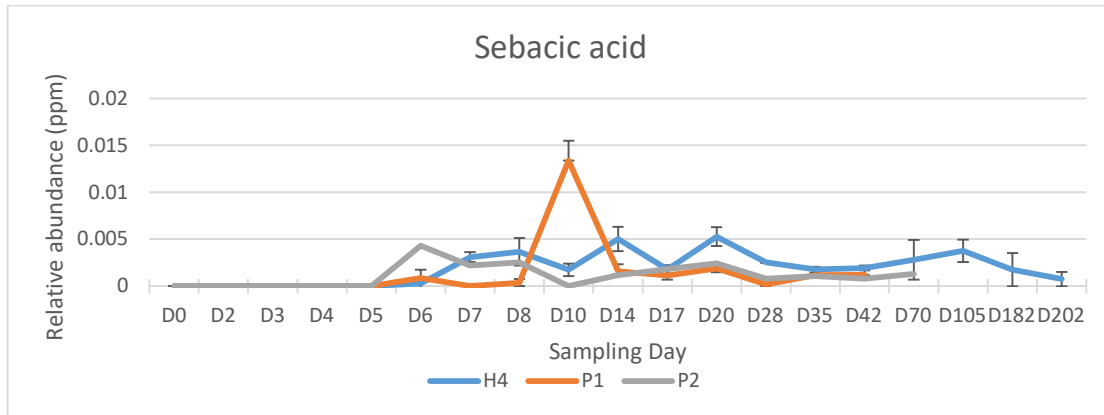


**Figure B-6:** Relative abundance graph of sebacic acid through decomposition period of H4, P1 and P2. X-axis represents sampling day and y-axis is relative abundance (ppm).

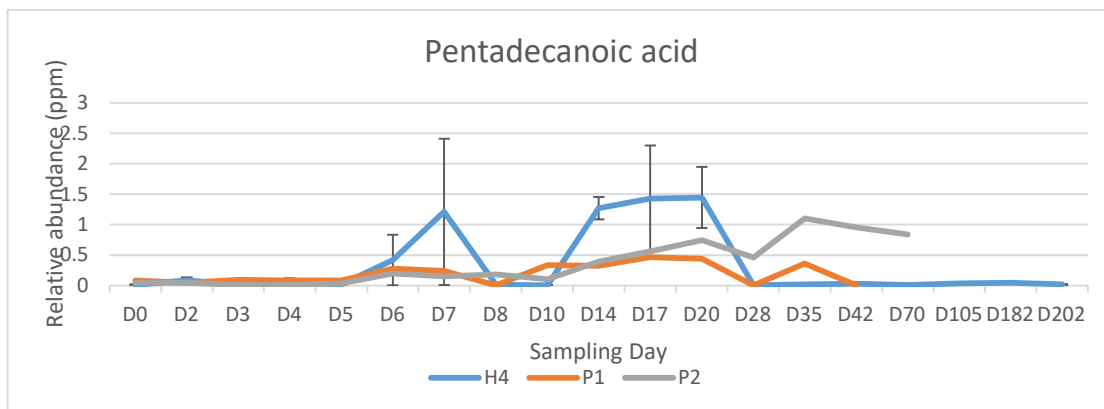


**Figure B-7:** Relative abundance graph of pentadecanoic acid through decomposition period of H4, P1 and P2. X-axis represents sampling day and y-axis is relative abundance (ppm).

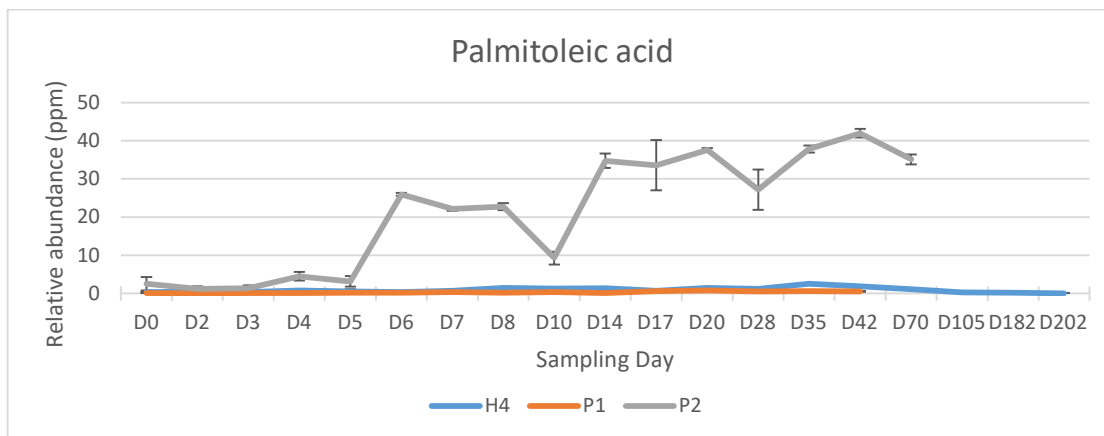


**Figure B-8:** Relative abundance graph of palmitoleic acid through decomposition period of H4, P1 and P2. X-axis represents sampling day and y-axis is relative abundance (ppm).

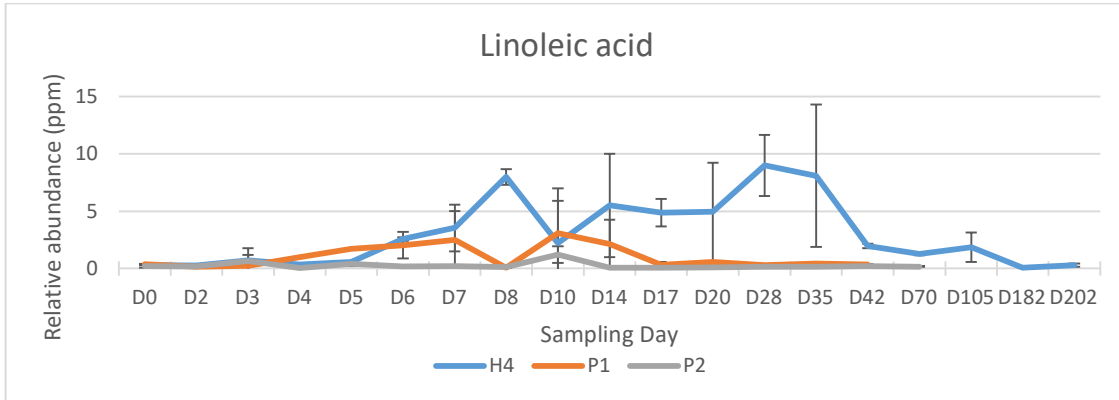


**Figure B-9:** Relative abundance graph of linoleic acid through decomposition period of H4, P1 and P2. X-axis represents sampling day and y-axis is relative abundance (ppm).

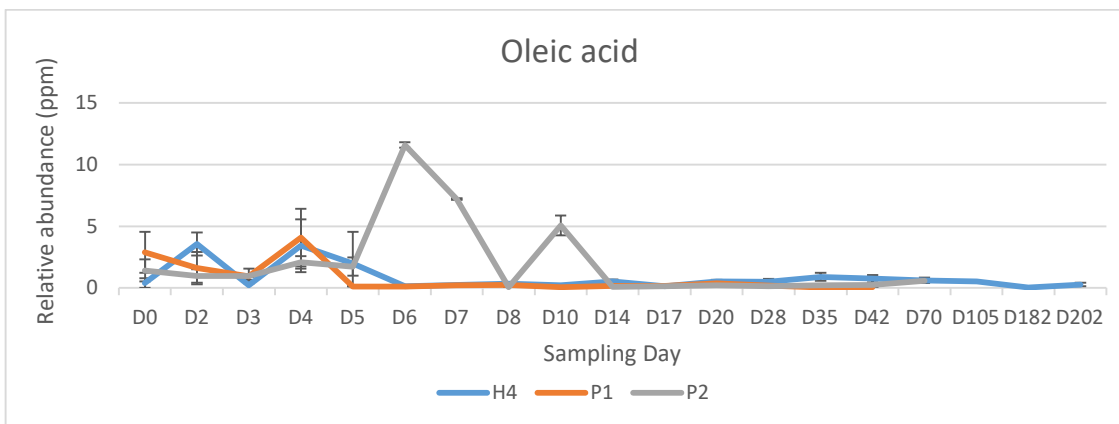


**Figure B-10:** Relative abundance graph of oleic acid through decomposition period of H4, P1 and P2. X-axis represents sampling day and y-axis is relative abundance (ppm).

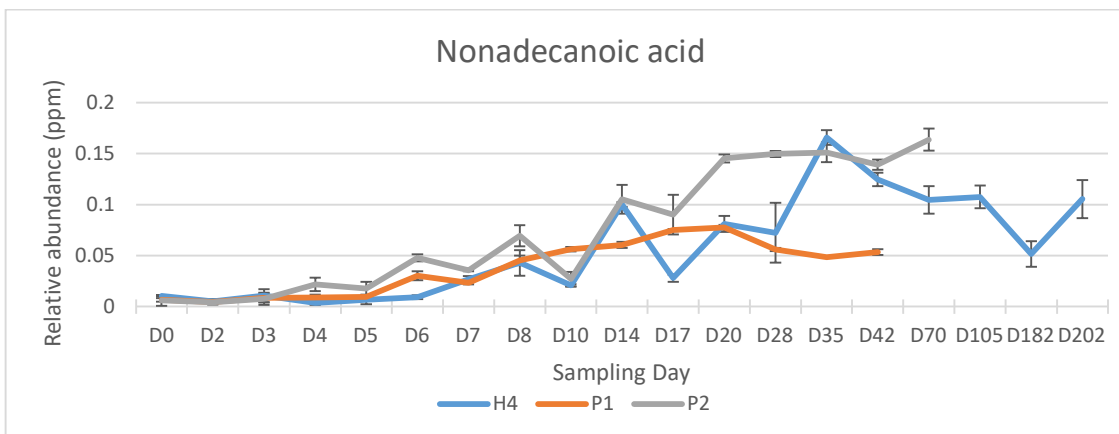


**Figure B-11:** Relative abundance graph of nonadecanoic acid through decomposition period of H4, P1 and P2. X-axis represents sampling day and y-axis is relative abundance (ppm).

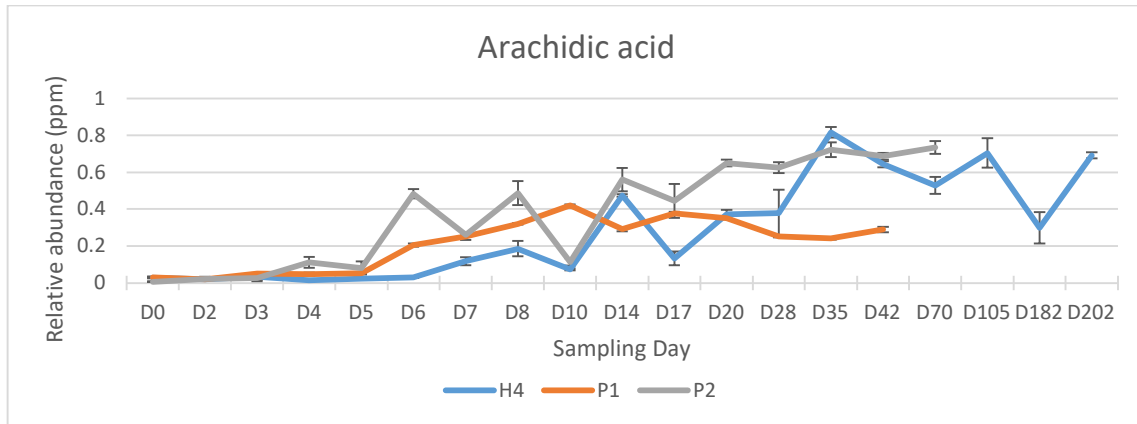


**Figure B-12:** Relative abundance graph of arachidic acid through decomposition period of H4, P1 and P2. X-axis represents sampling day and y-axis is relative abundance (ppm).

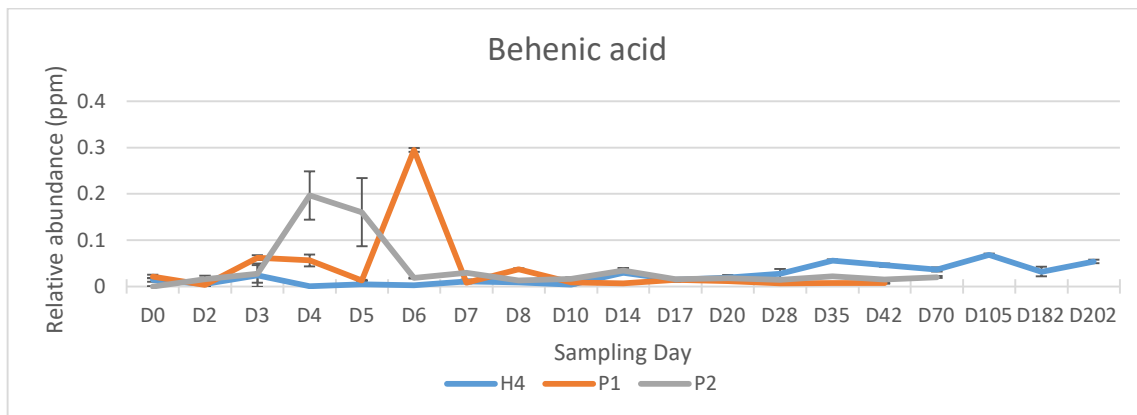


**Figure B-13:** Relative abundance graph of behenic acid through decomposition period of H4, P1 and P2. X-axis represents sampling day and y-axis is relative abundance (ppm).

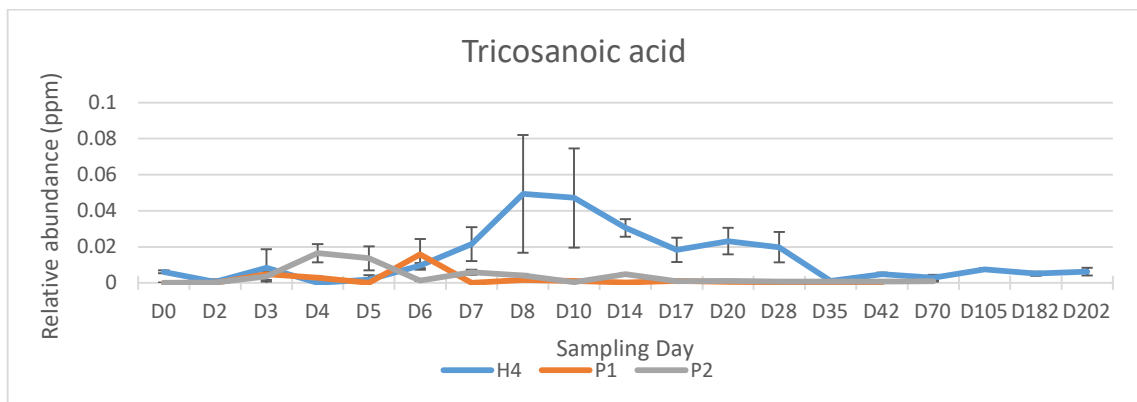


**Figure B-14:** Relative abundance graph of tricosanoic acid through decomposition period of H4, P1 and P2. X-axis represents sampling day and y-axis is relative abundance (ppm).

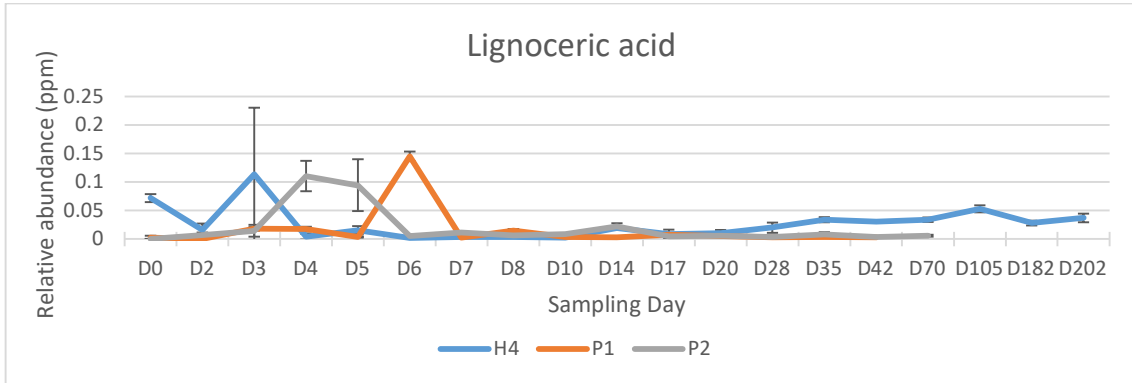


**Figure B-15:** Relative abundance graph of lignoceric acid through decomposition period of H4, P1 and P2. X-axis represents sampling day and y-axis is relative abundance (ppm).

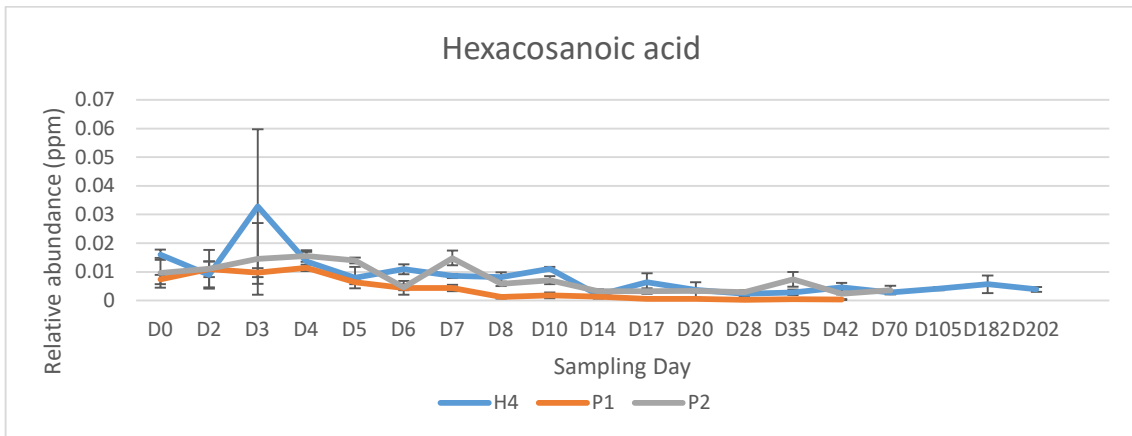


**Figure B-16:** Relative abundance graph of hexacosanoic acid through decomposition period of H4, P1 and P2. X-axis represents sampling day and y-axis is relative abundance (ppm).

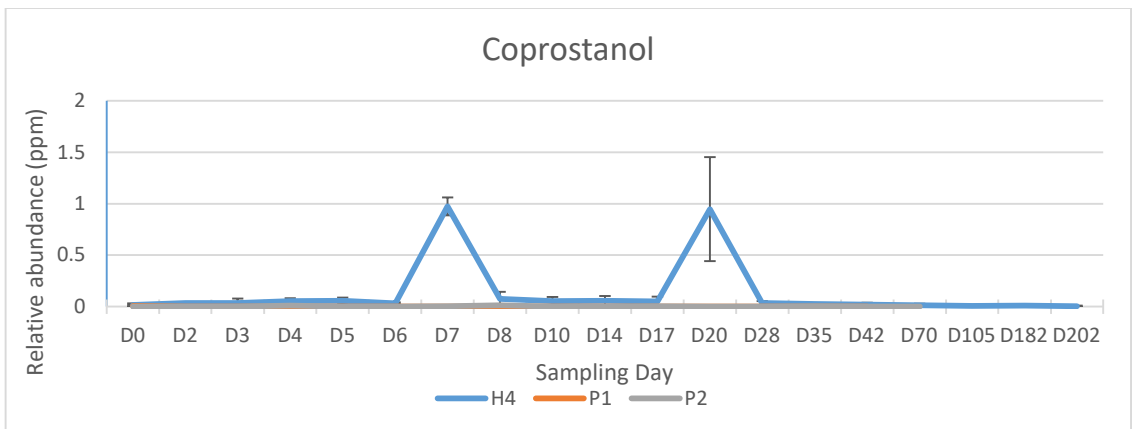




**Figure B-17:** Relative abundance graph of decanoic acid through decomposition period of H4, P1 and P2. X-axis represents sampling day and y-axis is relative abundance (ppm).

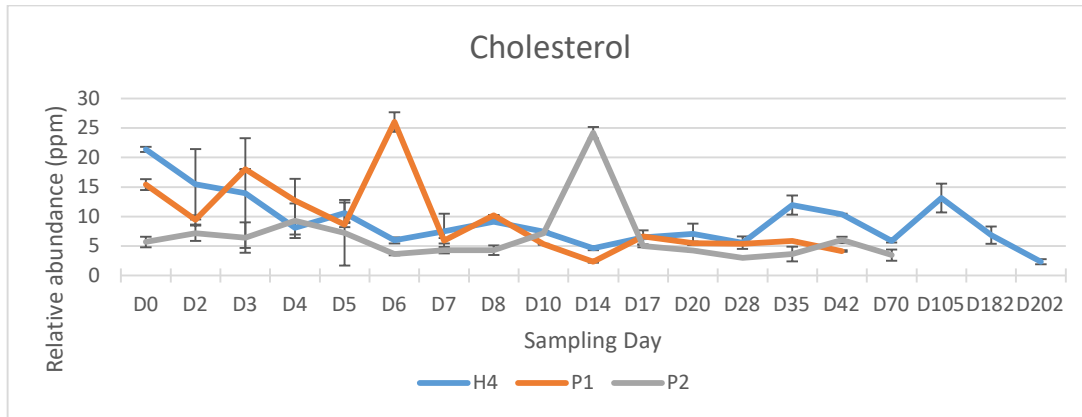


**Figure B-18:** Relative abundance graph of cholesterol through decomposition period of H4, P1 and P2. X-axis represents sampling day and y-axis is relative abundance (ppm).

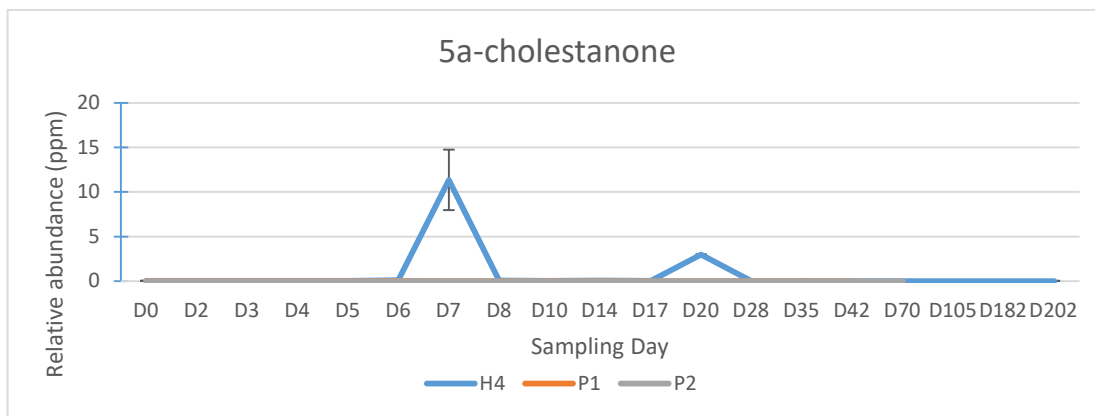


**Figure B-19:** Relative abundance graph of decanoic acid through decomposition period of H4, P1 and P2. X-axis represents sampling day and y-axis is relative abundance (ppm).

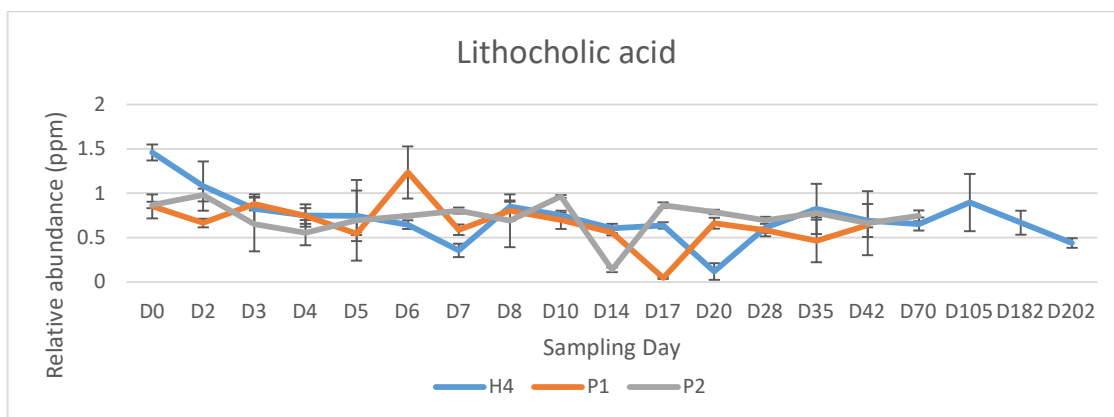


**Figure B-20:** Relative abundance graph of lithocholic acid through decomposition period of H4, P1 and P2. X-axis represents sampling day and y-axis is relative abundance (ppm).

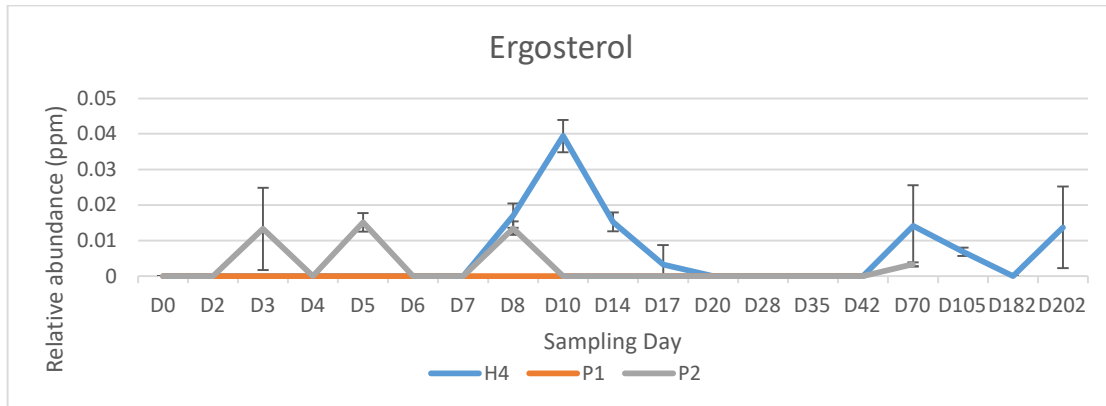


**Figure B-21:** Relative abundance graph of ergosterol through decomposition period of H4, P1 and P2. X-axis represents sampling day and y-axis is relative abundance (ppm).

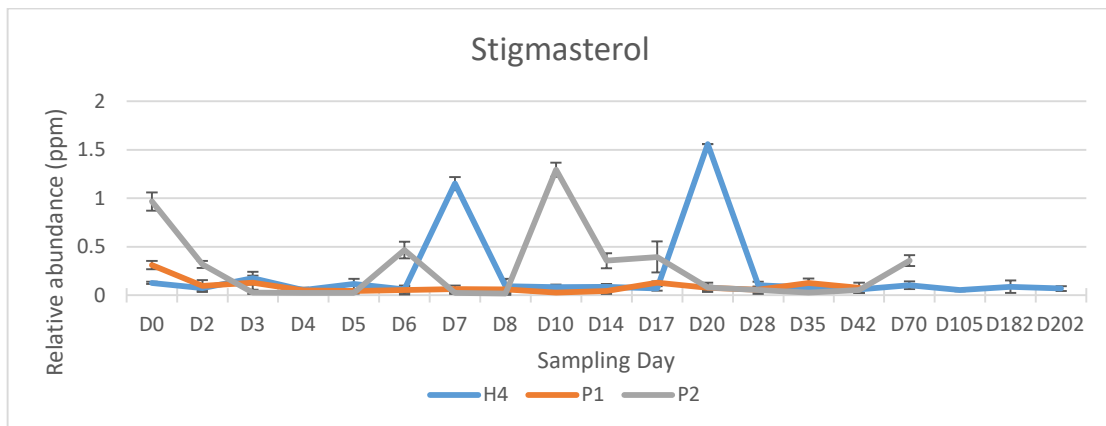


**Figure B-22:** Relative abundance graph of stigmasterol through decomposition period of H4, P1 and P2. X-axis represents sampling day and y-axis is relative abundance (ppm).

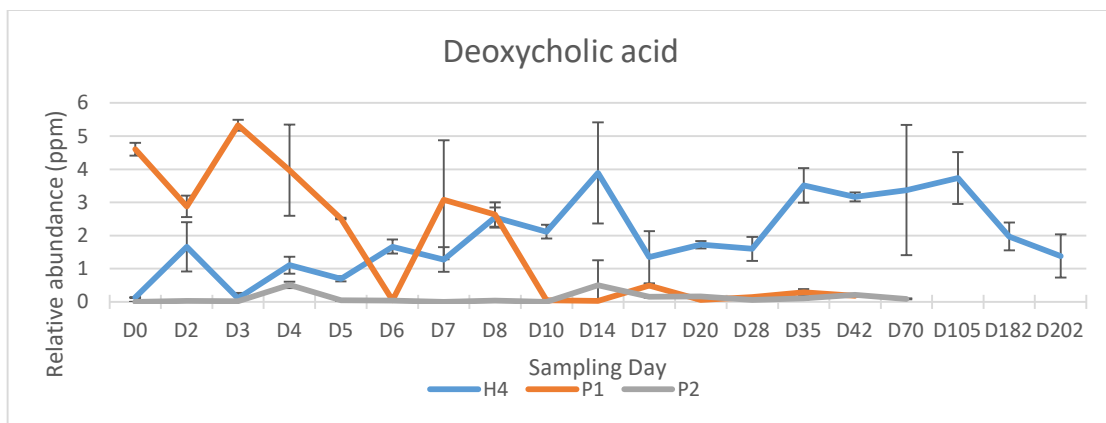


**Figure B-23:** Relative abundance graph of deoxycholic acid through decomposition period of H4, P1 and P2. X-axis represents sampling day and y-axis is relative abundance (ppm).

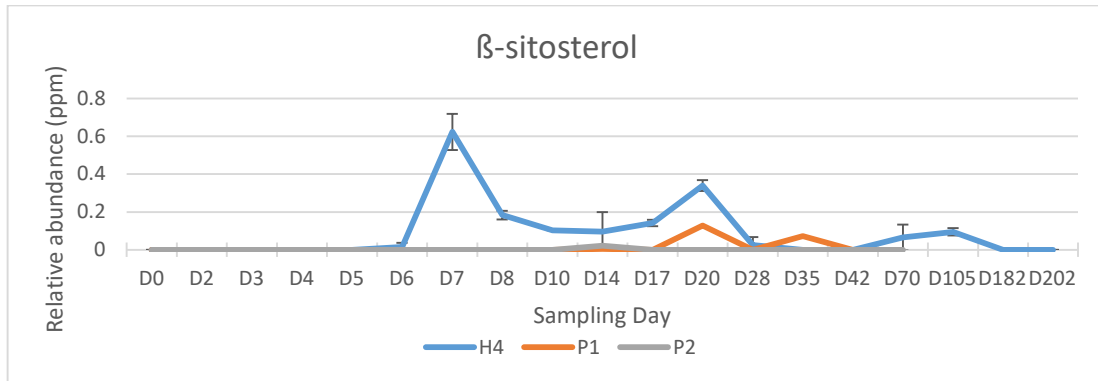


**Figure B-24:** Relative abundance graph of decanoic acid through decomposition period of H4, P1 and P2. X-axis represents sampling day and y-axis is relative abundance (ppm).

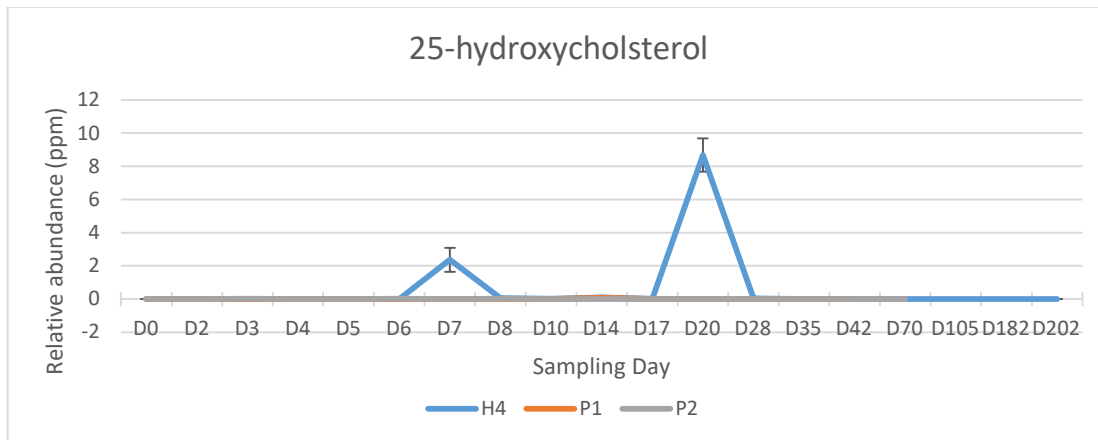


**Figure B-25:** Relative abundance graph of decanoic acid through decomposition period of H4, P1 and P2. X-axis represents sampling day and y-axis is relative abundance (ppm).

## APPENDIX C- WARMER SEASON STUDY: PIG VS HUMAN TISSUE

Comparison of H4, P1 and P2 individual lipid trends within the tissue of pigs and humans. The x-axis for all graphs represents relative abundance in parts per million (ppm), y-axis represents sampling day

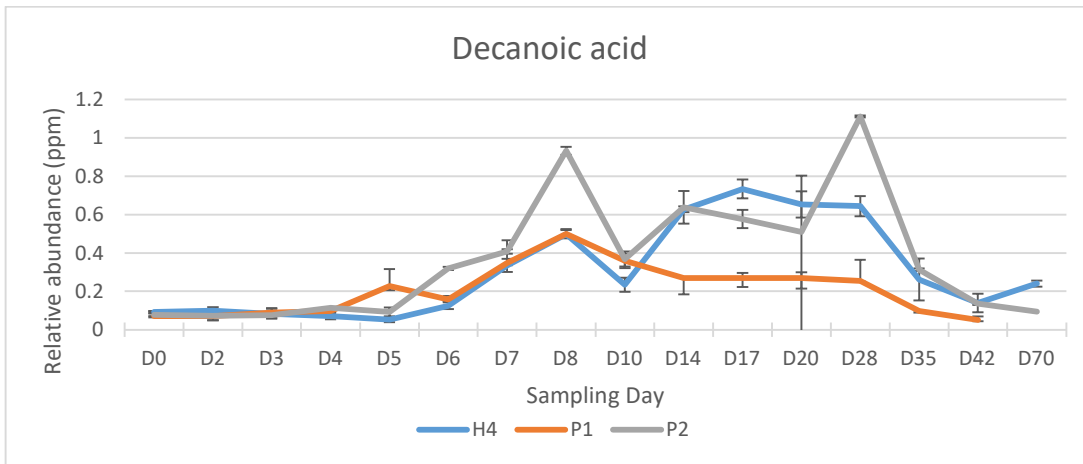


**Figure C-1:** Relative abundance graph of decanoic acid through decomposition period of H4, P1 and P2. X-axis represents sampling day and y-axis is relative abundance (ppm).

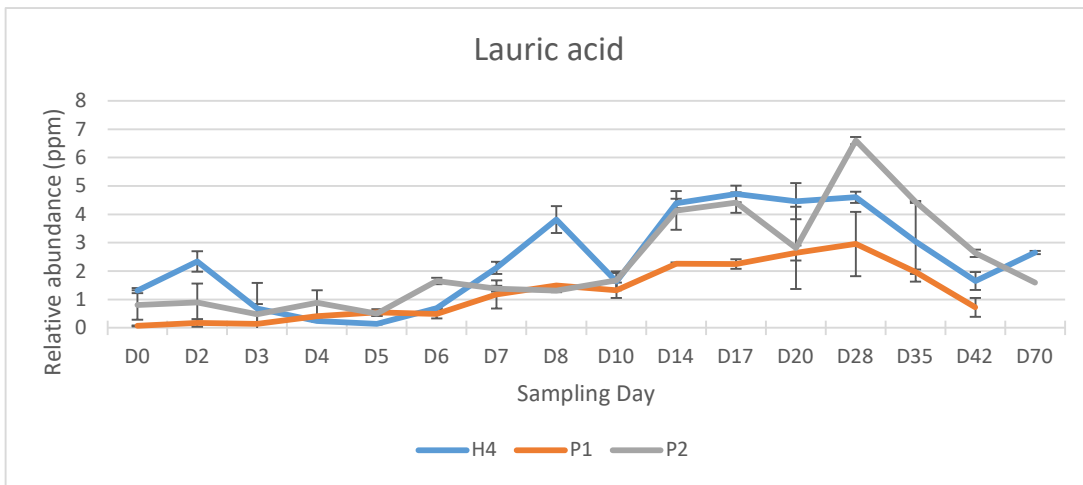


**Figure C-2:** Relative abundance graph of lauric acid through decomposition period of H4, P1 and P2. X-axis represents sampling day and y-axis is relative abundance (ppm).

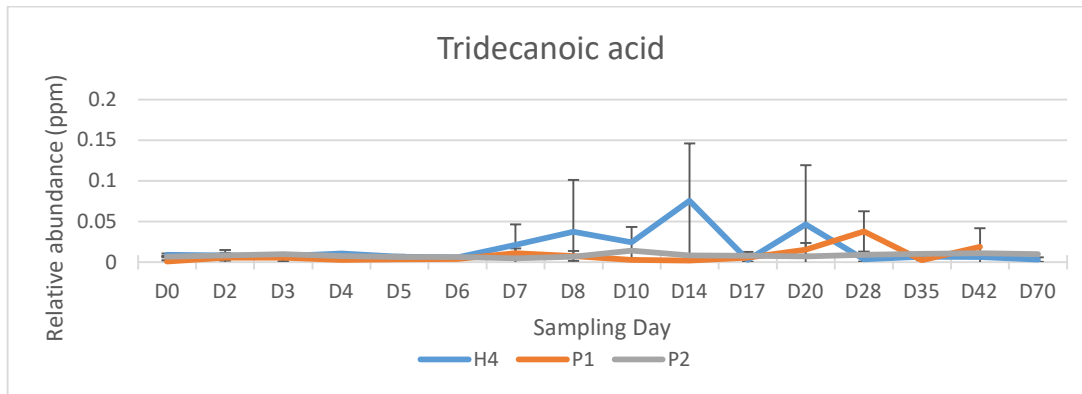


**Figure C-3:** Relative abundance graph of tridecanoic acid through decomposition period of H4, P1 and P2. X-axis represents sampling day and y-axis is relative abundance (ppm).

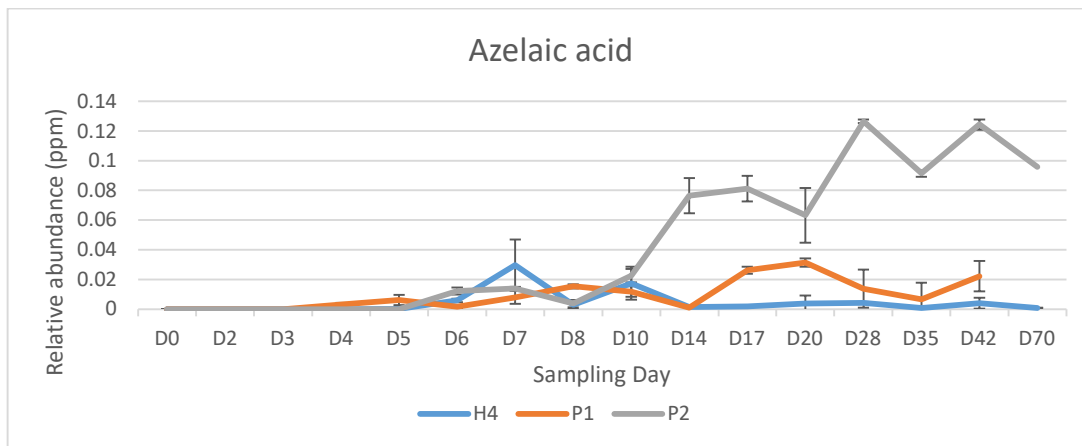


**Figure C-4:** Relative abundance graph of azelaic acid through decomposition period of H4, P1 and P2. X-axis represents sampling day and y-axis is relative abundance (ppm).

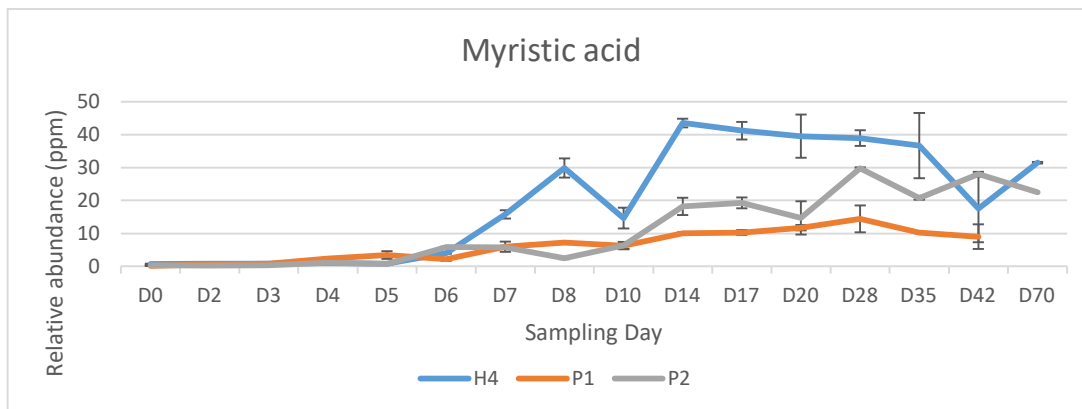


**Figure C-5:** Relative abundance graph of myristic acid through decomposition period of H4, P1 and P2. X-axis represents sampling day and y-axis is relative abundance (ppm).

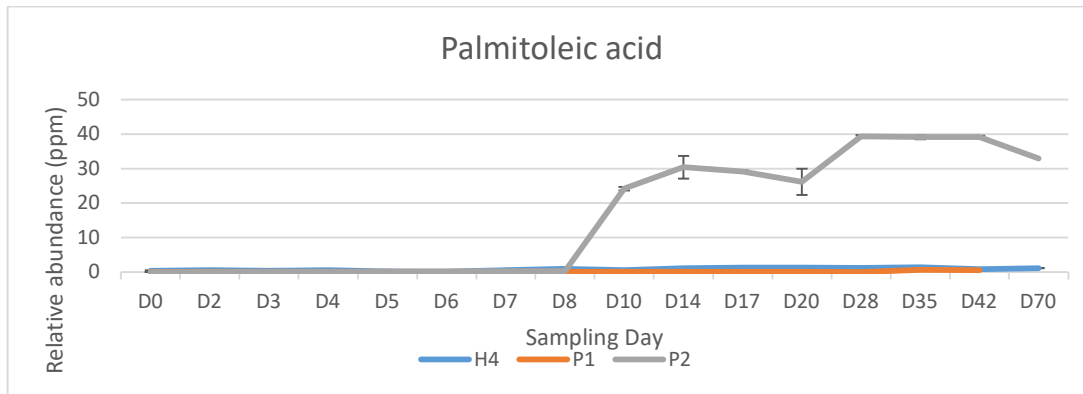


**Figure C-6:** Relative abundance graph of palmitoleic acid through decomposition period of H4, P1 and P2. X-axis represents sampling day and y-axis is relative abundance (ppm).

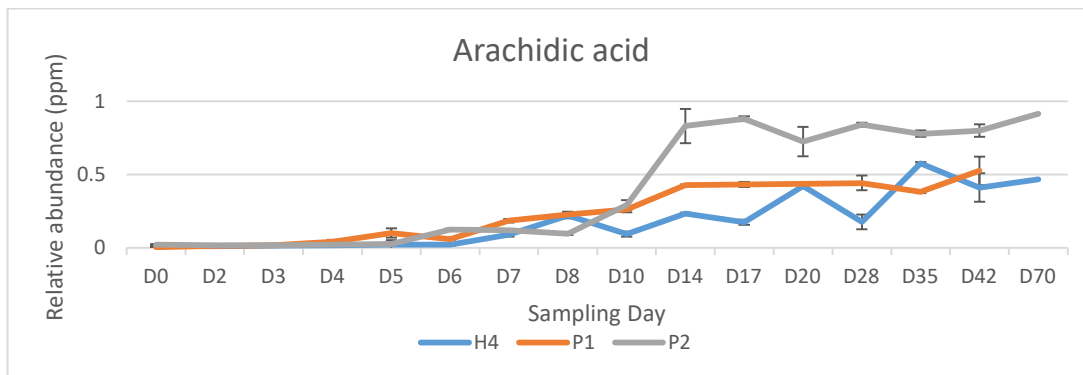


**Figure C-7:** Relative abundance graph of arachidic acid through decomposition period of H4, P1 and P2. X-axis represents sampling day and y-axis is relative abundance (ppm).

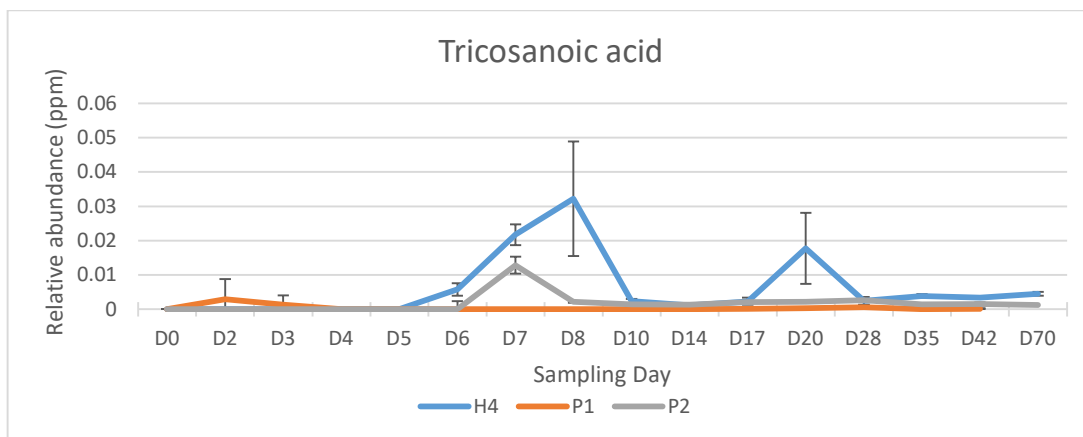


**Figure C-8:** Relative abundance graph of tricosanoic acid through decomposition period of H4, P1 and P2. X-axis represents sampling day and y-axis is relative abundance (ppm).

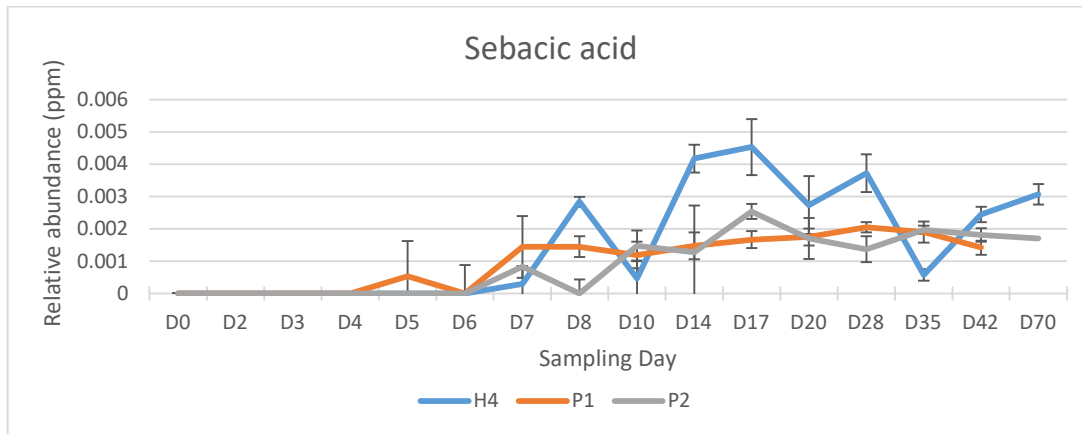


**Figure C-9:** Relative abundance graph of sebacic acid through decomposition period of H4, P1 and P2. X-axis represents sampling day and y-axis is relative abundance (ppm).

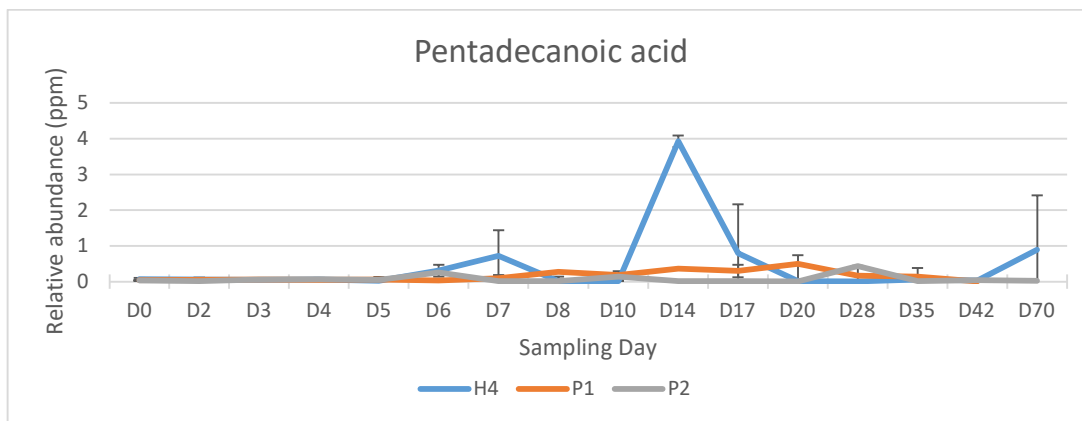


**Figure C-10:** Relative abundance graph of pentadecanoic acid through decomposition period of H4, P1 and P2. X-axis represents sampling day and y-axis is relative abundance (ppm).

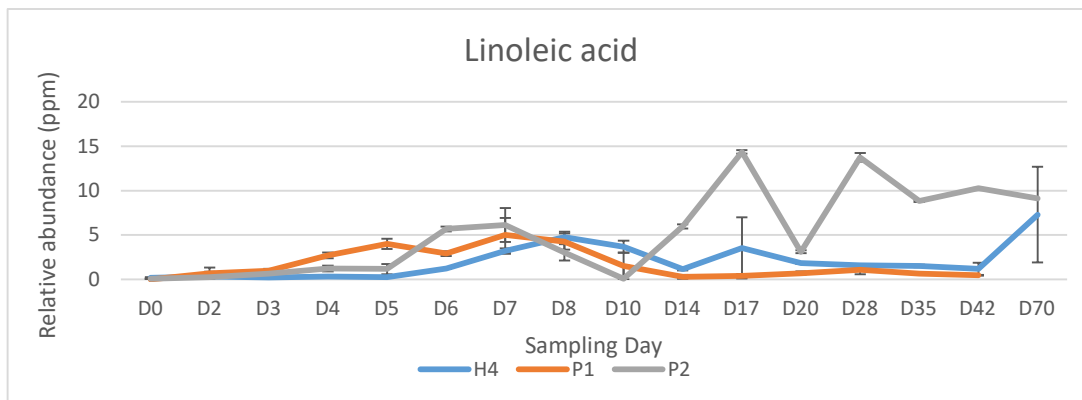


**Figure C-11:** Relative abundance graph of linoleic acid through decomposition period of H4, P1 and P2. X-axis represents sampling day and y-axis is relative abundance (ppm).



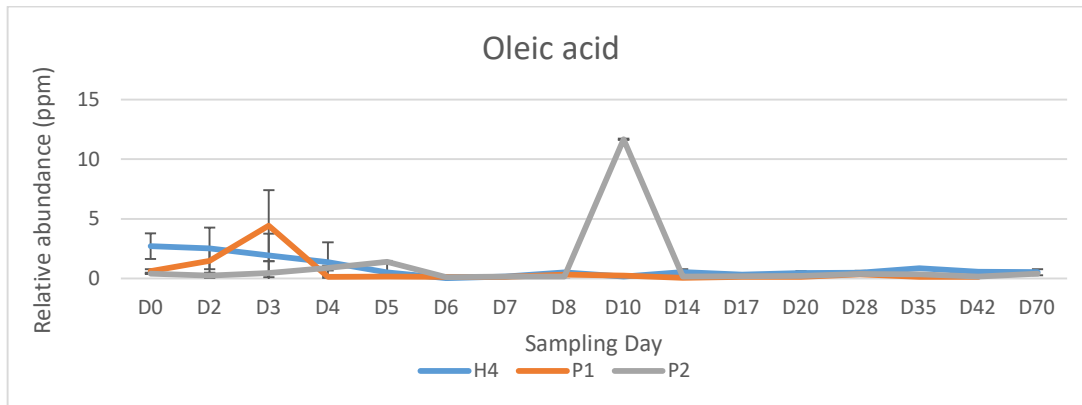


**Figure C-12:** Relative abundance graph of oleic acid through decomposition period of H4, P1 and P2. X-axis represents sampling day and y-axis is relative abundance (ppm).

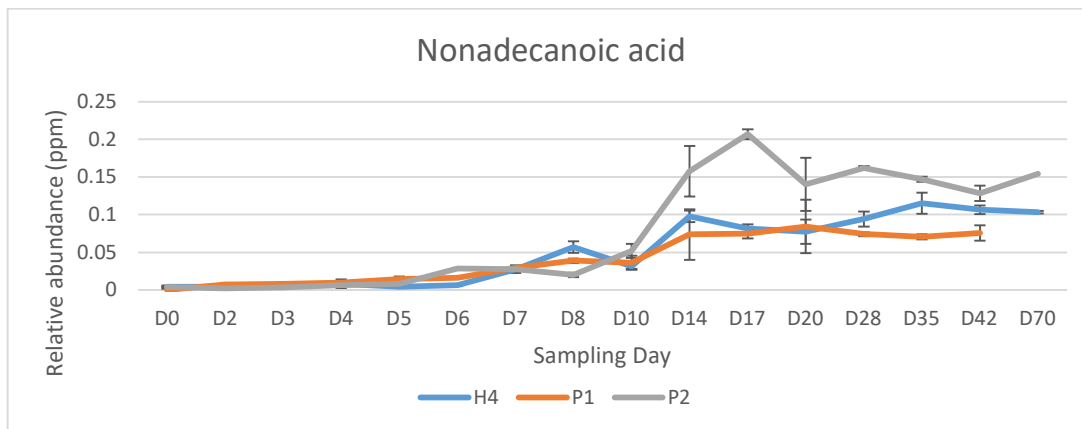


**Figure C-13:** Relative abundance graph of decanoic acid through decomposition period of H4, P1 and P2. X-axis represents sampling day and y-axis is relative abundance (ppm).

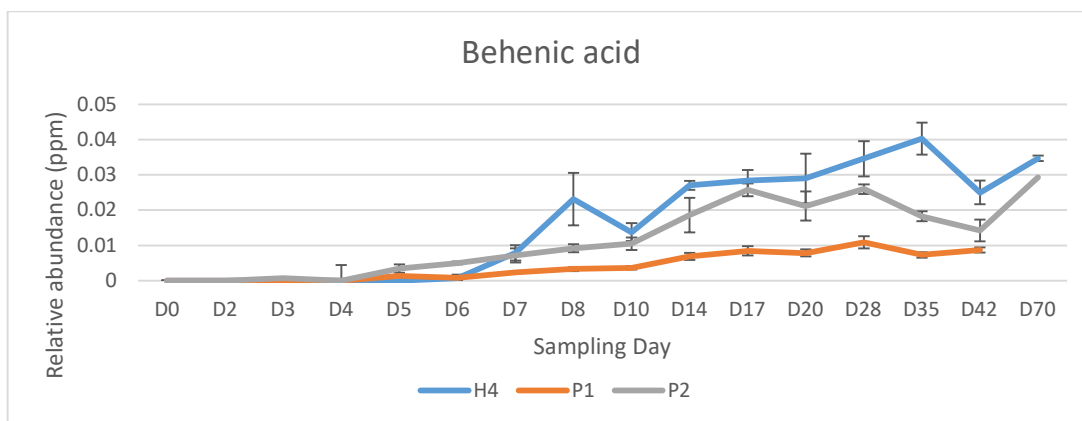


**Figure C-14:** Relative abundance graph of behenic acid through decomposition period of H4, P1 and P2. X-axis represents sampling day and y-axis is relative abundance (ppm).

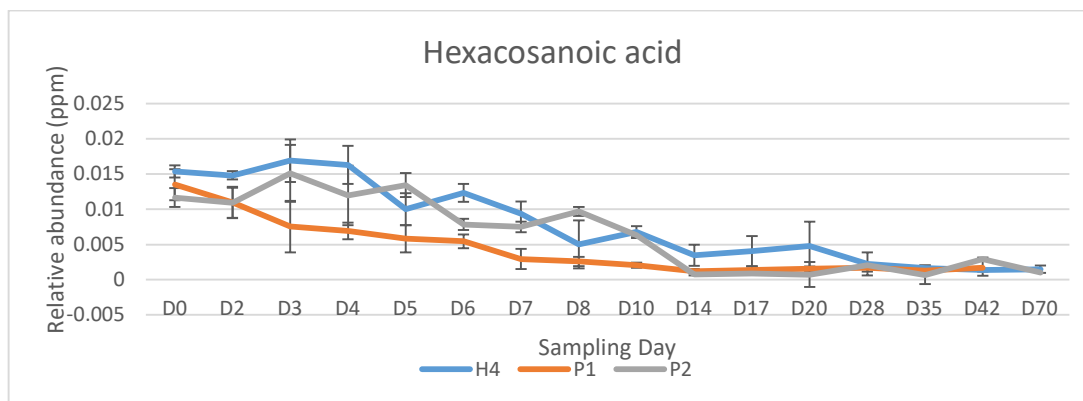


**Figure C-15:** Relative abundance graph of hexacosanoic acid through decomposition period of H4, P1 and P2. X-axis represents sampling day and y-axis is relative abundance (ppm).

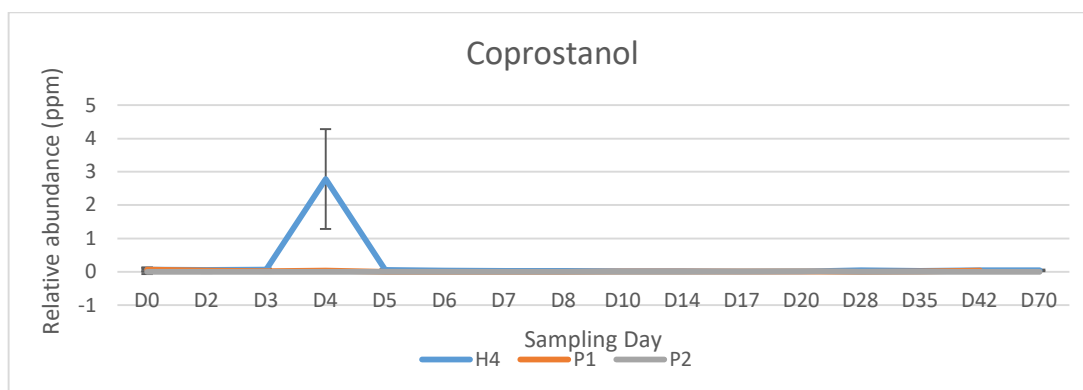


**Figure C-16:** Relative abundance graph of coprostanol through decomposition period of H4, P1 and P2. X-axis represents sampling day and y-axis is relative abundance (ppm).

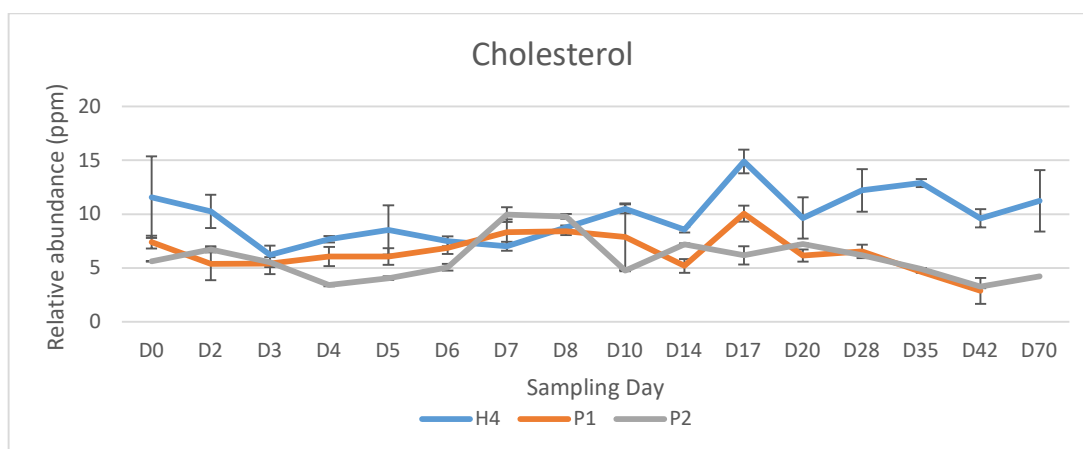


**Figure C-17:** Relative abundance graph of cholesterol through decomposition period of H4, P1 and P2. X-axis represents sampling day and y-axis is relative abundance (ppm).

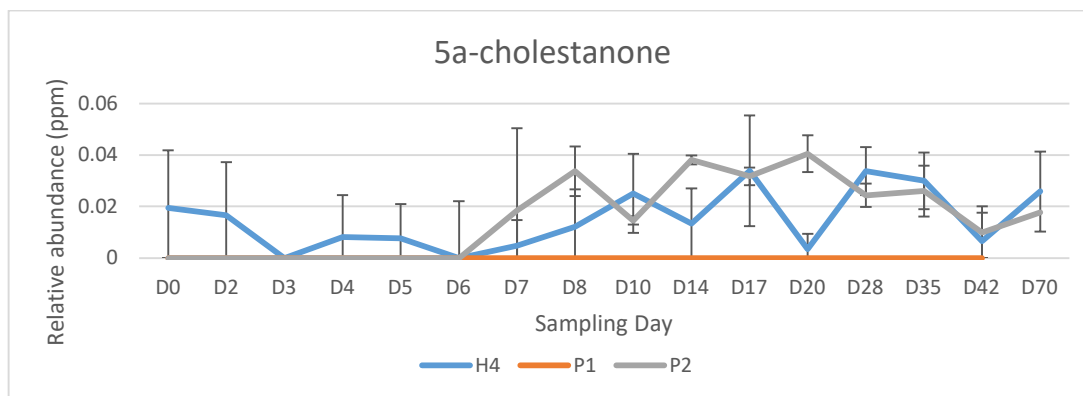


**Figure C-18:** Relative abundance graph of 5a-cholestanone through decomposition period of H4, P1 and P2. X-axis represents sampling day and y-axis is relative abundance (ppm).

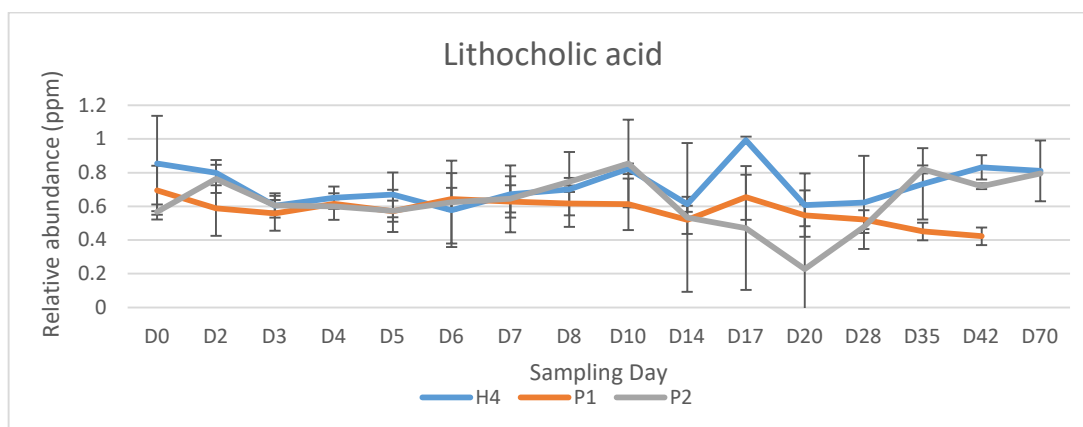


**Figure C-19:** Relative abundance graph of decanoic acid through decomposition period of H4, P1 and P2. X-axis represents sampling day and y-axis is relative abundance (ppm).

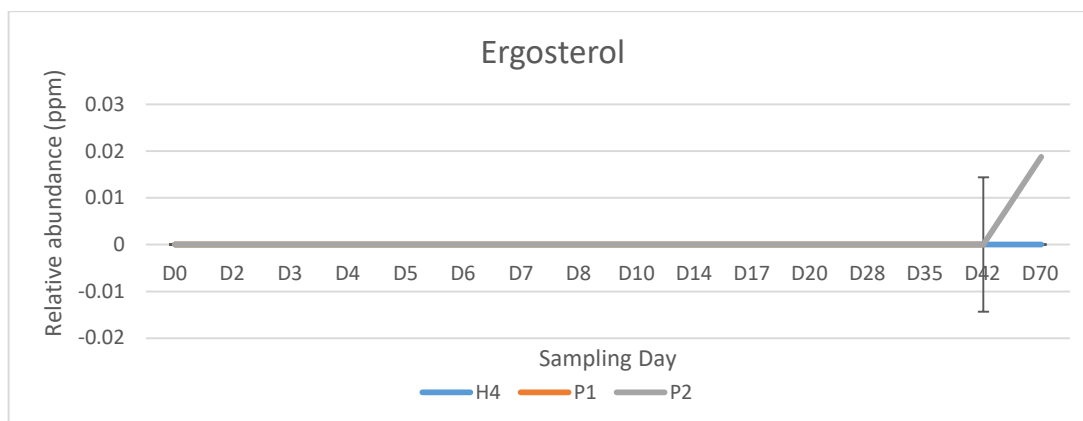


**Figure C-20:** Relative abundance graph of ergosterol through decomposition period of H4, P1 and P2. X-axis represents sampling day and y-axis is relative abundance (ppm).

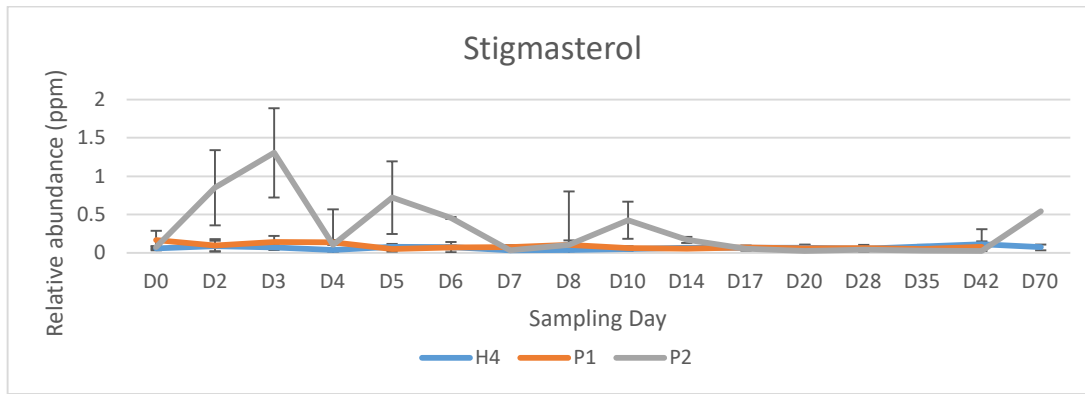


**Figure C-21:** Relative abundance graph of stigmasterol through decomposition period of H4, P1 and P2. X-axis represents sampling day and y-axis is relative abundance (ppm).

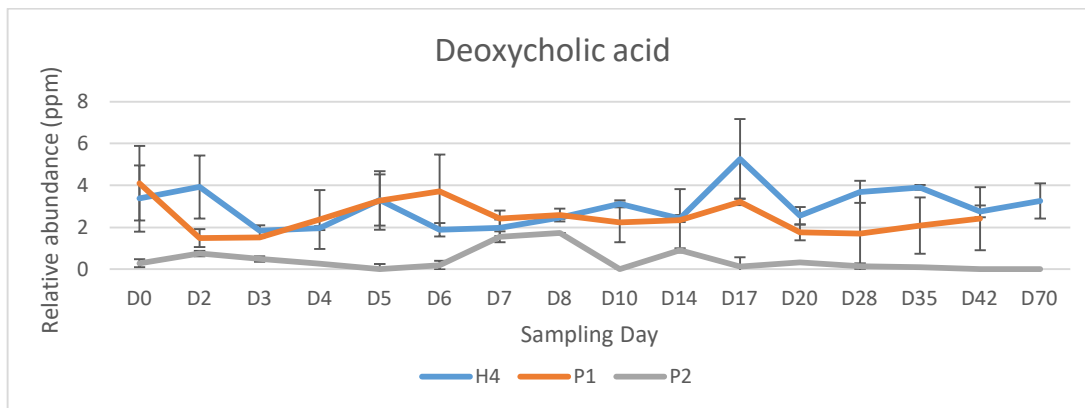


**Figure C-22:** Relative abundance graph of deoxycholic acid through decomposition period of H4, P1 and P2. X-axis represents sampling day and y-axis is relative abundance (ppm).

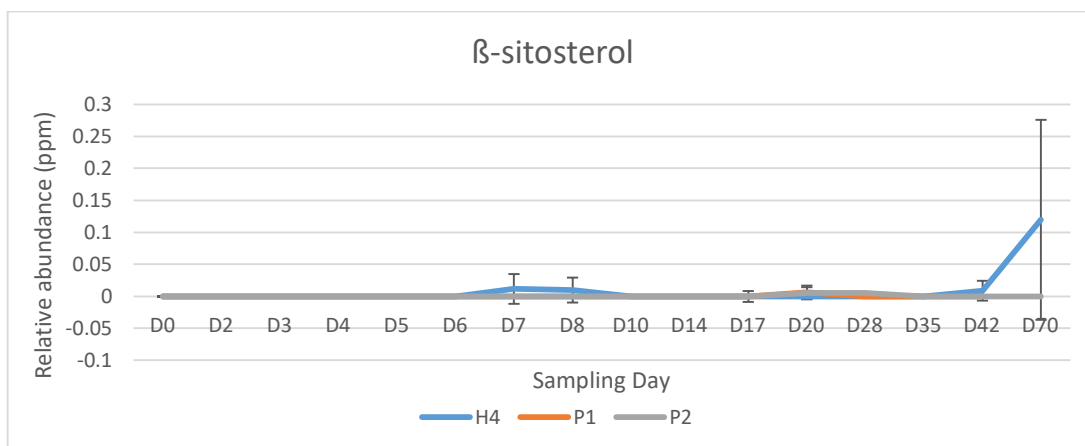


**Figure C-23:** Relative abundance graph of β-sitosterol through decomposition period of H4, P1 and P2. X-axis represents sampling day and y-axis is relative abundance (ppm).

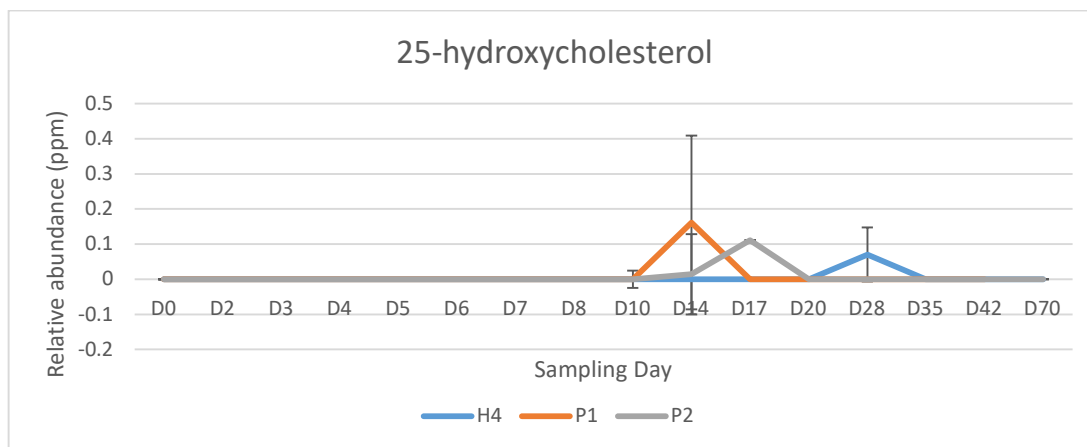


**Figure C-24:** Relative abundance graph of 25-hydroxycholesterol through decomposition period of H4, P1 and P2. X-axis represents sampling day and y-axis is relative abundance (ppm).

## APPENDIX D- COOLER SEASON STUDY: PIG VS HUMAN SKIN

Comparison of H5, P3 and P4 individual lipid trends within the skin of pigs and humans. The x-axis for all graphs represents relative abundance in parts per million (ppm), y-axis represents sampling day

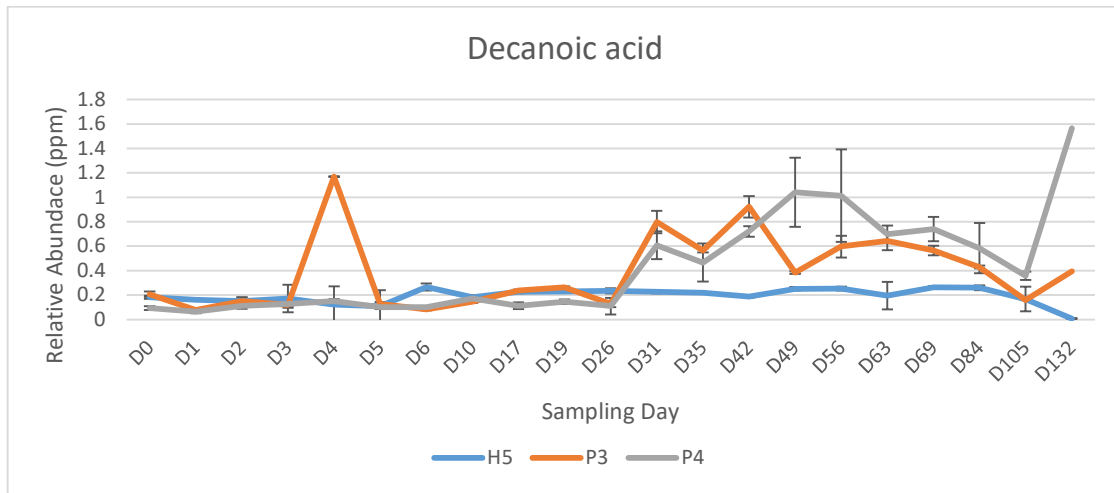


**Figure D-1:** Relative abundance graph of decanoic acid through decomposition period of H5, P3 and P4. X-axis represents sampling day and y-axis is relative abundance (ppm).

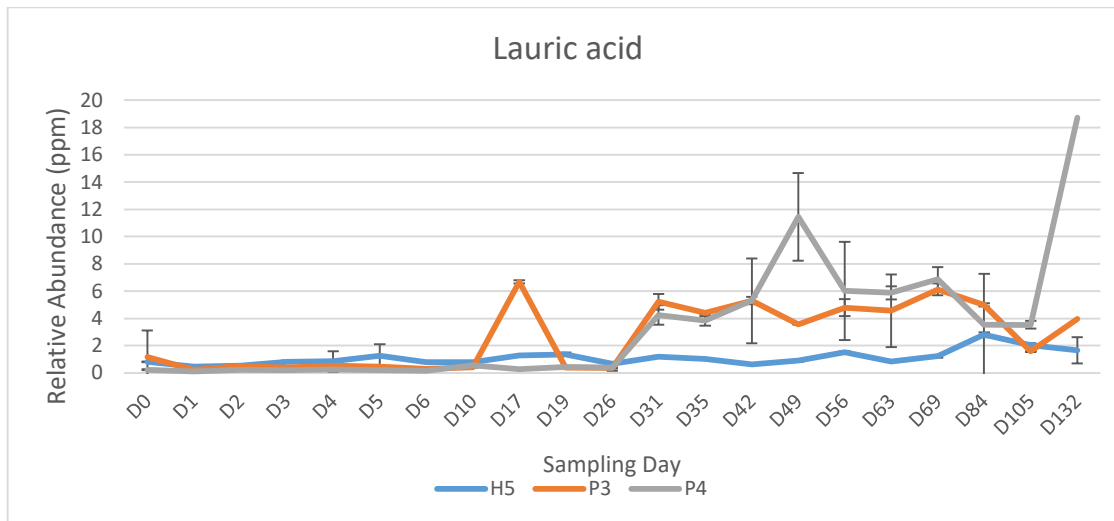


**Figure D-2:** Relative abundance graph of lauric acid through decomposition period of H5, P3 and P4. X-axis represents sampling day and y-axis is relative abundance (ppm).

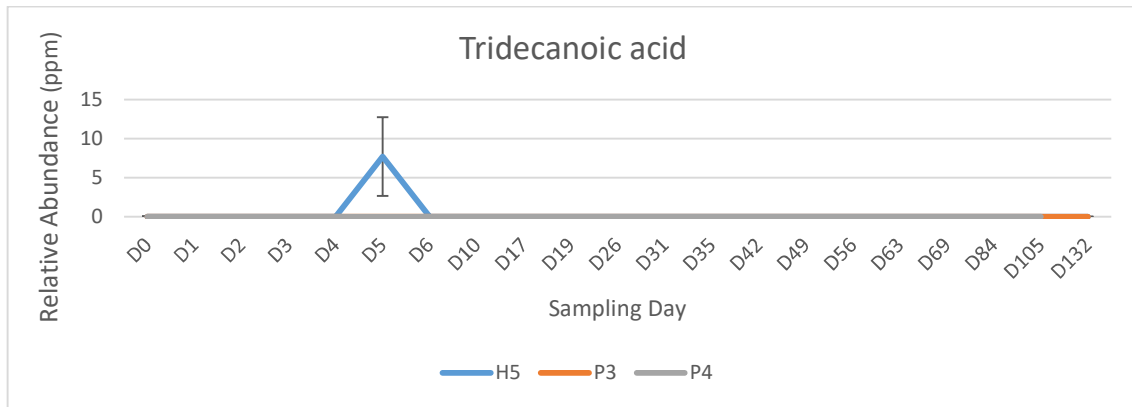


**Figure D-3:** Relative abundance graph of tridecanoic acid through decomposition period of H5, P3 and P4. X-axis represents sampling day and y-axis is relative abundance (ppm).

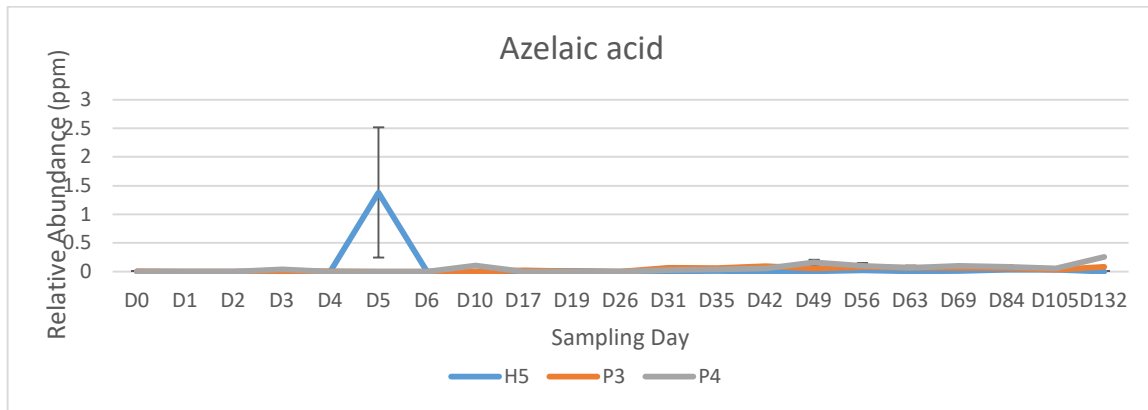


**Figure D-4:** Relative abundance graph of azelaic acid through decomposition period of H5, P3 and P4. X-axis represents sampling day and y-axis is relative abundance (ppm).

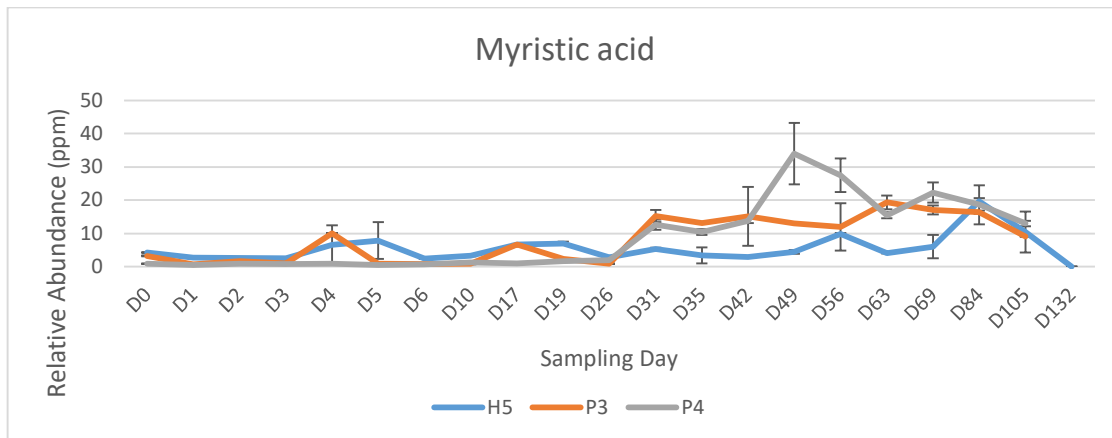


**Figure D-5:** Relative abundance graph of myristic acid through decomposition period of H5, P3 and P4. X-axis represents sampling day and y-axis is relative abundance (ppm).



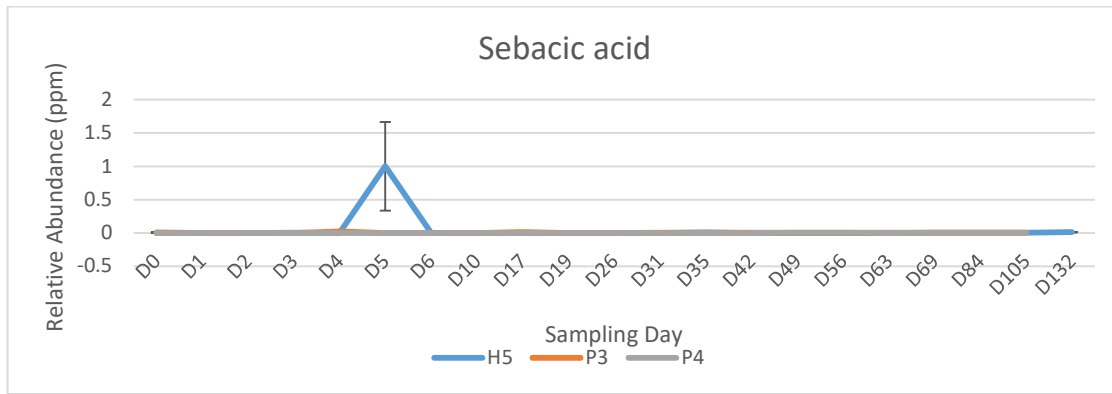


**Figure D-6:** Relative abundance graph of sebacic acid through decomposition period of H5, P3 and P4. X-axis represents sampling day and y-axis is relative abundance (ppm).

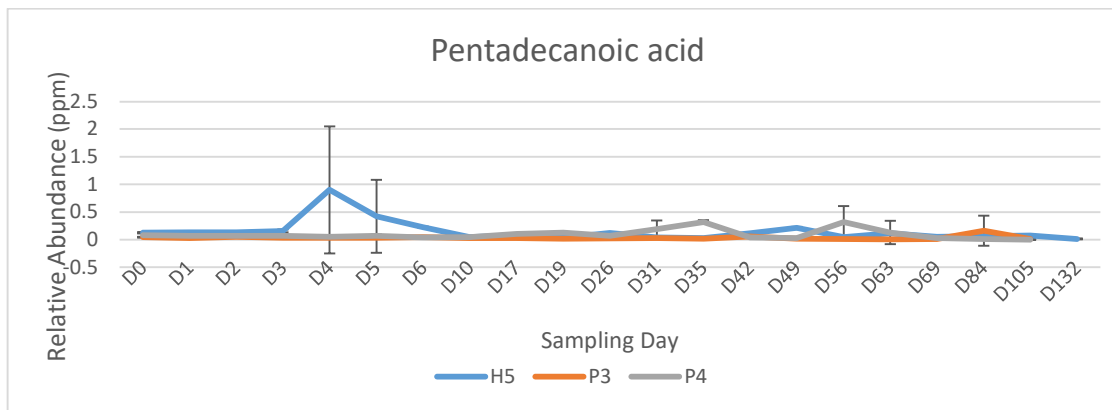


**Figure D-7:** Relative abundance graph of pentadecanoic acid through decomposition period of H5, P3 and P4. X-axis represents sampling day and y-axis is relative abundance (ppm).

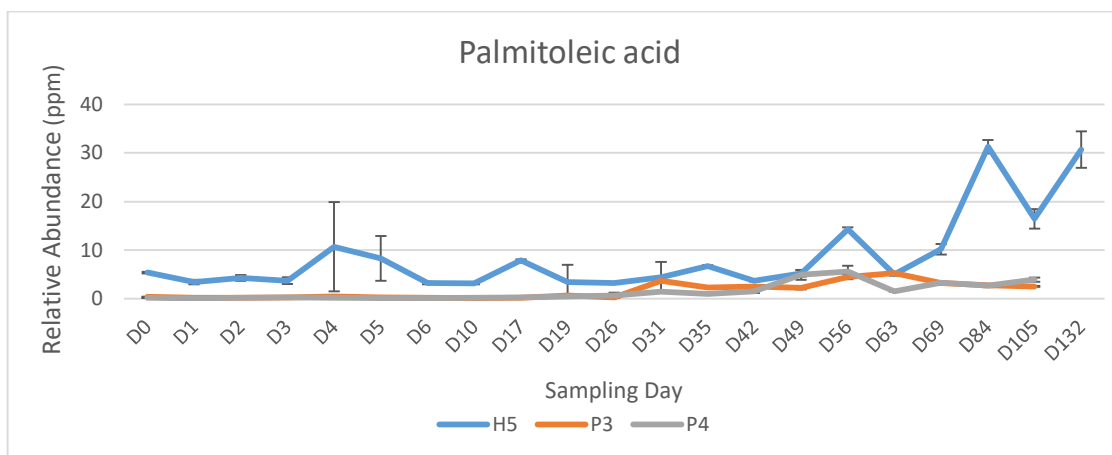


**Figure D-8:** Relative abundance graph of palmitoleic acid through decomposition period of H5, P3 and P4. X-axis represents sampling day and y-axis is relative abundance (ppm).

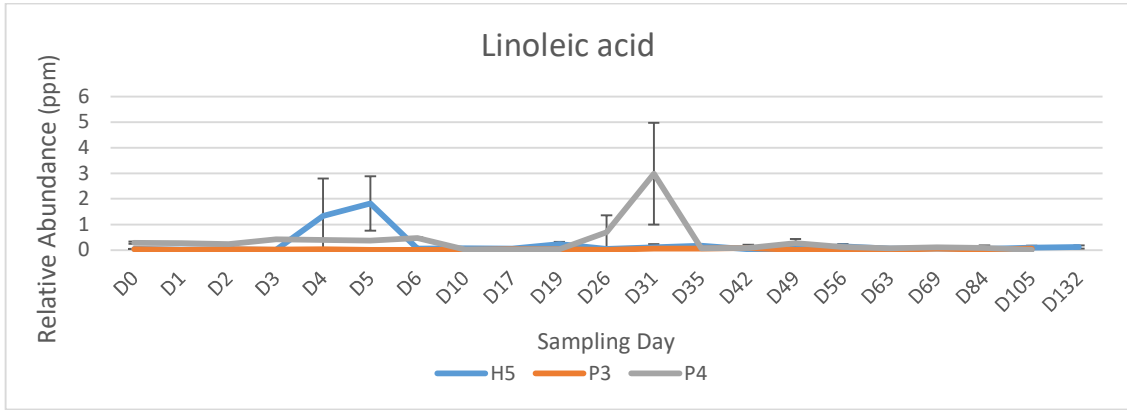


**Figure D-9:** Relative abundance graph of linoleic acid through decomposition period of H5, P3 and P4. X-axis represents sampling day and y-axis is relative abundance (ppm).

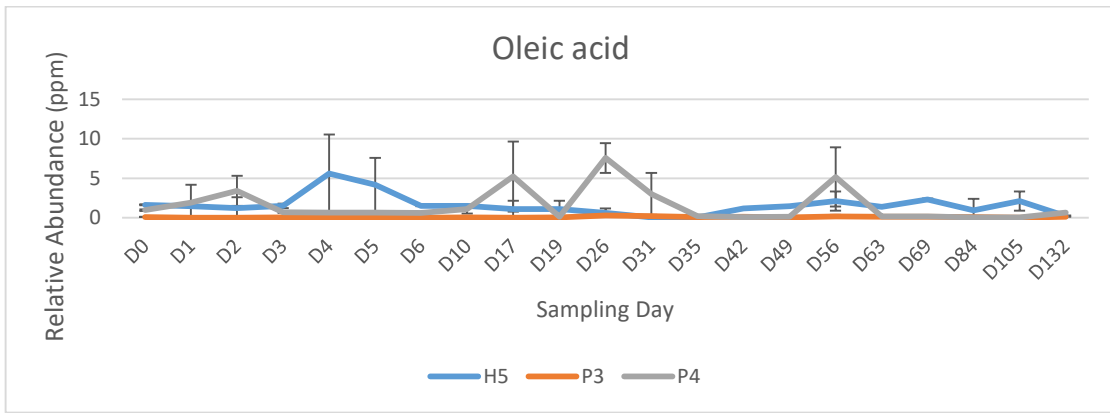


**Figure D-10:** Relative abundance graph of oleic acid through decomposition period of H5, P3 and P4. X-axis represents sampling day and y-axis is relative abundance (ppm).

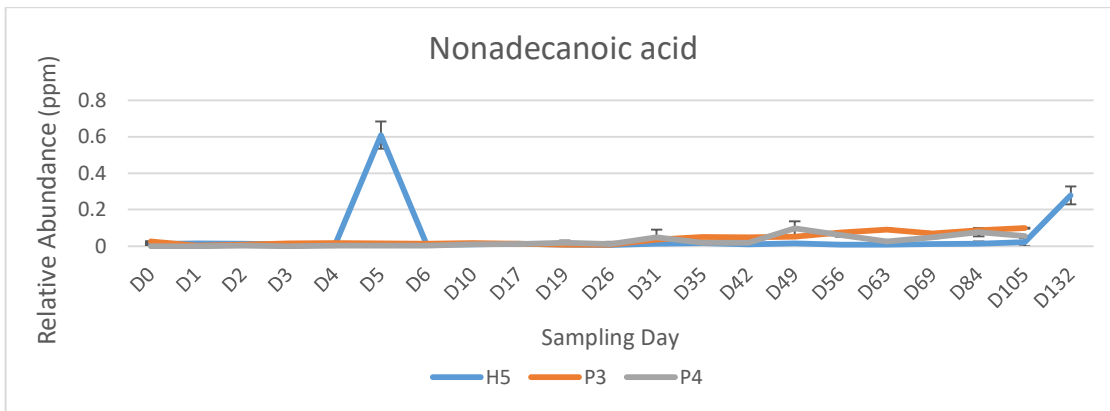


**Figure D-11:** Relative abundance graph of nonadecanoic acid through decomposition period of H5, P3 and P4. X-axis represents sampling day and y-axis is relative abundance (ppm)

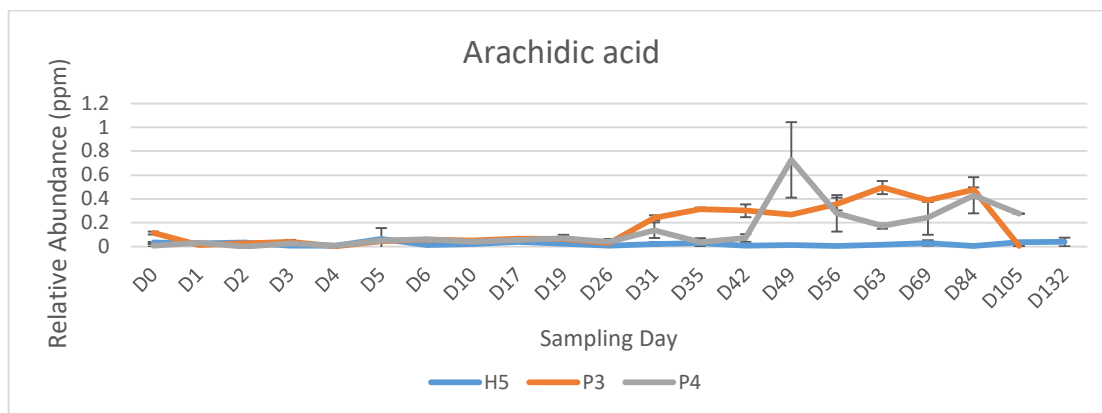


**Figure D-12:** Relative abundance graph of arachidic acid through decomposition period of H5, P3 and P4. X-axis represents sampling day and y-axis is relative abundance (ppm).

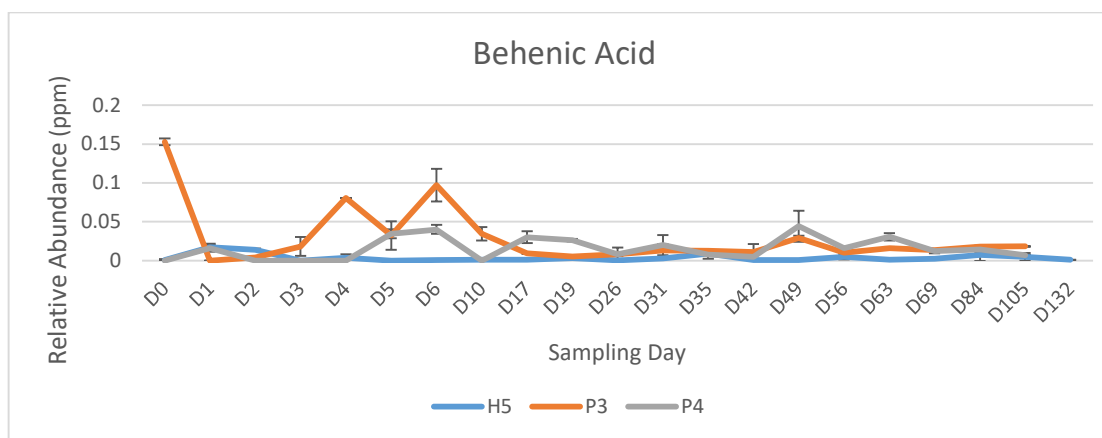


**Figure D-13:** Relative abundance graph of behenic acid through decomposition period of H5, P3 and P4. X-axis represents sampling day and y-axis is relative abundance (ppm).

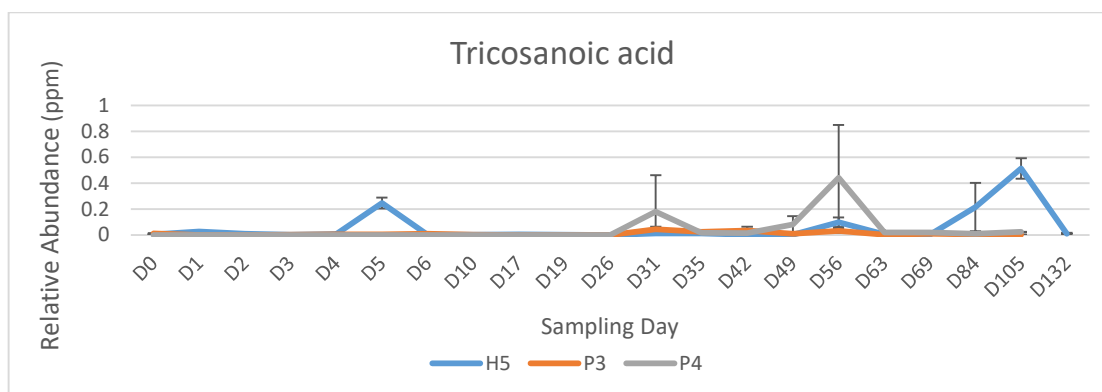


**Figure D-14:** Relative abundance graph of tricosanoic acid through decomposition period of H5, P3 and P4. X-axis represents sampling day and y-axis is relative abundance (ppm).

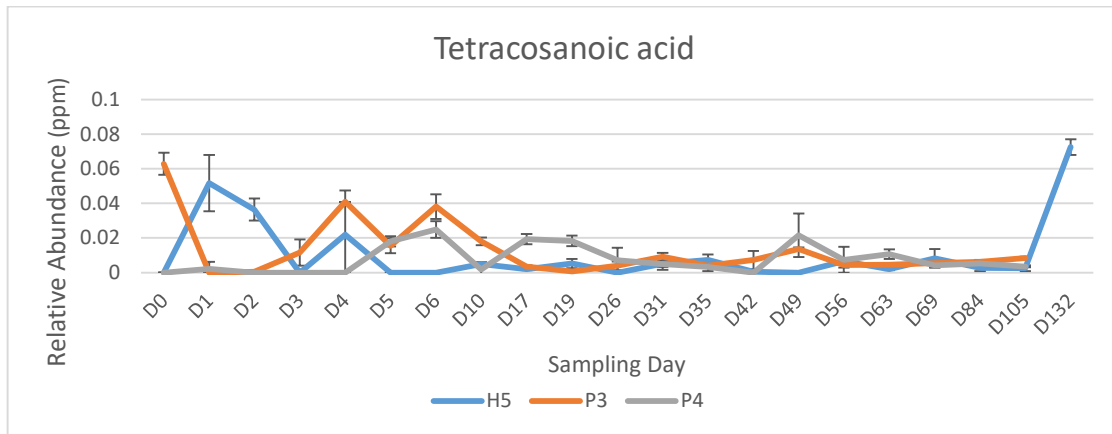


**Figure D-15:** Relative abundance graph of tetracosanoic acid through decomposition period of H5, P3 and P4. X-axis represents sampling day and y-axis is relative abundance (ppm).

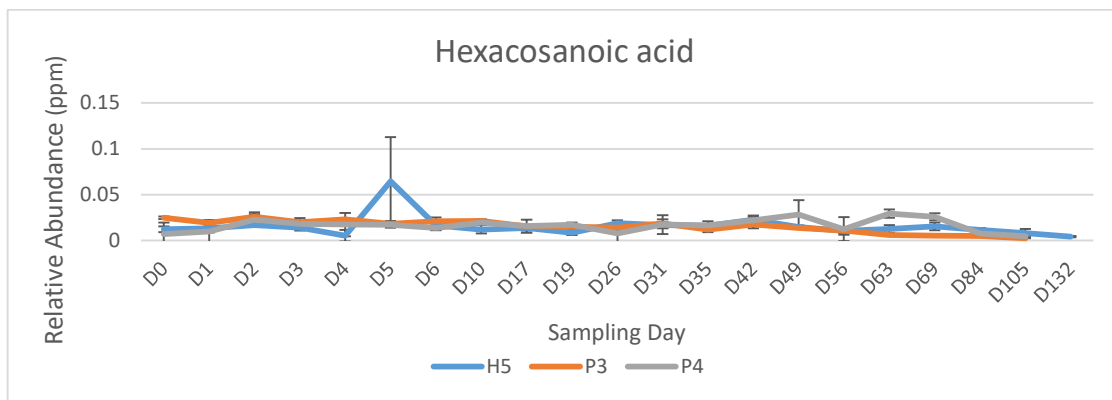


**Figure D-16:** Relative abundance graph of hexacosanoic acid through decomposition period of H5, P3 and P4. X-axis represents sampling day and y-axis is relative abundance (ppm).

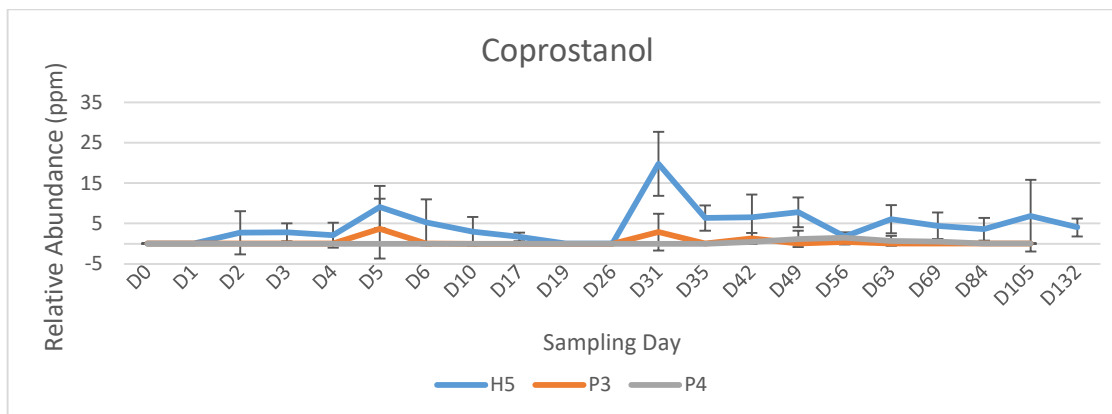


**Figure D-17:** Relative abundance graph of coprostanol through decomposition period of H5, P3 and P4. X-axis represents sampling day and y-axis is relative abundance (ppm).

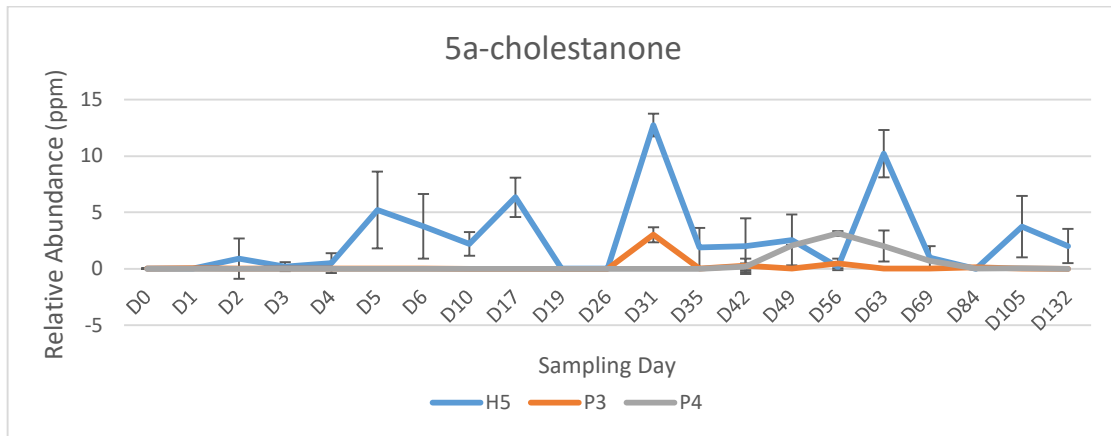


**Figure D-18:** Relative abundance graph of 5-cholestanone through decomposition period of H5, P3 and P4. X-axis represents sampling day and y-axis is relative abundance (ppm).

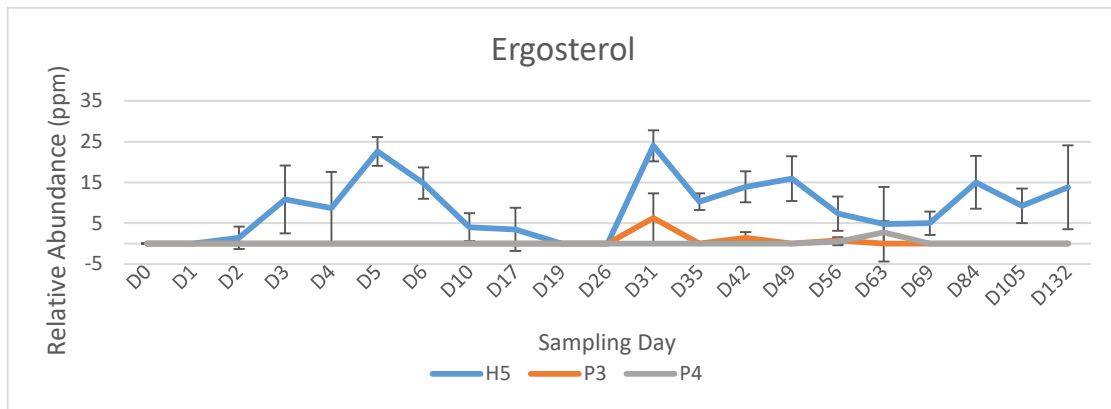


**Figure D-19:** Relative abundance graph of ergosterol through decomposition period of H5, P3 and P4. X-axis represents sampling day and y-axis is relative abundance (ppm).

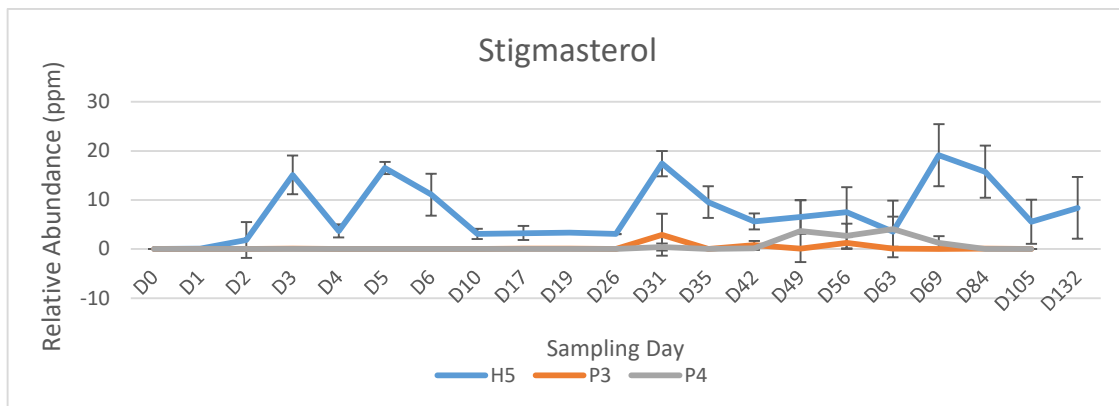


**Figure D-20:** Relative abundance graph of stigmasterol through decomposition period of H5, P3 and P4. X-axis represents sampling day and y-axis is relative abundance (ppm).

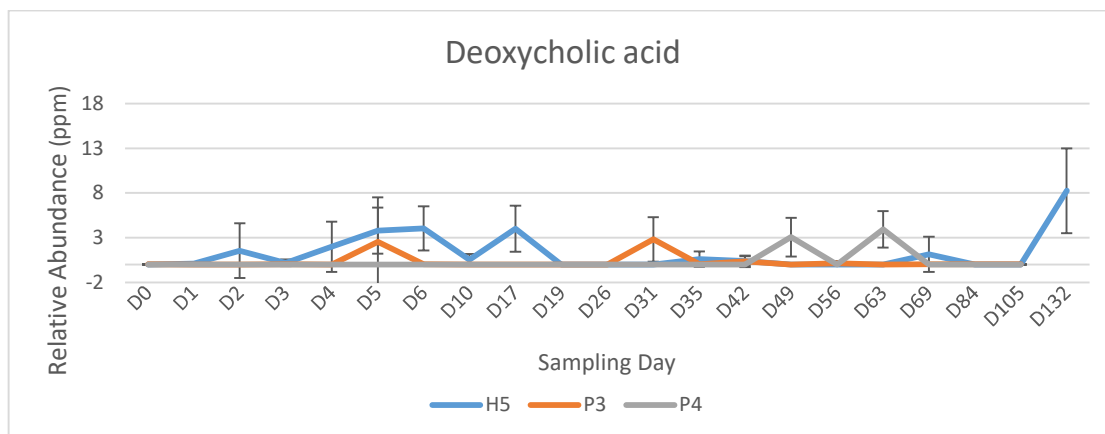


**Figure D-21:** Relative abundance graph of deoxycholic acid through decomposition period of H5, P3 and P4. X-axis represents sampling day and y-axis is relative abundance (ppm).

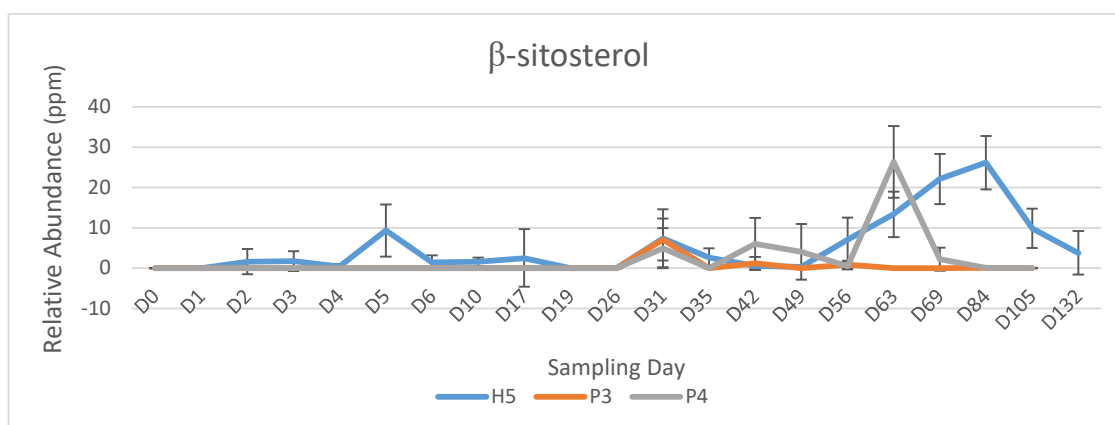


**Figure D-22:** Relative abundance graph of β-sitosterol through decomposition period of H5, P3 and P4. X-axis represents sampling day and y-axis is relative abundance (ppm).

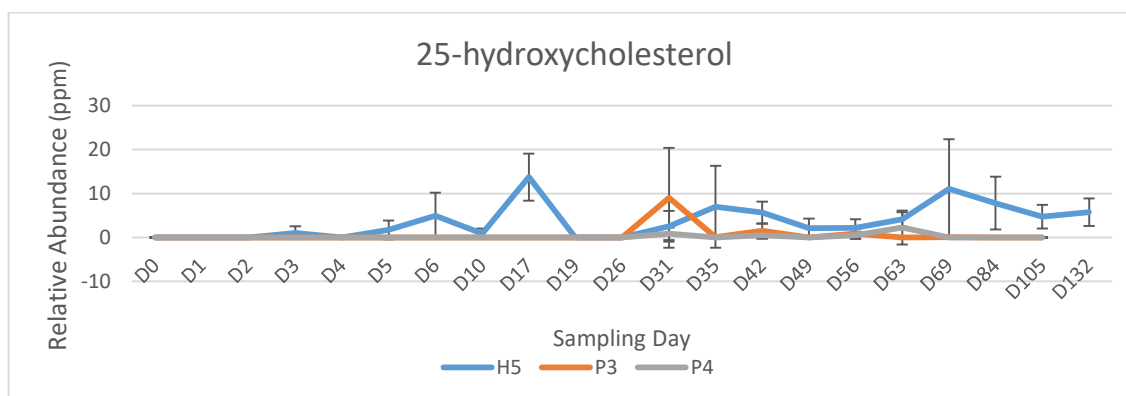


**Figure D-23:** Relative abundance graph of 25-hydroxycholesterol through decomposition period of H5, P3 and P4. X-axis represents sampling day and y-axis is relative abundance (ppm).

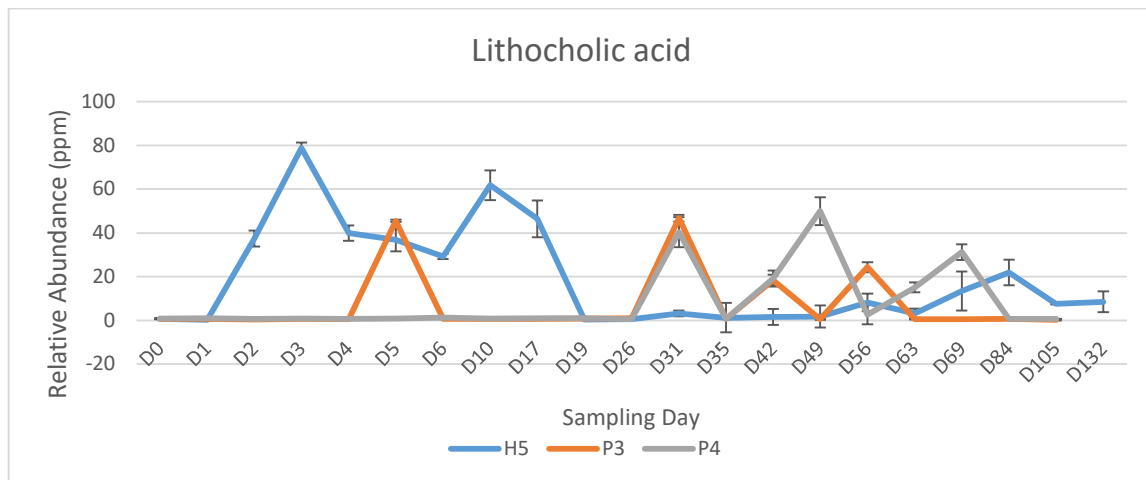


**Figure D-24:** Relative abundance graph of lithocholic acid through decomposition period of H5, P3 and P4. X-axis represents sampling day and y-axis is relative abundance (ppm).

## APPENDIX E- COOLER SEASON STUDY: PIG VS HUMAN TISSUE



Comparison of H5, P3 and P4 individual lipid trends within the tissue of pigs and humans. The x-axis for all graphs represents relative abundance in parts per million (ppm), y-axis represents sampling day

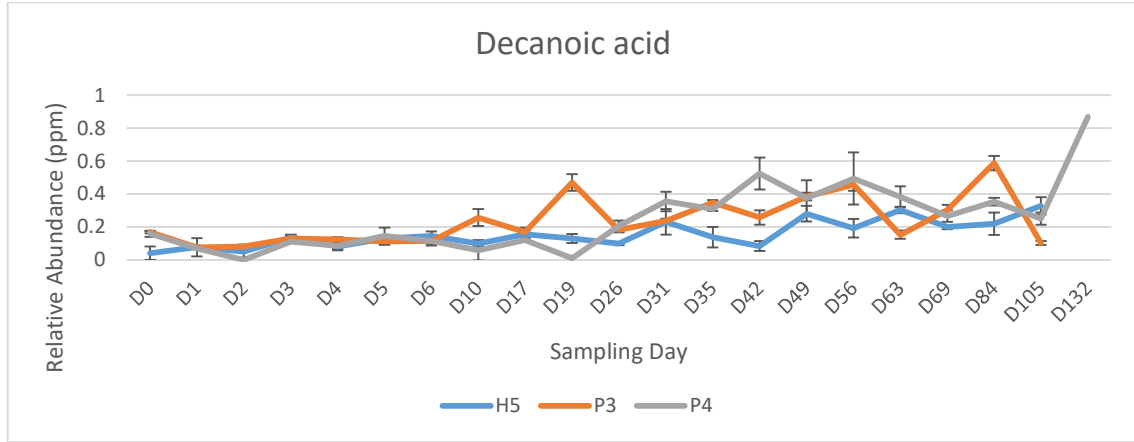


**Figure E-1:** Relative abundance graph of decanoic acid through decomposition period of H5, P3 and P4. X-axis represents sampling day and y-axis is relative abundance (ppm).

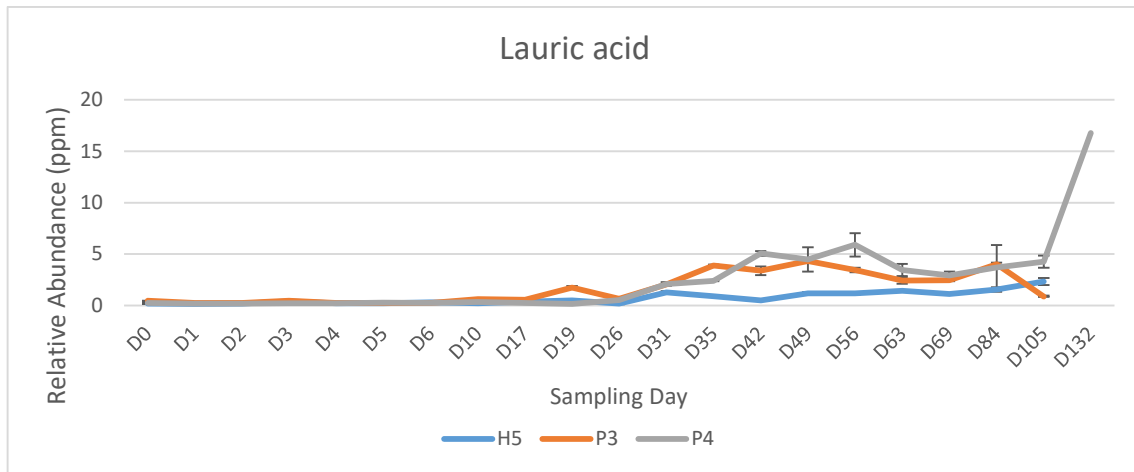


**Figure E-2:** Relative abundance graph of lauric acid through decomposition period of H5, P3 and P4. X-axis represents sampling day and y-axis is relative abundance (ppm).

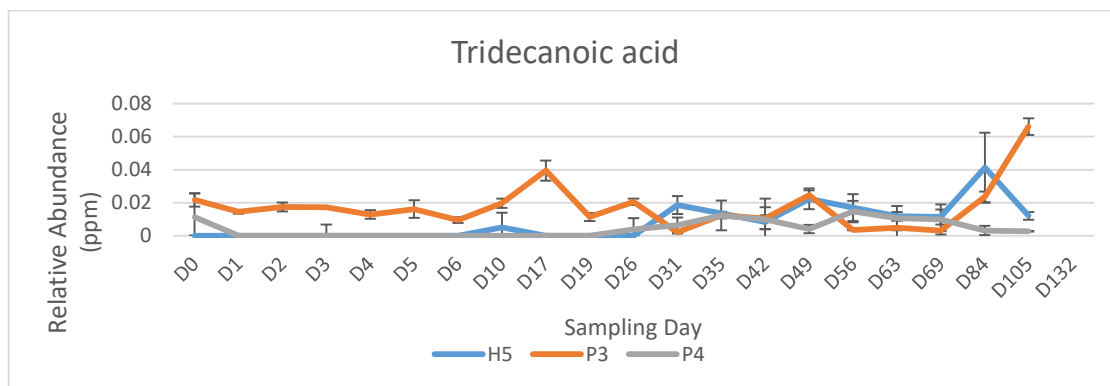


**Figure E-3:** Relative abundance graph of tridecanoic acid through decomposition period of H5, P3 and P4. X-axis represents sampling day and y-axis is relative abundance (ppm).

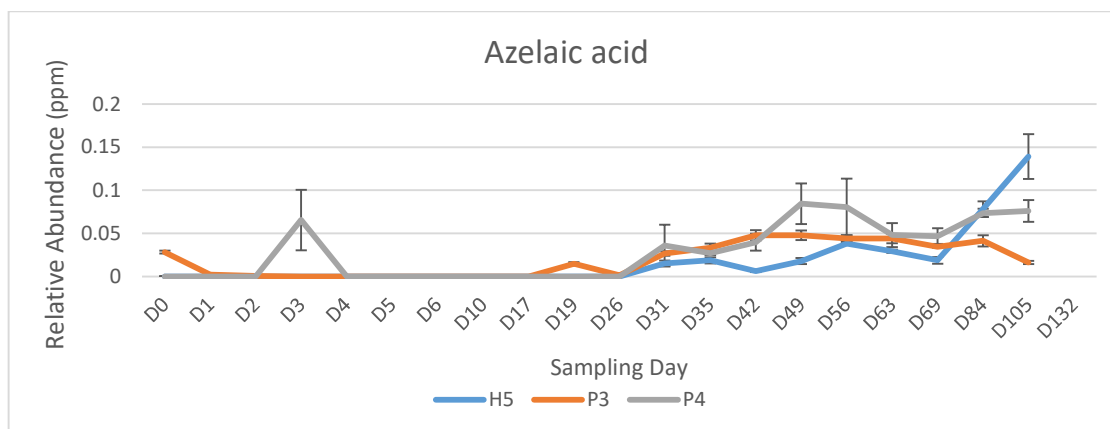


**Figure E-4:** Relative abundance graph of azelaic acid through decomposition period of H5, P3 and P4. X-axis represents sampling day and y-axis is relative abundance (ppm).

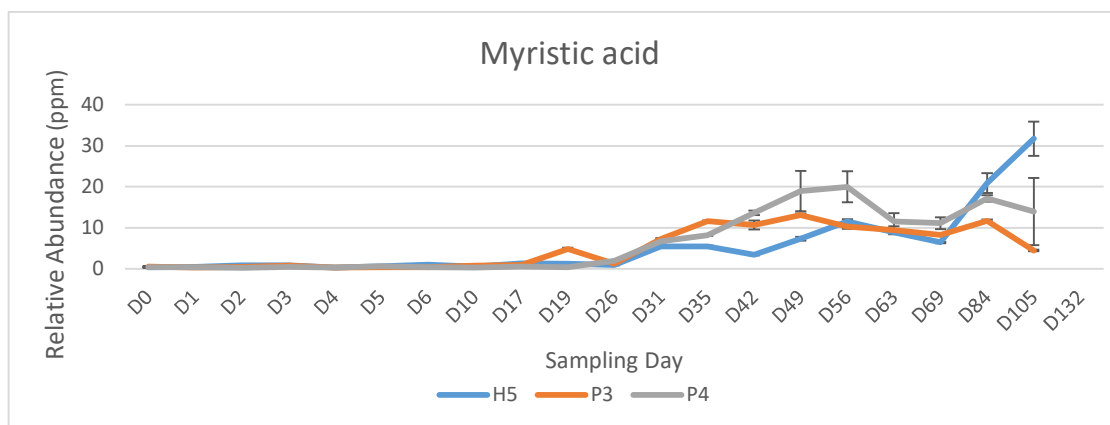


**Figure E-5:** Relative abundance graph of myristic acid through decomposition period of H5, P3 and P4. X-axis represents sampling day and y-axis is relative abundance (ppm).

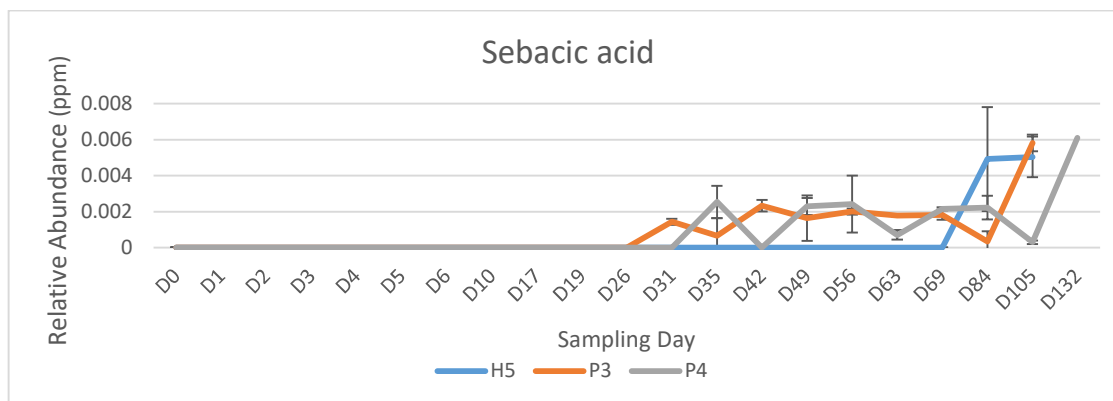


**Figure E-6:** Relative abundance graph of sebacic acid through decomposition period of H5, P3 and P4. X-axis represents sampling day and y-axis is relative abundance (ppm).

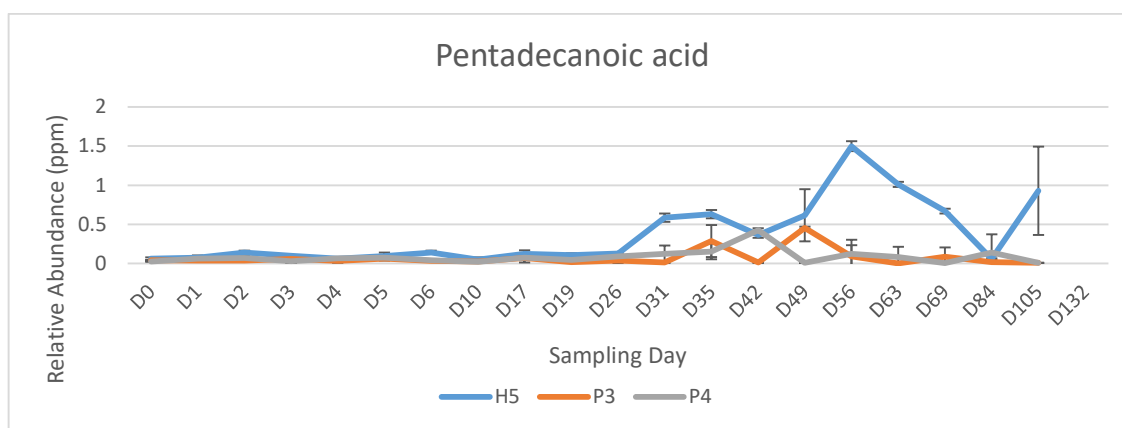


**Figure E-7:** Relative abundance graph of pentadecanoic acid through decomposition period of H5, P3 and P4. X-axis represents sampling day and y-axis is relative abundance (ppm).

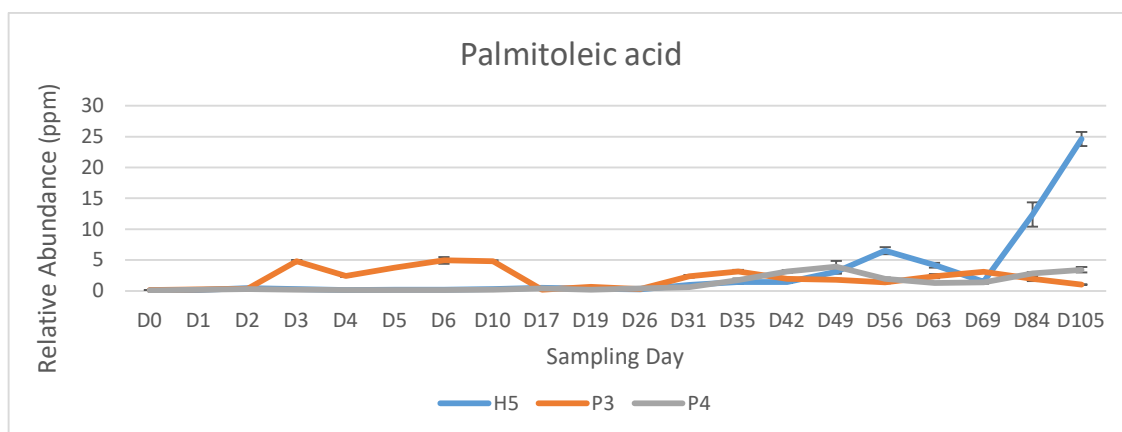


**Figure E-8:** Relative abundance graph of palmitoleic acid through decomposition period of H5, P3 and P4. X-axis represents sampling day and y-axis is relative abundance (ppm).

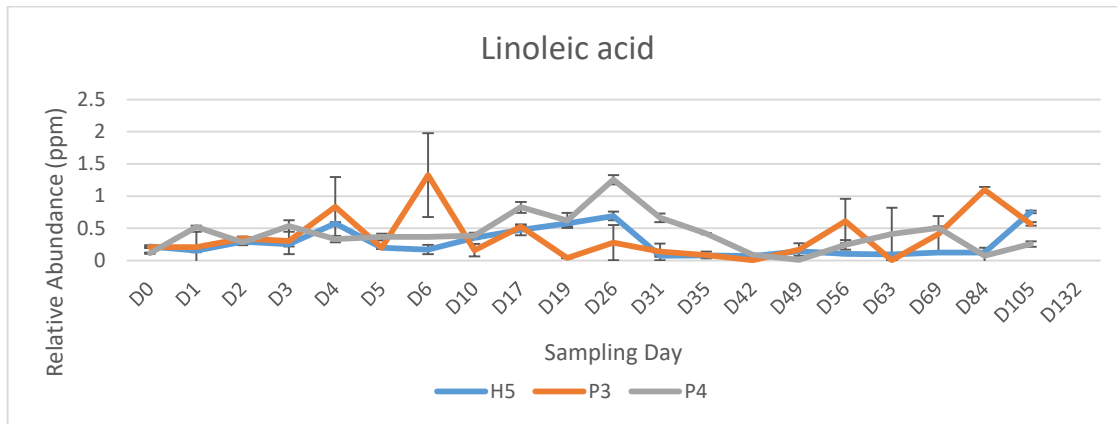


**Figure E-9:** Relative abundance graph of linoleic acid through decomposition period of H5, P3 and P4. X-axis represents sampling day and y-axis is relative abundance (ppm).

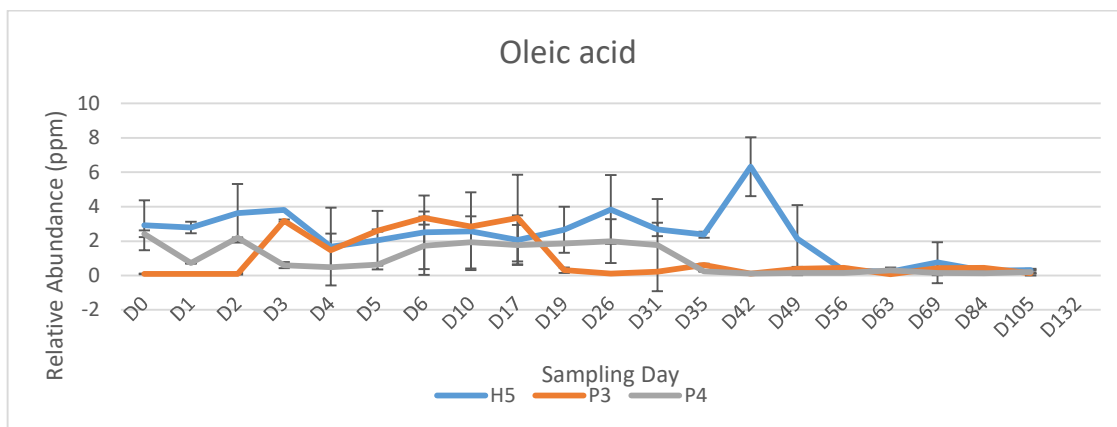


**Figure E-10:** Relative abundance graph of oleic acid through decomposition period of H5, P3 and P4. X-axis represents sampling day and y-axis is relative abundance (ppm).

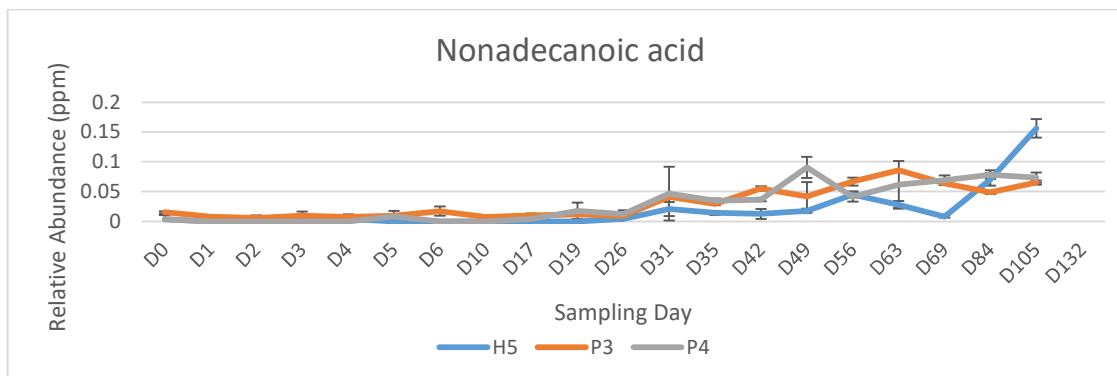


**Figure E-11:** Relative abundance graph of nonadecanoic acid through decomposition period of H5, P3 and P4. X-axis represents sampling day and y-axis is relative abundance (ppm).

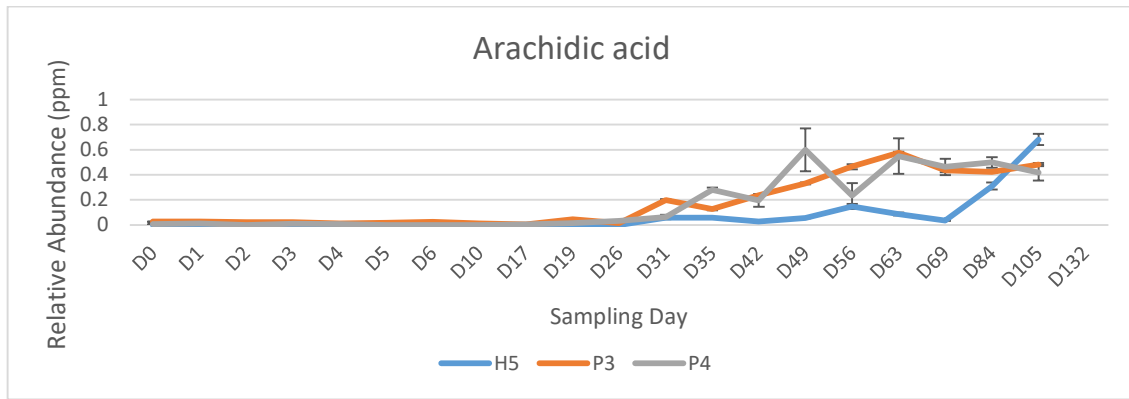


**Figure E-12:** Relative abundance graph of arachidic acid through decomposition period of H5, P3 and P4. X-axis represents sampling day and y-axis is relative abundance (ppm).

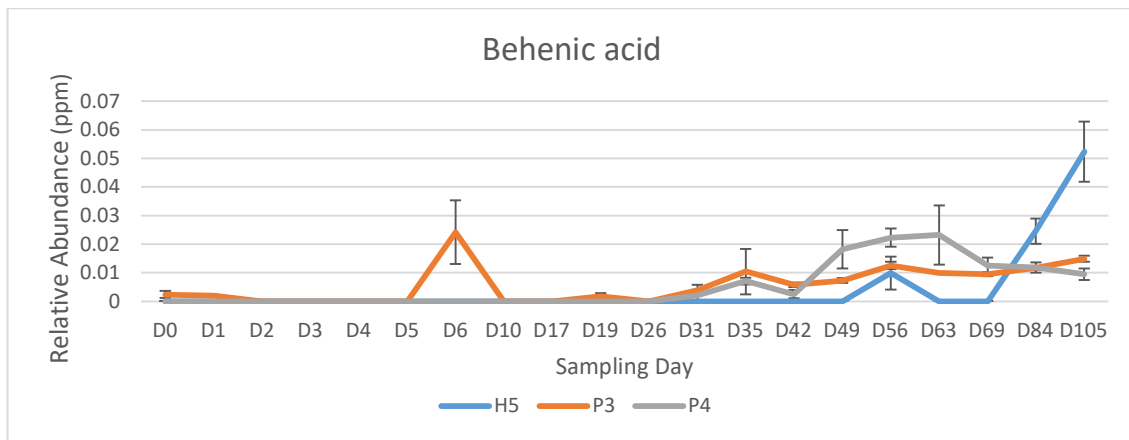


**Figure E-13:** Relative abundance graph of behenic acid through decomposition period of H5, P3 and P4. X-axis represents sampling day and y-axis is relative abundance (ppm).

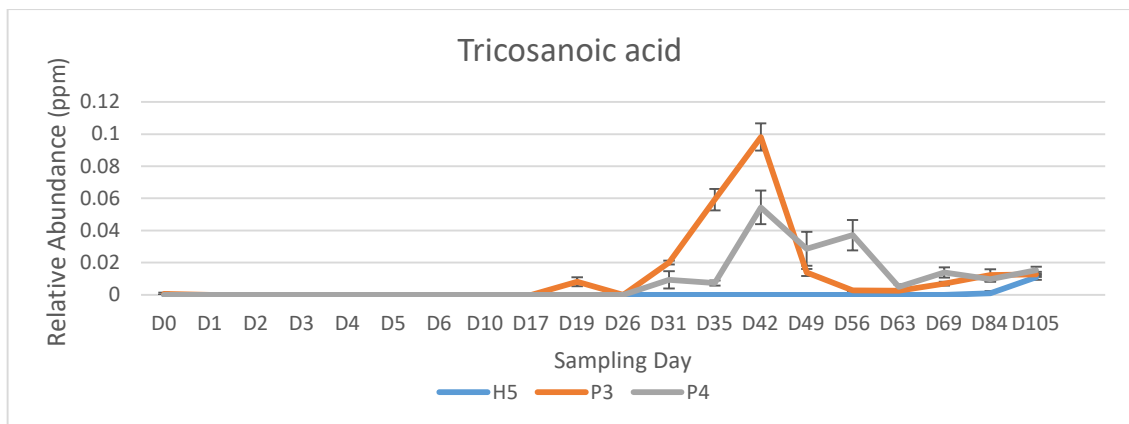


**Figure E-14:** Relative abundance graph of tricosanoic acid through decomposition period of H5, P3 and P4. X-axis represents sampling day and y-axis is relative abundance (ppm).

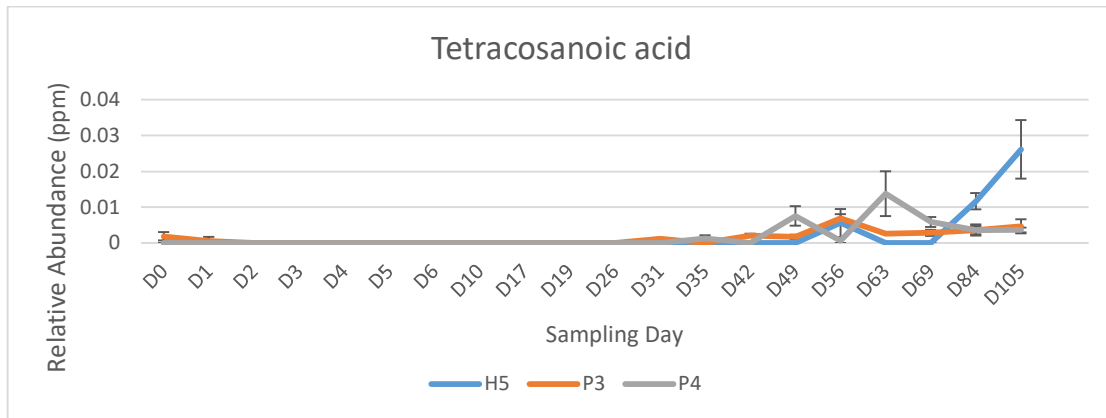


**Figure E-15:** Relative abundance graph of tetracosanoic acid through decomposition period of H5, P3 and P4. X-axis represents sampling day and y-axis is relative abundance (ppm).

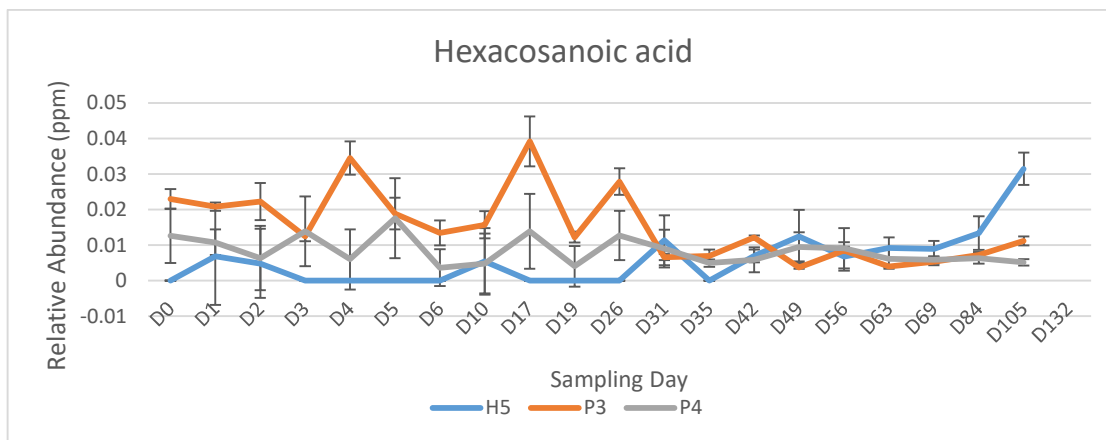


**Figure E-16:** Relative abundance graph of hexacosanoic acid through decomposition period of H5, P3 and P4. X-axis represents sampling day and y-axis is relative abundance (ppm).

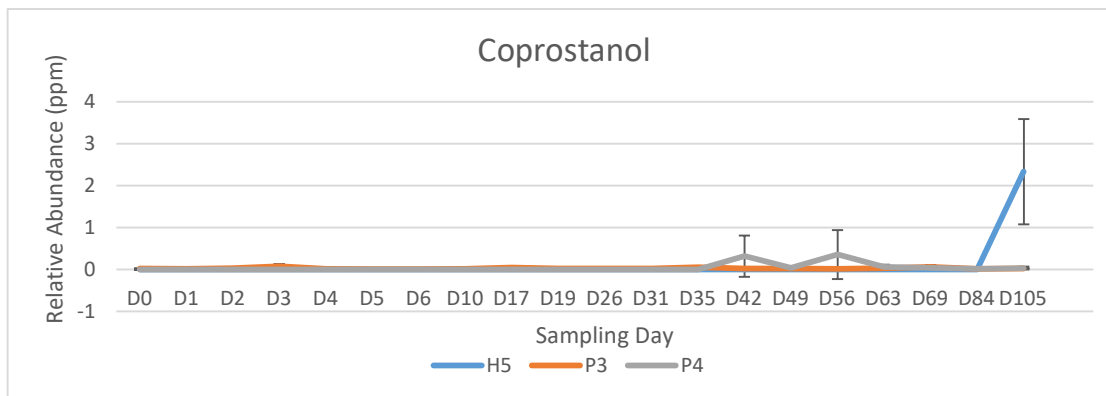


**Figure E-17:** Relative abundance graph of coprostanol through decomposition period of H5, P3 and P4. X-axis represents sampling day and y-axis is relative abundance (ppm).

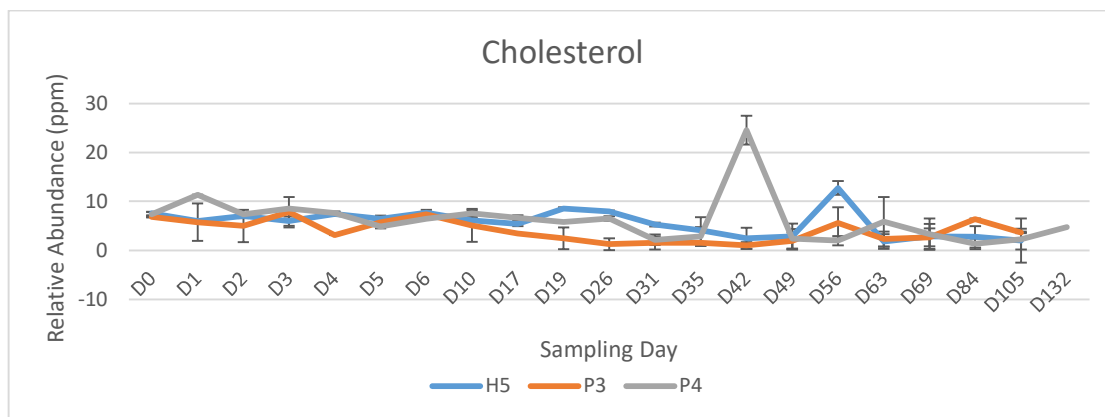


**Figure E-18:** Relative abundance graph of cholesterol through decomposition period of H5, P3 and P4. X-axis represents sampling day and y-axis is relative abundance (ppm).

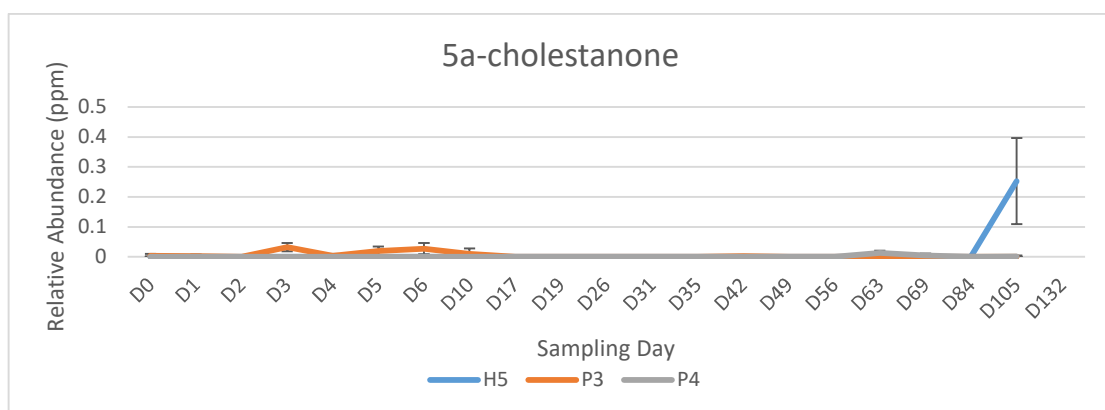


**Figure E-19:** Relative abundance graph of 5a-cholestanone through decomposition period of H5, P3 and P4. X-axis represents sampling day and y-axis is relative abundance (ppm).

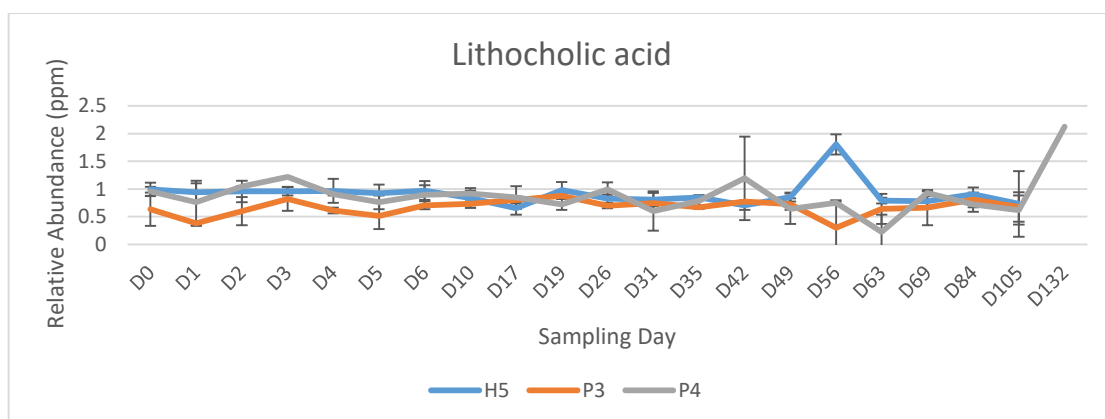


**Figure E-20:** Relative abundance graph of lithocholic acid through decomposition period of H5, P3 and P4. X-axis represents sampling day and y-axis is relative abundance (ppm).

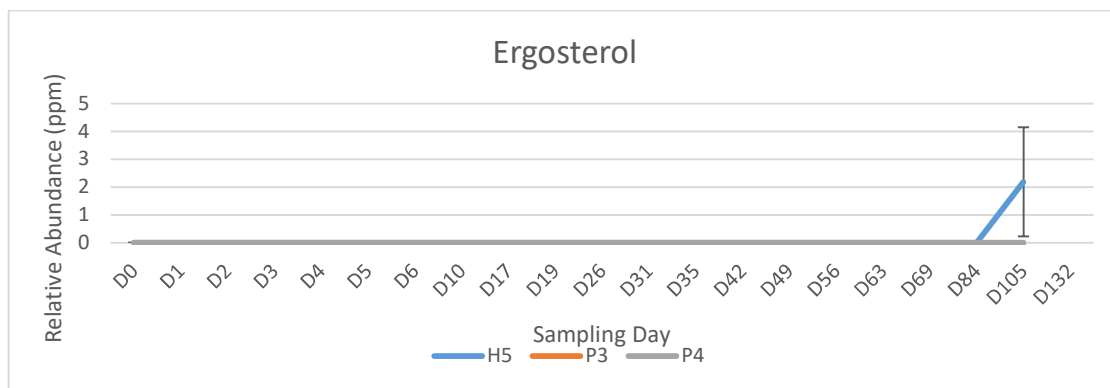


**Figure E-21:** Relative abundance graph of ergosterol through decomposition period of H5, P3 and P4. X-axis represents sampling day and y-axis is relative abundance (ppm).

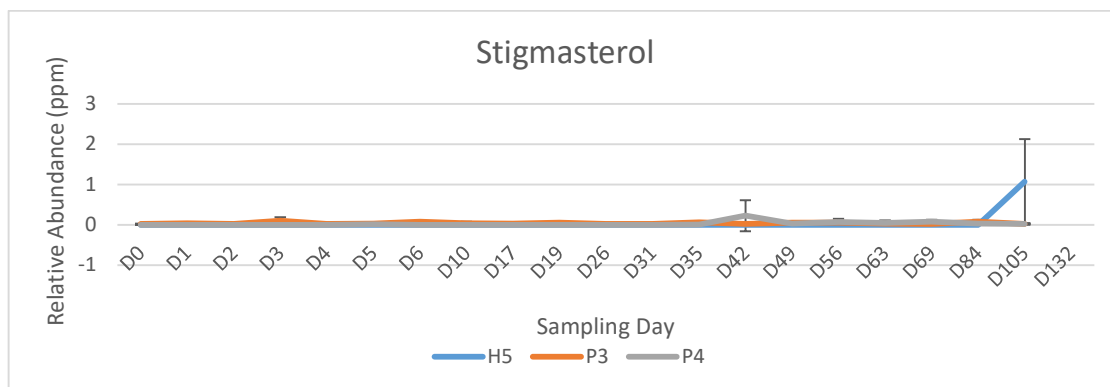


**Figure E-22:** Relative abundance graph of stigmasterol through decomposition period of H5, P3 and P4. X-axis represents sampling day and y-axis is relative abundance (ppm).

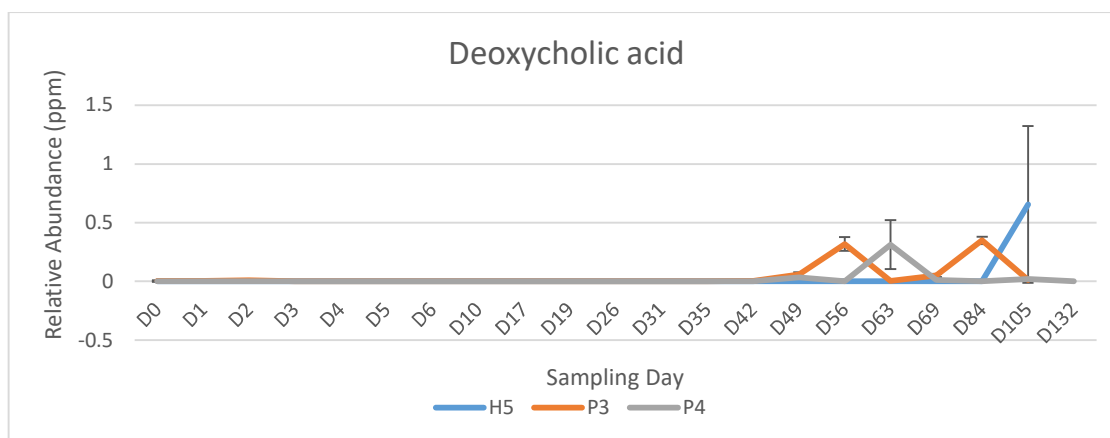


**Figure E-23:** Relative abundance graph of deoxycholic acid through decomposition period of H5, P3 and P4. X-axis represents sampling day and y-axis is relative abundance (ppm).



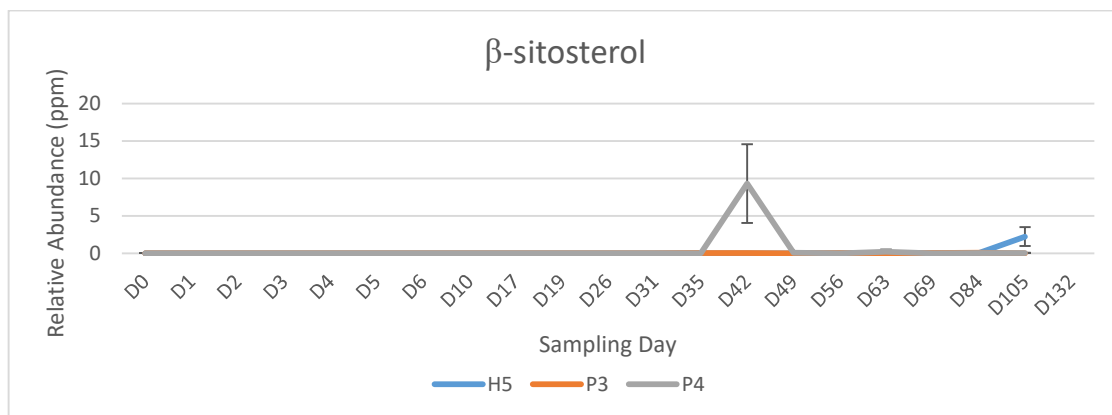


**Figure E-24:** Relative abundance graph of  $\beta$ -sitosterol through decomposition period of H5, P3 and P4. X-axis represents sampling day and y-axis is relative abundance (ppm).

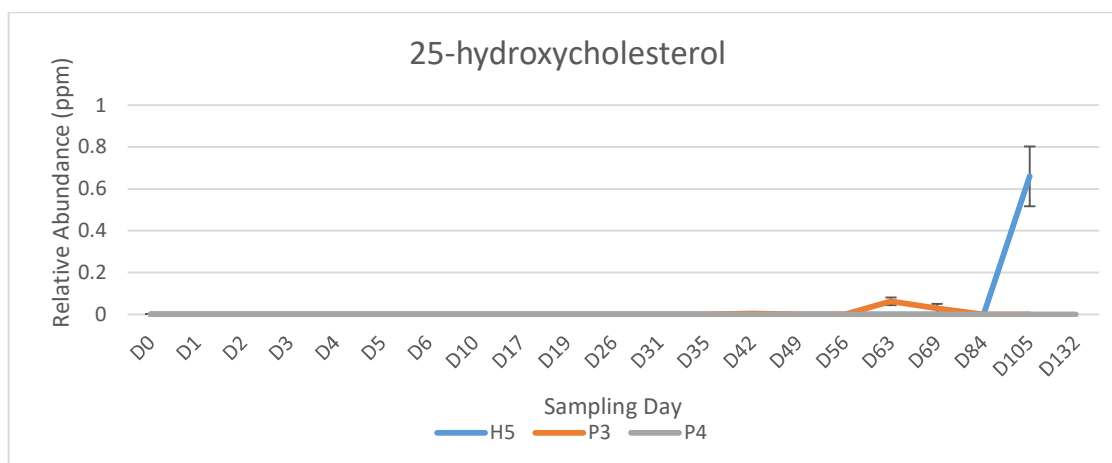


**Figure E-25:** Relative abundance graph of 25-hydroxycholesterol through decomposition period of H5, P3 and P4. X-axis represents sampling day and y-axis is relative abundance (ppm).

APPENDIX F- WARMER SEASON STUDY: PCA AND LOADINGS  
PLOT OF COMPOUNDS FOR PCA IN PIG VS HUMAN

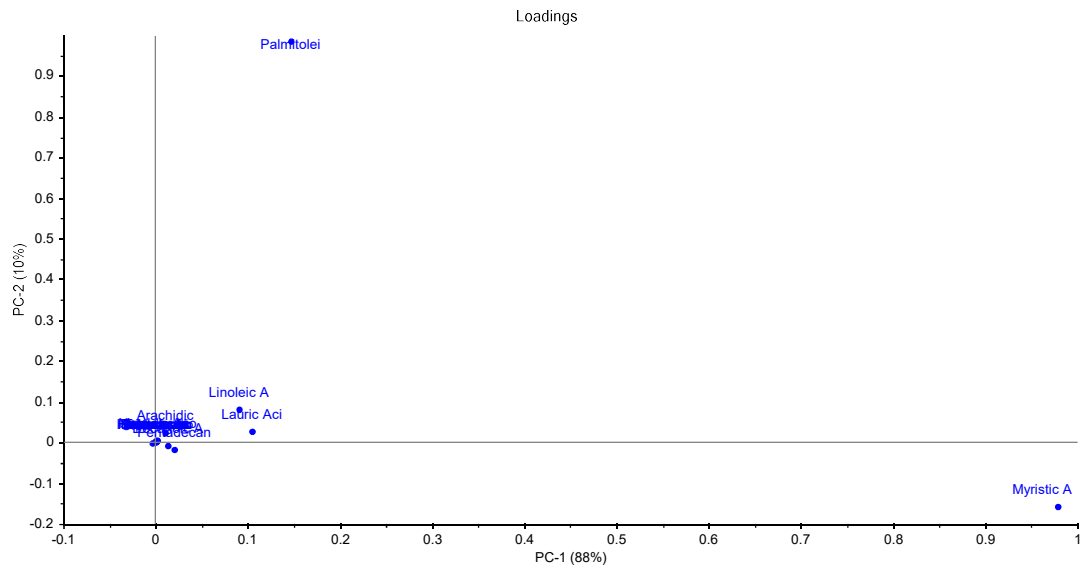


Figure F-1: Loadings plot of fatty acids within tissue of human vs pig.

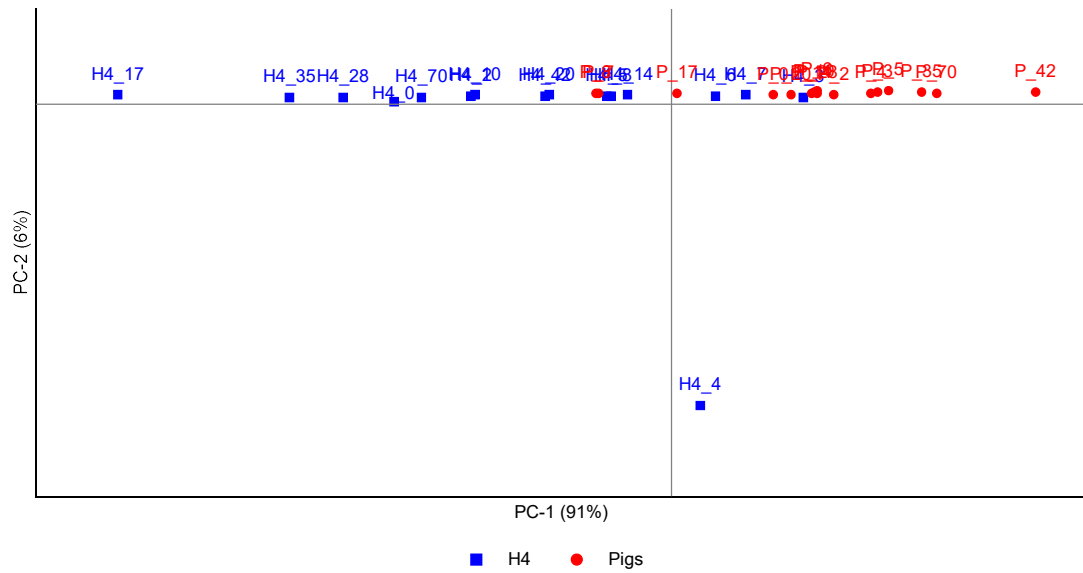


Figure F-2: PCA of sterols within tissue of human vs pigs.

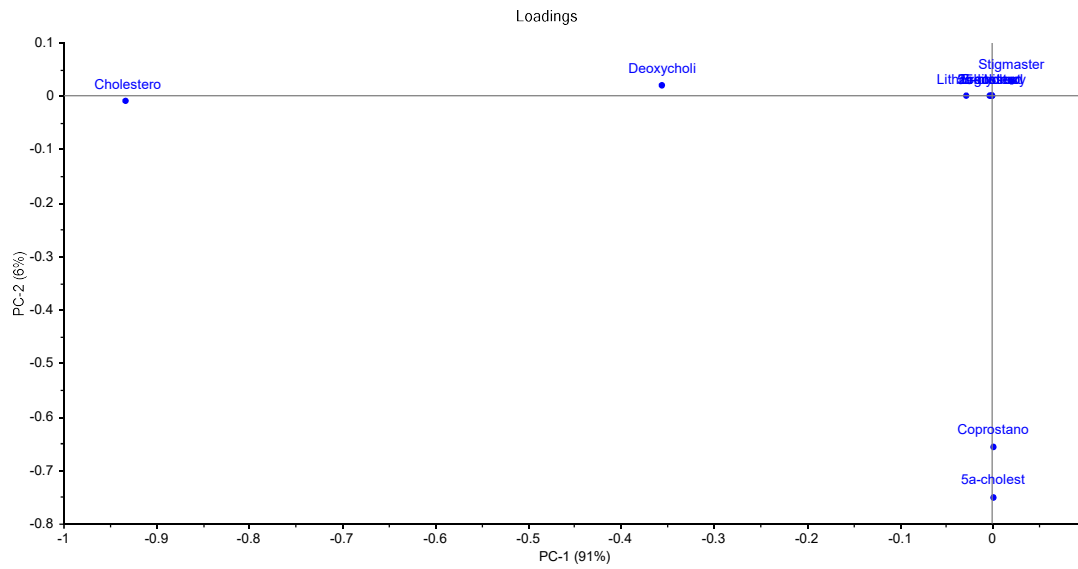


Figure F-3: Loadings plot of sterols within tissue of human vs pigs.

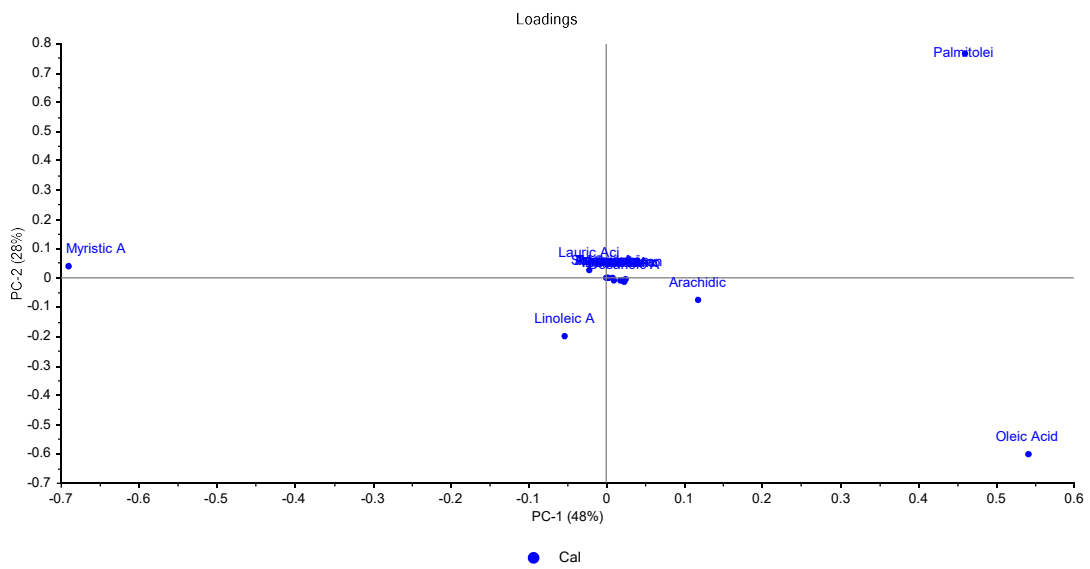


Figure F-4: Loadings plot of fatty acids within skin of human vs pigs.

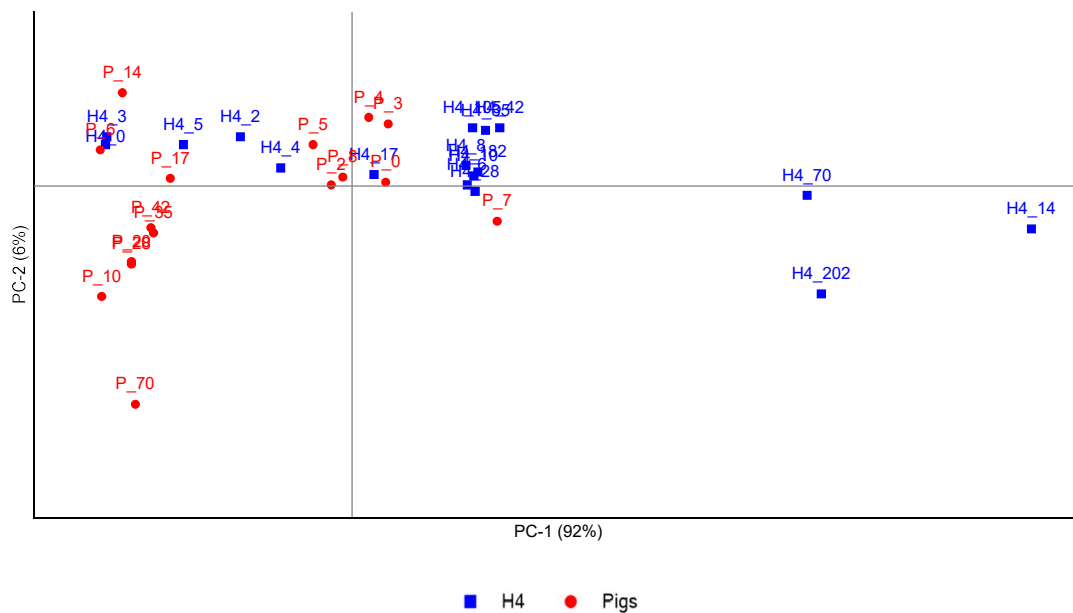


Figure F-5: PCA of sterols within skin of human vs pigs.

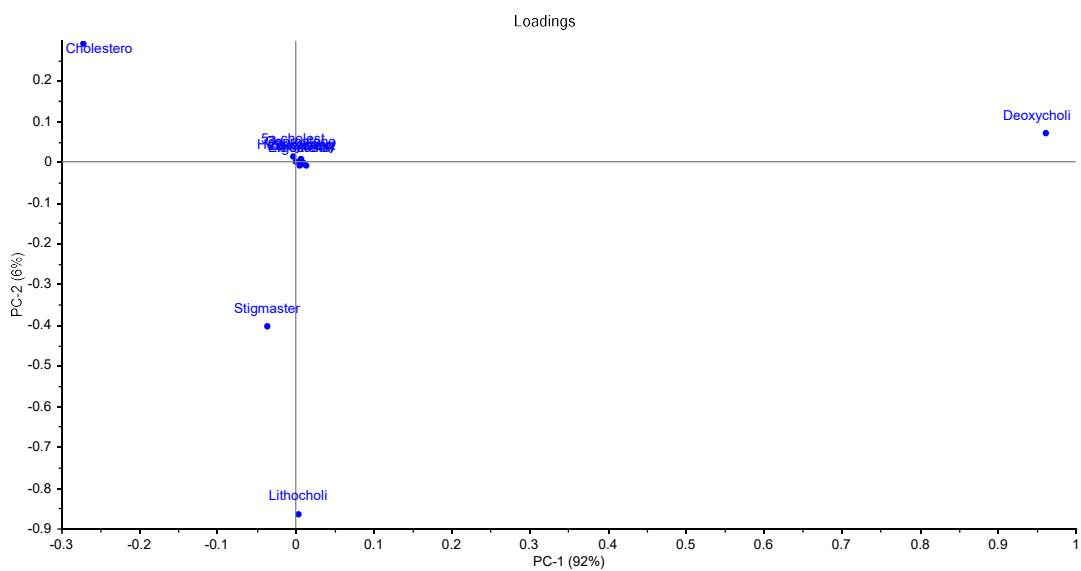


Figure F-6: Loadings plot of sterols within skin of human vs pigs.

APPENDIX G- COOLER SEASON STUDY: PCA AND LOADINGS PLOT  
OF COMPOUNDS FOR PCA IN PIG VS HUMAN

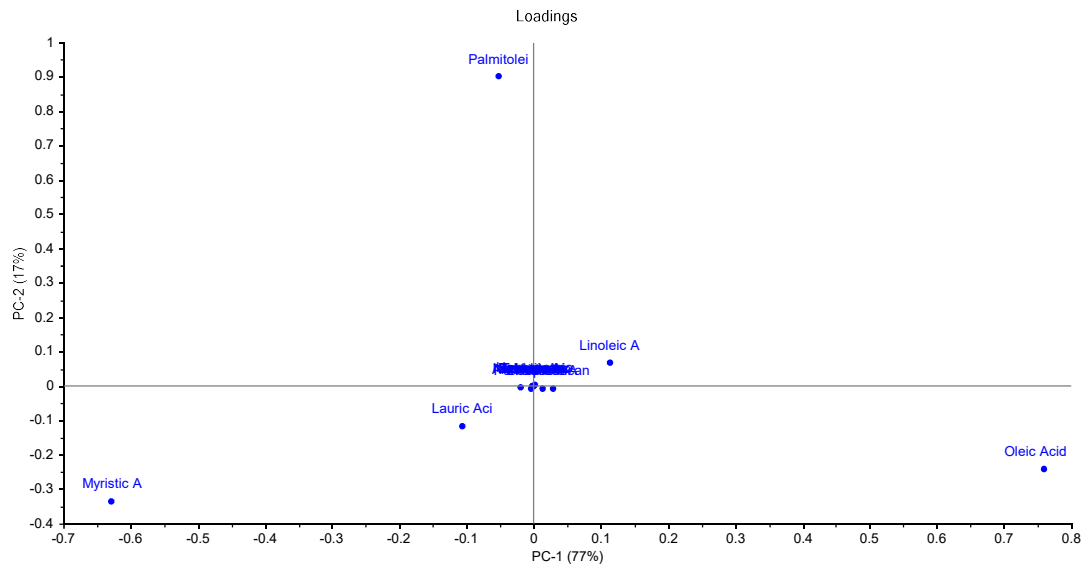


Figure G-1: Loadings plot of fatty acids within tissue of human vs pigs.

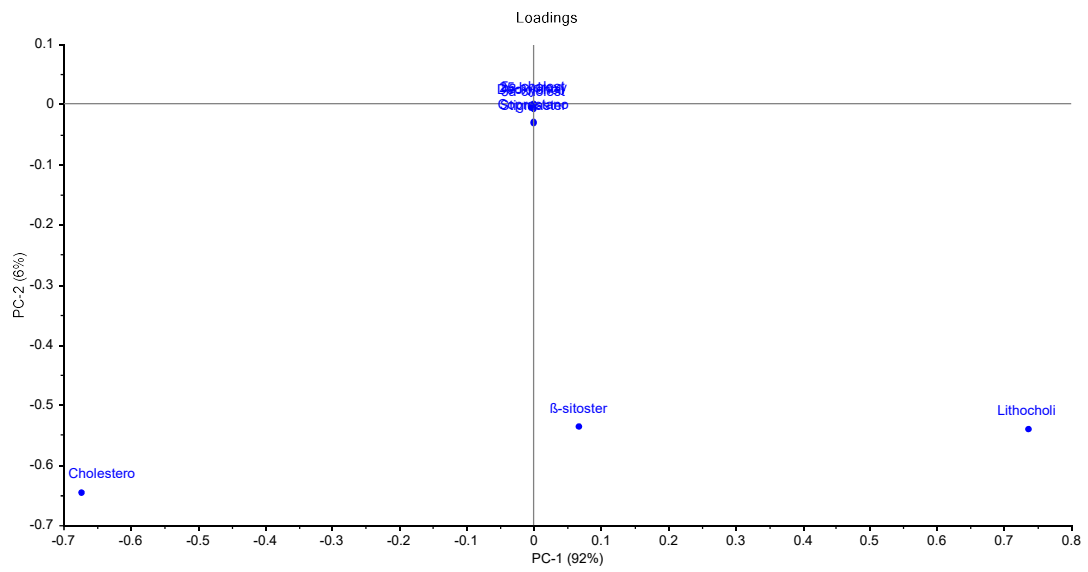


Figure G-2: Loadings plot of sterols within tissue of human vs pigs.

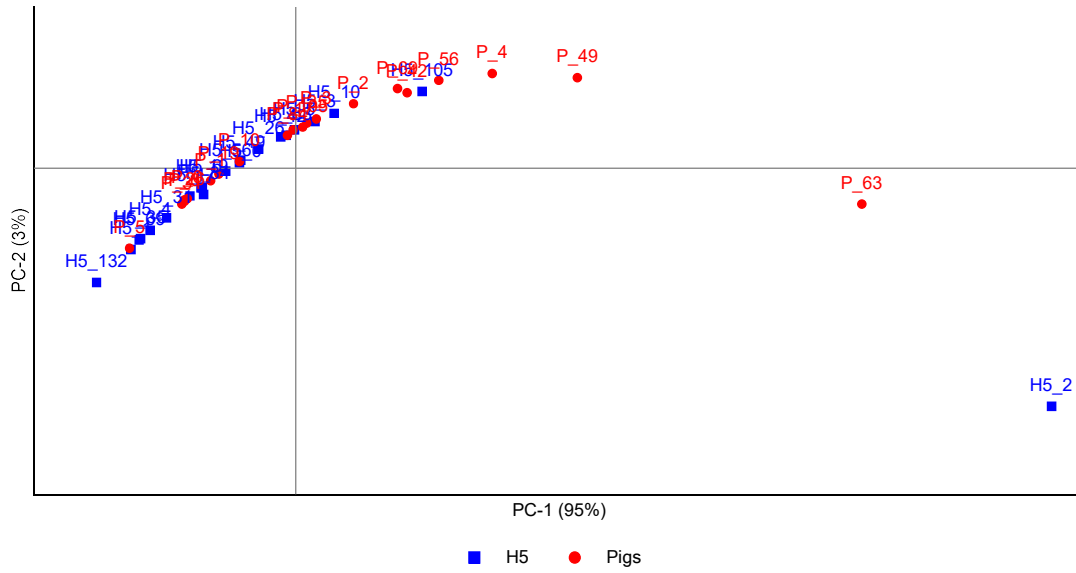


Figure G-3: PCA plot of fatty acids within skin of human vs pigs.

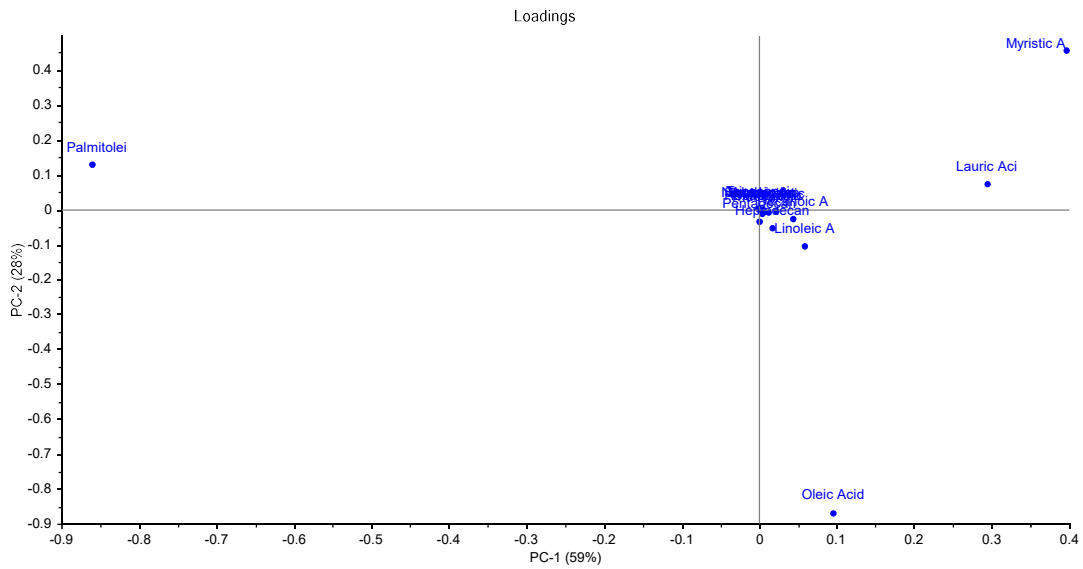


Figure G-4: Loadings plot of fatty acids within skin of human vs pigs.



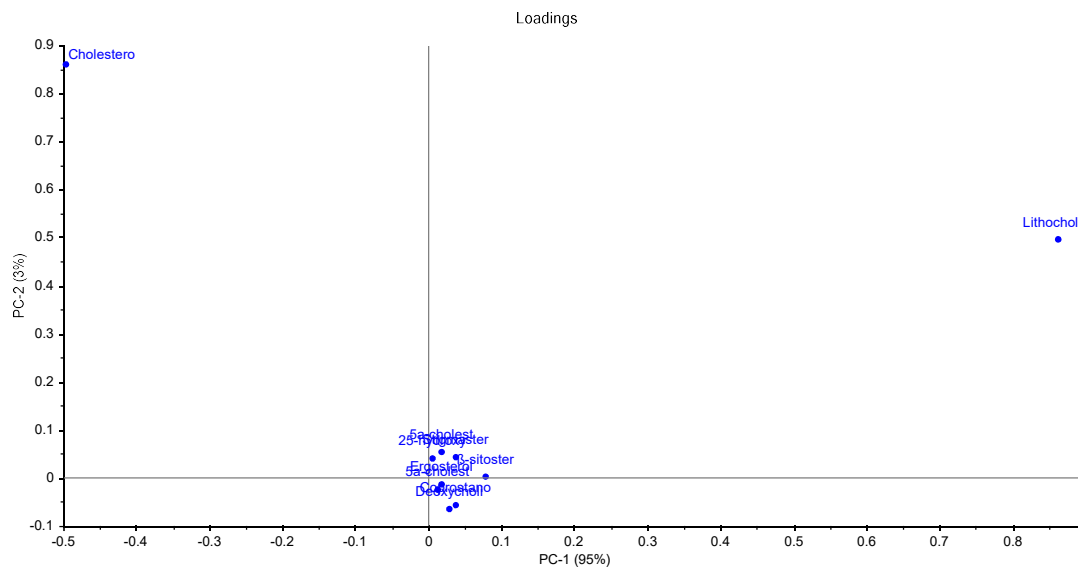


Figure G-5: Loadings plot of sterols within skin of human vs pigs.

APPENDIX H- LOADINGS PLOTS OF COMPOUNDS FOR PCA IN ALL  
HUMAN BODIES (HUMAN 2= H2, HUMAN 3= H3, HUMAN 4= H4,  
HUMAN 5= H5)

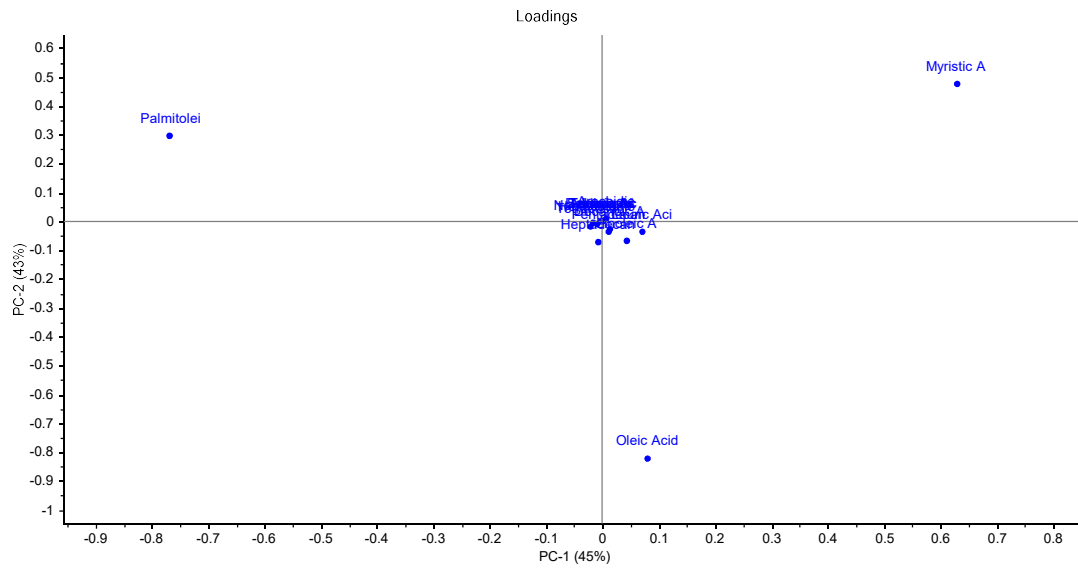


Figure H-1: Loadings plot of fatty acids within skin of H2, H3, H4 and H5.

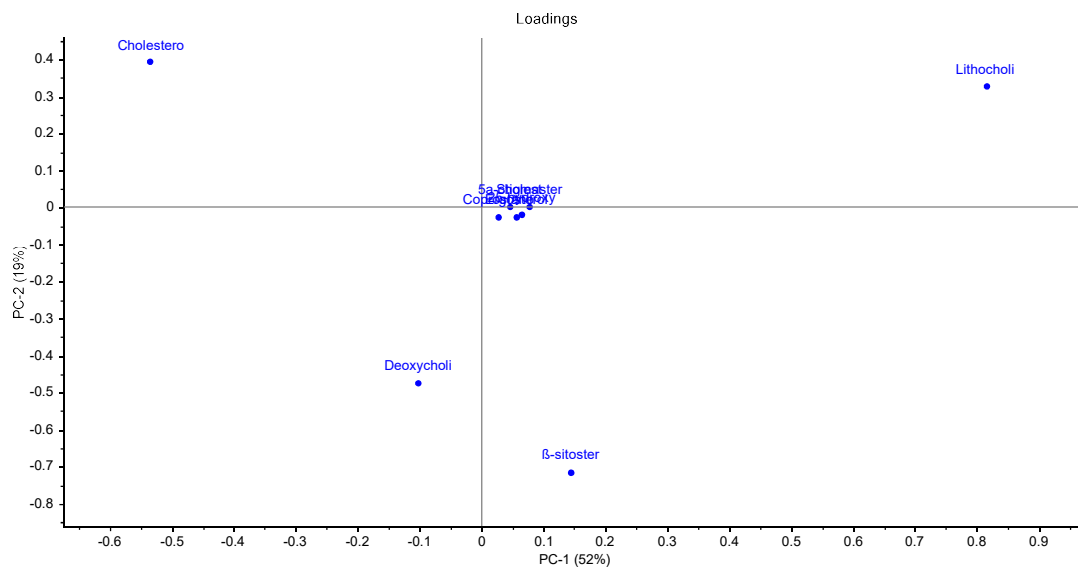


Figure H-2: Loadings plot of sterols within skin of H2, H3, H4 and H5.

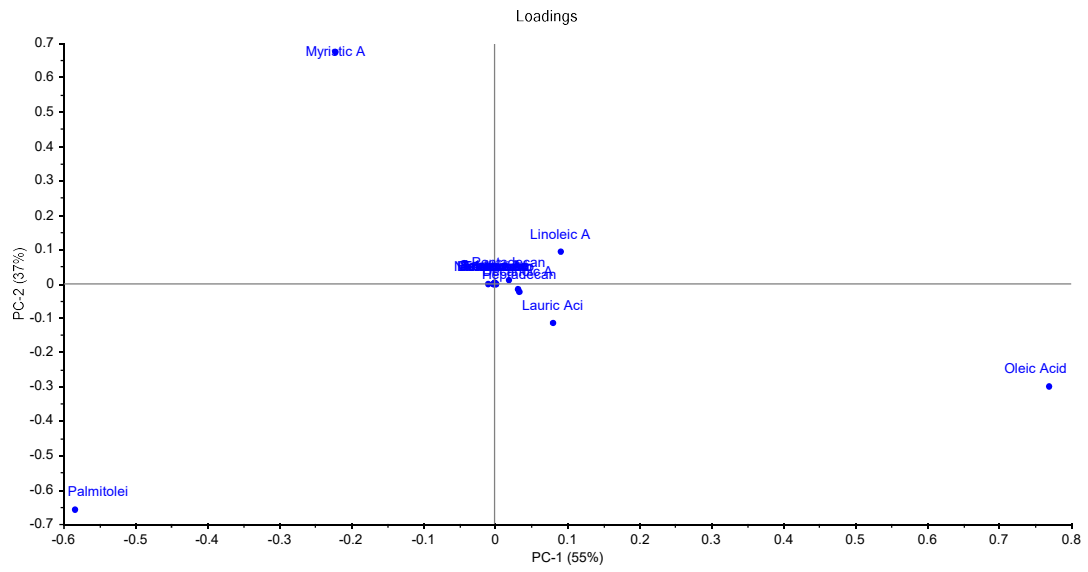


Figure H-3: Loadings plot of fatty acids within tissue of H2, H3, H4 and H5.

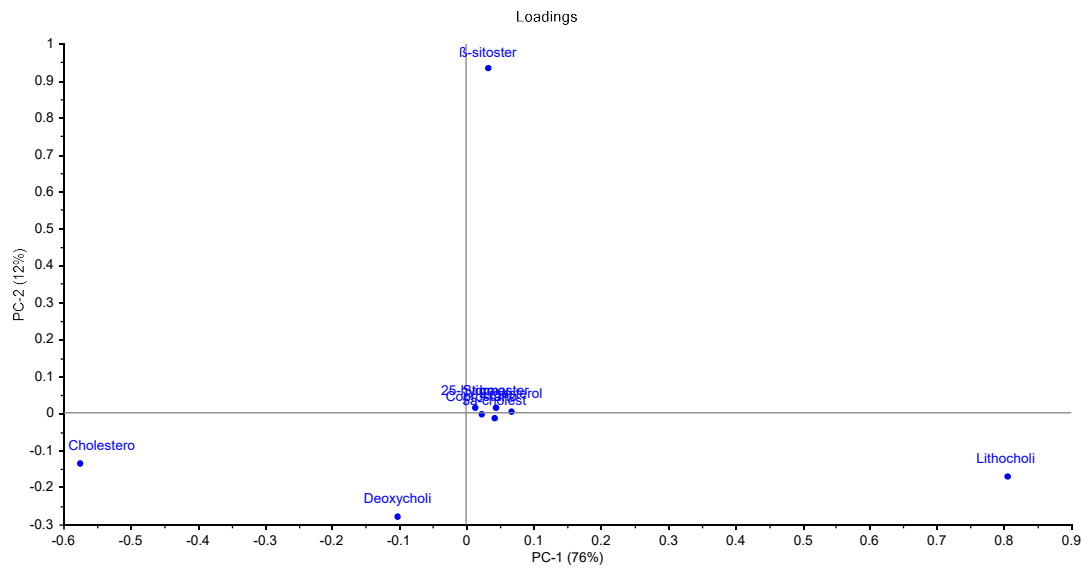
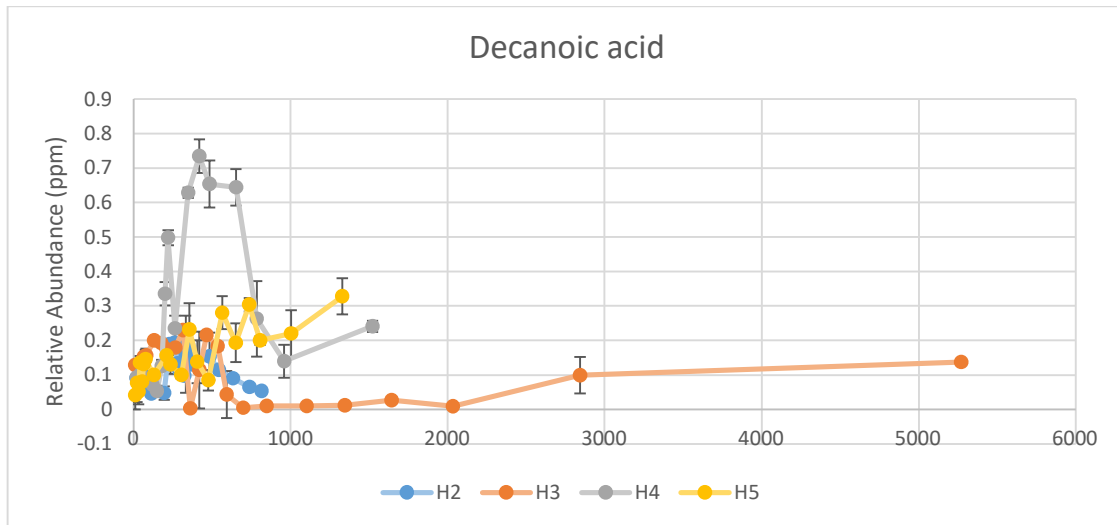


Figure H-4: Loadings plot of sterols within tissue of H2, H3, H4 and H5.

APPENDIX I- INDIVIDUAL COMPOUND TREND COMPARISON  
WITHIN THE SKIN OF ALL HUMAN BODIES

Comparison of individual lipid trends within the skin matrix of all humans (human 2= H2, human 3= H3, human 4= H4 and human 5= H5). The x-axis for all graphs represents relative abundance in parts per million (ppm), y-axis represents accumulated degree days.



**Figure I-1:** Comparison of decanoic acid through decomposition period of H2, H3, H4 and H5. X-axis represents relative abundance in ppm. Y-axis represents accumulated degree days (ADD).

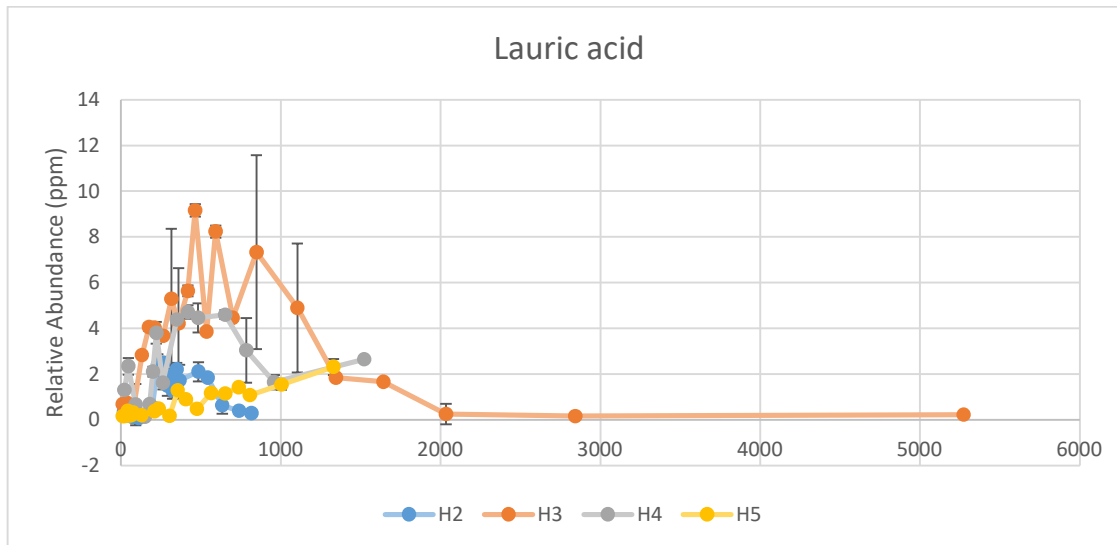


**Figure I-2:** Comparison of lauric acid through decomposition period of H2, H3, H4 and H5. X-axis represents relative abundance in ppm. Y-axis represents accumulated degree days (ADD).

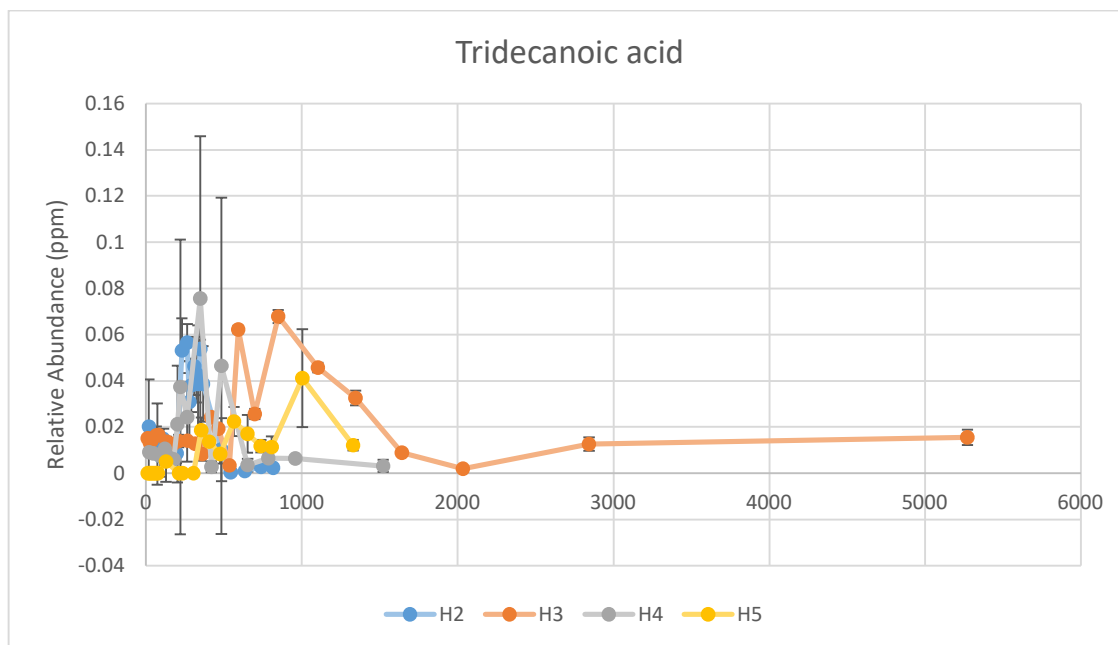


**Figure I-3:** Comparison of tridecanoic acid through decomposition period of H2, H3, H4 and H5. X-axis represents relative abundance in ppm. Y-axis represents accumulated degree days (ADD).

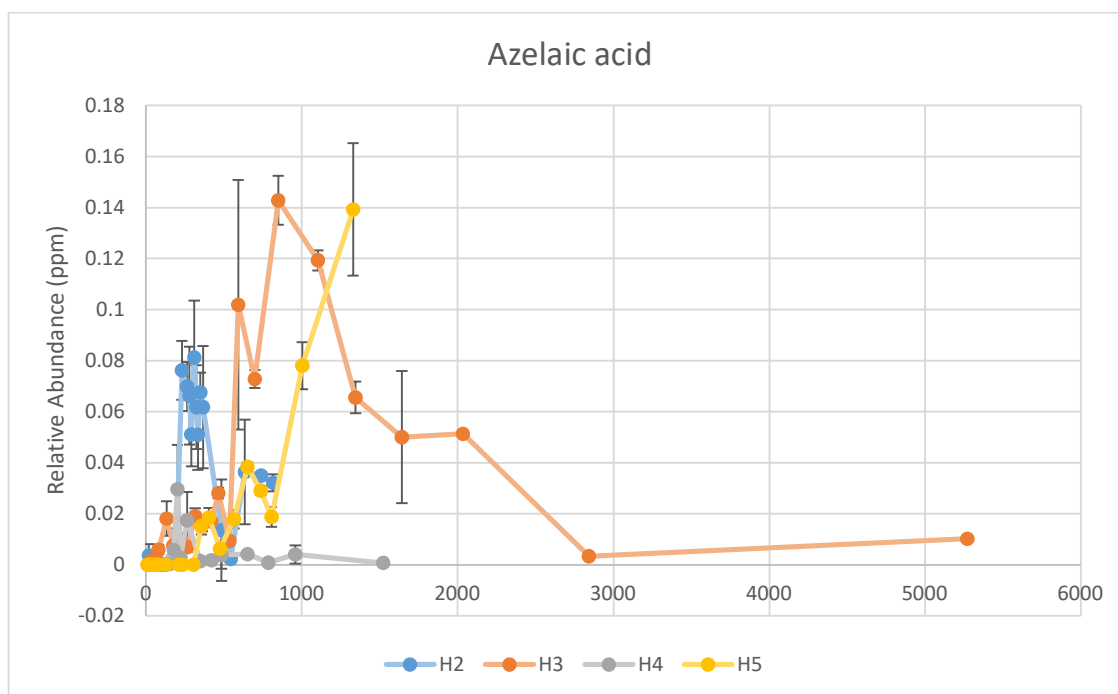


**Figure I-4:** Comparison of azelaic acid through decomposition period of H2, H3, H4 and H5. X-axis represents relative abundance in ppm. Y-axis represents accumulated degree days (ADD).

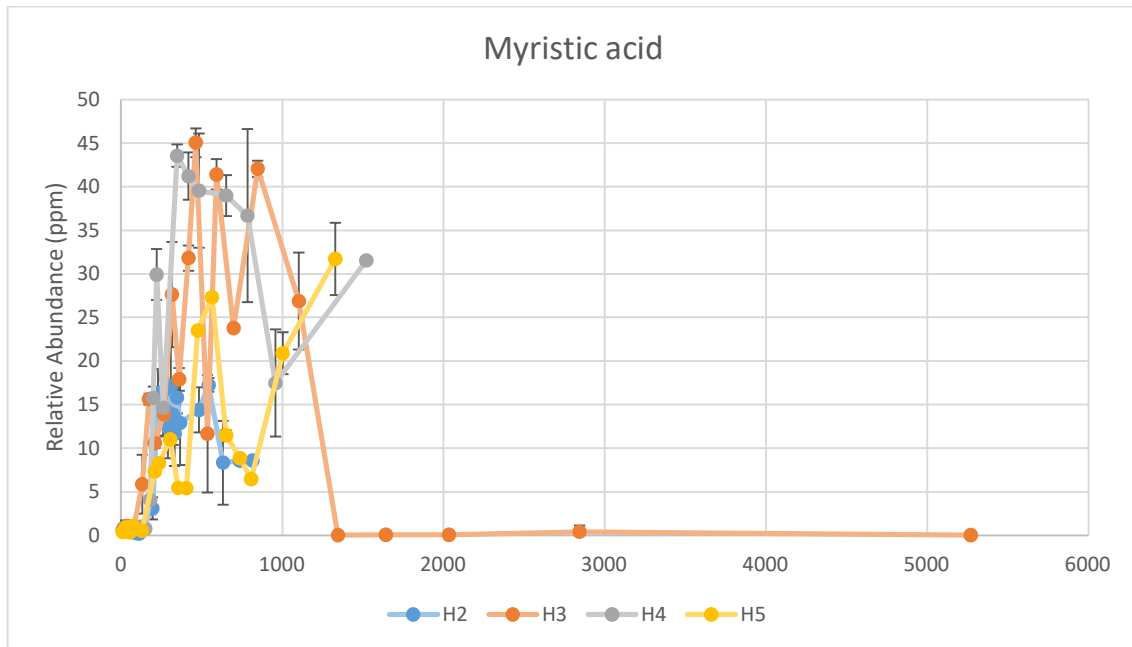


**Figure I-5:** Comparison of myristic acid through decomposition period of H2, H3, H4 and H5. X-axis represents relative abundance in ppm. Y-axis represents accumulated degree days (ADD).

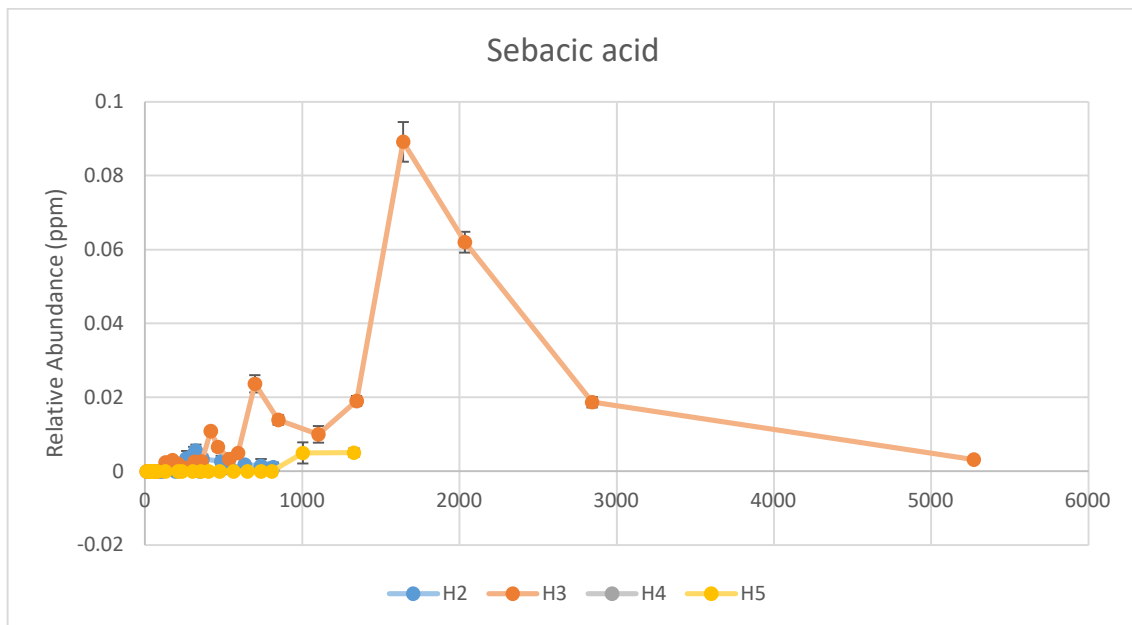


**Figure I-6:** Comparison of sebacic acid through decomposition period of H2, H3, H4 and H5. X-axis represents relative abundance in ppm. Y-axis represents accumulated degree days (ADD).



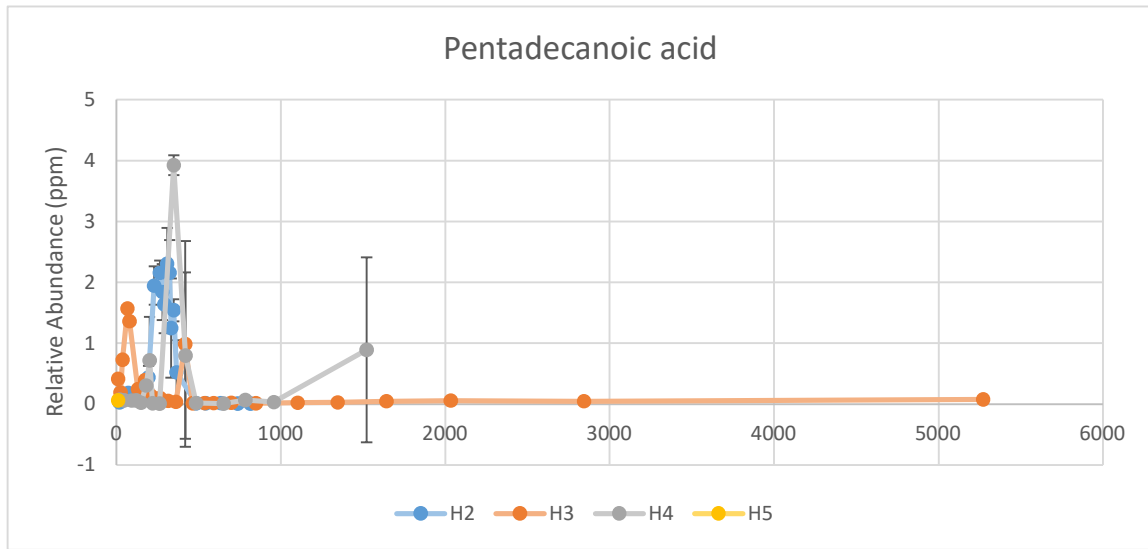


**Figure I-7:** Comparison of pentadecanoic acid through decomposition period of H2, H3, H4 and H5. X-axis represents relative abundance in ppm. Y-axis represents accumulated degree days (ADD).

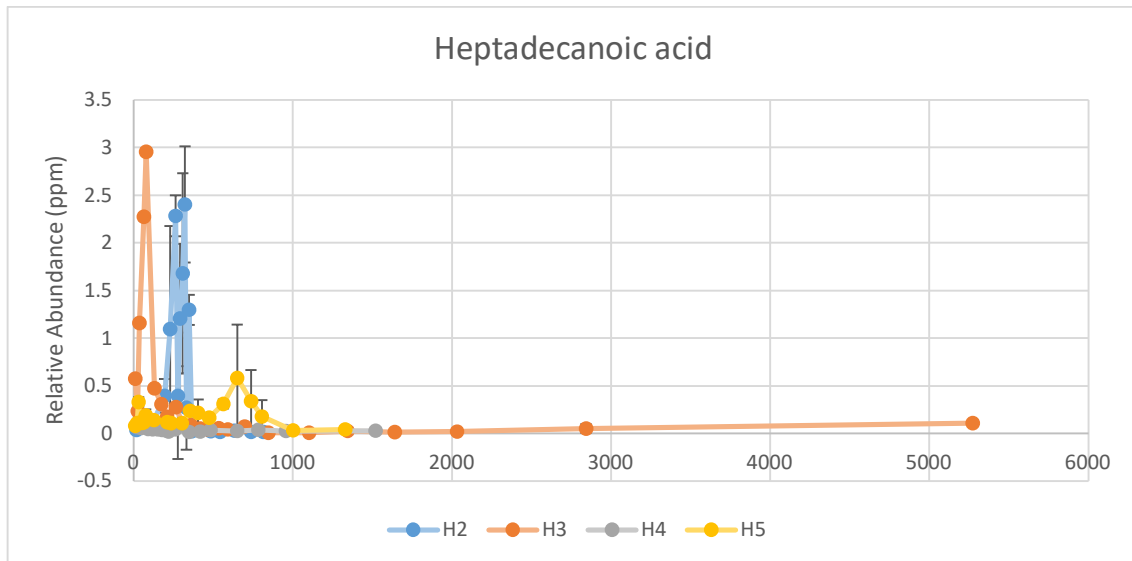


**Figure I-8:** Comparison of heptadecanoic acid through decomposition period of H2, H3, H4 and H5. X-axis represents relative abundance in ppm. Y-axis represents accumulated degree days (ADD).

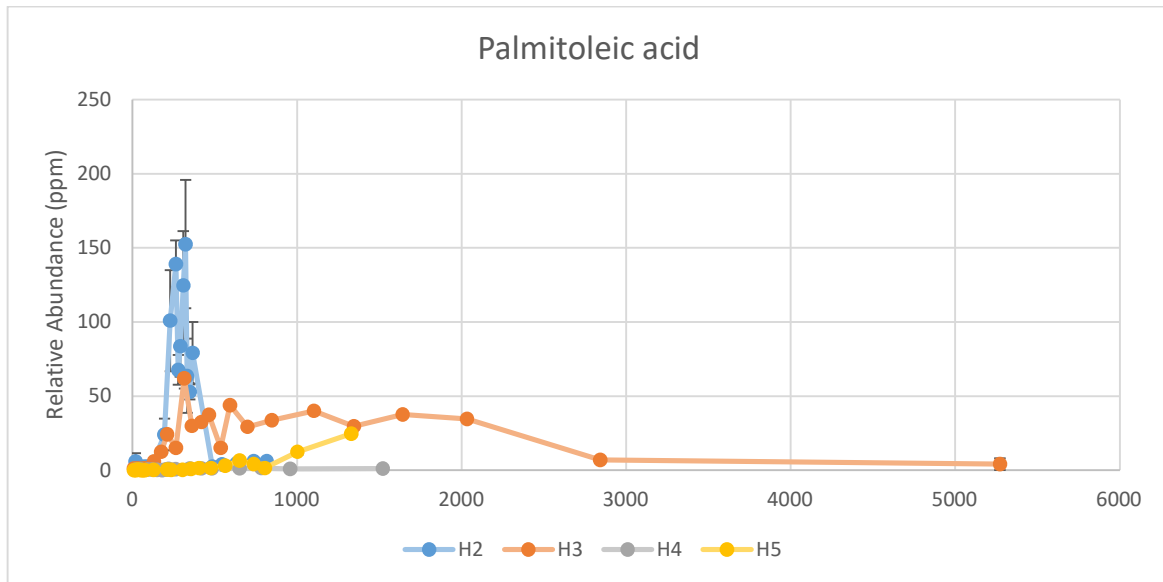


**Figure I-9:** Comparison of palmitoleic acid through decomposition period of H2, H3, H4 and H5. X-axis represents relative abundance in ppm. Y-axis represents accumulated degree days (ADD).

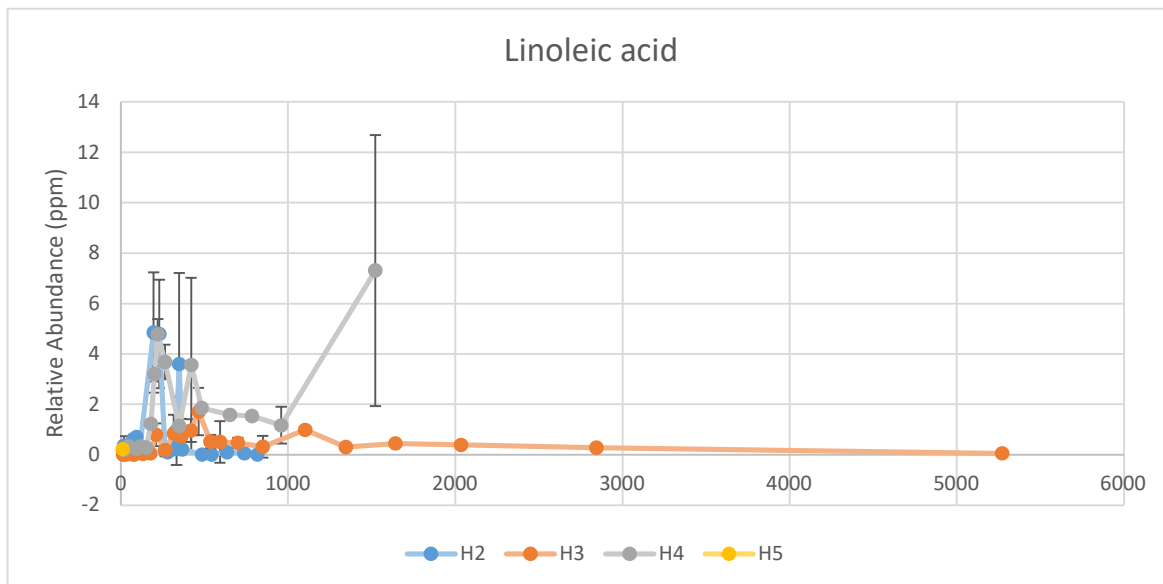


**Figure I-10:** Comparison of linoleic acid through decomposition period of H2, H3, H4 and H5. X-axis represents relative abundance in ppm. Y-axis represents accumulated degree days (ADD).

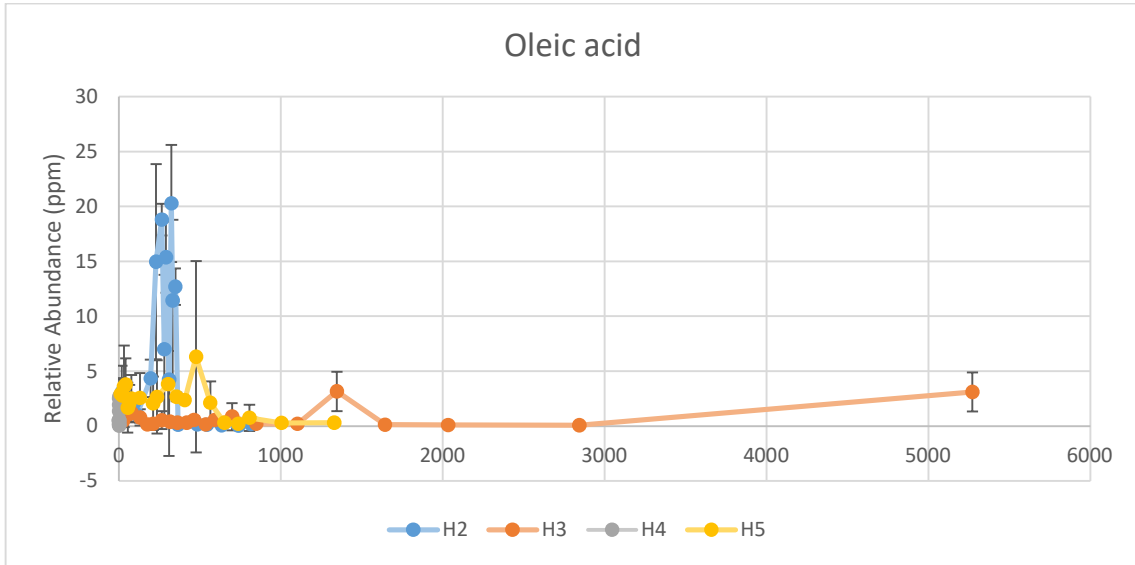


**Figure I-11:** Comparison of oleic acid through decomposition period of H2, H3, H4 and H5. X-axis represents relative abundance in ppm. Y-axis represents accumulated degree days (ADD).

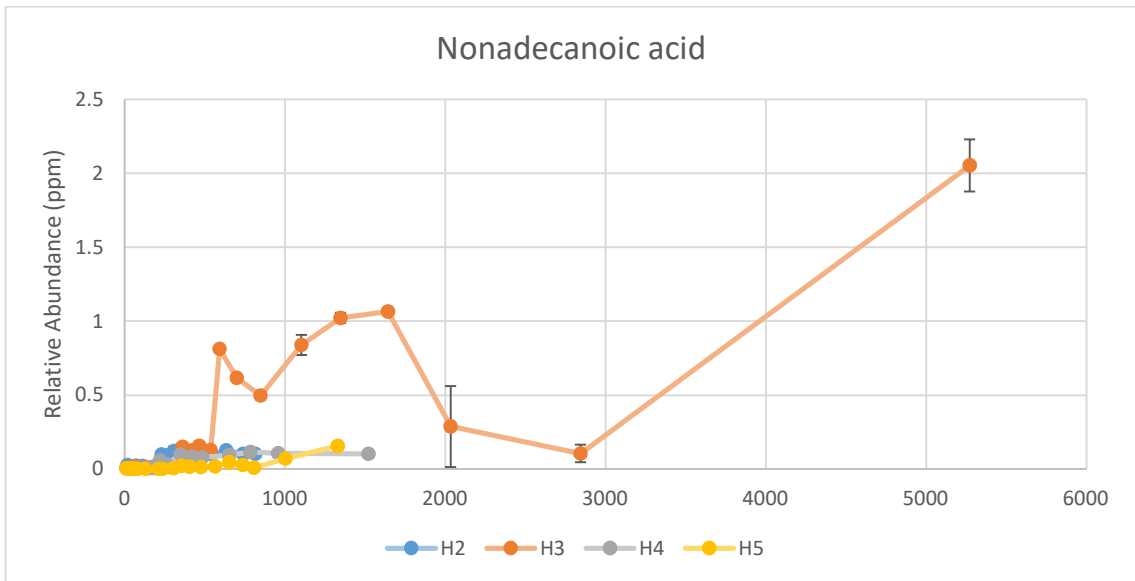


**Figure I-12:** Comparison of nonadecanoic acid through decomposition period of H2, H3, H4 and H5. X-axis represents relative abundance in ppm. Y-axis represents accumulated degree days (ADD).

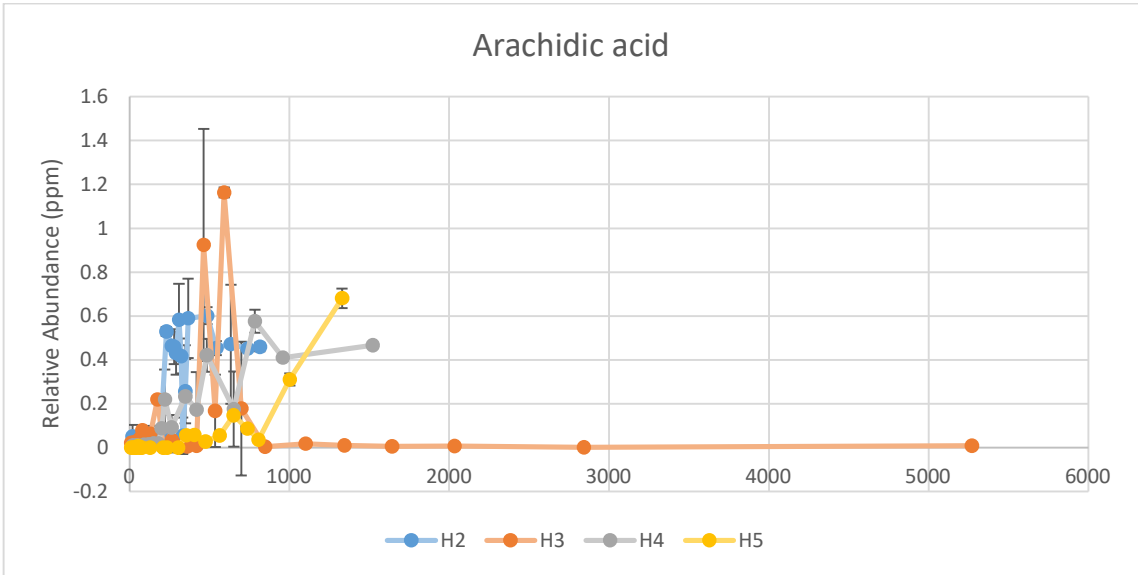


**Figure I-13:** Comparison of arachidic acid through decomposition period of H2, H3, H4 and H5. X-axis represents relative abundance in ppm. Y-axis represents accumulated degree days (ADD).

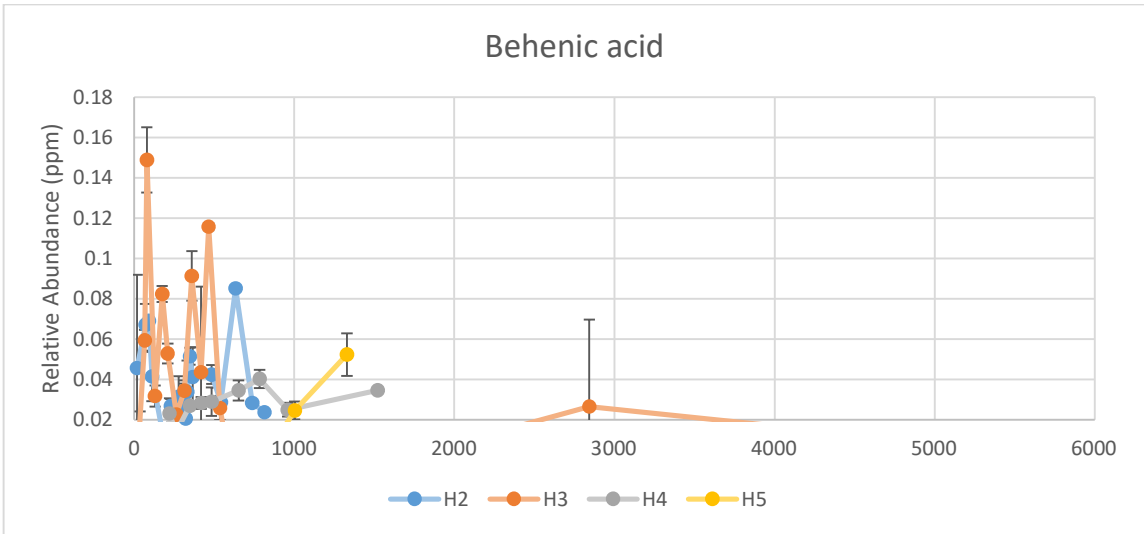


**Figure I-14:** Comparison of behenic acid through decomposition period of H2, H3, H4 and H5. X-axis represents relative abundance in ppm. Y-axis represents accumulated degree days (ADD).

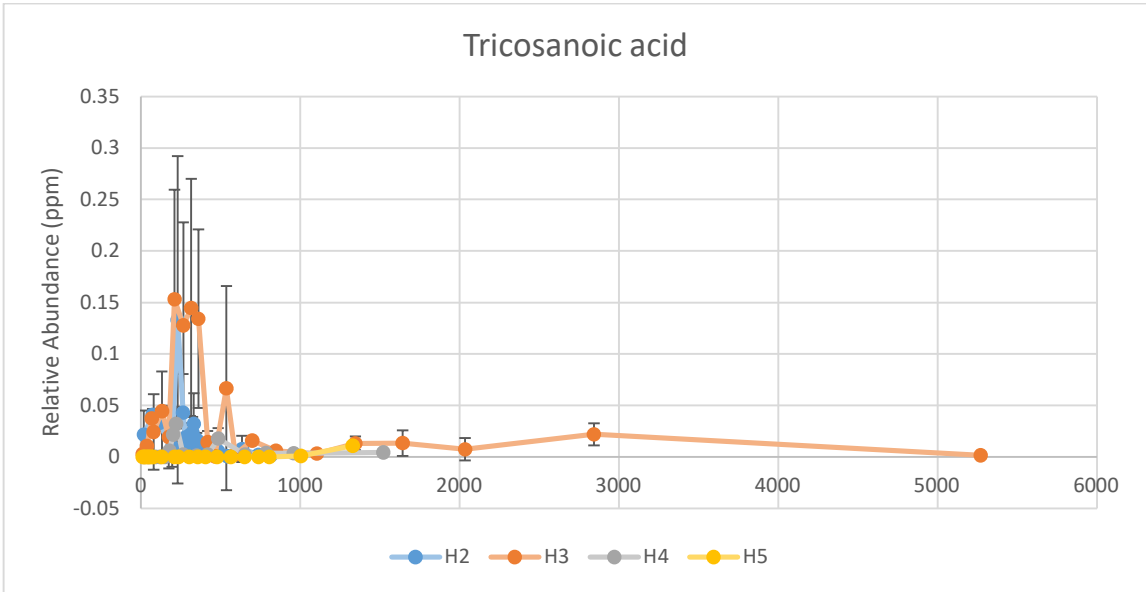


**Figure I-15:** Comparison of tricosanoic acid through decomposition period of H2, H3, H4 and H5. X-axis represents relative abundance in ppm. Y-axis represents accumulated degree days (ADD).

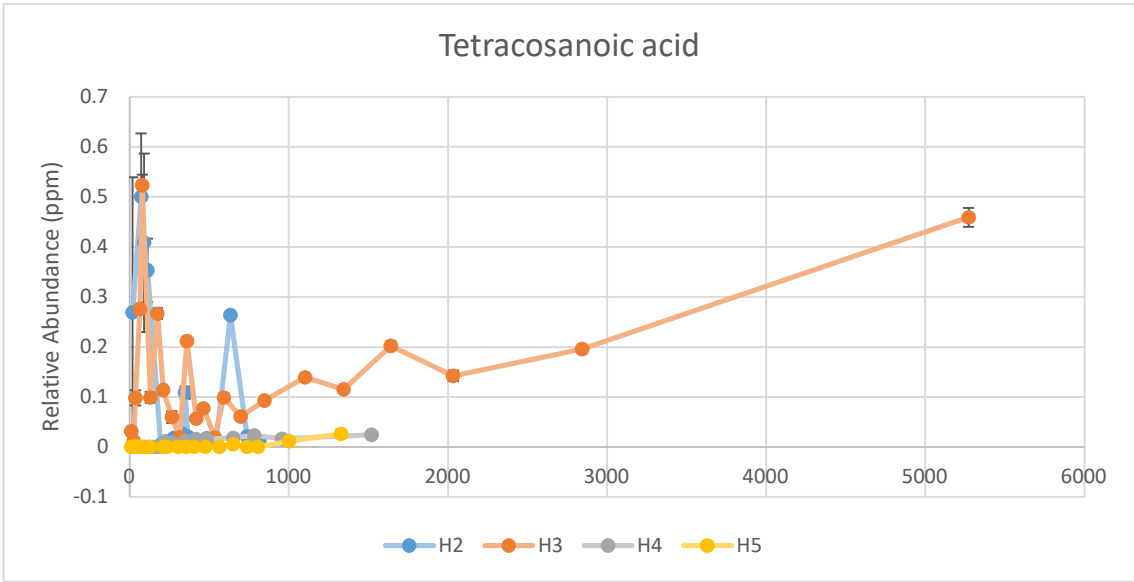


**Figure I-16:** Comparison of tetracosanoic acid through decomposition period of H2, H3, H4 and H5. X-axis represents relative abundance in ppm. Y-axis represents accumulated degree days (ADD).

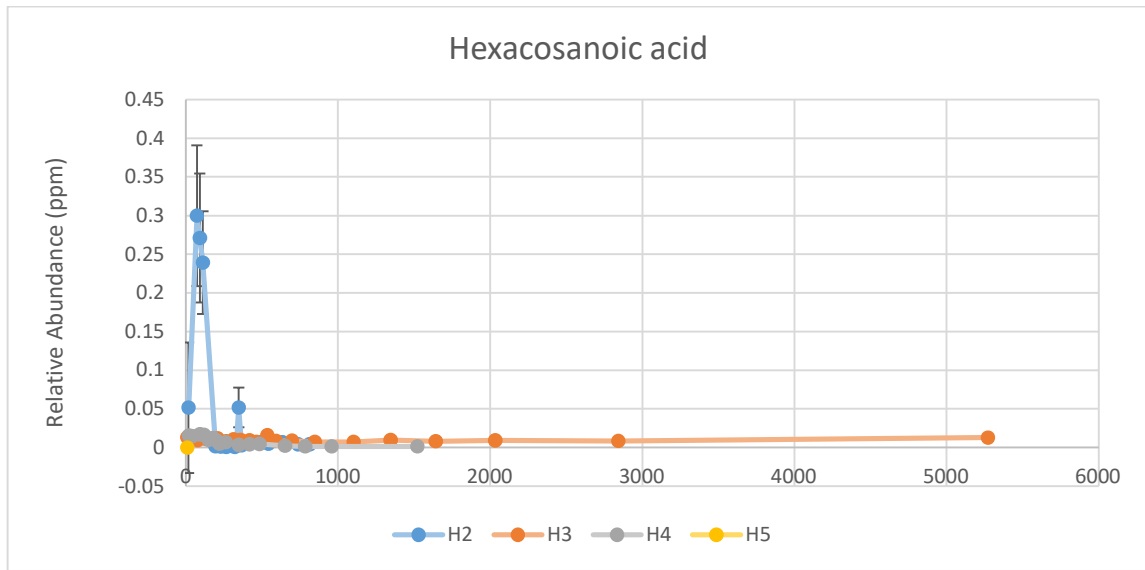


**Figure I-17:** Comparison of hexacosanoic acid through decomposition period of H2, H3, H4 and H5. X-axis represents relative abundance in ppm. Y-axis represents accumulated degree days (ADD).

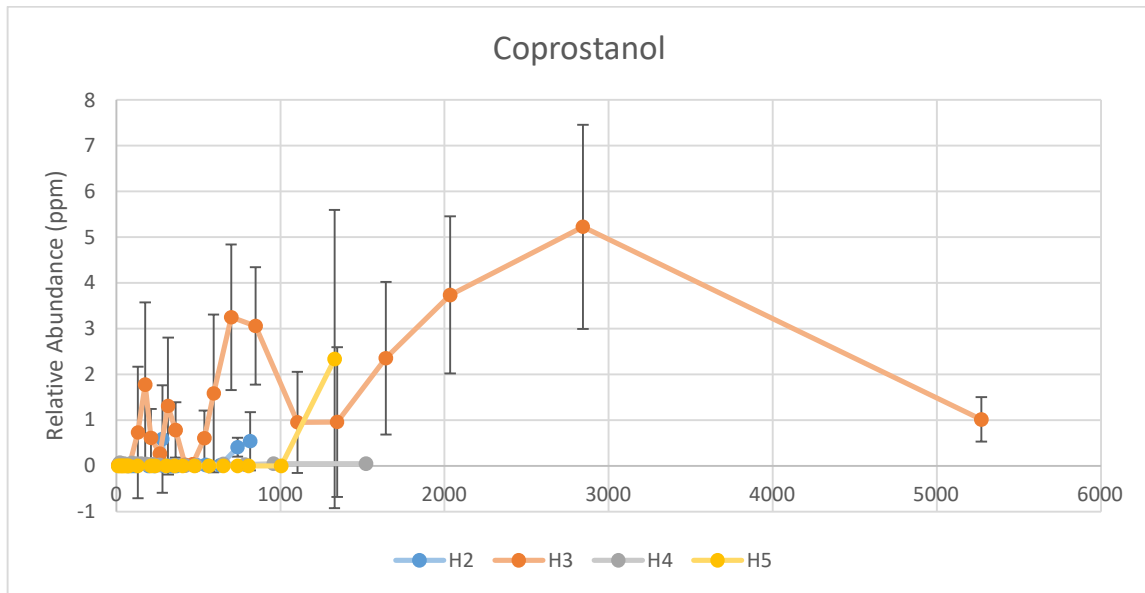


**Figure I-18:** Comparison of coprostanol through decomposition period of H2, H3, H4 and H5. X-axis represents relative abundance in ppm. Y-axis represents accumulated degree days (ADD).

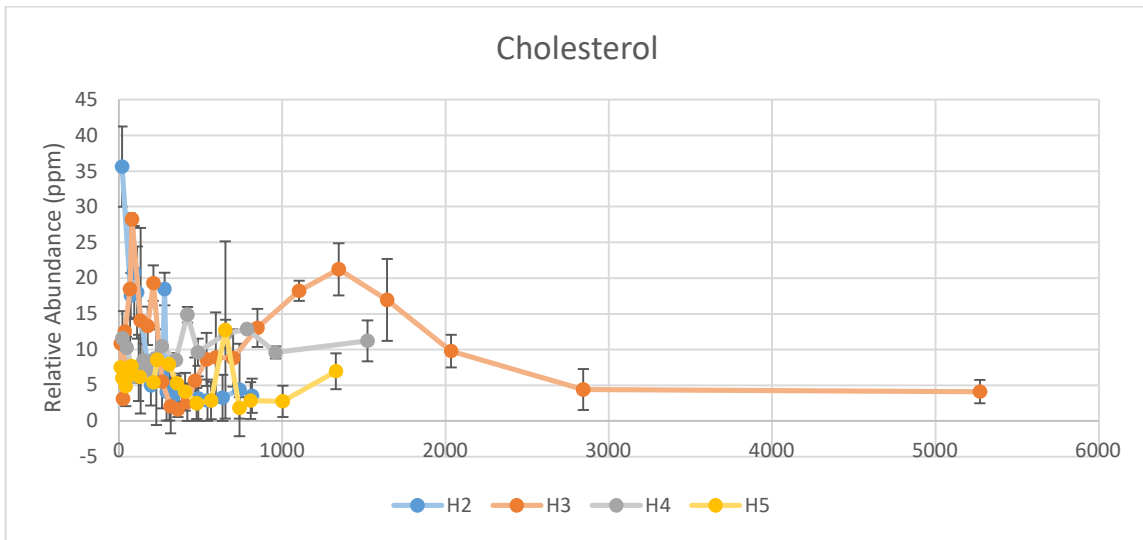


**Figure I-19:** Comparison of cholesterol through decomposition period of H2, H3, H4 and H5. X-axis represents relative abundance in ppm. Y-axis represents accumulated degree days (ADD).

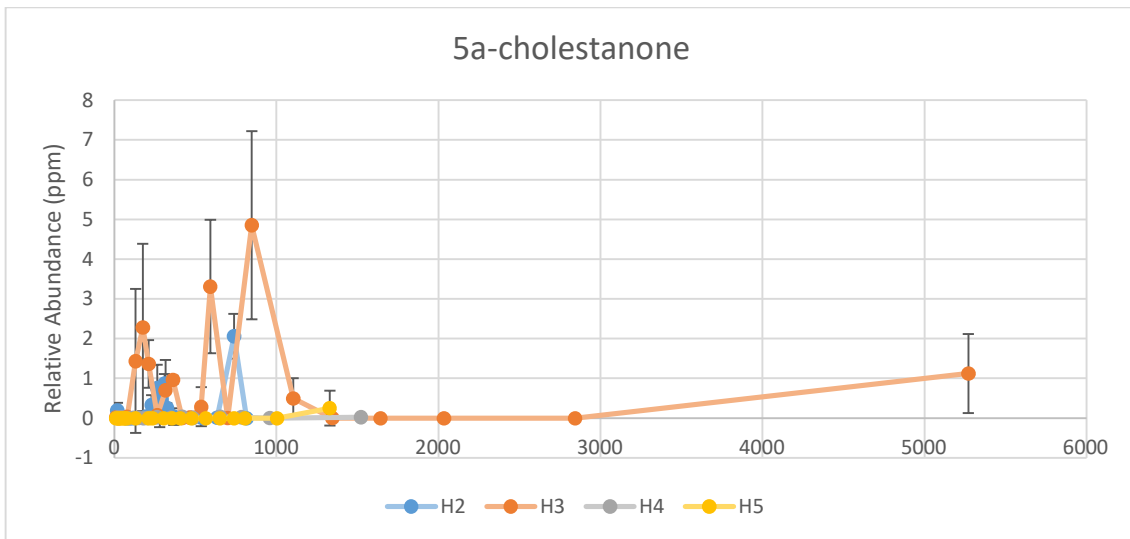


**Figure I-20:** Comparison of 5a-cholestanone through decomposition period of H2, H3, H4 and H5. X-axis represents relative abundance in ppm. Y-axis represents accumulated degree days (ADD).

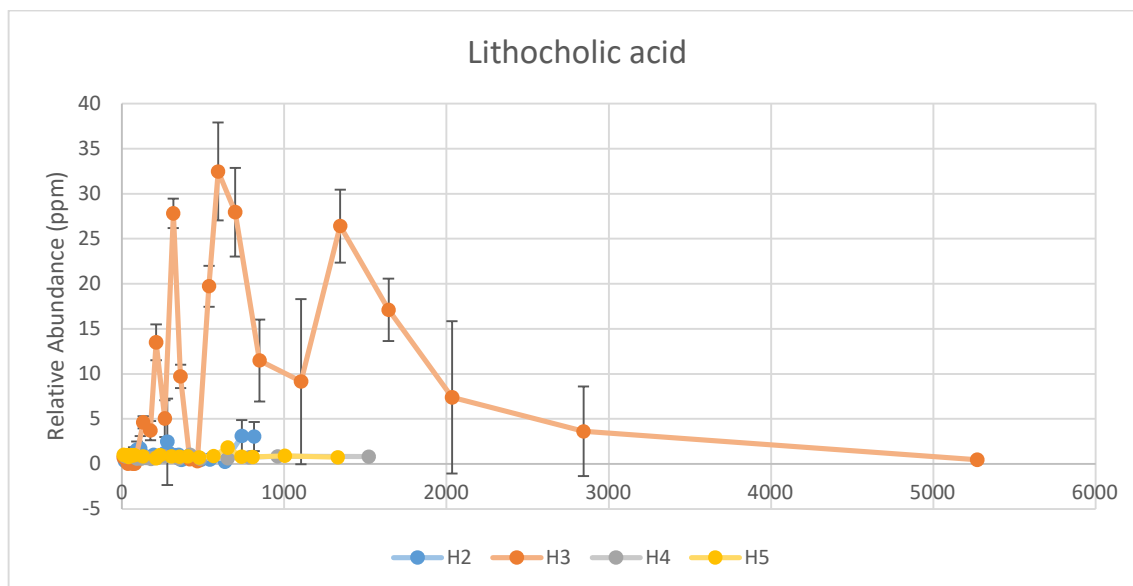


**Figure I-21:** Comparison of lithocholic acid through decomposition period of H2, H3, H4 and H5. X-axis represents relative abundance in ppm. Y-axis represents accumulated degree days (ADD).

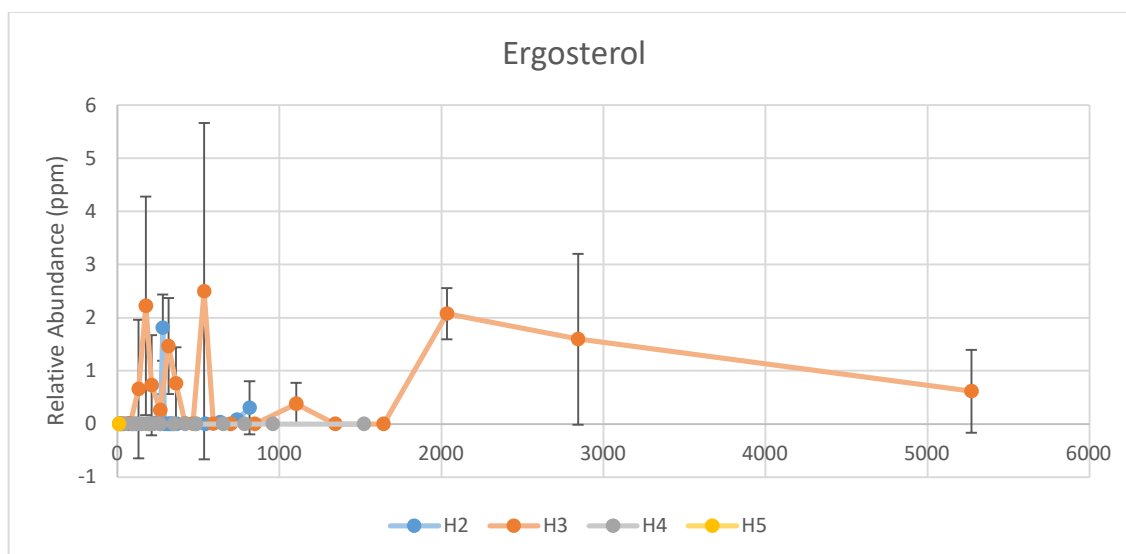


**Figure I-22:** Comparison of ergosterol through decomposition period of H2, H3, H4 and H5. X-axis represents relative abundance in ppm. Y-axis represents accumulated degree days (ADD).



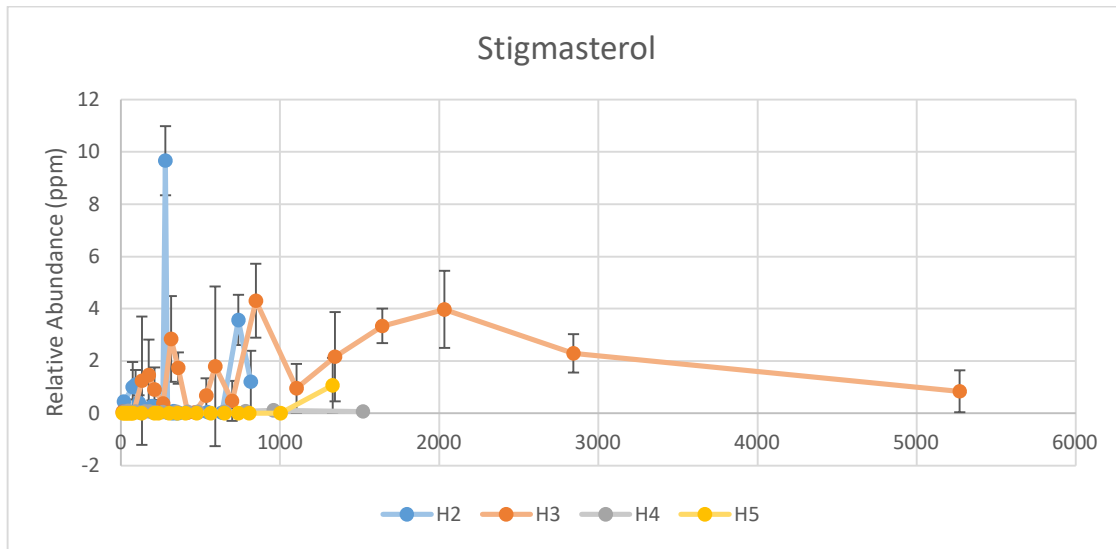


**Figure I-23:** Comparison of stigmasterol through decomposition period of H2, H3, H4 and H5. X-axis represents relative abundance in ppm. Y-axis represents accumulated degree days (ADD).

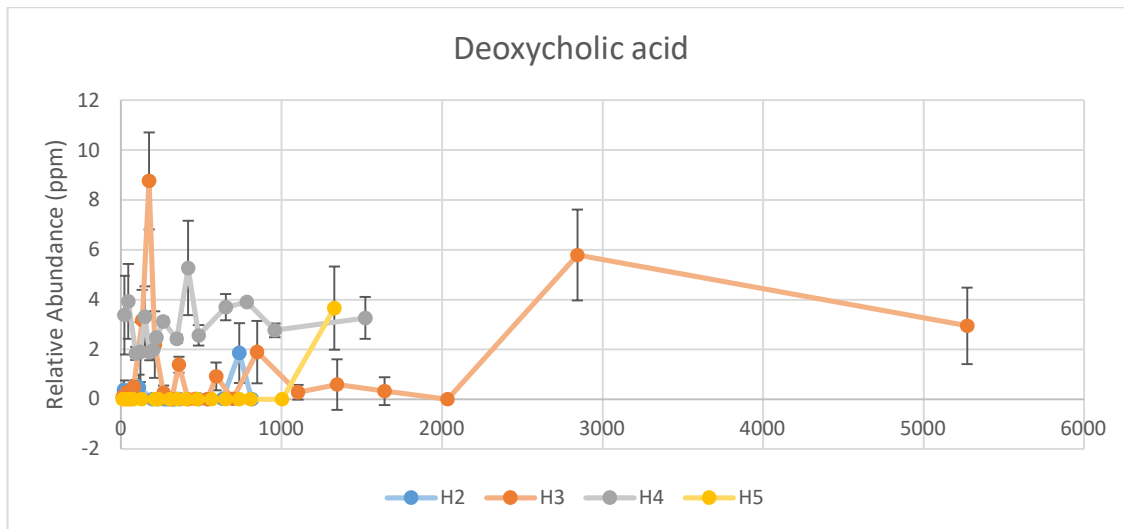


**Figure I-24:** Comparison of deoxycholic acid through decomposition period of H2, H3, H4 and H5. X-axis represents relative abundance in ppm. Y-axis represents accumulated degree days (ADD).

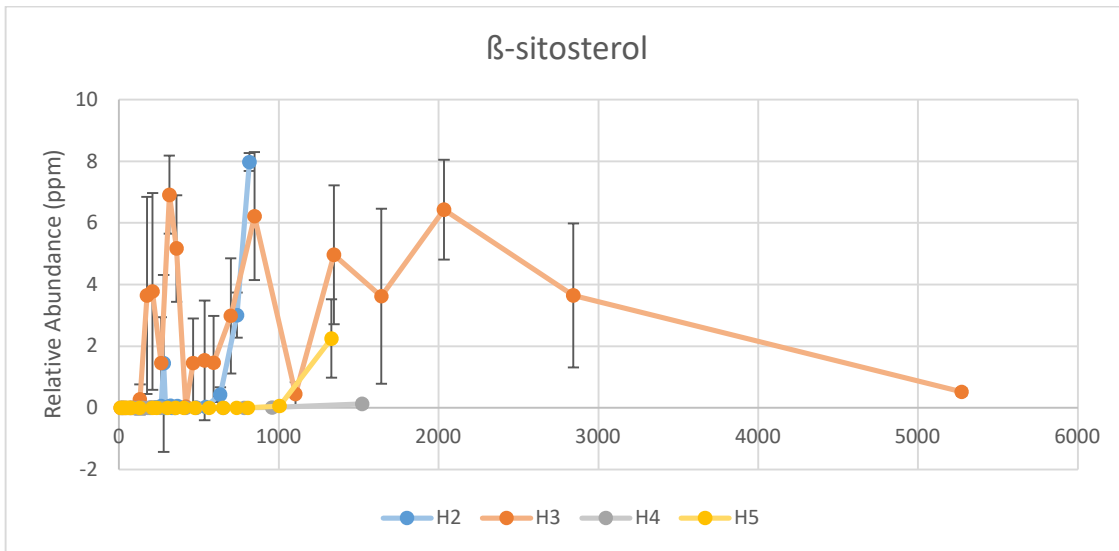


**Figure I-26:** Comparison of β-sitosterol through decomposition period of H2, H3, H4 and H5. X-axis represents relative abundance in ppm. Y-axis represents accumulated degree days (ADD).

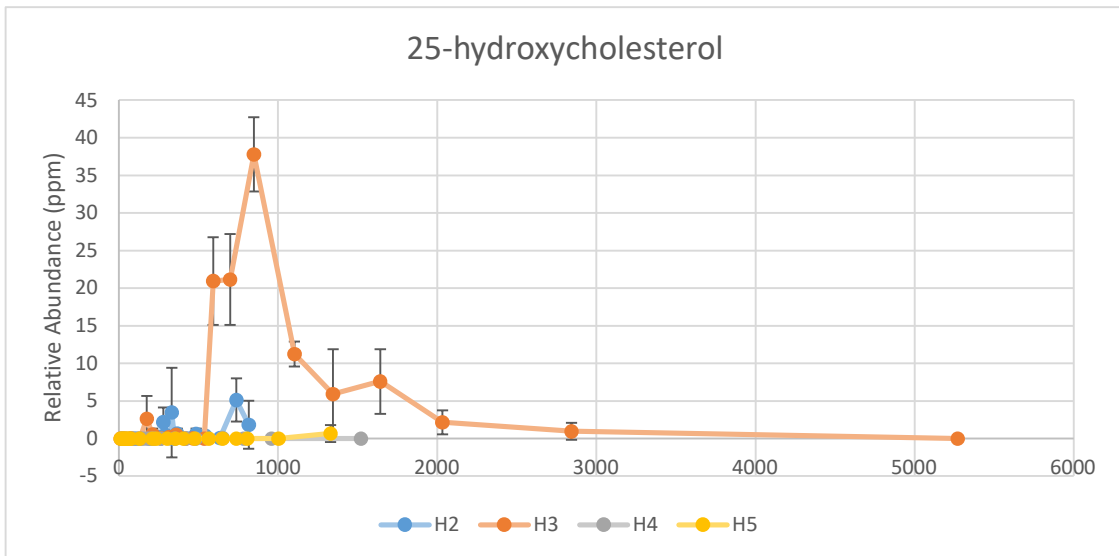


**Figure I-27:** Comparison of 25-hydroxycholesterol through decomposition period of H2, H3, H4 and H5. X-axis represents relative abundance in ppm. Y-axis represents accumulated degree days (ADD).

APPENDIX J- INDIVIDUAL COMPOUND TREND COMPARISON  
WITHIN THE TISSUE OF ALL HUMAN BODIES

Comparison of individual lipid trends within the tissue matrix of all humans (human 2= H2, human 3= H3, human 4= H4 and human 5= H5). The x-axis for all graphs represents relative abundance in parts per million (ppm), y-axis represents accumulated degree days

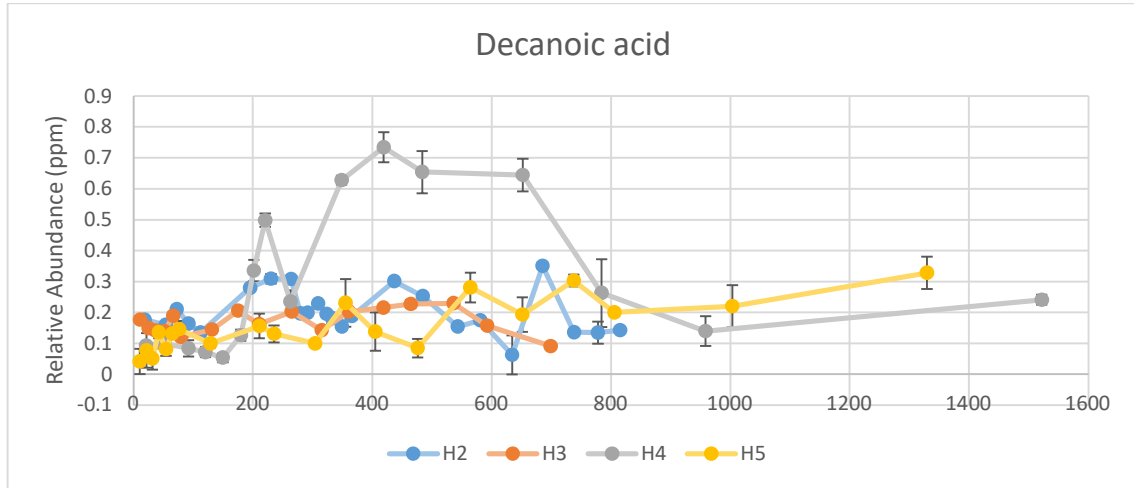


**Figure J-1:** Comparison of decanoic acid through decomposition period of H2, H3, H4 and H5. X-axis represents relative abundance in ppm. Y-axis represents accumulated degree days (ADD).

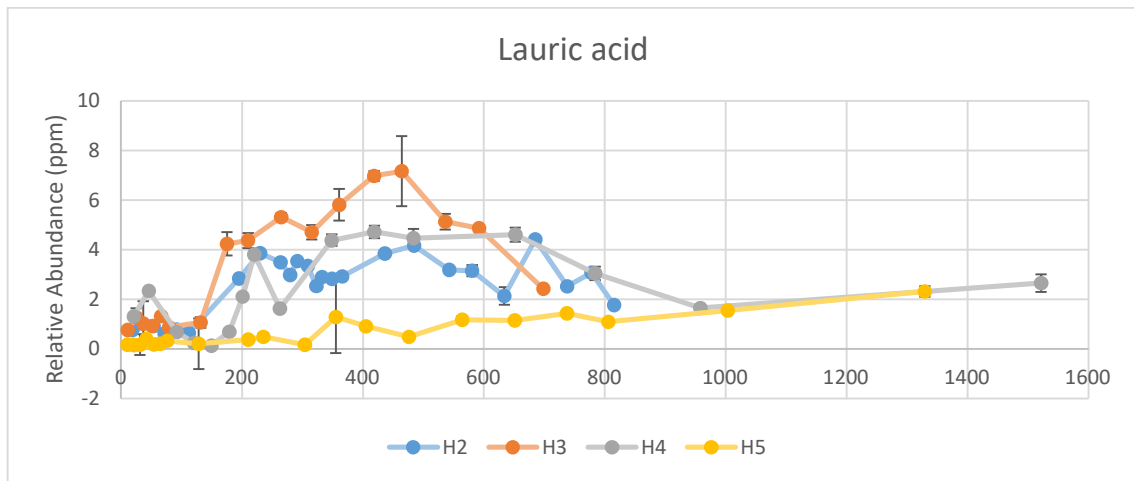


**Figure J-2:** Comparison of lauric acid through decomposition period of H2, H3, H4 and H5. X-axis represents relative abundance in ppm. Y-axis represents accumulated degree days (ADD).

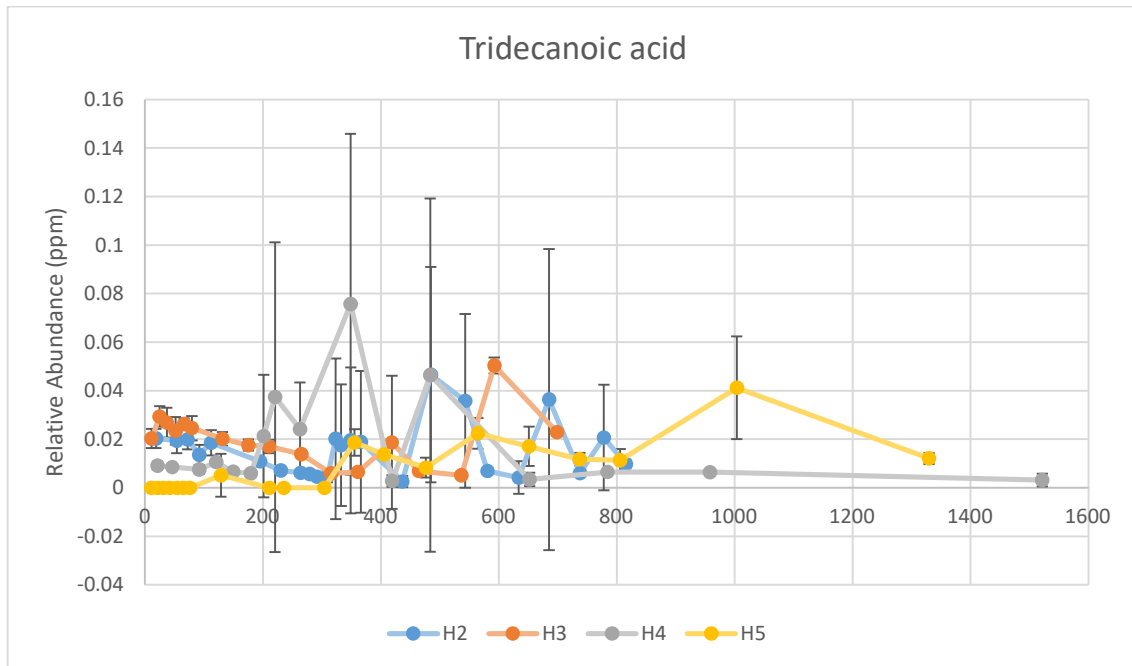


**Figure J-3:** Comparison of tridecanoic acid through decomposition period of H2, H3, H4 and H5. X-axis represents relative abundance in ppm. Y-axis represents accumulated degree days (ADD).

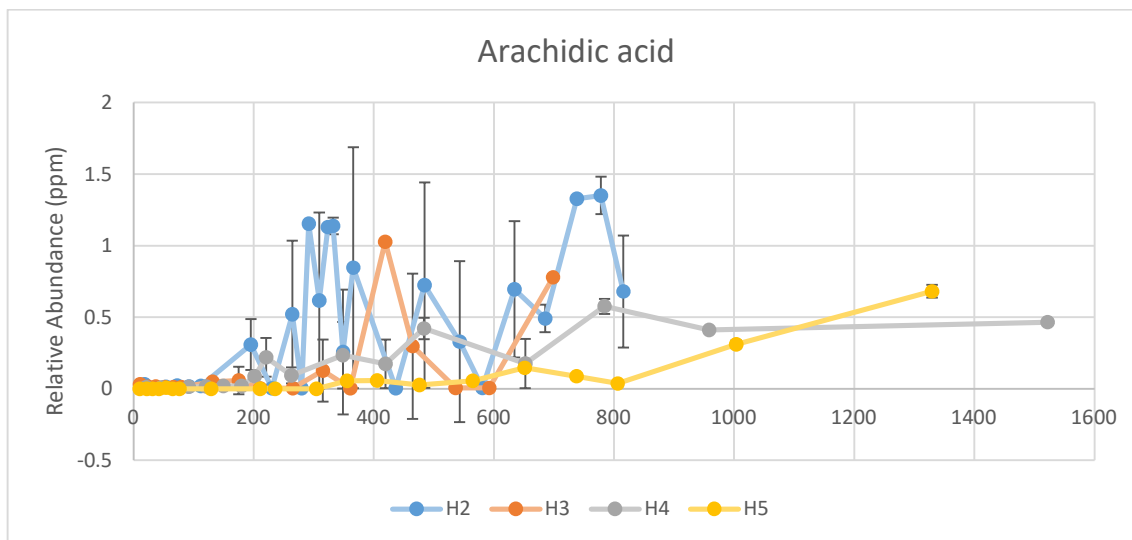


**Figure J-4:** Comparison of azelaic acid through decomposition period of H2, H3, H4 and H5. X-axis represents relative abundance in ppm. Y-axis represents accumulated degree days (ADD).

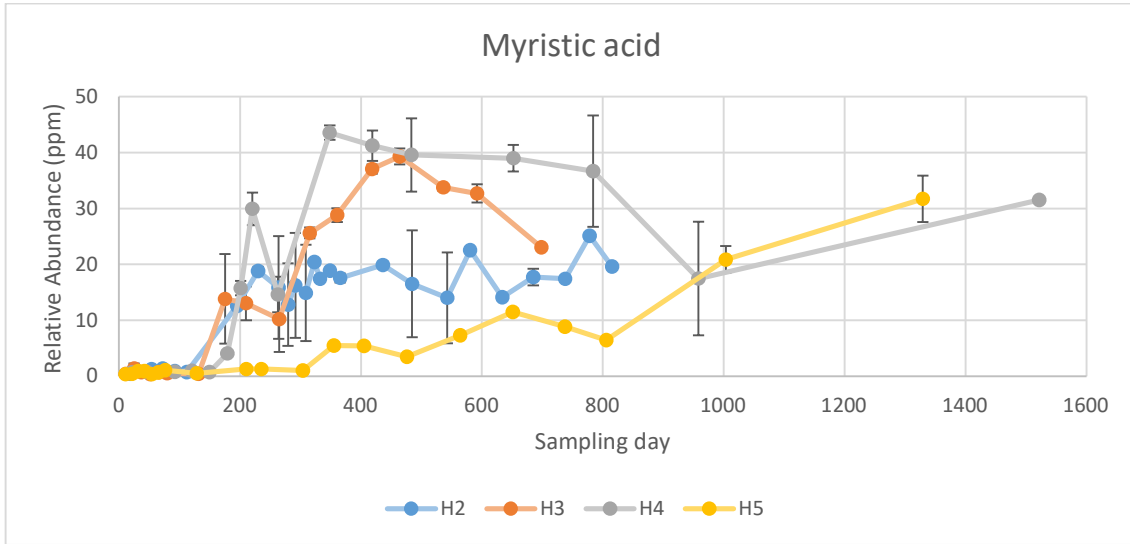


**Figure J-5:** Comparison of myristic acid through decomposition period of H2, H3, H4 and H5. X-axis represents relative abundance in ppm. Y-axis represents accumulated degree days (ADD).

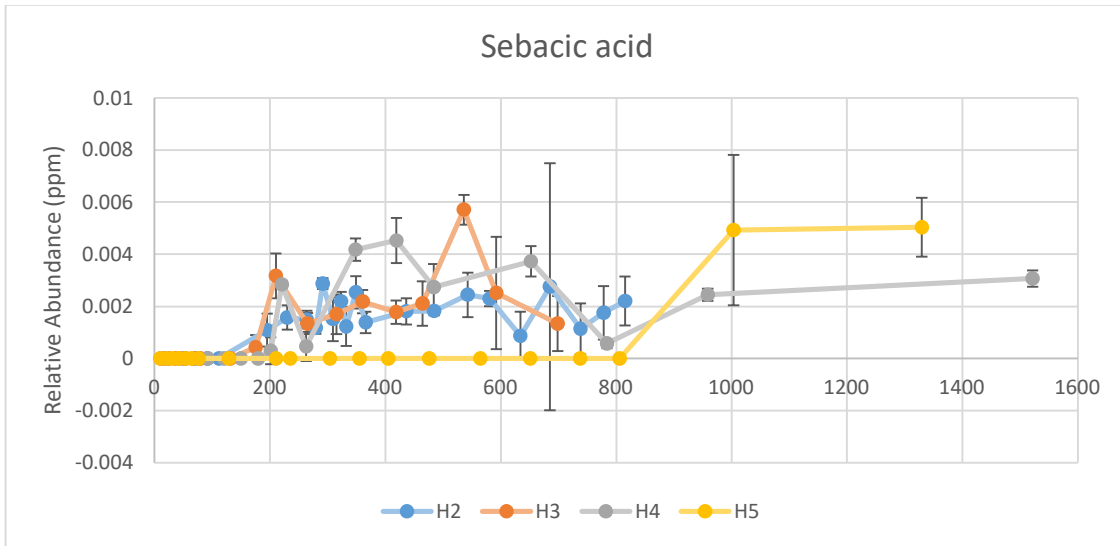


**Figure J-6:** Comparison of sebacic acid through decomposition period of H2, H3, H4 and H5. X-axis represents relative abundance in ppm. Y-axis represents accumulated degree days (ADD).

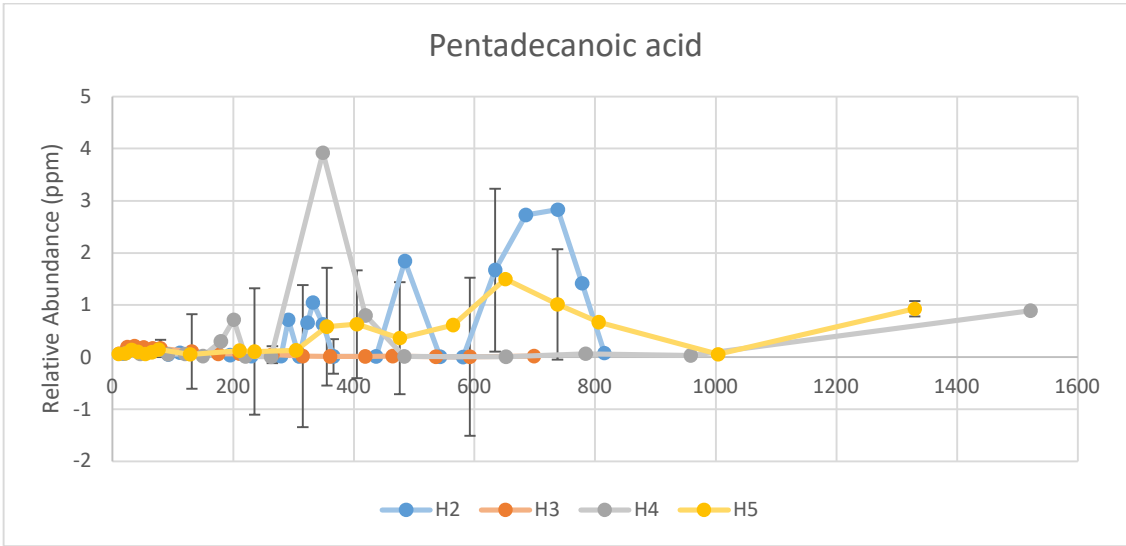


**Figure J-7:** Comparison of pentadecanoic acid through decomposition period of H2, H3, H4 and H5. X-axis represents relative abundance in ppm. Y-axis represents accumulated degree days (ADD).

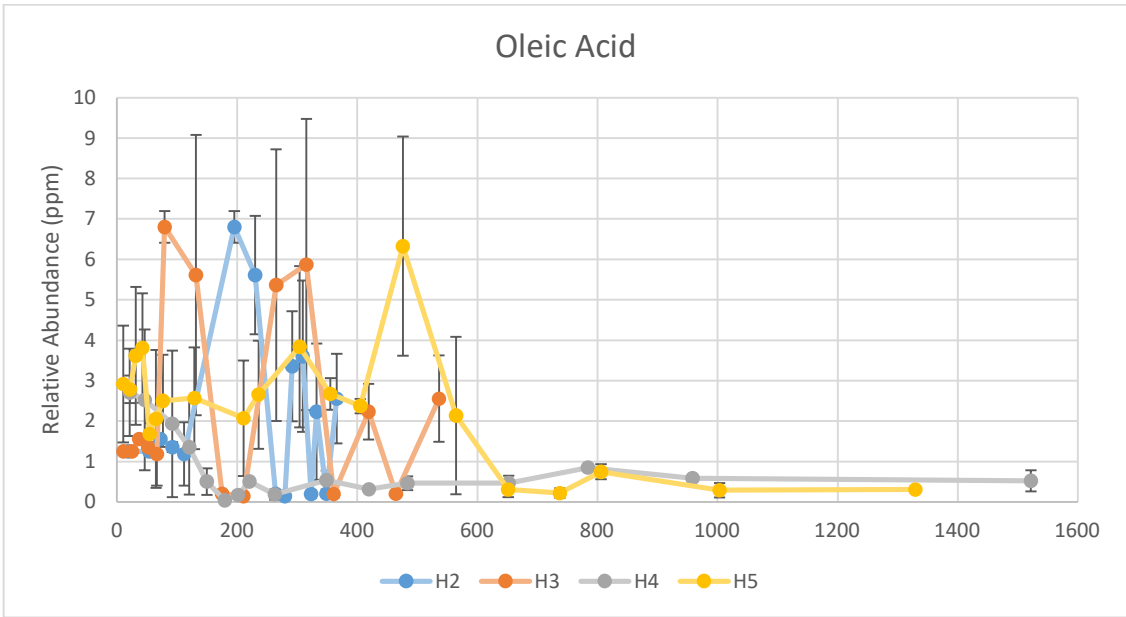


**Figure J-8:** Comparison of oleic acid through decomposition period of H2, H3, H4 and H5. X-axis represents relative abundance in ppm. Y-axis represents accumulated degree days (ADD).

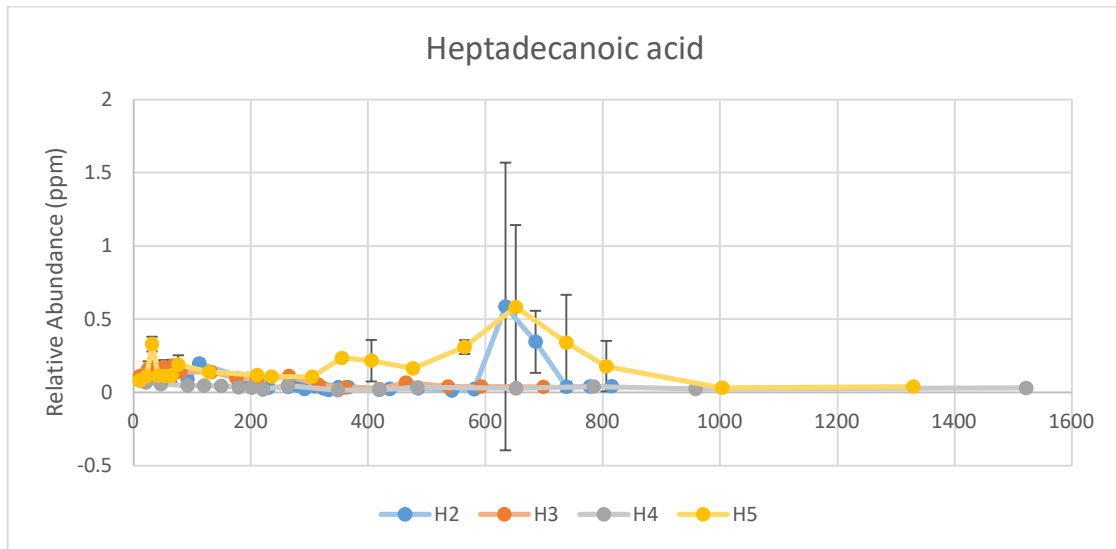


**Figure J-9:** Comparison of heptadecanoic acid through decomposition period of H2, H3, H4 and H5. X-axis represents relative abundance in ppm. Y-axis represents accumulated degree days (ADD).

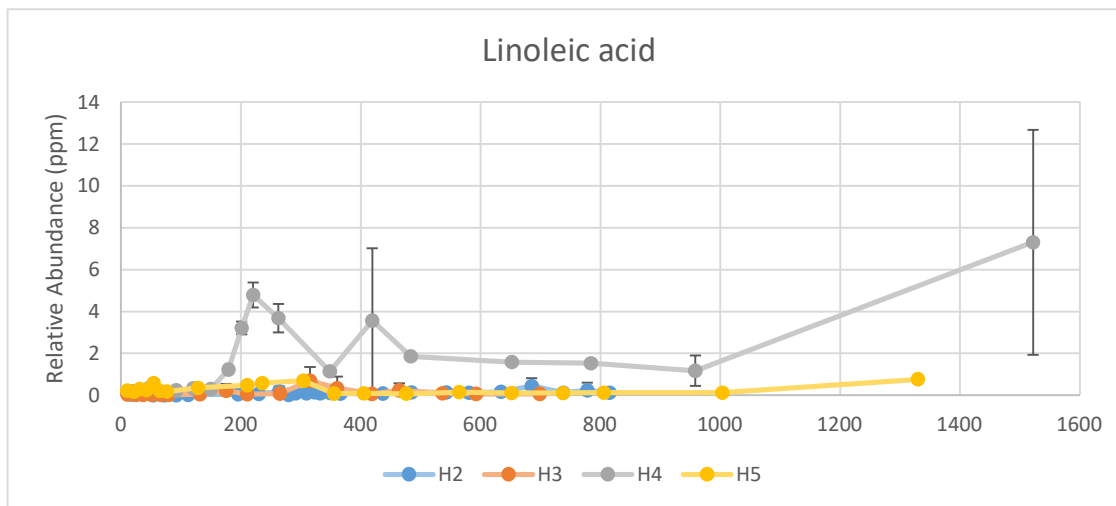


**Figure J-10:** Comparison of linoleic acid through decomposition period of H2, H3, H4 and H5. X-axis represents relative abundance in ppm. Y-axis represents accumulated degree days (ADD).



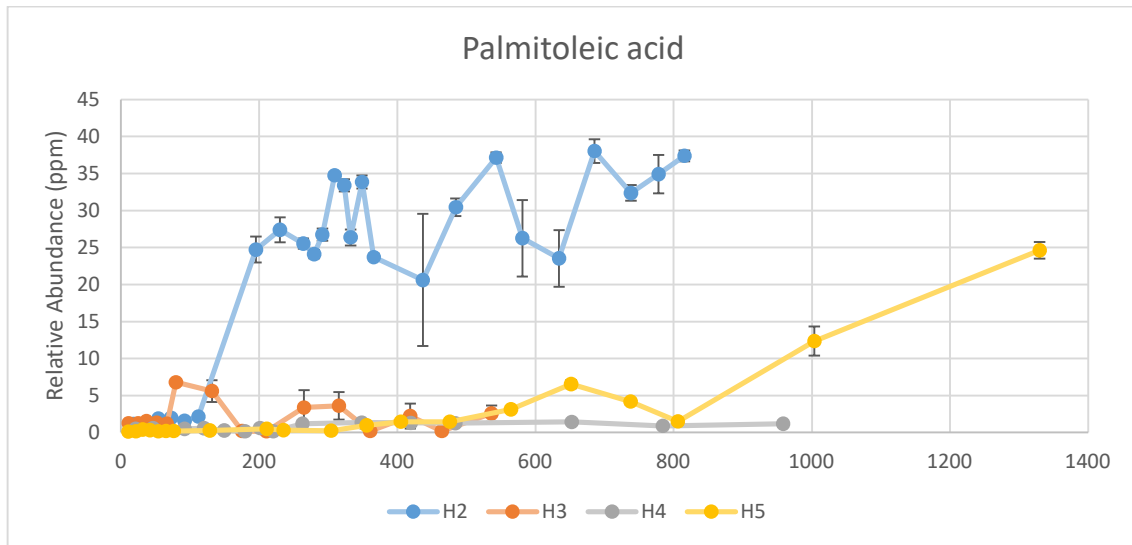


**Figure J-11:** Comparison of palmitoleic acid through decomposition period of H2, H3, H4 and H5. X-axis represents relative abundance in ppm. Y-axis represents accumulated degree days (ADD).

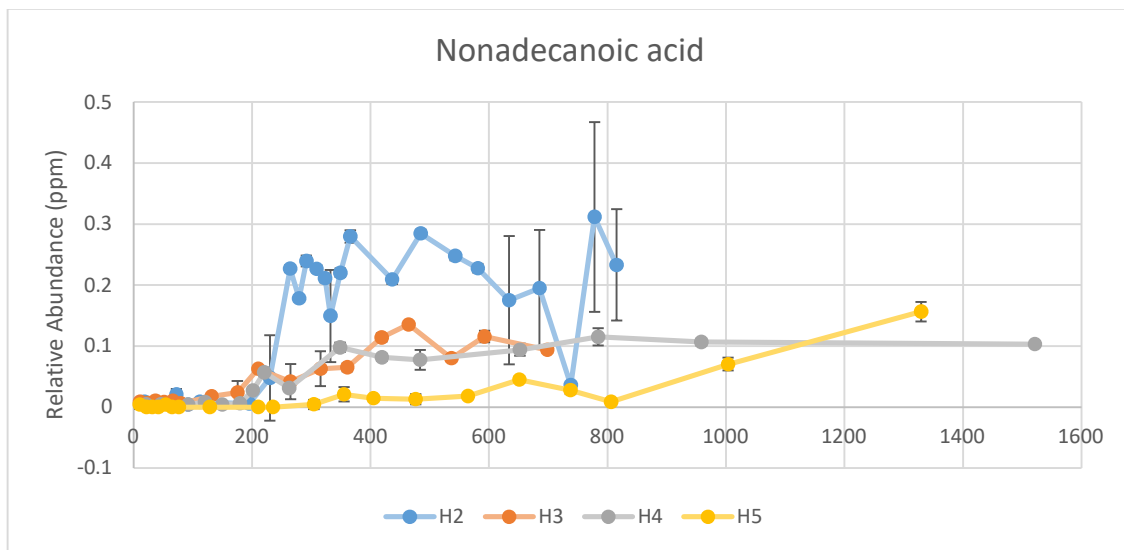


**Figure J-12:** Comparison of nonadecanoic acid through decomposition period of H2, H3, H4 and H5. X-axis represents relative abundance in ppm. Y-axis represents accumulated degree days (ADD).

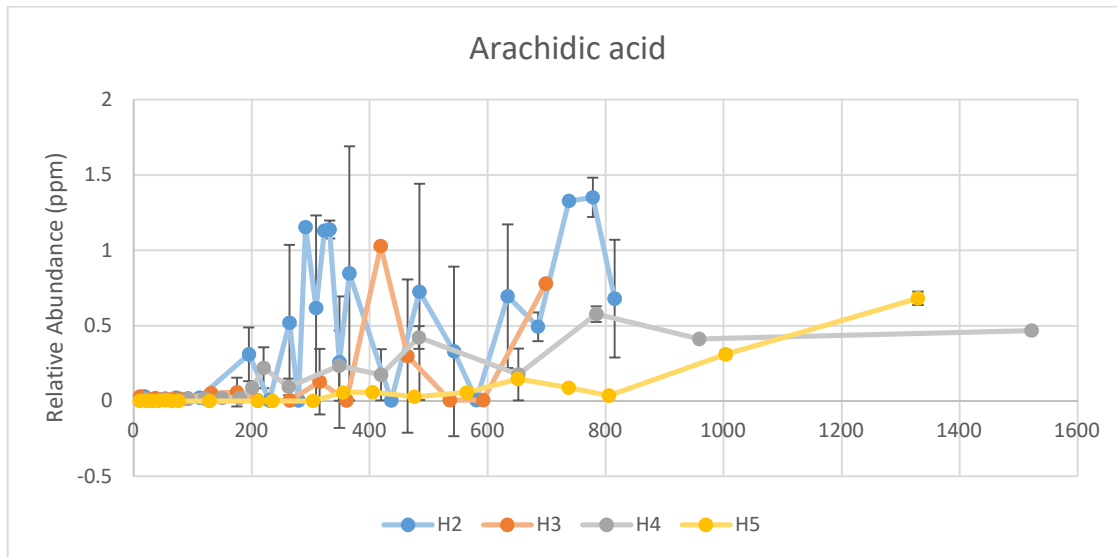


**Figure J-13:** Comparison of arachidic acid through decomposition period of H2, H3, H4 and H5. X-axis represents relative abundance in ppm. Y-axis represents accumulated degree days (ADD).

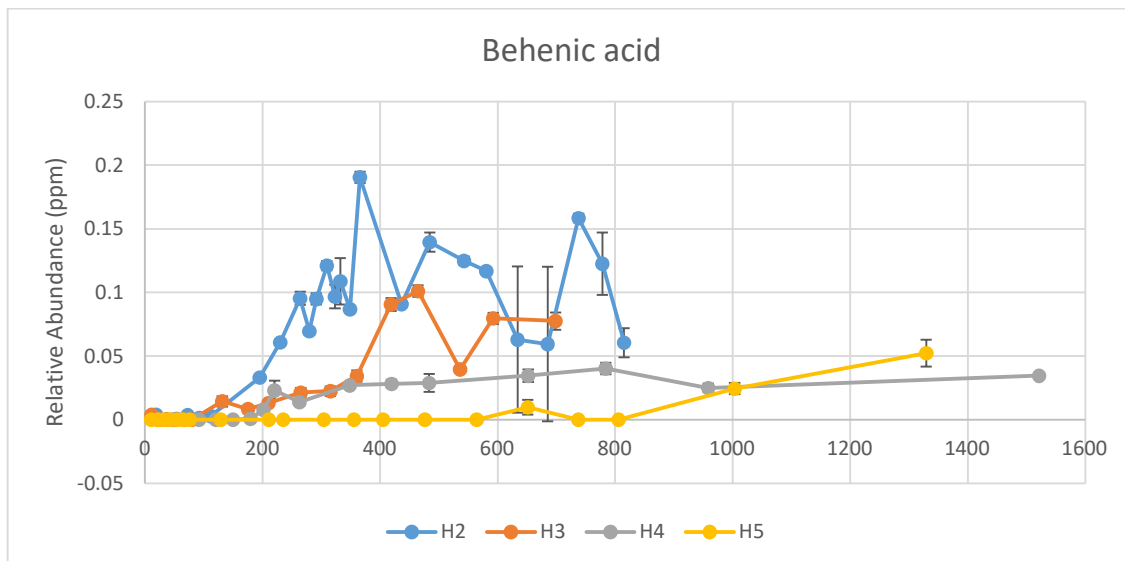


**Figure J-14:** Comparison of behenic acid through decomposition period of H2, H3, H4 and H5. X-axis represents relative abundance in ppm. Y-axis represents accumulated degree days (ADD).

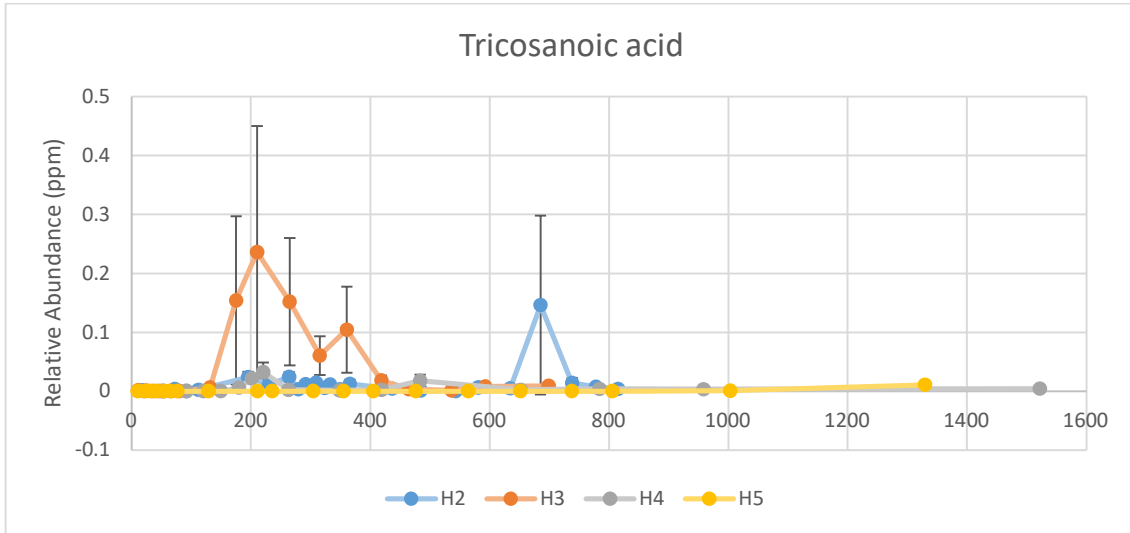


**Figure J-15:** Comparison of tricosanoic acid through decomposition period of H2, H3, H4 and H5. X-axis represents relative abundance in ppm. Y-axis represents accumulated degree days (ADD).

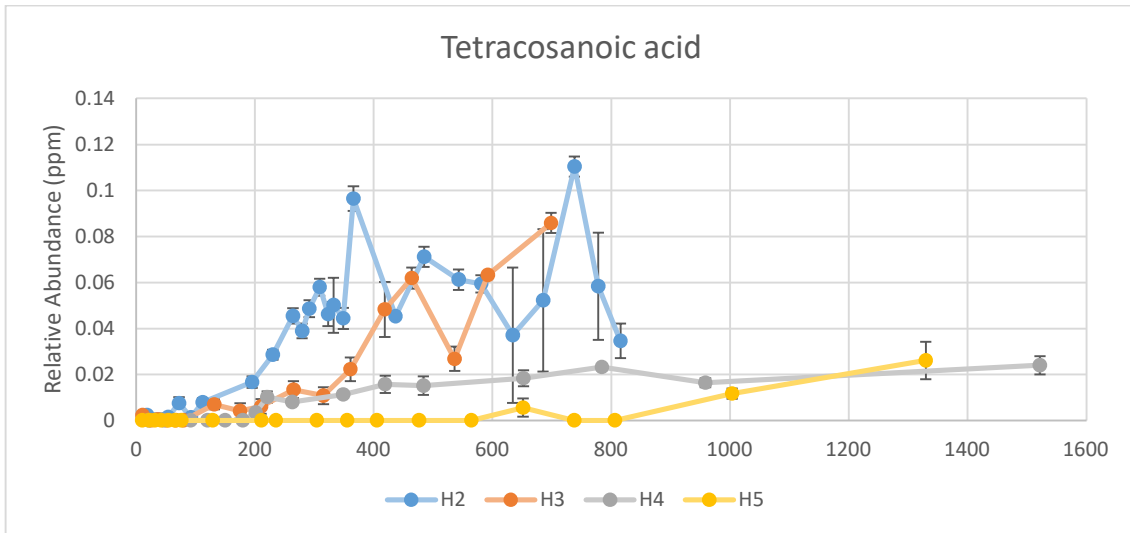


**Figure J-16:** Comparison of tetracosanoic acid through decomposition period of H2, H3, H4 and H5. X-axis represents relative abundance in ppm. Y-axis represents accumulated degree days (ADD).

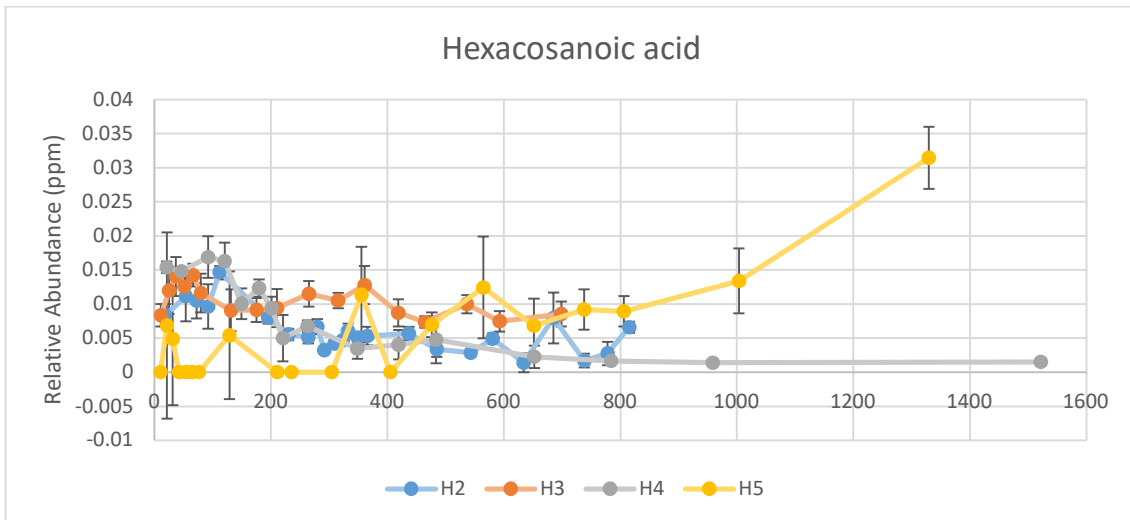


**Figure J-17:** Comparison of hexacosanoic acid through decomposition period of H2, H3, H4 and H5. X-axis represents relative abundance in ppm. Y-axis represents accumulated degree days (ADD).

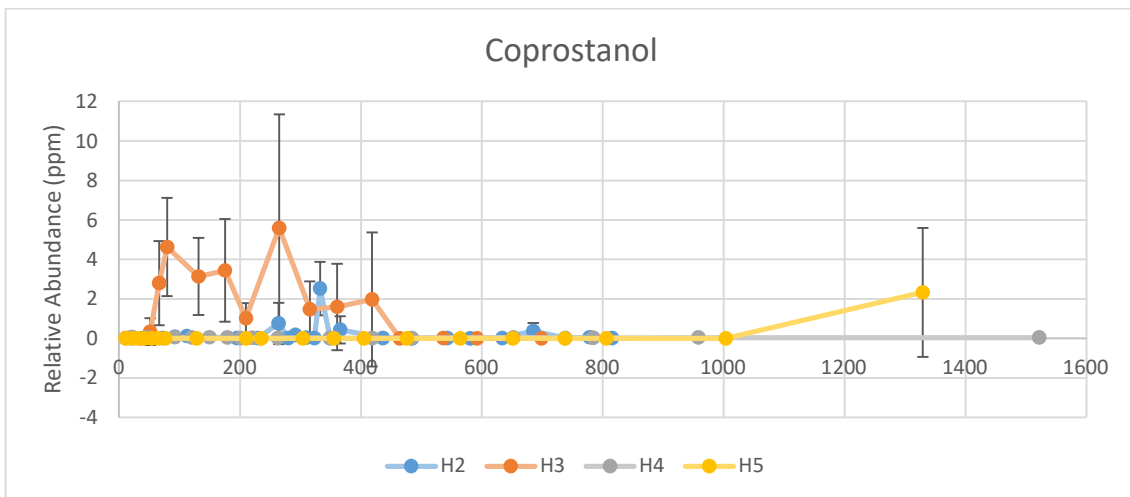


**Figure J-18:** Comparison of coprostanol through decomposition period of H2, H3, H4 and H5. X-axis represents relative abundance in ppm. Y-axis represents accumulated degree days (ADD).

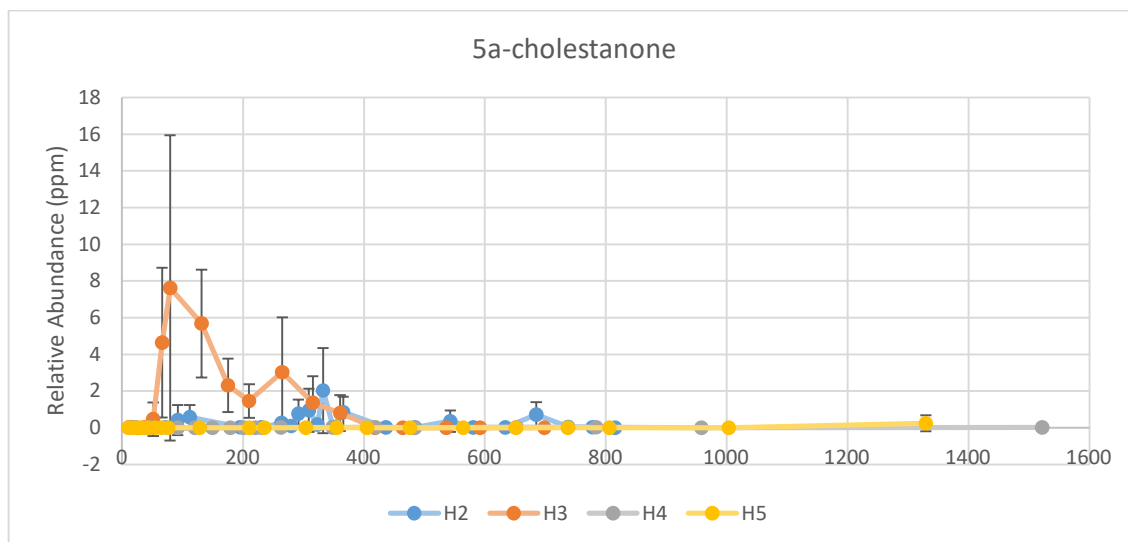


**Figure J-19:** Comparison of 5a-cholestanone through decomposition period of H2, H3, H4 and H5. X-axis represents relative abundance in ppm. Y-axis represents accumulated degree days (ADD).

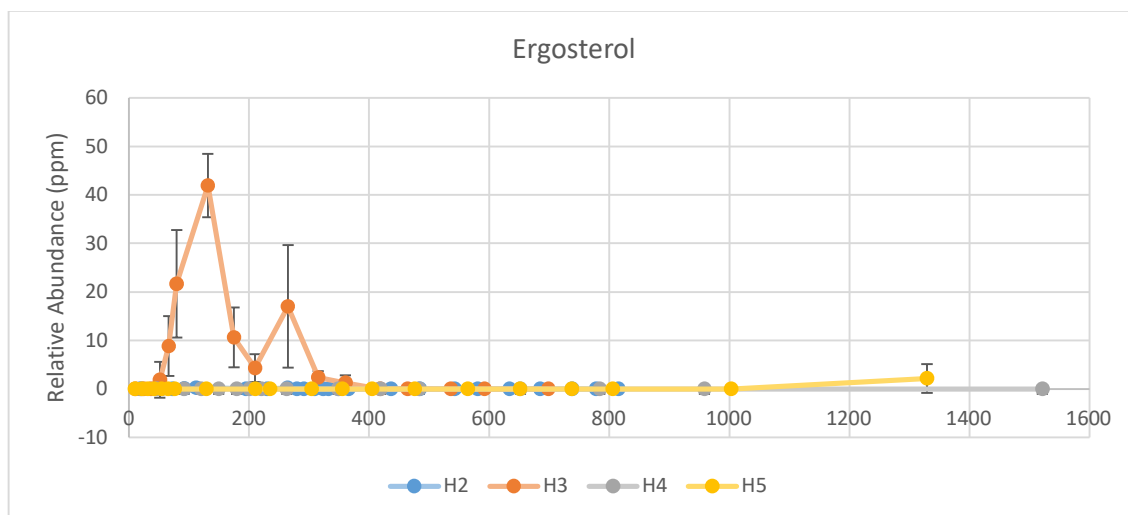


**Figure J-20:** Comparison of ergosterol through decomposition period of H2, H3, H4 and H5. X-axis represents relative abundance in ppm. Y-axis represents accumulated degree days (ADD).

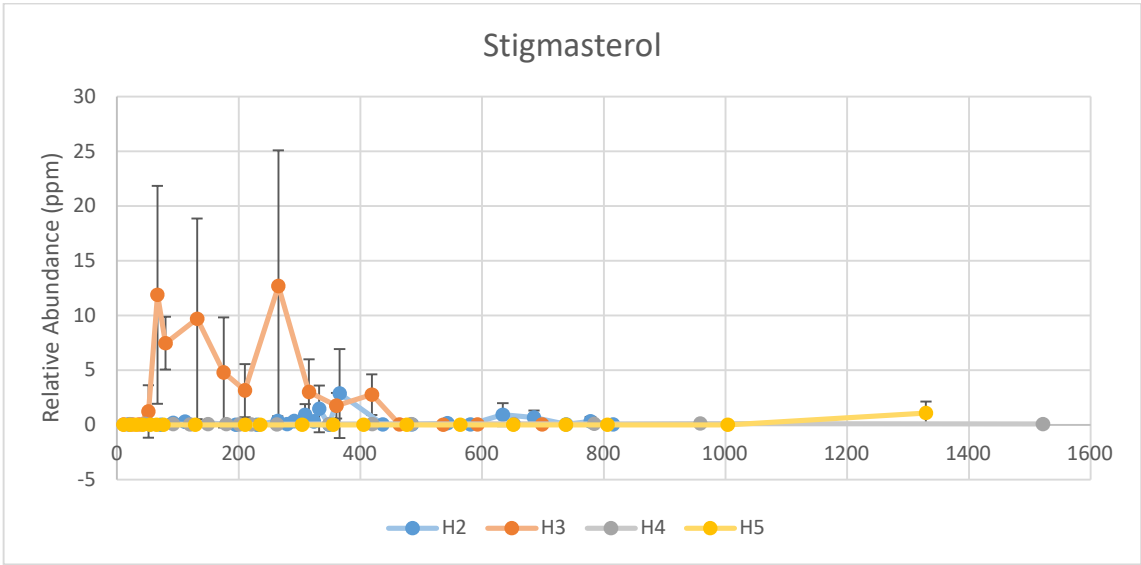


**Figure J-21:** Comparison of stigmasterol through decomposition period of H2, H3, H4 and H5. X-axis represents relative abundance in ppm. Y-axis represents accumulated degree days (ADD).

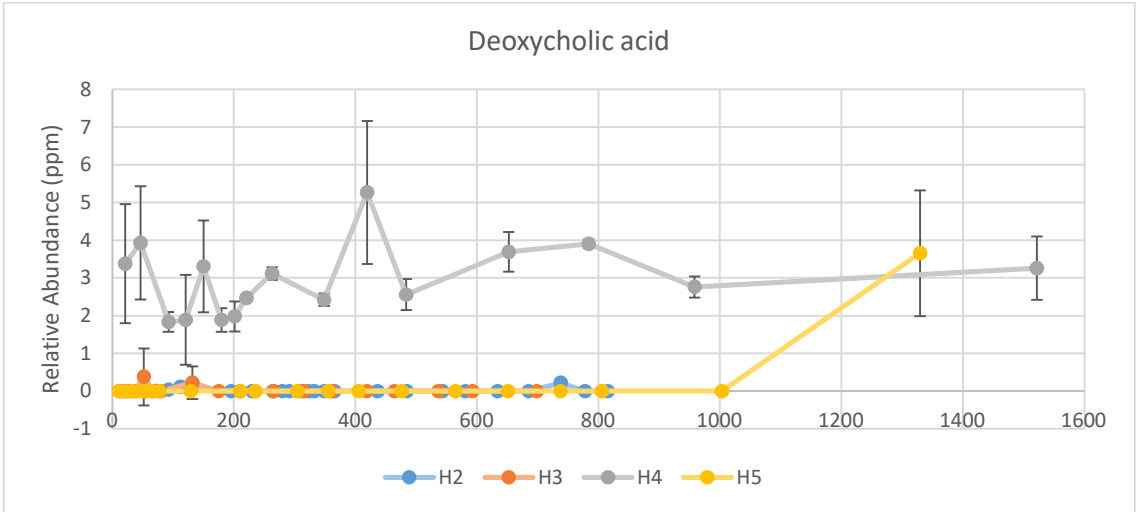


**Figure J-22:** Comparison of deoxycholic acid through decomposition period of H2, H3, H4 and H5. X-axis represents relative abundance in ppm. Y-axis represents accumulated degree days (ADD).

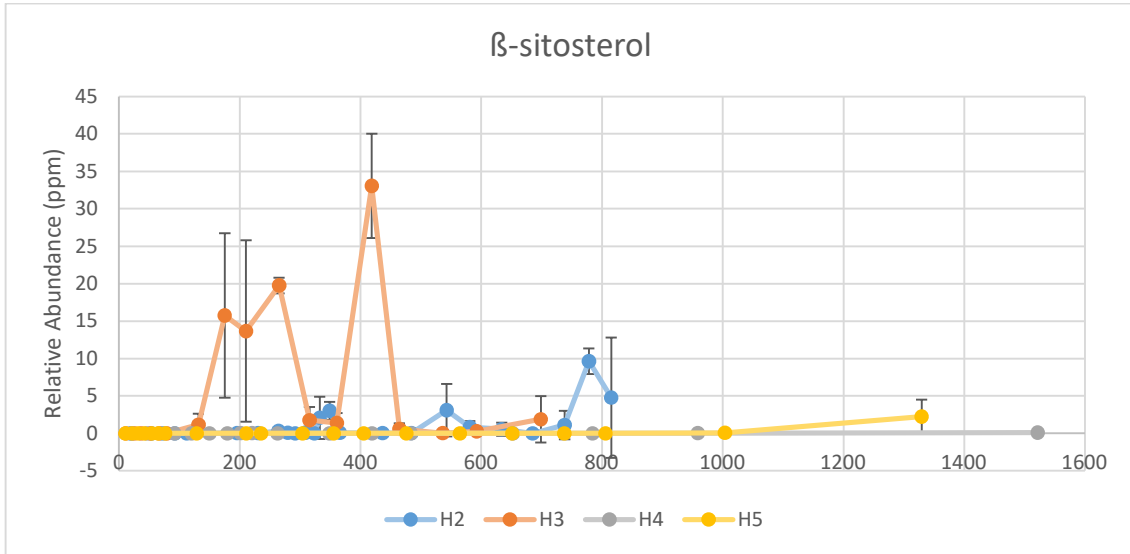


**Figure J-23:** Comparison of β-sitosterol through decomposition period of H2, H3, H4 and H5. X-axis represents relative abundance in ppm. Y-axis represents accumulated degree days (ADD).

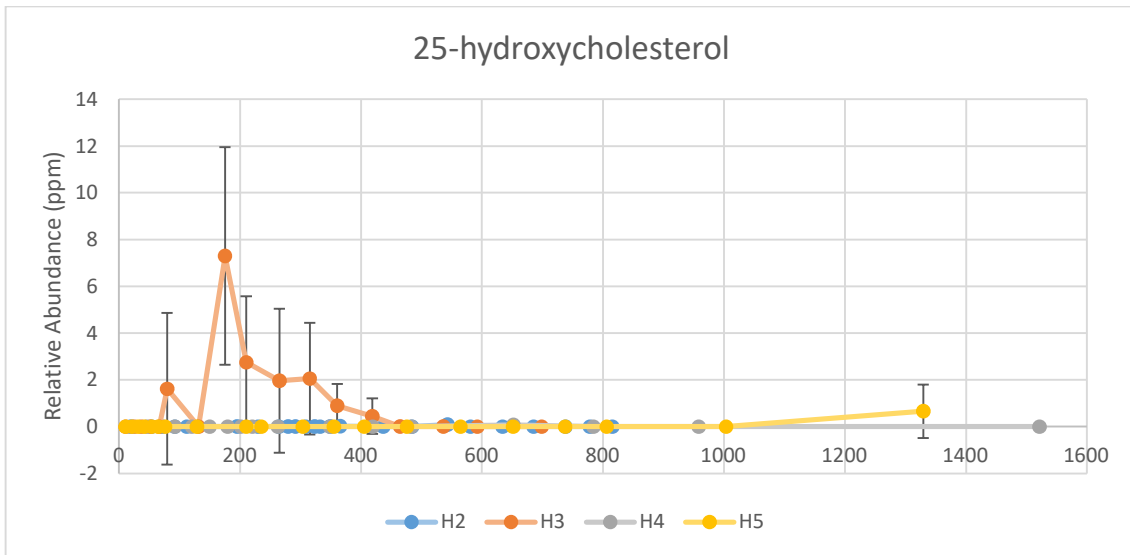







**Figure J-24:** Comparison of β-sitosterol through decomposition period of H2, H3, H4 and H5. X-axis represents relative abundance in ppm. Y-axis represents accumulated degree days (ADD).

## APPENDIX K- PHOTOGRAPHS OF ALL STUDIED BODIES

Disclaimer: The following content contains sensitive images related to forensic studies and human decomposition. Viewer discretion is advised. The purpose of including these images is solely for educational and research purposes within the context of forensic taphonomy.

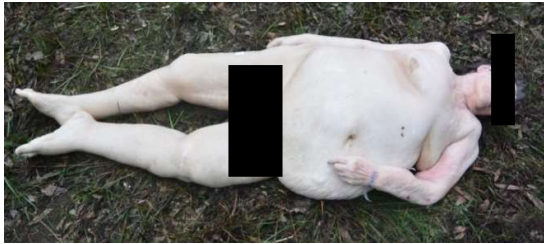


**Table K-1:** Human 2 (H2) photographs

Photograph & Sampling Day	
 <p>Day 0</p>	 <p>Day 1</p>
 <p>Day 2</p>	 <p>Day 3</p>
 <p>Day 4</p>	 <p>Day 6</p>



Day 7



Day 10



Day 12



Day 14



Day 16



Day 18





Day 20



Day 22



Day 24



Day 26



Day 28



Day 30



Day 35



Day 40



Day 45



Day 50



Day 55



Day 60



Day 65









Day 70



Day 75



Table K-2: Human 3 (H3) photographs

Photograph & Sampling Day	
 <p>Day 0</p>	 <p>Day 1</p>
 <p>Day 2</p>	 <p>Day 3</p>
 <p>Day 4</p>	 <p>Day 5</p>



Day 6



Day 9



Day 12



Day 13



Day 16



Day 19





Day 23



Day 26



Day 30



Day 33



Day 37



Day 40





Day 47



Day 55



Day 68









Day 82



Day 114

Table K-3: Human 4 (H4) photographs

Photograph and Sampling Day	
 <p>Day 0</p>	 <p>Day 1</p>
 <p>Day 2</p>	 <p>Day 3</p>
 <p>Day 4</p>	 <p>Day 5</p>





Day 6



Day 7



Day 8



Day 10



Day 14



Day 17



Day 20



Day 28



Day 35



Day 42



Day 70



Day 105











Day 182



Day 202

Table K-4: Human 5 (H5) photographs

Photograph and Sampling Day	
 <p>Day 0</p>	 <p>Day 1</p>
 <p>Day 2</p>	 <p>Day 3</p>
 <p>Day 4</p>	 <p>Day 5</p>





Day 6



Day 10



Day 13



Day 17



Day 23



Day 26



Day 31



Day 35



Day 42



Day 49



Day 56



Day 63



Day 69



Table K-5: Pig 1 (P1) photographs

Photographs and sampling day	
 <p>Day 0</p>	 <p>Day 1</p>
 <p>Day 2</p>	 <p>Day 3</p>



Day 4



Day 5



Day 7



Day 8



Day 10



Day 14





Day 17



Day 28



Day 35







Pig 42



Day 70

Table K-6: Pig 2 (P2) photographs

Photograph and Sampling Day	
 <p>A pig wearing a white t-shirt is lying on grass. There is a significant amount of blood on its head and neck area.</p>	 <p>A pig wearing a white t-shirt is lying on grass, viewed from the side. The pig appears to be in a resting or sedated state.</p>
Day 0	Day 1
 <p>A pig wearing a white t-shirt is lying on grass, viewed from the side. The pig's body is covered in numerous small dark spots, likely lesions.</p>	 <p>A pig wearing a white t-shirt is lying on grass, viewed from the side. The pig's body is covered in numerous small dark spots, similar to Day 3.</p>
Day 3	Day 5





Day 7



Day 8



Day 10



Day 14



Day 17



Day 28



Day 35









Day 42



Day 70



Table K-7: Pig 3 (P3) photographs

Photograph and Sampling Day	
 <p>Day 0</p>	 <p>Day 1</p>
 <p>Day 2</p>	 <p>Day 3</p>
 <p>Day 4</p>	 <p>Day 5</p>





Day 6



Day 10



Day 13



Day 17



Day 23



Day 26





Day 31



Day 35



Day 42



Day 49



Day 56









Day 63



Day 69



Table K-8: Pig 4 (P4) photographs

Photographs and Sampling days	
 <p>Day 0</p>	 <p>Day 1</p>
 <p>Day 2</p>	 <p>Day 3</p>
 <p>Day 4</p>	 <p>Day 5</p>



Day 6



Day 10



Day 13



Day 17



Day 23



Day 26





Day 31



Day 35



Day 42



Day 49



Day 56



Day 63



Day 69